1180

TRANSPORTATION RESEARCH RECORD

Bridge Design and Testing

Transportation Research Record 1180

Contents

Foreword

There are 13 papers in this Record on bridge design and construction, including strengthening, laboratory and field testing, estimation and economic analysis of replacement costs, and analytical procedures used for structural performance predictions.

Klaiber et al. summarize the development of a manual containing eight different bridge-strengthening procedures, which was carried out under National Cooperative Highway Research Program Project 12-28(4). The manual includes an equivalent uniform annual cost (EUAC) procedure, which makes possible cost comparisons of different economic lives. In another paper on strengthening, Eberline et al. present a review of research on and applications of epoxy-bonded steel plates. Information on the bonding procedure, including surface preparation, adhesion, selection, and application, is provided.

Vasishth and Itani document a two-part research program consisting of a full-scale test of a 48-ft-long precast concrete girder and a corresponding analytical study. The two studies showed that blocks can be eliminated from simply supported precast concrete girders of the Washington Department of Transportation Series 14 and 10 design. Girder standards were revised, with a cost savings of 7 percent.

To explain an unexpected fracture in the top flange of a steel tie, Hanson et al. present the results of chemical and physical tests and fractographic and metallographic examinations used to characterize the quality of the steel and to reconstruct the history of the fracture. The $2^3/_8$-in.-thick A588 plate in which the fracture occurred did not meet the toughness requirements of the Iowa Department of Transportation.

Anderson describes the field testing of a 100-year-old solid-rib arch bridge consisting of two 258-ft spans, one of which has three hinges and the other, two hinges. The testing demonstrated that deteriorated $^3/_8$-in. steel batten plates were controlling the load rating and required immediate replacement. The test findings also helped develop rehabilitation alternatives.

Laboratory testing of 26 stringer-stiffened steel deck grids, as reported by GangaRao et al., is used to develop design equations. Conclusions include items on reduction of bending stresses due to composite action, bending moments as affected by main-bar direction compared with traffic direction, stresses induced by field welding, residual stresses, fatigue life, galvanization, and riveted connections.

Hill et al. describe the design and construction of a 488-ft six-span prestressed concrete bulb tee beam bridge with a 2-in. concrete overlay. The construction was completed in 5 months for $450/square yard, an estimated 25 percent savings.

The computer program SEISAB is used by Chen and Van Lund to examine the effect of high-strength concrete (HSC) on the response of concrete bridge piers and columns subjected to seismic forces. Vibration characteristics, displacement, and shears and moments suggest that the use of HSC on rigid foundation systems can reduce material costs up to 33 percent.

Fanous et al. use the general-purpose finite-element computer program ANSYS to study curved shell elements with attached deck slabs. Detailed analyses of four different cross sections indicated that shell-type bridges can be used for short- or medium-span emergency bridges.

Two papers address the structural response of curved prestressed-concrete box girder bridges. Choudhury and Scordelis use a finite-element numerical analysis method based on thin-walled beam theory to make a linear-elastic analysis of force distributions in a complex prestressed-concrete curved box girder bridge. In addition, a nonlinear analysis procedure is used to trace the response of the same bridge to loads through elastic, inelastic, and ultimate load ranges. Computer programs used for the analyses are LAPBOX and NAPBOX. In the second paper, Mari et al. use a filament beam model and a box beam straight element composed of concrete panels with steel layers to analyze a curved prestressed-concrete box girder bridge constructed in Spain. On the basis of the analysis results, observations are made concerning nonlinearity of

the bridge after concrete cracking, redistribution of forces, loading conditions, ultimate load capacity, effect of transverse prestressing, torsion, and bending.

A mathematical model that incorporates the effects of bridge age on bridge condition is presented by Jiang et al. Further work is under way to incorporate effects of truck traffic and climatic condition into the model.

Saito et al. present the results of a study of bridge replacement costs for the Indiana Department of Highways bridge management system. It was found that superstructure, substructure, and approach-cost estimates must be made separately to obtain reasonable results. Substructures were grouped into stem piers or pile piers. Approach costs were related to length and amount of earthwork. Statistical analyses were used to identify variability of costs from average values.

Methods of Strengthening Existing Highway Bridges

F. Wayne Klaiber, Kenneth F. Dunker, Terry J. Wipf, and Wallace W. Sanders, Jr.

This paper briefly reviews the results of NCHRP Project 12-28(4), Methods of Strengthening Existing Highway Bridges. The initial task in this investigation was a thorough review of international literature to determine strengthening procedures currently being used and to investigate innovative ideas now being considered. The types of structures that show the most need for cost-effective strengthening were identified. A procedure for determining equivalent uniform annual costs was developed to assist the engineer in determining whether to strengthen or replace a given bridge. The culmination of the study was the development of a strengthening manual for practicing engineers. The eight sections of that manual, which contain different strengthening procedures, are briefly summarized in this paper.

About one-half of the approximately 600,000 highway bridges in the United States were built before 1940. Many of these bridges have not been adequately maintained and were designed for lower traffic volumes, smaller vehicles, slower speeds, and smaller live loads than are common today. In addition, deterioration caused by environmental factors is a growing problem. According to FHWA, almost 40 percent of the nation's bridges are classified as deficient and in need of rehabilitation or replacement. Many of these bridges are deficient because their load-carrying capacity is inadequate for today's traffic. Strengthening can often be used as a cost-effective alternative to replacement or posting.

The live-load capacity of various types of bridges can be increased by using different methods such as adding members, providing continuity, providing composite action, modifying load paths, and so forth. Some of these methods have been widely used, but others are new and have not been fully developed. The need to compile, evaluate, and improve existing methods as well as to develop new procedures, equipment, and materials for increasing or restoring the load-carrying capacity of existing bridges was the reason for this investigation. This project is one of a series that was funded by the National Cooperative Highway Research Program (NCHRP) to address the serious bridge problems confronting the United States. The purpose of this paper is to summarize the results of NCHRP Project 12-28(4), Methods of Strengthening Existing Highway Bridges.

The objectives of this investigation were to evaluate the feasibility and cost-effectiveness of current strengthening

Bridge Engineering Center, Town Engineering Building, Iowa State University, Ames, Iowa 50011.

methods as applied to various types of bridges and to identify cost-effective innovative methods. The objectives required completion of the following tasks:

Task 1: Thoroughly review available literature and contact appropriate organizations to identify, describe, and categorize methods for strengthening existing highway bridges. Innovative ideas as well as established methods should be considered.

Task 2: Determine which types of structures show the greatest need for broad application of cost-effective techniques for strengthening.

Task 3: Evaluate the cost-effectiveness of each method for strengthening bridge structures. Identify new materials and innovative techniques for further study.

Task 4: Prepare a manual for use by practicing engineers that describes the most effective techniques for strengthening existing highway bridges.

Task 5: Prepare a final report documenting all research. The manual prepared in Task 4 should be the main entity of the final report. The additional findings of the investigation should simply provide supplementary or background information.

The final report of this investigation [NCHRP 12-28(4)] was submitted to NCHRP in July 1987; this report has recently been published by the Transportation Research Board as NCHRP Report 293 (1). In the following sections the approach taken to complete Tasks 1 through 4 and a brief summary of the results will be presented.

TASK 1

As noted earlier, the purpose of Task 1 was to determine what techniques and procedures are now being used to strengthen existing bridges.

The research team used three different approaches to obtain the desired information: literature review, questionnaires, and personal correspondence.

Highway Research Information Service and the Computerized Engineering Index were searched to obtain articles in English on bridge strengthening. In an attempt to locate German and French articles, volume indexes from 1945 to the present were reviewed. Over 500 articles on bridge strengthening and closely related areas were located. Of these articles, approximately 95 were written in a foreign language. Over 375 of the articles located were included in the bibliography of the final report (1). In recent years FHWA and NCHRP have sponsored several studies on bridge repair, rehabilitation, and

retrofitting. Because these procedures also increase the strength of a given bridge, the final reports of these investigations (2–12) are excellent references. Note that the references have been listed in chronological order. Two of these references (3, 4) are of specific interest in strengthening work. Reference 3 is an FHWA investigation into methods of increasing the load-carrying capacity of bridges whose capacities are inadequate for current service loads, and Reference 4 presents several techniques for increasing the capacity of various bridge components. Two questionnaires were developed to obtain unpublished information on bridge-strengthening techniques and to identify agencies involved with bridge strengthening. Questionnaire 1 was developed for distribution to government bridge engineers, consultants, and members of various technical committees, and Questionnaire 2 was developed to obtain information from manufacturers of products related to bridge strengthening. A total of 767 questionnaires was mailed; the response rate was slightly over 38 percent. The state bridge engineers had the highest response rate of all the groups surveyed; all but 3 of the 50 state bridge engineers returned the questionnaire. This high rate of response can be partially attributed to their interest and experience with bridge strengthening.

The majority of the respondents had successfully employed one or more techniques to strengthen a given bridge. The following list of strengthening techniques was provided on the questionnaires for reference to assist the respondents:

1. Replace an existing deck with a lighterweight deck.
2. Provide composite action between deck and supporting members.
3. Increase the transverse stiffness of bridge deck.
4. Replace deficient members.
5. Replace structurally significant portions of deficient members.
6. Increase the cross section of deficient members.
7. Add supplemental members.
8. Poststress members.
9. Add supplemental spanning mechanisms.
10. Strengthen critical connections.
11. Add supplemental supports to reduce span lengths.
12. Convert a series of simple spans to a continuous span.
13. Other.

Shown in Figure 1 are the responses to one of the questions on the survey that requested information on strengthening procedures that had been used; the strengthening method reference numbers correspond to those on the foregoing list. The survey results indicate that replacing deficient members and increasing the cross section of deficient members have been the two most frequently used strengthening techniques.

To locate foreign published and unpublished bridge-strengthening information, the research team made personal contacts with colleagues in foreign countries as well as in the United States. Over 70 different individuals and agencies were contacted for such information. Included in this list are the 21 foreign members of the Organisation for Economic Cooperation and Development (OECD) Committee. This group met in Paris in 1983 and developed a report entitled *Bridge Rehabilitation and Strengthening (13)*. The report reviewed
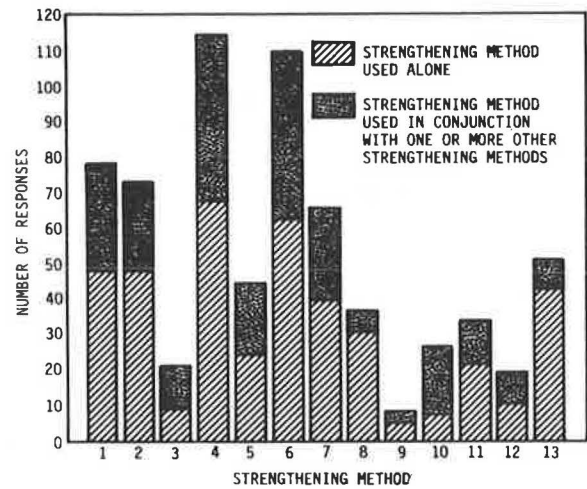
FIGURE 1 Number of responses for strengthening methods 1–13 (see section on Task 1 for description of strengthening methods).

the needs, policies, and techniques used for bridge rehabilitation and strengthening in the OECD member countries. The material provided by a large number of the respondents was quite valuable and has been included in various sections of the final report.

TASK 2

Task 2 involved determining the types of structures that show the most need for cost-effective strengthening. The research team used data from the previously described questionnaires, data in the National Bridge Inventory (NBI), and a limited number of site inspections to address this task. Preliminary findings from this task have been published elsewhere; thus only limited information on this task will be presented in this paper. The most direct approach to determine the types of bridges in need of strengthening is to examine the improvements recommended by bridge inspectors in the NBI. For the 15 common bridge types, inspectors recommended some type of improvement in more than 40 percent of the bridges. As can be seen in Figure 2, the overwhelming choice of improvement, accounting for two-thirds of the recommendations, was replacement due to condition. The inspectors' recommendations, if followed and extrapolated to all bridges, would require that one-third of the nation's bridges be replaced in the near future. Also shown in Figure 2 is that only approximately 1 percent of the recommendations were to strengthen bridges. There are several probable reasons for the few recommendations for strengthening; for example, inspectors did not recognize strengthening as a means of prolonging bridge life, inspectors in some states did not have strengthening as an option, and limitations in the NBI coding system.

For those bridges for which strengthening was recommended, the responses ranked by number and bridge type are shown in Figure 3. The recommendations for strengthening steel stringer bridges account for more than one-half of the recommendations. The next four bridge types in the ranking are steel-through-truss, steel-girder floor-beam, timber stringer, and concrete slab. Although there is some variation in
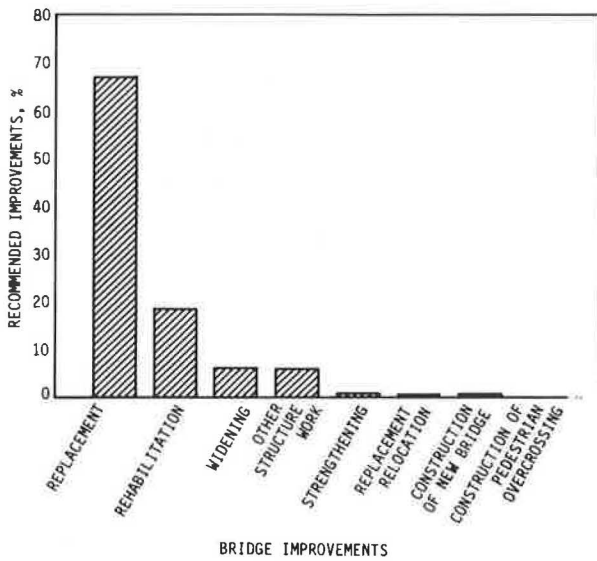
FIGURE 2 Bridge improvements recommended by inspector (NBI).
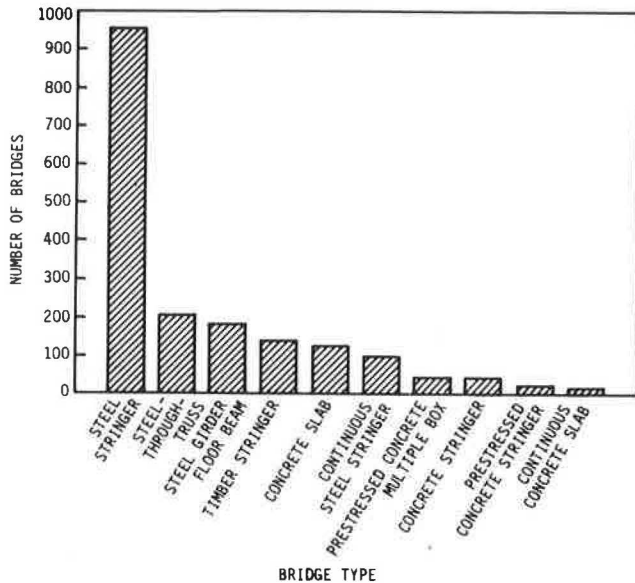
FIGURE 3 Strengthening recommended by inspector, ranked by bridge type (NBI).

FIGURE 4 Number of steel-stringer bridges constructed and anticipated retirements by 5-year periods (NBI).

which bridges show the greatest need for strengthening, data from the questionnaires and site visits essentially agree with the NBI data. To develop some concept of the urgency of the strengthening needs, the number of anticipated bridge retirements was examined for each of the common bridge types. A representative sample of the type of curve showing anticipated bridge retirements is given in Figure 4 for steel-stringer bridges. The dashed line represents the number of bridges constructed in each 5-year period. Steel-stringer bridges constructed in 1900 and all previous years are represented by the first point on the dashed line. The average life, 57 years in this case, was computed from NBI data for each bridge type by adding the age computed from the year built and the estimated remaining life. The solid line in Figure 4, which represents anticipated bridge retirements, was obtained by extending the

construction date into the future by the average life. Although the average life may contain some inaccuracies, it is the best statistic available in the NBI for predicting bridge life.

Figure 4 [and the figures for other types of bridges presented in the final report (*1*)] indicate which types of bridges have large numbers of anticipated retirements in the near future; these bridges show a definite need for effective strengthening methods.

TASK 3

Task 3 consisted of two separate parts: the development of a procedure for determining the cost-effectiveness of strengthening methods for various bridges and the identification of new materials and innovative strengthening techniques.

The bridge engineer has three alternatives when faced with a bridge having a deficient load rating: (a) replace the existing bridge, (b) strengthen the existing bridge (which includes selecting the "best" strengthening method from those available), or (c) leave the existing bridge in its present state. To assist the engineer in making this decision, an equivalent uniform annual cost (EUAC) procedure was developed that makes possible cost comparisons between alternatives of different economic lives. A related paper, Cost-Effectiveness Analysis for Strengthening Existing Bridges (*14*), provides additional background and detail on the economic model.

Listed below are various factors that are considered in the economic analysis models:

Replacement structure first cost: The initial replacement cost has the greatest effect on the EUAC for the replacement model.

Structure service life: Information obtained indicated that a minimum service life of 50 years is commonly assigned to new structures in a life-cycle cost analysis.

Interest rate: Although difficult to predict over a long time period, interest rate significantly affects the EUAC. In general, a higher interest rate favors future expenditures (i.e., strengthening), whereas a lower interest rate favors the immediate expenditure of capital (i.e., replacement).

Bridge maintenance costs: This factor is probably the most difficult life-cycle cost to predict. However, improvements in

bridge maintenance accounting procedures should soon provide data to make more accurate forecasts possible.

Level-of-service factor: This factor is a measure of the cost difference in the level of service provided to the road user between a new and an existing bridge. Level-of-service factors as presented in this model are principally functions of bridge geometry.

Maintenance of essential traffic flow: This construction aspect is very situation dependent and is difficult to quantify accurately.

In the search for new material that might have application in bridge strengthening, essentially no new materials were identified that would be suitable for use in bridge strengthening. Composite materials—that is, materials consisting of two or more distinct parts—were the only "new materials" identified. Composite materials are new to the construction industry; however, they have been used in the aircraft industry for over 20 years. Although composite materials are sensitive to the environment, their main disadvantage in bridge work is the cost. The procedure of bonding steel plates to steel and to concrete is somewhat related to the topic of new materials. Some work on bonding steel to steel has been done in the United States; however, no work has been done in the area of bonding steel plates to concrete. Other countries, such as the United Kingdom and Japan, have been bonding steel plates to concrete for strengthening for over 20 years. Although a literature review of bonding steel plates to concrete has been included in an appendix to the final report, this procedure has not been included in the strengthening manual.

TASK 4

For the information accumulated in Task 1 to be useful to the practicing engineer, it must be organized and presented in a manual format that is readily accessible and easy to use. The development of such a manual was the objective of Task 4. The strengthening manual obviously could be organized by bridge type or by strengthening method. After a conference with the project panel, it was decided to organize the strengthening manual by strengthening method. Although the procedures have been placed in sections according to the method or procedure, for the convenience of the user, a table is provided that is arranged according to bridge type. In the table, the user is referred to a section or sections in which strengthening information for a particular bridge may be found. Obviously, a single strengthening procedure is applicable to more than one type of bridge or stringer.

Strengthening procedures included in the manual are procedures that have been successfully used in the field or have been sufficiently tested in the laboratory so that they can be employed in the field with minimal difficulty. Each strengthening procedure in the manual includes a description of its use, a description of its limitations, and basic cost information. For most procedures, decision aids are provided to assist users in determining the adequacy of the strengthening procedure for particular situations. For several of the procedures, design aids are also given to assist the users. References are provided for each strengthening procedure, describing where the technique has been employed and where additional information may be obtained.

Every effort has been made to present the different strengthening techniques in clear, practical formats to facilitate their use. However, because of the wide range of variables involved (e.g., span lengths, amount of overstress, and type of loading), most of the strengthening systems presented are conceptual, and the designs and dimensions, where given, are for illustration only.

Described in the following paragraphs are the eight sections of Chapter 3 of the final report in which the various strengthening techniques and procedures are categorized. A brief description of the material in each section is presented.

Lightweight Deck Replacement

One of the more fundamental approaches to increase the live-load capacity of a bridge is to reduce the dead load. Significant reductions in dead load can be obtained by removing an existing concrete deck and replacing it with a lighterweight deck. Lightweight deck replacement is a feasible strengthening technique for bridges with structurally inadequate but sound steel stringers. Several types of lightweight decks, including steel grid, Exodermic, laminated timber, lightweight concrete, and aluminum and steel orthotropic plate, are available. Decision aids are included to indicate the relative increase in live-load capacity for each type of lightweight deck.

Providing Composite Action Between Bridge Deck and Stringer

Modification of an existing stringer and deck system to a composite system is a common method of increasing the flexural strength of a bridge. The composite action of the stringer and deck reduces not only the live-load stresses but also deflections as a result of the increase in the moment of inertia. Composite action can effectively be developed between steel stringers and various deck materials, such as normal-weight reinforced concrete (precast or cast-in-place), lightweight reinforced concrete (precast or cast-in-place), laminated timber, and concrete-filled steel grids. In general, composite action is slightly more beneficial in short spans than in long spans, and the larger the stringer spacing, the larger the stress reduction when composite action is added.

Increasing Transverse Stiffness of a Bridge

Increasing transverse stiffness is applicable only as a secondary method for strengthening a bridge. Transverse stiffening can increase the rating of a bridge but does not increase the overall longitudinal moment strength. Increasing the transverse stiffness of a steel-stringer bridge can reduce live-load stresses in stringers by as much as 15 percent. Maximum reductions occur for interior stringers in wider and longer span bridges.

Improving the Strength of Various Bridge Members

One of the most common procedures used to strengthen existing steel stringer bridges is the addition of steel cover plates to

existing members. The additional steel is normally attached to the flanges of existing sections, thus increasing the section modulus and thereby increasing the flexural capacity of the member.

A common method of strengthening compression members in steel-truss bridges is to add steel cover plates to the existing members. The steel cover plates will increase the cross-sectional area of the members and, if properly applied, will also reduce the slenderness ratio of the compression member.

The shear strength of reinforced concrete beams or prestressed concrete beams can be improved by adding external steel straps, plates, or stirrups. For more efficient use of the material added, the new material should be posttensioned so that it carries both dead and live loads.

Improving the strength of timber or concrete piles and pier columns can be achieved by encasing the column in a concrete or steel jacket. Jacketing, which may be applied to the full length of the column or only to severely deteriorated sections, increases the cross-sectional area of the column and reduces the column's slenderness ratio.

Adding or Replacing Members

Reinforced concrete, prestressed concrete, steel, and timber stringer bridges can be strengthened by the addition or replacement of one or more stringers. Adding stringers not only increases the deck capacity, but also reduces the magnitude of the loads distributed to the existing stringers.

Adding supplementary members to truss frames is most commonly applied to Warren and Pratt trusses. The supplementary members are normally most effective in reducing the unbraced length of the top chord member, which can increase the load capacity of the top chord by as much as 15 to 20 percent.

Posttensioning Various Bridge Components

Since the 19th century, timber structures have been strengthened by means of king post and queen post tendon arrangements. These arrangements are still in use today; however, since the 1950s, posttensioning has been applied as a strengthening method in many more configurations to almost all common bridge types. A review of the engineering literature revealed that approximately one-half of the reported uses of posttensioning for bridge strengthening are for the current decade. Posttensioning can be applied to an existing bridge to meet a variety of objectives: relieve tension overstresses with respect to service load and fatigue-allowable stresses, reduce or reverse undesirable displacements, add ultimate strength to an existing bridge, and change basic behavior of a bridge from a series of simple spans to continuous spans.

Strengthening Critical Connections

The types of connections addressed in the manual include cover and splice-plate connections as well as truss connections. Although several methods of strengthening the various types of connections are presented in this section, only two will be briefly described here. One of the more common joint-strengthening techniques is to replace loose or broken rivets with new high-strength bolts. These bolts increase the shear capacity and have been shown to increase the fatigue life of the connected material by reducing fatigue cracking. The use of high-strength bolts at the ends of welded cover plates has also been shown to significantly reduce or eliminate the fatigue cracking often associated with the ends of cover plates.

Developing Additional Bridge Continuity

There are two basic methods of adding continuity to a given bridge. Supplemental supports can be added to reduce the span length and thereby reduce the maximum positive moment in a given bridge. By changing a single-span bridge to a continuous, multiple-span bridge, stresses in the bridge can be altered dramatically, thereby improving the bridge's maximum live-load capacity. Even though this method may be expensive, it may be desirable in certain situations. Several adjacent simple spans may be converted into a continuous span by connecting the simple spans together with moment and shear-type connections. The desired decrease, however, is accompanied by the development of negative moment over the interior supports.

SUMMARY

The results of a study on the various methods of strengthening highway bridges have been presented. The literature review resulted in a bibliography of more than 375 references. Types of structures that show the greatest need for cost-effective strengthening techniques were identified; these are steel stringer bridges, timber stringer bridges, steel-through-truss bridges, and steel-girder floor-beam bridges. An economic analysis for determining the cost-effectiveness of the various strengthening procedures, developed as part of the investigation, is briefly described. The major effort of the study was the development of a strengthening manual for use by practicing engineers. The organization of the strengthening manual and a brief description of the information included have been presented. In the opinion of the authors, the final report of the project in question (*1*) is an excellent reference for engineers faced with the problem of strengthening a deficient bridge.

REFERENCES

1. F. W. Klaiber, K. F. Dunker, T. J. Wipf, and W. W. Sanders, Jr. *NCHRP Report 293: Methods of Strengthening Existing Highway Bridges.* TRB, National Research Council, Washington, D.C., 1987, 114 pp.
2. *Extending the Service Life of Existing Bridges by Increasing Their Load Carrying Capacity.* Report FHWA-RD-78-133. FHWA, U.S. Department of Transportation, June 1978, 75 pp.
3. J. W. Fisher, H. Hausamann, M. D. Sullivan, and A. W. Pense. *NCHRP Report 206: Detection and Repair of Fatigue Damage in Welded Highway Bridges.* TRB, National Research Council, Washington, D.C., June 1979, 85 pp.
4. *NCHRP Report 222: Bridges on Secondary Highways and Local Roads—Rehabilitation and Replacement.* TRB, National Research Council, Washington, D.C., May 1980, 73 pp.
5. G. O. Shanafelt and W. B. Horn. *NCHRP Report 226: Damage Evaluation and Repair Methods for Prestressed Concrete Bridge Members.* TRB, National Research Council, Washington, D.C., Nov. 1980, 66 pp.
6. H. W. Mishler and B. N. Leis. *Evaluation of Repair Techniques for Damaged Steel Bridge Members: Phase I.* Final Report, NCHRP Project No. 12-17, May 1981, 131 pp.
7. *NCHRP Report 243: Rehabilitation and Replacement of Bridges on Secondary Highways and Local Roads.* TRB, National Research Council, Washington, D.C., Dec. 1981, 46 pp.
8. G. M. Sabnis. *Innovative Methods of Upgrading Structurally and Geometrically Deficient Through Truss Bridges.* Report FHWA-RD-82-041. FHWA, U.S. Department of Transportation, April 1983, 130 pp.
9. *Seismic Retrofitting Guidelines for Highway Bridges.* Report FHWA-RD-83-007. FHWA, U.S. Department of Transportation, Dec. 1983, 219 pp.
10. G. O. Shanafelt and W. B. Horn. *NCHRP Report 271: Guidelines for Evaluation and Repair of Damaged Steel Bridge Members.* TRB, National Research Council, Washington, D.C., June 1984, 64 pp.
11. M. M. Sprinkle. *NCHRP Synthesis of Highway Practice 119: Prefabricated Bridge Elements and Systems.* TRB, National Research Council, Washington, D.C., Aug. 1985, 75 pp.
12. G. O. Shanafelt and W. B. Horn. *NCHRP Report 280: Guidelines for Evaluation and Repair of Prestressed Concrete Bridge Members.* TRB, National Research Council, Washington, D.C., Dec. 1985, 84 pp.
13. *Bridge Rehabilitation and Strengthening.* Organisation for Economic Cooperation and Development, Paris, France, 1983, 103 pp.
14. T. J. Wipf, D. L. Erickson, and F. W. Klaiber. Cost-Effectiveness Analysis for Strengthening Existing Bridges. In *Transportation Research Record 1113*, TRB, National Research Council, Washington, D.C., 1988, pp. 9–17.

Bridge Strengthening with Epoxy-Bonded Steel Plates

Donita K. Eberline, F. Wayne Klaiber, and Kenneth Dunker

Epoxy-bonded steel plates have been used to strengthen or repair concrete bridges in many countries around the world. Because most of the information pertaining to this subject has been published outside the United States, an extensive literature review was undertaken; this paper summarizes some of the research and applications related to this strengthening technique. Information relevant to the bonding procedure is provided, including methods for preparing the bonding surfaces and guidelines for adhesive selection and application. Research results pertaining to variations in the plate geometry, the effects of cyclic loading, and steel-to-steel bonding are also presented. Numerous applications of this strengthening technique are described. Although no original research results are presented, an extensive bibliography and a formatted table indicating the topics addressed are included for convenient reference.

Epoxy-bonded steel plates have been used to strengthen or repair bridges and buildings in many countries around the world, including South Africa, Switzerland, France, USSR, Japan, United Kingdom, Australia, Belgium, and Poland. Because this strengthening technique has not been widely researched or implemented in the United States, this paper was prepared to introduce the concept of strengthening with epoxy-bonded plates and to summarize some of the related research. In addition, a description of some applications of this procedure primarily related to bridge strengthening will be presented.

The principle of this strengthening technique is rather simple: an epoxy adhesive is used to bond steel plates to overstressed regions of reinforced-concrete members. The steel plates are typically located in the tension zone of a beam; however, plates located in the compression and shear zones have also been utilized. The adhesive provides a shear connection between the reinforced-concrete beam and the steel plate, resulting in a composite structural member. The addition of plates in the tension zone not only increases the area of tension steel, but also lowers the neutral axis, resulting in a reduction of live-load stresses in the existing reinforcement. The tension plates effectively increase the flexural stiffness, thereby reducing cracking and deflection of the member.

Epoxy-bonded steel plates have been used to repair bridges that have been damaged by accident, fire, or explosion. The technique has also been used to strengthen bridges with insufficient load-carrying capacity because of increased load requirements or a design or construction error. When applied to

Bridge Engineering Center, Department of Civil and Construction Engineering, Iowa State University, Ames, Iowa 50011.

bridges, this strengthening technique has several advantages. The plates can be easily handled and placed, thus allowing the procedure to be carried out relatively quickly, with minimal disruption to traffic. Also, because the plates are thin, there is almost no loss of overhead clearance. This strengthening technique is not recommended, however, for application to bridges with unsound concrete or to bridges where corrosion has been a problem unless the source of the problem is corrected.

ASSEMBLY METHODS

Critical to the success of this strengthening technique are the selection and application of an appropriate adhesive and the preparation of the bonding surfaces (1). The steel plates must be free from oil, grease, rust, mill scale, and dirt. Oil and grease should be removed with a chemical cleaning agent. Grit blasting is the preferred method of removing dirt, scale, and rust. In research reported by Cusens and Smith (2), it was found that the shear strength of the joint improved with increased roughness of the bonding surfaces. Cleaning of the steel plates must be done shortly before bonding to avoid the development of surface corrosion or recontamination.

Preparation of the concrete surface requires the removal of all loose and unsound material. For a new concrete member, the surface laitance must be removed to expose the aggregate. Sand-blasting or grinding or both are generally used to prepare the concrete surfaces in this manner, followed by a thorough cleaning to remove all dust and debris.

There are several things to consider when an adhesive is selected for this type of application. Practical considerations to simplify the placement of the plates include the following: the temperature requirements for mixing, applying, and curing of the adhesive should be consistent with those that will exist in the field; the adhesive should also have a viscosity and pot life suitable for the particular application; and the adhesive, in most applications, should develop its strength rapidly. Long-term performance characteristics that need to be considered include the following: the shear strength of the resin should equal or exceed that of the concrete, and the adhesive should demonstrate good durability and tolerance to moisture and chemicals (1, 3).

Epoxy resin adhesives typically consist of two components: a resin and a hardener. Care must be taken when mixing the two components to ensure that the components are mixed completely and in the proper proportions. The adhesive is generally applied to both the concrete and steel bonding surfaces. The steel plate is then put in contact with the concrete surface and pressure is applied until the adhesive cures. An

alternative method involves the pressure injection of the epoxy resin between the concrete and steel surfaces. For this method, the steel plates are fastened to the concrete with bolts, using shims and spacers to maintain the desired gap between the two surfaces. After the edges of the plates have been sealed, the adhesive is pressure injected (4).

There is general agreement among the researchers that the adhesive layer should be as thin as possible while still remaining free of voids. Adhesive thicknesses ranging from 1 to 1.5 mm (0.04 to 0.06 in.) are suggested (5).

RESEARCH

The steel plates should be designed so that the full flexural strength of the composite member can be achieved, thus ensuring ductility. Macdonald (6) reported that rapid shear failure of the concrete can be prevented with proper sizing of the bonded plates. In this study, steel plates of different widths and thicknesses but of constant cross-sectional area were epoxy-bonded to concrete beams and subjected to four-point bending tests. It was found that beams with thick, narrow plates exhibited sudden, horizontal shear failures. Thin, wide plates, on the other hand, remained bonded to the beams at the maximum sustained load, resulting in ductile failures. Macdonald suggested that an optimum width/thickness (b/t) ratio exists at which the maximum increase in failure load and a significant increase in stiffness can be obtained while still maintaining a ductile failure. Macdonald estimated this optimum ratio to be 60.

Further research pertaining to the effects of plate geometry was reported by Swamy et al. (7). They conducted tests on a series of beams with bonded plates of constant width but varying thicknesses. Single plates with thicknesses of 1.5, 3.0, and 6 mm (0.06, 0.12, and 0.24 in.) were bonded to 155- × 255-mm (6.1- × 10.0-in.) reinforced concrete beams. In addition, beams with two layers of 1.5-mm-thick bonded plates were tested and compared with beams with a single 3-mm plate. All of the beams with plates 1.5 mm thick ($b/t = 83.3$) failed in flexure with no bond distress. Beams with single plates 3.0 mm thick and two layers of plates 1.5 mm thick all exhibited a shear-bond failure; however, the shear-bond failures occurred at loads that approached the theoretical flexural strength of the beams. All of the beams with plates 6 mm thick failed by shearing of the concrete at the level of the reinforcing bars. On the basis of these results, Swamy et al. suggested two tentative design criteria: first, the b/t ratio should be no less than 50; in addition, the neutral axis depth should not be greater than 0.4 times the effective depth.

One advantage of this strengthening technique, when applied to bridges, is that the work can be accomplished with little or no interruption of traffic. The effects of cyclic loading during curing of the adhesive were examined by Swamy and Jones (8) and by Macdonald (9). Swamy and Jones found that the cyclic loading had no effect on the ultimate strength of the beams. Two different adhesives were used in the study conducted by Macdonald. The test beams with one adhesive displayed a 7 to 31 percent reduction in shear strength due to cyclic loading. No reduction in strength was recorded for the test beams with the other adhesive.

Although most of the literature pertaining to epoxy-bonded plates involves bonding steel plates to concrete beams, some research has also been reported (especially in the United States) related to bonding steel plates to steel beams. Researchers at Case Western Reserve University (10) examined the fatigue life of cover plates epoxy-bonded to the tension flanges of steel wide-flange beams. In a similar application, researchers at the University of Maryland (11, 12) combined end-bolting with the adhesive bonding of steel plates to steel beams. Both studies concluded that the use of adhesives improved the fatigue life of cover plates. The adhesive helps to distribute and transfer the load over a larger area, thus reducing stress concentrations. Findings in the study conducted by Albrecht et al. (12) indicate that adhesive bonding increased the fatigue life of cover plates by a factor of 20 over that of conventionally welded cover plates. Though Albrecht et al. advised that the method of adhesive bonding needs further research, they concluded that adhesive bonding, combined with end-bolting, has the potential of making cover plates on steel bridge girders fatigueproof.

A major problem associated with bridge strengthening using epoxy-bonded plates is the long-term durability of the connection. Ongoing exposure tests are being conducted by Calder (13). Unreinforced-concrete beams with epoxy-bonded plates were exposed to three climates, each characterized by varying levels of annual rainfall, mean temperature, and atmospheric chloride and sulfur content. Calder found that the failure load for the beams decreased rapidly during the first 8 months of exposure to approximately 60 to 80 percent of the original load. The failure loads recorded after 1 and 2 years of exposure were only slightly different from the 8-month failure loads. A significant amount of corrosion was noted at the steel–epoxy interface. The reduction in overall strength was attributed to the corrosion.

Hoigard and Longinow (14) investigated the durability of steel-to-steel bonded joints. The bonded joints were subjected to a simulated rain environment and tested after 100 and 696 hr of submersion. The author estimated that for a midwestern climate this represented 88 and 609 days of normal weathering. The specimens displayed a 9 and 12 percent loss in strength after 100 and 696 hr of submersion.

Numerous parameters related to epoxy-bonded plates have been examined by researchers. Some of these parameters are summarized in Table 1. The references, organized in chronological order, indicate the areas investigated by each of the researchers (15–31).

APPLICATIONS

One of the first documented applications of strengthening with epoxy-bonded plates was in 1964 in Durban, South Africa, when the reinforcing steel required in a concrete beam located in a new apartment complex was accidentally omitted during construction.

In the early to mid-1970s, several buildings in Switzerland were strengthened by means of epoxy-bonded steel plates (32, 33). Reinforced-concrete floor slabs and supporting reinforced-concrete beams in a building located in Zurich were strengthened to carry additional live load. Plates were bonded to the undersides of the floor slabs and to the soffits of

TABLE 1 RESEARCH RELATED TO EPOXY BONDING

Author of Investigation	Year	Country	Reference No.	Pre-cracked Section	Reinforced & Unreinforced Sections	Under & Over Reinforced Sections	Effects of Shear Reinforcement	Dimensions of Concrete Beam	Compressive Strength of Concrete	Surface Preparation of Concrete & Steel	Surface Moisture of Concrete	Type of Adhesive	Glue Thickness	Bond Length	Mechanical Fasteners	Variations in Plate Geometry or Section	Multiple Layers of Plates	Plate Lapping	Cyclic Loading During Glue Hardening	Nature of Loading (Static, Dynamic)	Rate of Loading	Fatigue Tests	Creep	Exposure to Environmental Conditions	Temperature Effects	Humidity & Moisture Effects	Use in Actual Structure	Field Tests	Moment-Curvature Relationships	Steel to Steel	Steel to Concrete
Kajfasz	1967	Poland	15												▨																	▨
L'Hermite, Bresson	1971	France	16												▨												▨				▨	
Bresson	1971	France	17									▨			▨																▨	
Ladner, Flueler	1974	Switzerland	18		▨		▨								▨	▨		▨														▨
Irwin	1975	United Kingdom	19																											▨		
Calder	1979	United Kingdom	13																							▨	▨					
Teoh Han	1979	Malaysia	20	▨																												
Cusens, Smith	1980	United Kingdom	2						▨			▨		▨						▨		▨				▨					▨
Jones, et al.	1980	United Kingdom	21									▨					▨															
Raithby	1980	United Kingdom	22	▨								▨				▨				▨							▨					
Swamy, Jones	1980	United Kingdom	8																	▨									▨			▨
VanGemert	1980	Belgium	23								▨					▨													▨			▨
DeBuck, et al.	1981	Belgium	24					▨		▨	▨	▨				▨											▨					
MacDonald	1981	United Kingdom	9														▨														▨	
Kostasy, et al.	1981	West Germany	25						▨	▨		▨		▨		▨		▨		▨											▨
Jones, Swamy	1982	United Kingdom	5				▨																									
MacDonald	1982	United Kingdom	6	▨								▨	▨							▨											▨
Mays, Tilly	1982	United Kingdom	26																			▨			▨			▨			▨
Cardon, Boulpaep	1983	Belgium	27																▨					▨							▨
Albrecht, et al.	1984	United States	11							▨									▨					▨						▨	
Jones, Swamy, Salman	1985	United Kingdom	28				▨					▨		▨																	▨
Mecklenburg, ET AL	1985	United States	29																	▨				▨					▨		
VanGemert, VandenBosch	1985	Belgium	30																					▨							▨
Hoigard, Longinow	1986	United States	14																					▨	▨			▨			
Wiener, Jirsa	1986	United States	31						▨					▨																	
Swamy, Jones, Bloxham	1987	United Kingdom	7	▨								▨			▨																▨

the beams. Shear-reinforcing plates were also bonded to the sides of the beams.

The strengthening of a reinforced-concrete tee-beam bridge in France was reported in 1972 (*34*). The skewed highway bridge, constructed in 1960, had developed a permanent deflection of 8 cm (3.15 in.) near the midspan of the most heavily loaded beam. The probable cause of the excessive deflection was fatigue. To strengthen the bridge, steel plates were bonded to both the sides and bottoms of the beams. At joints between adjacent plates, lap plates were bonded to provide continuous reinforcing. Up to four layers of flexural cover plates were bonded to the bottom surface of the beams.

In 1974, a highway bridge that crosses the Saint-Denis Canal in France was repaired with epoxy-bonded steel plates (*35*). Reinforcing plates were added to the reinforced-concrete tee-beam bridge for both flexure and shear. Traffic was maintained during preparation of the beams; however, the bridge was closed to traffic during bonding.

In the Russian city of Karastan, a continuous-span, reinforced-concrete bridge, which was constructed in 1912, was repaired with bonded plates (*36*). This work was completed before 1974. As a result of poor drainage, up to 25

percent of the reinforcing steel had corroded away. In negative moment regions, steel plates were bonded to the cleaned deck surface. Bolts were welded to exposed reinforcing steel in positive moment regions, and plates were then bolted and bonded to the underside of the beams. The bridge was kept open to traffic, one lane at a time, during strengthening.

By 1975, over 200 bridges on an elevated motorway in Japan had been strengthened with bonded steel plates. Thin steel plates were attached to the bottom surface of slabs by using a resin adhesive and anchor bolts (*37*). This strengthening technique was used on cracked slabs, slabs that displayed excessive spalling or scaling, slabs with insufficient thickness, and slabs with insufficient reinforcement. Both assembly techniques previously described (applying the adhesive directly to the bonding surfaces before setting or pressure injecting the adhesive after setting the plate) were utilized.

Also in 1975, a group of four reinforced-concrete slab bridges near Quinton, England, were strengthened with epoxy-bonded plates after cracks in the soffits were discovered (*38–40*). Investigations showed that inadequate tension steel had originally been provided in the cracked regions. A total of

1,376 plates, mostly 254 mm (10.0 in.) wide by 6.4 mm (0.26 in.) thick with lengths up to 3.6 m (11.8 ft), were bonded to the underside of the four bridges. In some locations, the effective thickness of the steel was increased by bonding two or three plates together. The bridges were open to normal traffic while the plates were attached and the epoxy was cured. Two additional bridges located in the United Kingdom, near Swanley, Kent, were strengthened in a similar manner in 1977. Shortly after the bridges were opened to traffic, cracks were discovered in the soffit of the beams. After it was determined that the continuous deck slabs were deficient in longitudinal steel, steel plates were epoxy bonded to the top surface as well as to the underside of the slabs.

In 1978, steel plates were epoxy bonded to the top of the concrete piers of the Shelley Bridge in Perth, Australia (41). About the time that the bridge was to be opened to traffic, shear cracks were discovered in the cantilevered portions of the piers. Plates 200 mm (7.9 in.) wide and 6 mm (0.24 in.) thick were adhesively bonded and bolted in three layers on top of each pier. Work was carried out in the winter, requiring the top of the piers to be heated to maintain a minimum temperature of 15°C (59°F) while the epoxy cured.

Two bridges over the Netekanaal in Belgium were rehabilitated in the late 1970s (24). The bridges were two of four nearly identical three-span, continuous, prestressed concrete bridges built in 1955. The rehabilitation program for the bridges included external posttensioning and epoxy-bonded steel plates. The steel plates were bonded to the undersides of the concrete stringers in the positive moment region of the center span. Additional steel plates were bonded around the webs and lower flanges of the stringers near the posttensioning anchorage beams in the end spans.

The application of adhesively bonded plates has been found to be one of the most economical and practical methods of strengthening bridges in Poland (42). Adhesively bonded plates have been used to strengthen several reinforced-concrete and prestressed-concrete bridges. In one example, flat steel strips were bonded to the upper surface of the slab bridge in the negative moment areas. Other repair work has included the bonding of flat strips to the lower surface of the concrete bridge deck, in which the strips were fastened at the ends with bolts or bonded and anchored with bolts to the side surfaces of concrete slabs.

SUMMARY

Epoxy-bonded steel plates can effectively be used to increase the live-load capacity of a concrete bridge. By adding tension reinforcement, the neutral axis of a member is lowered and the stresses in the existing reinforcement are reduced. The strengthened member acquires increased flexural stiffness, resulting in a reduction in cracking and deflection. The procedure requires careful preparation of the bonding surfaces and proper mixing and application of a suitable epoxy adhesive. The steel plates should be designed so that failure, if it occurs, is a ductile failure instead of a sudden, shear-bond failure. To meet this requirement, researchers suggest that the b/t ratio of the plate be no less than 50.

Although this strengthening technique has primarily been applied to concrete members, research related to bonding steel plates to steel members has also been undertaken. The fatigue life of bonded steel cover plates increased by a factor of 20 over that of conventionally welded cover plates.

An area needing more research is the long-term durability of the bonded connection. Significant corrosion and loss in strength have been noted in both steel-to-concrete and steel-to-steel bonded connections after they were subjected to exposure tests. Until this problem is resolved, this strengthening procedure is not recommended as a permanent solution.

ACKNOWLEDGMENT

REFERENCES

1. P. J. Moss. *Structural Uses of Epoxy Resin Adhesives.* Road Research Unit Bulletin 68. National Roads Board of New Zealand, Wellington, 1984, 159 pp.
2. A. R. Cusens and D. W. Smith. A Study of Epoxy Resin Adhesive Joints in Shear. *Structural Engineer*, Vol. 58A, No. 1, Jan. 1980, pp. 13–18.
3. G. C. Mays. Structural Applications of Adhesives in Civil Engineering. *Materials Science and Technology*, Vol. 1, Nov. 1985, pp. 937–943.
4. R. F. Mander. Use of Resins in Road and Bridge Construction and Repair. *International Journal of Cement Composites and Lightweight Concrete*, Vol. 3, No. 1, Feb. 1981, pp. 27–39.
5. R. Jones, R. N. Swamy, J. Bloxham, and A. Bouderbalah. Composite Behaviour of Concrete Beams with Epoxy Bonded External Reinforcement. *International Journal of Cement Composites and Lightweight Concrete*, Vol. 2, No. 2, May 1980, pp. 91–107.
6. M. D. Macdonald. *The Flexural Performance of 3.5 m Concrete Beams with Various Bonded External Reinforcements.* Supplementary Report 728. U.K. Transport and Road Research Laboratory, Department of the Environment, Crowthorne, Berkshire, England, 1982, 41 pp.
7. R. N. Swamy, R. Jones, and J. W. Bloxham. Structural Behaviour of Reinforced-Concrete Beams Strengthened by Epoxy-Bonded Steel Plates. *Structural Engineer*, Vol. 65A, No. 2, Feb. 1987, pp. 59–68.
8. R. N. Swamy and R. Jones. Technical Notes—Behaviour of Plated Reinforced-Concrete Beams Subjected to Cyclic Loading During Glue Hardening. *International Journal of Cement Composites*, Vol. 2, No. 4, Nov. 1980, p. 233.
9. M. D. Macdonald. Strength of Bonded Shear Joints Subjected to Movement During Cure. *International Journal of Cement Composites and Lightweight Concrete*, Vol. 3, No. 4, Nov. 1981, pp. 267–272.
10. H. Nara and D. Gasparini. *Fatigue Resistance of Adhesively Bonded Connections.* Report FHWA-OH-81-001. FHWA, U.S. Department of Transportation, Nov. 1981, 130 pp.

11. P. Albrecht, A. Sahli, D. Crute, P. Albrecht, and B. Evans. *Application of Adhesives to Steel Bridges.* Report FHWA-RD-84-037. FHWA, U.S. Department of Transportation, Nov. 1984, pp. 1–30, 106–147.

12. P. Albrecht, F. Watter, and A. Sahli. Toward Fatigue-Proofing Cover Plate Ends (W. H. Munse Symposium on Behavior of Metal Structures, Research to Practice). *Proc., ASCE*, 1983, pp. 24–44.

13. A. J. J. Calder. *Exposure Test on Externally Reinforced-Concrete Beams—First Two Years.* U.K. Transport and Road Research Laboratory, Department of the Environment, Crowthorne, Berkshire, England, 1979, pp. 19–27.

14. K. Hoigard and A. Longinow. The Effects of Hostile Environment on Adhesively Bonded Steel Bridge Connections. In *Proceedings, Third Annual International Bridge Conference*, 1986, pp. 87–92.

15. S. Kajfasz. Concrete Beams with External Reinforcement Bonded by Gluing—Preliminary Investigation. In *Proc., Symposium on Synthetic Resins in Building Construction*, Réunion Internationale des Laboratoires d'Essais et de Recherches sur les Matériaux et les Constructions (RILEM), Paris, France, Vol. 1, Sept. 1967, pp. 142–151.

16. R. L'Hermite and J. Bresson. Concrete Reinforced with Bonded Reinforcing. (Beton armé d'armatures collées.) In *Proc., Symposium on Synthetic Resins in Building Construction*, RILEM, Paris, France, Sept. 1967, pp. 175–203.

17. J. Bresson. New Research and Applications of the Utilization of Bonding in Structures—Concrete Plates. (Nouvelles recherches et applications concernant l'utilisation de collage dans les structures. Beton plaque.) *Annales de l'Institut Technique de Bâtiment et des Travaux Publics*, No. 278, Feb. 1971, pp. 22–55.

18. M. Ladner and P. Flueler. Tests of Reinforced Concrete Members with Adhesive Bonded Reinforcing. (Versuche an Stahlbeton Bauteilen mit geklebter Armierung.) *Schweizerische Bauzeitung*, Vol. 92, No. 19, May 1974, pp. 463–470.

19. C. A. K. Irwin. *The Strengthening of Concrete Beams by Bonded Steel Plates.* Supplementary Report 160 UC. U.K. Transport and Road Research Laboratory, Department of the Environment, Crowthorne, Berkshire, England, 1975, 21 pp.

20. T. Han. The Effect of Bonded Mild Steel Plates in the Strengthening and Repairing of Reinforced Concrete Beams. *Journal of I.E.M.*, Vol. 26, June/Dec. 1979, pp. 31–37.

21. R. Jones, R. N. Swamy, and T. H. Ang. Under- and Over-Reinforced Concrete Beams with Glued Steel Plates. *International Journal of Cement Composites and Lightweight Concrete*, Vol. 4, No. 1, Feb. 1982, pp. 19–32.

22. K. D. Raithby. *External Strengthening of Concrete Bridges with Bonded Steel Plates.* Supplementary Report 612. U.K. Transport and Road Research Laboratory, Department of the Environment, Crowthorne, Berkshire, England, 1980, 17 pp.

23. D. Van Gemert, J. Van Aelst, J. De Buck, and J. Van Der Mijnsbrugge. Force Transfer in Bonded Concrete-Steel Connections. (Krachtsoverdracht in Gelijmde Beton Staalverbinden.) *Tijdschrift der Openbare Werken van Belgie*, No. 6, 1980, pp. 1–13 (in Flemish).

24. J. DeBuck, T. Van Essche, D. Van Gemert, K. Gamski, R. Degeimbre, J. M. Rigo, and J. Wiertz. Conception, Computation and Test Program for the Repair of Two Prestressed Concrete Bridges. (Konceptie, Berekening en Proefprogramma voor de Herstelling van Twee Bruggen in Voorgespannen Beton.) *Tijdschrift der Openbare Werken van Belgie*, No. 2, 1981, pp. 1–35 (in Flemish and French).

25. F. S. Rostasy, E. H. Ranisch, and W. Alda. Subsequent Strengthening of Prestressed Concrete Bridges in Construction Joint Regions by Means of Bonded Steel Plates. (Nachträgliche Verstärkung von Spannbetonbrücken im Koppelfugenbereich durch geklebte Stahllaschen.) *Forschung Strassenbau und Strassenverkehrstechnik*, No. 326, 1981, pp. 95–142 (in German).

26. G. C. Mays and G. P. Tilly. Long Endurance Fatigue Performance of Bonded Structural Joints. *International Journal of Adhesion and Adhesives*, Vol. 2, No. 2, April 1982, pp. 109–114.

27. A. H. Cardon and F. Boulpaep. Adhesion Between Traditional Materials and Epoxy Resins. (Adhesion entre les matériaux traditionnels et les résines epoxy.) In *Strengthening of Building Structures—Diagnosis and Therapy*, International Association for Bridge and Structural Engineering, Zurich, Switzerland, Vol. 46, 1983, pp. 211–216 (in French).

28. R. Jones, R. N. Swamy, and F. A. R. Salman. Structural Implications of Repairing by Epoxy Bonded Steel Plates. In *Structural Faults 85: Proceedings of the 2nd International Conference on Structural Faults and Repair*, Westminster, London, England, April 30–May 2, 1985, pp. 75–80.

29. M. F. Mecklenburg, P. Albrecht, and B. M. Evans. *Screening of Structural Adhesives for Application to Steel Bridges.* FHWA, U.S. Department of Transportation, Feb. 1985, 102 pp.

30. D. A. Van Gemert and M. C. J. VandenBosch. Repair and Strengthening of Reinforced Concrete Structures by Means of Epoxy Bonded Steel Plates. Presented at International Conference on Deterioration, Bahrain, October 26–29, 1985.

31. D. F. Wiener and J. O. Jirsa. Attaching Steel Members to Reinforced Concrete Elements. In *Dynamic Response of Structures: Proceedings of the 3rd Conference Organized by the Engineering Mechanics Division*, American Society of Civil Engineers, Los Angeles, Calif., March 31–April 2, 1986, pp. 302–309.

32. Araldit Epoxy Resin for Exterior Reinforcing. (Araldit-Epoxidharze für Aussenarmierungen.) *Aspekte*, No. 2, 1979, pp. 2–6 (in German).

33. Araldit for a Bridge: Bonded Reinforcing Instead of Replacement. (Araldit für eine Brücke: Klebarmierung statt Neubau.) *Aspekte*, No. 4, 1982, pp. 2–4 (in German).

34. J. Bresson. Strengthening by Bonded Reinforcing of the Underpass on CD 126 on the Southern Autoroute. (Renforcement par collage d'armatures du passage inférieur du CD 126 sous l'autoroute du sud.) *Annales de l'Institut Technique de Bâtiment et des Travaux Publics*, No. 297, Sept. 1972, pp. 2–24.

35. J. P. Sevene. Three Examples of Repair and Strengthening Work for Structures. (Trois examples de travaux de réparation et de renforcements d'ouvrages.) *Annales de l'Institut Technique de Bâtiment et des Travaux Publics*, No. 349, April 1983, pp. 69–76.

36. Strengthening of a Reinforced-Concrete Highway Bridge in the USSR. (Verstärkung einer Stahlbeton-Strassenbrücke in den USSR.) *Schweizerische Bauzeitung*, Vol. 92, No. 16, April 1974, pp. 390–391.

37. Y. Maeda, S. Matsui, I. Shimada, and H. Kato. Deterioration and Repairing of Reinforced-Concrete Slabs of Highway Bridges in Japan. III. Inspection and Repairing of Cracked Slabs. *Technology Reports of Osaka University*, Vol. 31, No. 1599, 1981, pp. 135–144.

38. I. J. Dussek. Strengthening of Bridge Beams and Similar Structures by Means of Epoxy-Resin-Bonded External Reinforcement. In *Transportation Research Record 785*, TRB, National Research Council, Washington, D.C., 1980, pp. 21–24.

39. T. Sommerard. Swanley's Steel-Plate Patch-Up. *New Civil Engineer*, June 16, 1977, pp. 18–19.

40. K. D. Raithby and F. D. Lyndon. Lightweight Concrete in Highway Bridges. *International Journal of Cement Composites and Lightweight Concrete*, Vol. 2, No. 3, May 1981, pp. 133–146.

41. P. M. Palmer. Repair and Maintenance of Concrete Bridges with Particular Reference to the Use of Epoxies. *Australian Road Research Board, Proc.* Sept. 1979, 21 pp.

42. M. Rybak. Reinforcement of Bridges by Bonded Reinforcing. (Renforcement des ponts par collage de l'armature.) *Matériaux et Constructions*, Vol. 16, No. 91, Jan./Feb. 1983, pp. 13–17.

43. *NCHRP Report 293: Methods of Strengthening Existing Highway Bridges.* TRB, National Research Council, Washington, D.C., 1987.

Analytical Investigation for Shell Structures Utilized as Emergency Bypass Bridges

F. Fanous, D. Andrey, and F. W. Klaiber

Bridges are one of the most important elements of any country's surface transportation system. Closing a bridge always causes inconvenience to the public. Thus, a critical need exists for a "bypass" bridge that can be assembled quickly, economically, and easily at the original site or close to the bridge that is being repaired or replaced. Analytical studies indicated that integrated shell-deck segments can be used to construct short or medium-span emergency bridges. A simply supported bridge with four different shell cross sections was investigated; dead load and various patterns of live loads were considered. The analysis of these shells was performed using the ANSYS general purpose finite-element program. The results of this investigation demonstrated that shell structures can be utilized for emergency bridges.

Bridges are one of the vital segments of any country's surface transportation system. According to the latest FHWA figures, there are approximately 575,000 bridges on all highway systems in the United States. In a recent article by Galambos (1), it was noted that approximately 25 percent of these bridges are structurally deficient and 21 percent of those are functionally obsolete. Data in this article indicated that more than twice as many bridges in the non-federal-aid road system are rated deficient as compared with bridges in the federal-aid system.

In addition, several bridge failure accidents have been reported each year: during the first quarter of 1987, one bridge collapsed in the state of Pennsylvania, one bridge collapsed in the state of California, three bridges failed in the state of Missouri, and, more recently, two bridge failures occurred in the state of New York. These frequent incidents and the large number of deficient bridges obviously are of concern to the public. Even though several billions of dollars have been spent since 1982 on strengthening, repairing, or replacing some of the nation's deficient bridges, the United States still has major bridge problems.

Closing a bridge for maintenance or emergency repairs always causes costly delays and inconvenience to the traveling public. This is especially true of bridges subjected to high volumes of traffic or isolated bridges where the next available bridge is several miles away. Thus, to help alleviate or, in some instances, completely eliminate these problems, the need exists for "bypass" bridges that can be quickly, economically,

and easily constructed at the original sites or close to existing bridges that are being repaired or replaced.

Prefabricated elements and systems offer a unique solution for replacing or widening deficient bridges at a low cost. Many such elements and systems are now available. Precast, prestressed concrete units, such as prestressed beams and slabs, have been used for short-span bridges that require no intermediate supports. When longer spans are needed, these units require one or more intermediate supports; however, the construction of intermediate supports is costly and cannot be accomplished in a short period of time.

Although the previous comments obviously pertain to highway bridges, similar problems exist in the railroad industry. In some instances, the problem is even more critical in the railroad industry because of the limited number of railway lines and, thus, the limited number of possible reroutings if a bridge needs to be repaired or replaced. Thus, a critical need exists for a structural system that can be used for longer spans without intermediate supports or even for longer spans if intermediate supports are provided. The authors summarize some of the results of a research project; the primary objective of their study was to investigate using shell structures as emergency bypass bridges.

SHELL STRUCTURES FOR BRIDGES: A NEW CONCEPT

The shell structural system does not require intermediate supports and can be utilized for short or long spans (2–4). Shell structures for roof systems are classified as either short or long shells (see Figure 1a and b). The short shells offer the economy of arch action when a long but narrow area is to be covered. The long shell, that is, one in which the length of the shell is large compared with its width, structurally behaves like a beam. Circular or elliptical cross-sectional shapes are common for short or long shells. In contrast to straight structural elements (beam-and-slab systems), relatively thin shells can be used for long spans. Because of the strength and the relatively light weight of the shell elements, they are able to support relatively large live loads. The following comparison of structural systems verifies the previous statements. In the structural system shown in Figure 1c, the loads are essentially carried transversely by the slab and longitudinally by the beam. If the slab thickness is decreased to reduce the dead load of the system, transverse beams will be required. An alternative that improves the behavior and reduces the weight of

Bridge Engineering Center, Town Engineering Building, Iowa State University, Ames, Iowa 50011.
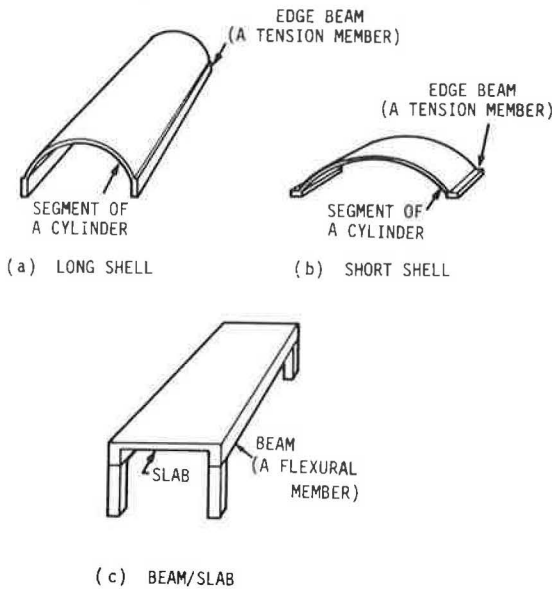
FIGURE 1 Roof systems.

the system shown in Figure 1c is to reduce moments in a transverse direction by using arch action. In the longitudinal direction, the behavior of the beam-and-slab and shell systems is also significantly different. In Figure 1c, the longitudinal beams that are composite with the slab carry the entire load. On the other hand, the entire shell system shown in Figure 1a acts as a beam with curved cross sections to carry the load.

As a result of the behavior of curved surface structures, short- or long-span bridges can be built using a shell-shaped cross section. Precast shell elements with an attached deck (Figure 2) could be transported to the bridge site and used to construct a bypass bridge. These units can be cast over a single form, an air-supporting system, or even on form work sculptured in the soil. Air-supporting systems, also known as air-bag forms, are currently being used with ease and rapidity in building inexpensive small bridges and culverts (5). This type of form needs no surface preparation or intermediate shoring and can be modified and reused to build structures of different sizes and shapes. Depending on the desired bridge span, the proposed shell-deck segments can be posttensioned together to the desired length by using external or internal tendons, or both. If rapid construction is desired, precast abutments can be positioned to support the shell bridge.
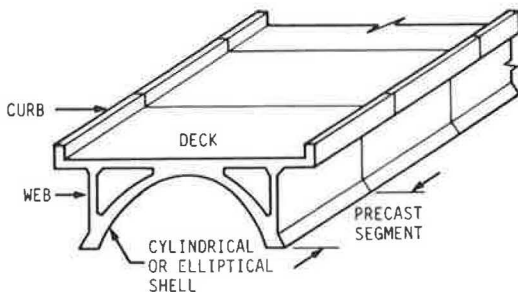

FIGURE 2 Shell structure for emergency bypass bridges.

The shell elements can also be used to construct permanent bridges. Techniques used to build precast segmental box-girder bridges can be employed to build shell-deck segmental bridges. Thus, the shell elements previously described can have dual use—in temporary "bypass" bridges, which can be disassembled and retained for future use, or in permanent bridges.

ANALYTICAL INVESTIGATION

Fifteen different cross sections that can be used in emergency bypass bridges were initially investigated. From these, four were selected for additional study. The finite-element method was used to perform the structural analysis of these sections.

Geometry of Selected Cross Sections

The four sections selected as promising candidates for emergency bypass bridges are shown in Figure 3. The cross sections shown in Figure 3a and b consist of a deck slab attached to a cylindrical shell. These cross sections can be cast in horizontal or vertical positions. In most instances, casting these sections in a vertical position can be accomplished in one pour; however, casting these sections in a horizontal position requires at least two pours.

In the first pour, the shell portion will be cast after the appropriate shell reinforcement and the reinforcement required to ensure continuity between the shell and the deck have been placed. During the curing of the shell portion, the form work and reinforcement required in the deck slab can be positioned. By reinforcing the deck slab to act compositely with the shell, the cross sections shown in Figure 3a or b are obtained. In these two cross sections, because the deck is only supported by the shell at its crown, large bending stresses are induced at this connection.

Appropriate voids can be used (Figure 3b) to remove structurally insignificant material and thus to reduce the structure's dead weight. In Figure 3c, two thin webs are used to connect the deck to the shell. These webs reduce both longitudinal and transverse stresses in the shell-deck section despite the fact that they increase the dead weight of the structure.

The cross section shown in Figure 3d is a modified version of the one in Figure 3c. In Figure 3d, longitudinal beams are used along the edges of the shell and the deck. The beams along the shell and deck are connected by using either vertical posts or inclined members. These members could be either cast in place or precast and added before the element is transported to the field. The beams along the edges of the deck function to reduce the transverse bending stresses in the deck and to serve as curbs. Posttension tendons required to assemble the shell-deck segments can be positioned internally or attached to the edge beams along the shell.

The integrated shell-deck cross sections shown in Figure 3a, c, and d were analyzed assuming a simply supported concrete segment 100 ft long and 30 ft wide. In the analysis, the deck and the shell thickness were assumed to be 8 in. and 5 in., respectively. The deck thickness is similar to that found in segmental box-girder bridges. However, the assumed shell thickness is small in comparison with the thickness of webs and bottom flanges in segmental box-girder bridges. In shell
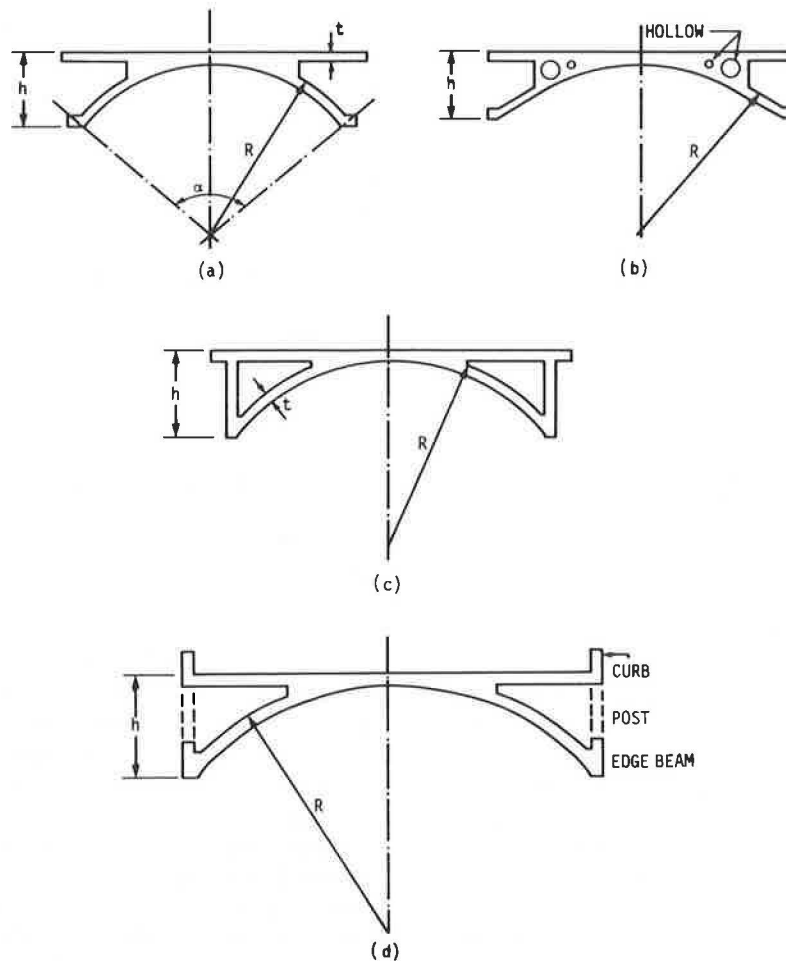
FIGURE 3 Cross sections for shell bridges.

structures, the aperture angle in Figure 3a typically ranges between 60 and 90 degrees. This limits the curvature of the shell and hence eliminates the need for double forms during horizontal casting of the shell. In this study an angle of 80 degrees was selected. For a 30-ft-wide bridge, this resulted in a shell radius of 23 ft and a height h of 6 ft 11/2 in. (see Figure 3). The width and the height of the curb beam were assumed to be 8 in. and 16 in., respectively. A square cross section of 8 in. × 8 in. was employed for the web members. As a result of symmetry (in the dead load case only), it was only necessary to model one-fourth of the bridge; symmetry boundary conditions were imposed on edges 1 to 2, 2 to 3, and 2 to 4 as shown in Figure 4.

Finite-Element Software

A general-purpose finite-element program ANSYS (6) was used to determine the dead- and live-load stresses induced in the 100-ft long, 30-ft wide simply supported concrete bridge. A concrete compressive strength of 4 ksi was assumed throughout this investigation. Several elements, such as quadrilateral, isoparametric shell, and solid elements, are available in the ANSYS program for modeling the proposed shell bridge. The cylindrical roof system given by Cook (7) was analyzed using isoparametric shell elements and solid ele-

ments to calibrate the ANSYS results and to select an element to model the shell bridge. The results of both analyses agreed with those presented by Cook (7); the difference in the results was less than 3 percent. In this study, solid elements were selected to model the shell-deck structure. This type of element was employed instead of the isoparametric shell element to ensure an adequate idealization of the connection between the shell and the deck.

Finite-Element Results

Dead Loads

The finite-element model for the bridge example with 16 inclined posts is shown in Figure 5. Dead-load stresses and displacements obtained from the finite-element analyses of the bridge example are summarized in Figures 6–9. Shown in Figures 6 and 7 are the transverse and longitudinal stresses at midspan. As expected, the largest stresses and deflections occurred in the cross section shown in Figure 3a. In an attempt to reduce the stresses and deflections in this section, the cross section in Figure 3a was reanalyzed by using a wider shell-deck connection. The maximum transverse stress was reduced by about 33 percent (see Figure 6). However, the maximum deflection was slightly increased (see Figures 8 and 9). This slight increase would be expected, because increasing the deck
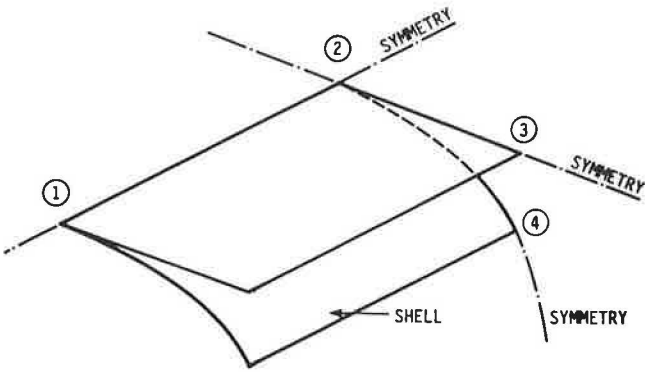
FIGURE 4   Boundary conditions for bridge.
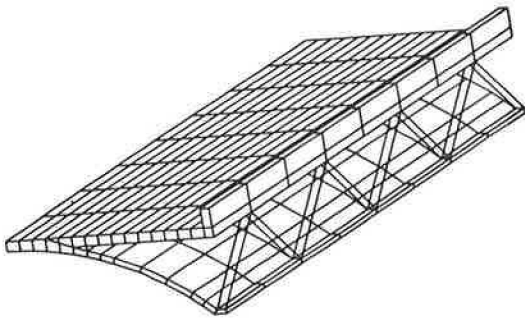
FIGURE 5   Finite-element model of shell-deck structure.
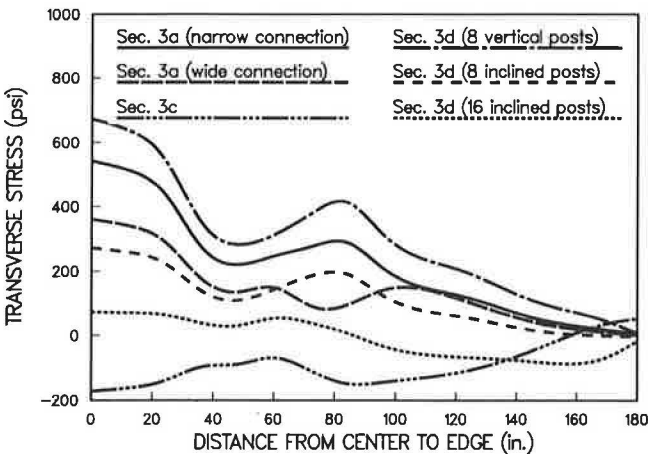
FIGURE 6   Transverse stresses across the deck (midspan).

FIGURE 7   Longitudinal stresses across the deck (midspan).

FIGURE 8   Vertical displacement across the deck (midspan).

and shell connection increases the dead weight of the section and does not significantly increase the stiffness of the cross section. Deflections obviously can be reduced by reducing the dead weight of the cross section by using appropriate voids as shown in Figure 3b. Another alternative to improve the structural behavior in Figure 3a is to use a section similar to that shown in Figure 3d. Connecting the deck to the shell by using eight diagonal members reduces the maximum transverse stress and vertical displacement by 50 and 20 percent, respectively (see Figures 6 and 8). The reduction in the transverse stress was very obvious (see Figure 6) when 16

diagonal members were used to connect the deck to the shell. Doubling the number of the diagonals also reduced the vertical displacement along the edges of the deck (see Figures 8 and 9). Using vertical posts did not improve the structural behavior of the shell deck, as may be seen in Figure 3a. Using diagonal members in conjunction with the edge beams introduces truss action along the edges of the bridge. This results in reducing deflections and stresses as shown in Figures 6–9 (compare the results of Figure 3d using vertical posts or diagonals). The cross sections with a wider shell-deck connection, 16 inclined posts, and two thin webs were selected for further investigation when the bridge is subjected to live loads.

Live Loads

The previously described bridge was reanalyzed considering truck live loads recommended by the American Association of State Highway and Transportation Officials (AASHTO) (8). Live loads as defined in the AASHTO specifications were positioned on the bridge deck as shown in Figures 10 and 11 to induce maximum longitudinal, transverse, and shear stresses. However, because of the limitations imposed by the finite-element idealization, the lane loads for the load case that induces maximum shear stresses were applied along the nodes
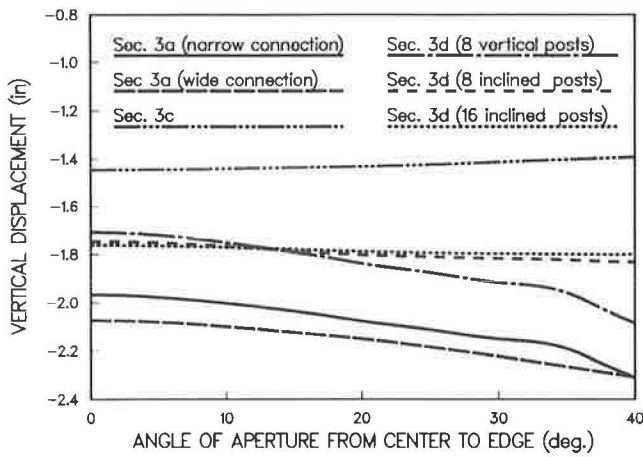
FIGURE 9   Vertical displacement across the shell (midspan).
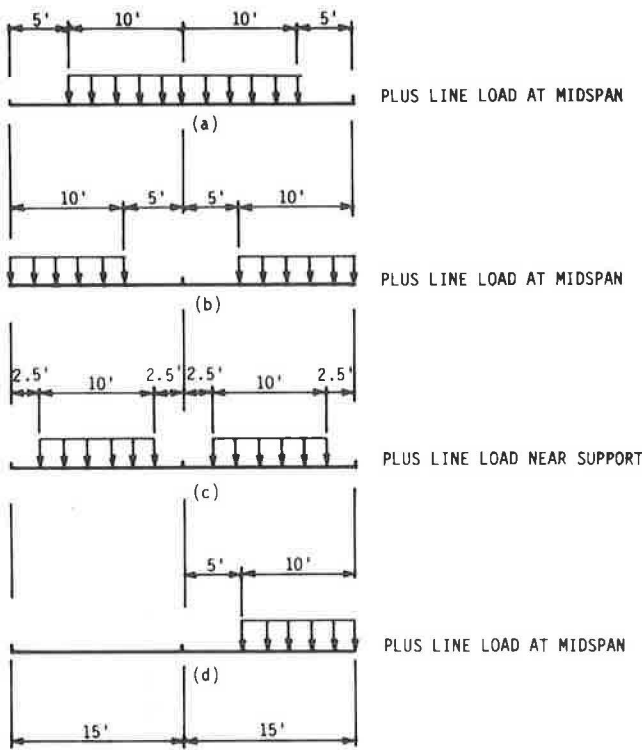
FIGURE 10   Arrangement of lane loads.

adjacent to the support and not on the nodes above the support. For the finite-element model, quarter symmetry was used when the load cases shown in Figure 10a, b, and c were analyzed. This idealization may appear incorrect for the load case that produces maximum shear stresses (see Figure 10c). However, to compensate for the errors that resulted from placing the line load near the support and not above it, equal line loads must be applied at a similar distance from the other end. These loads will induce the miscalculated fraction of the shearing force at the near support that resulted from misplacing the line loads along the location described earlier. Hence, quarter symmetry still can be used for the analysis of this particular load case. The entire bridge system was modeled for the analysis of load case 10d.
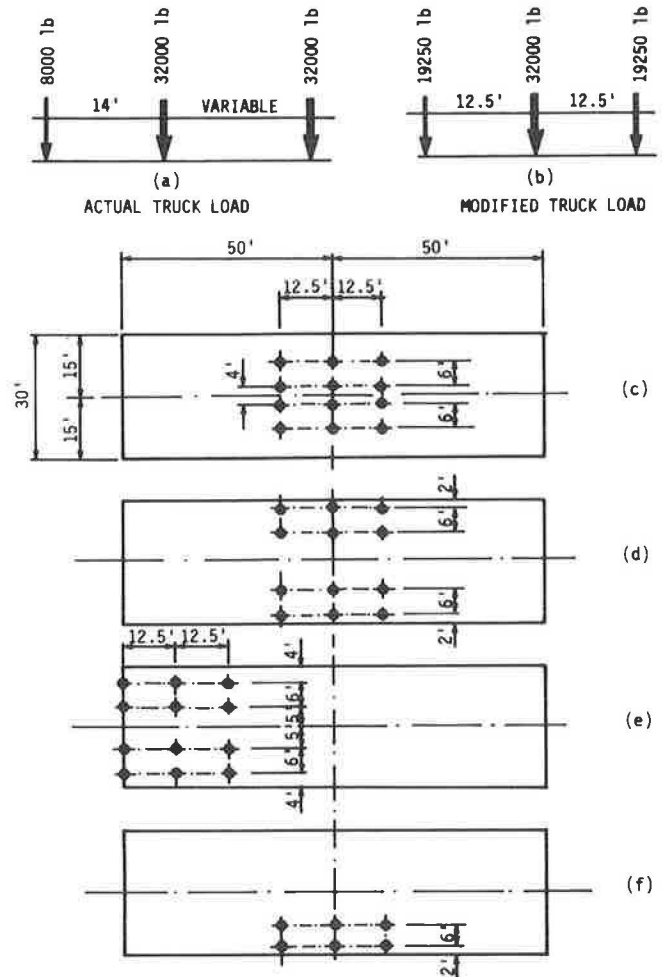
FIGURE 11   Arrangement and magnitude of truck loads.

The bridge considered herein was also reanalyzed considering AASHTO truck loading (8). Figure 11 shows the location of trucks for each of the four loading cases analyzed. Note that the loads per each axle as well as the distance between the axles are not equal (see Figure 11a), and hence one must idealize the entire structure for the finite-element analysis. However, to minimize the computation time and to make use of symmetry conditions, some modifications to the truck loading were necessary. This was accomplished using a simple beam analysis considering a modified truck load that predicts the same maximum bending stresses as the actual truck loading. The modified load obtained from this analysis is shown in Figure 11b. This load was applied to the bridge example previously described; the results were compared with those obtained from the analysis using the actual truck loading. Differences between the results obtained using the modified loading and the actual AASHTO loading were within 2 percent, and hence it was satisfactory to replace the AASHTO truck loading with the modified loading in subsequent analysis. For the reader's interest, using the modified load in conjunction with a quarter symmetry resulted in saving 50 min of CPU time on the VAX 11/780 computer. In summary, quarter symmetry was employed in the analysis of the load cases shown in Figure 11c and d, half symmetry was used to

analyze load case 11e, and the entire structure was modeled to analyze load case 11f. The actual truck loading and the assumption that the axles are 12 ft apart were employed in the analysis of the load case shown in Figure 11e.

The results of the analyses of the bridge example demonstrated that the truck-load cases yielded larger displacement and stresses than those induced by lane loads. The maximum displacement because of any of the foregoing live loadings, however, was less than that allowed by the AASHTO specifications, that is, was less than 1/800 of the span of the bridge.
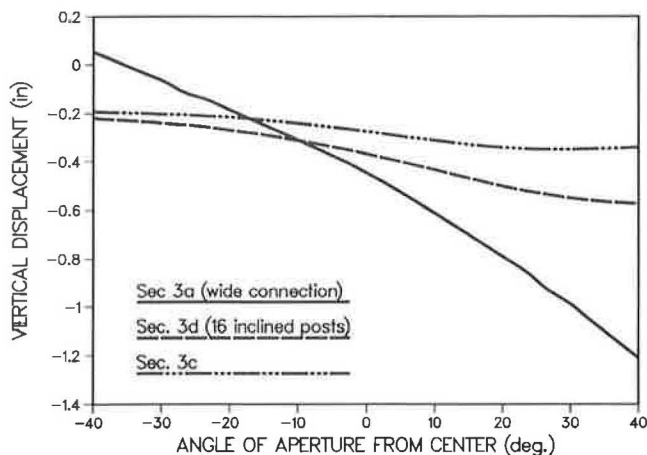
FIGURE 12   Distribution of vertical displacements caused by loads shown in Figure 11f.
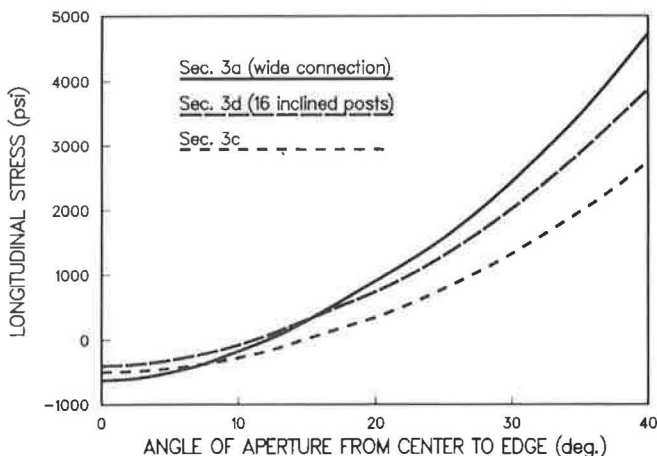
FIGURE 13   Distribution of longitudinal stresses across the bridge sections for load self-weight and loads shown in Figure 11d.

Figure 12 shows the displacement distribution across the bridge at midspan for the live load shown in Figure 11f to the three different cross sections shown in Figure 3a, c, and d. As can be seen, the cross section without webs or inclined posts to connect the deck to the shell experiences large differential displacements between the two edges. However, connecting the shell to the deck significantly increases the torsional behavior of the section.

The results of the analyses of the load cases shown in Figure 11 demonstrated that the bridge with inclined posts experiences stresses and displacements bounded by those induced in the cross sections built with and without thin webs. This is shown in Figures 12 and 13. Maximum longitudinal stress induced by applied live loads and dead loads of the structure is given in Table 1. Also listed are those stresses calculated using a flexure stress analysis. The data illustrate that the cross section without posts or thin webs experiences the largest stresses despite the fact that this section weighs less than the others. In addition, it may be noted that the heaviest cross section, that is, the one with thin webs, experiences smaller displacement and stresses (see Figures 12 and 13). Because of the similar behavior of the cross section with inclined posts and the cross section with thin webs (see Figures 12 and 13), the cross section with inclined posts was selected for additional investigation.

SUMMARY AND CONCLUSIONS

Closing a bridge for repair or maintenance always causes inconvenience to the traveling public. Shell elements with an attached deck slab for emergency bypass bridges were analytically investigated. Several cross sections that can be utilized for these types of bridges were initially studied, and a subset of four was selected for further investigation. These cross sections consist of a deck slab attached to a shell element at its crown over a wide or a narrow connection and shell-deck elements connected by either inclined truss elements or by two thin webs. The finite-element technique was employed to perform the analysis of a simply supported bridge built considering these three different shell-deck sections.

The results demonstrated that shell bridges can be used to construct short- or medium-span emergency bridges. The displacements and transverse and longitudinal stresses caused by the structure self-weight and the live loads were influenced by connecting the deck to the shell. The cross section with inclined posts connecting the deck to the shell was found to be the most appropriate section for this new bridge concept. In addition, these sections were constructed using a procedure

TABLE 1   LONGITUDINAL STRESS NEAR EDGE OF SHELL CAUSED BY SELF-WEIGHT AND TRUCK LOAD

Section	Area (in.²)	Inertia (in.⁴) × 10³	Centroidal Axis from Bottom (in.)	Weight (lb/ft)	Finite Element (psi)	Flexural Stress Analysis (psi)
Wide connection	4,935	1,382	58.55	4,969	4,700	4,705
Inclined post	5,012	1,756	58.95	5,212	3,800	3,850
Two thin webs	5,724	2,374	53.75	5,764	2,740	2,785

NOTE: See Figure 11d.

similar to that used in building small bridges and culverts utilizing air-bag forms.

ACKNOWLEDGMENT

REFERENCES

1. C. F. Galambos. Bridge Design, Maintenance and Management. *Public Roads*, Vol. 50, No. 4, March 1987.
2. D. P. Billington. *Thin Shell Concrete Structures*. McGraw-Hill, New York, 1965.
3. A. M. Hass. *Precast Concrete—Design and Applications*. Applied Science Publishers, New York, 1983.
4. S. Timoshenko and S. Woinowsky-Krieger. *Theory of Plates and Shells*. McGraw-Hill, New York, 1978.
5. *Contractor's Concrete Advantage*. Concrete Construction Institute, Addison, Ill., 1986.
6. G. J. DeSalvo and J. A. Swanson. *ANSYS Engineering Analysis System User's Manual*. Swanson Analysis System, Inc., Houston, Pa., 1985, Vols. 1 and 2.
7. R. D. Cook. *Concepts and Application of Finite Element Analysis*, 2nd ed. John Wiley & Sons, New York, 1981.
8. *Standard Specifications for Highway Bridges*, 13th ed. American Association of State Highway and Transportation Officials, Washington, D.C., 1983.

Bridge Replacement Cost Analysis

MITSURU SAITO, KUMARES C. SINHA, AND VIRGIL L. ANDERSON

As part of a study to develop a comprehensive bridge manage-
ment system for the Indiana Department of Highways, statis-
tical analyses were performed on bridge replacement costs. It
was found that unit superstructure cost can be estimated
reasonably well in terms of dollars per square foot of deck
area. However, the current practice of expressing unit sub-
structure cost in terms of dollars per square foot of deck area
only by superstructure type may not adequately account for
the difference in substructure costs caused by different sub-
structure types such as solid-stem piers and pile-bent piers.
Average unit substructure costs should be computed sepa-
rately by substructure type as well as by superstructure type.
Estimation of approach construction costs has been consid-
ered difficult and impractical because of various factors af-
fecting such costs. However, an analysis of variance (ANOVA)
can be used. Although approach costs vary significantly from
site to site, it was possible to develop cost prediction models
that would provide reasonably reliable preliminary cost esti-
mates for bridge engineers and inspectors.

As part of a study to develop a comprehensive bridge manage-
ment system for the Indiana Department of Highways (IDOH),
statistical analyses were performed on bridge replacement
costs. It was found that unit superstructure cost can be esti-
mated reasonably well in terms of dollars per square foot of
deck area by superstructure type. However, the current prac-
tice of computing unit substructure cost per square foot of
deck area only by superstructure type may not be adequate to
fully account for the difference in costs caused by different
types of substructures, such as solid-stem piers and pile-bent
piers. It was also found that approach construction costs can be
estimated fairly accurately. An ANOVA approach was used to
find mean costs and their 95 percent confidence intervals for a
group of approach-length and approach-earthwork
combinations.

Detailed descriptions and results of statistical analyses per-
formed on unit structure costs and approach construction costs
are discussed; these analyses were part of the replacement cost
analysis.

DATA BASE

Only state-owned bridges were used for this analysis. Bridges
replaced between 1980 and 1985 were selected for statistical
analyses. Two hundred seventy-nine state-owned bridges were
replaced during this period in Indiana. Currently, IDOH
groups newly designed bridges into five types: reinforced-

K. C. Sinha and V. L. Anderson, School of Civil Engineering, Purdue
University, West Lafayette, Ind. 47907. M. Saito, Institute for Trans-
portation, City College of New York, Convent Avenue at 138th Street,
New York, N.Y. 10031.

concrete box beam, reinforced-concrete slab, concrete I-beam,
steel beam, and steel girder. Because only a few box beam
bridges have been designed, they were grouped with rein-
forced-concrete slab bridges. The Bridge Design Section of
IDOH keeps all the records needed for this analysis.

Cost data used in this analysis were actual bridge contract
costs awarded to contractors and unit costs computed by
IDOH from these contract costs. Replacement costs in dif-
ferent years were adjusted to the 1985 price using the FHWA
construction price invoices (1).

Data obtained were examined for their suitability to subse-
quent analyses. It was found that some bridge construction
contracts included two bridges together. Where it was difficult
to separate costs for each bridge, such data were excluded
from the input data set. Bridges with unnecessarily high or low
costs relative to the normal range of construction costs were
also excluded. Furthermore, bridges that had no approach-road
length were considered outside the population of interest for
this study.

RESULTS OF PRELIMINARY ANALYSES

After preliminary analyses, it was found that predictions
would be practical and reliable if some cost items were
grouped. Four cost components were defined: superstructure,
substructure, approach, and "other." The "other" cost in-
cluded other structure, mobilization and demobilization, traffic
control, demolition, and miscellaneous costs, which included
construction engineering, training, and field office costs.

Table 1 shows percentage splits of these four cost compo-
nents by bridge and superstructure type. The superstructure
cost component accounted for about one-third of the total
bridge construction cost for concrete and steel beam bridges,
whereas it was about 45 percent for steel girder bridges. The
second largest cost component was the approach construction

TABLE 1 AVERAGE PERCENTAGE OF CONTRIBUTION
TO TOTAL BRIDGE COST BY FOUR COST COMPONENTS

Cost Compo-nent	Bridge Type				
	A	B	C	D	All
I	31.11	31.10	33.42	45.63	32.63
II	11.82	16.69	15.64	15.50	13.53
III	39.45	36.84	36.94	26.35	37.52
IV	17.63	15.38	14.01	12.51	16.33

NOTE: Cost components: I = superstructure; II = substructure; III =
approach; IV = other. Bridge types: A = box beam and RC slab (112
samples); B = concrete I-beam (36 samples); C = steel beam (22
samples); D = steel girder (16 samples).

cost; it accounted for about one-third of the total construction cost. The remaining one-third was split between the substructure cost and other cost.

STUDY APPROACH

ANOVA was performed to evaluate the degree of the impact of classification factors on unit costs. Three factors were used for analyses: superstructure type, substructure type, and highway type. Table 2 shows the levels of these three fixed factors

TABLE 2 CLASSIFICATION FACTORS CONSIDERED FOR UNIT STRUCTURE REPLACEMENT COST ANALYSIS

Factor	Level
Superstructure type	Box beam and RC slab
	Concrete I-beam
	Steel beam
	Steel girder
Substructure type	Solid-stem piers
	Pile-type piers
	Abutment only or arch type[a]
Highway type	Interstate[a]
	Primary
	Secondary
	Urban
	Off-system

[a]Only a few samples were available for analysis.

originally considered in the analysis. Superstructure type is the main structure type, as specified by the FHWA guide (2). Four superstructure types were considered: reinforced-concrete slab and box beam, concrete I-beam, steel beam, and steel girder.

For substructure type, three groups were used. Bridges with hammerhead piers and solid-stem piers were classified as belonging to the same group because the only difference between these two types was the cantilever portion of the hammerhead piers. Bridges with pile-type piers require far less material than those with solid-stem piers. Therefore, these bridges were grouped separately. The last group includes bridges that do not have piers: bridges supported solely by abutments and arch bridges.

Highway type was considered to determine whether functional highway classification, such as Interstate or primary, would affect the construction cost of superstructures. FHWA requires the state to provide separate unit costs for different highway types, such as those listed in Table 2.

RESULTS OF ANALYSIS OF VARIANCE

Unit Structure Costs

Unit structure costs were divided into three groups: superstructure, substructure, and total structure costs. FHWA requires the state to report these unit costs by superstructure and highway types. One major objective was to examine whether these factors would substantially affect the estimation of unit structure costs.

Unit Superstructure Cost

Because the model used for the ANOVA on unit superstructure cost had unequal cell frequencies, the MANOVA procedure of the SPSS package was used (3). A model of four superstructure types and five highway types was originally designed.

However, it was found that only a few bridges were replaced on Interstate highways and urban federal-aid highways. Therefore, these two highway types were excluded from the analysis. Among the remaining three highway types, however, bridges on off-system highways caused a significant heterogeneity of variance in this model. As shown in Figure 1, standard deviations of unit costs of bridges on primary and secondary highways appeared to be fairly constant at different levels of mean values. However, the standard deviation of unit costs of bridges on the off-system state highways showed substantial differences at various levels of mean values, causing the heterogeneity of variances for this three-level model. The existence of heterogeneous variances among the cells violates one of the basic assumptions of the ANOVA.

It was not possible to reduce this large variance by commonly used transformations of raw data values. Because of the persistent disturbance of homogeneity of variances created by unit costs of bridges on the off-system state highways and the relatively few bridges replaced on this highway system, it was decided that off-system bridges be excluded from the analysis and the number of levels for highway types be reduced to two, primary and secondary highways. Strictly speaking, therefore, the inference drawn from this analysis can be made only for these two highway types. Unit structure costs of bridges on Interstate, urban, federal-aid, and off-system highways need to be analyzed after an adequate number of bridges have been replaced on these systems.

Consequently, the reduced ANOVA model performed was

$$C_{ijk} = \mu + H_i + S_j + HS_{ij} + \varepsilon_{(ij)k}$$

where

$$
\begin{aligned}
C_{ijk} &= \text{unit superstructure cost,} \\
\mu &= \text{the grand mean,} \\
H_i &= \text{highway type,} \\
S_j &= \text{bridge type,} \\
HS_{ij} &= \text{interaction of highway type by} \\
&\quad \text{superstructure type, and} \\
\varepsilon_{(ij)k} &= \text{error term.}
\end{aligned}
$$

The k subscript on the error term was included to emphasize replication of unit cost samples. Both classification factors were treated as fixed factors. With the reduced model, the Cochran C-test statistic was 0.227 and the homogeneity of variance was accepted at $\alpha = 0.03$. Anderson and McLean (4) state that if the homogeneity test is accepted at $\alpha = 0.01$, there is no need to transform the data. Therefore, no data transformation was performed, and the ANOVA was conducted on the raw data.

Because of the sequential sum-of-squares method used by the MANOVA procedure (3), the result of the ANOVA is affected by the order in which the two main factors, superstructure type and highway type, are introduced into the model. The sums of squares for each factor effect are adjusted for all effects previously entered into the model (3). Therefore, two runs were made, one with the superstructure type as the first entry and the other with the highway type as the first entry. Table 3 is one of these ANOVA tables resulting from the reduced model. It was found that in both cases effects of highway type and the interaction of two factors on the mean
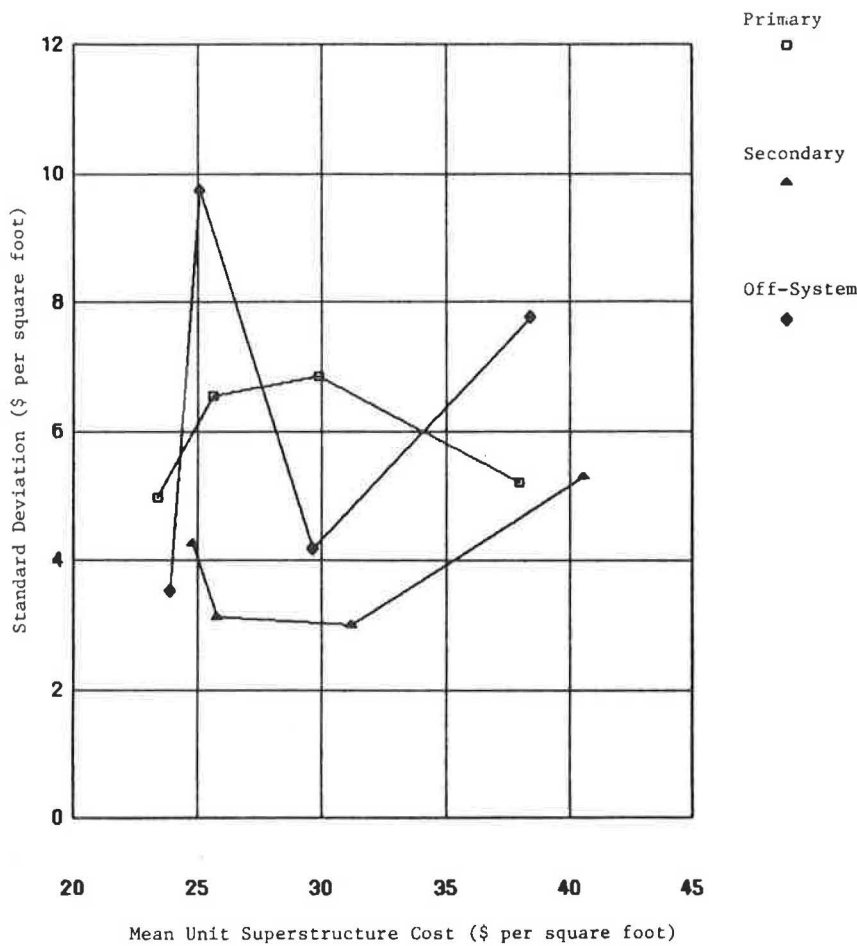
FIGURE 1 Mean versus standard deviation of unit superstructure cost.

TABLE 3 ANOVA FOR HIGHWAY TYPE BY SUPERSTRUCTURE TYPE ON UNIT SUPERSTRUCTURE COSTS

Source of Variation	Sum of Squares	Degrees of Freedom	Mean Square	F-Value	Significance of F
Within cells (error term)	4,554.65	190	23.97		
Constant	141,876.18	1	141,876.18	5,918.45	0^a
HWYTP	11.81	1	11.81	0.49	0.484^b
SUPTP	2,716.48	3	905.49	37.77	0^a
HWYTP by SUPTP	25.49	3	8.5	0.35	0.786^b

NOTE: Cochran C-statistic = 0.227; probability = 0.030 (approximately); SUPTP = superstructure type (main effect); HWYTP = highway system type (main effect); SUPTP by HWYTP = interaction effects of highway type by superstructure type.

[a]Significant at the 0.05 level.
[b]Not significant at the 0.05 level.

unit costs were not significant at a 5 percent level. Therefore, with available data, it was concluded that as far as unit superstructure cost is concerned, the only major factor affecting mean cost values was superstructure type. Table 4 shows the mean unit costs, standard errors of the mean (SE), and the upper limit (UL) and lower limit (LL) of the 95 percent confidence intervals. This table shows that only a small difference exists between the mean unit costs and the 95 percent confidence intervals of the two highway types.

Unit Substructure Cost

Unit substructure costs are currently expressed in dollars per square foot of deck area and classified by highway and super-

structure type. Considering the diverse factors affecting substructure constructions, such as the location of the foundation and the substructure type, it may be too simplistic to classify unit costs only by superstructure type for accurately estimating actual substructure cost. An ANOVA was therefore performed on unit substructure costs using the superstructure type and the substructure type as the main effects to examine whether the substructure type should be considered to compute unit substructure costs. The substructure type was selected because it was the next logical choice for factoring unit substructure costs. Effects of highway class were assumed to be small judging from the results of analyses on unit superstructure costs.

TABLE 4   TWO-WAY ANOVA DESIGN FOR UNIT SUPERSTRUCTURE COST ANALYSIS

| Highway Type | Superstructure Type | | | |
	Box Beam and RC Slab	Concrete I-Beam	Steel Beam	Steel Girder
Primary				
N	47	23	14	10
Mean	25.62	23.40	29.90	37.94
SE	0.71	1.02	1.31	1.55
LL	24.23	21.40	27.33	34.90
UL	27.01	25.40	32.47	40.98
Secondary				
N	72	21	7	4
Mean	25.81	24.81	31.19	40.58
SE	0.58	1.07	1.85	2.45
LL	24.67	22.71	27.56	35.78
UL	26.95	26.91	34.82	45.38

NOTE: N = number of samples; mean = mean unit superstructure cost ($/ft^2 of deck area); SE = standard error of the mean; LL = lower limit of 95 percent confidence interval; UL = upper limit of 95 percent confidence interval.

Table 5 shows the model considered in this analysis along with mean unit costs, standard errors of the mean, and 95 percent confidence intervals. Two substructure types were used—solid-stem piers and pile-type piers. The third type, bridges with only abutments or arch support, was excluded from this analysis because only a few samples were found in this group.

Table 6 is the ANOVA table for the model considered. The Cochran C-test statistic was 0.225 and the homogeneity test was accepted at $\alpha = 0.05$. Therefore, there was no need for data transformation. It was found that the interaction of the two main effects was significant at the 5 percent level as well as the main effects, as shown in Table 6. The unit substructure costs for the different superstructure and substructure combinations indicated that superstructure type had less effect on unit substructure cost for the bridges with solid-stem type piers than for the bridges with pile-type piers. This differential

influence of superstructure type, which depends on the type of substructure, implies that the superstructure and substructure factors interact in their effect on unit substructure costs. Thus, one should not ordinarily discuss the effects of each factor separately in terms of the factor-level means.

Generally, pile-type substructures are expected to cost less. This trend was found for superstructures made of reinforced concrete. However, for steel-beam bridges, pile-type substructures became more expensive than solid-stem piers. The result therefore did not substantiate the expected trend. The small number of samples for this type might have affected the result. However, from these analyses, it can be concluded that the substructure type does affect the unit substructure cost in terms of dollars per square foot of deck area and that adding the substructure grouping should help improve the accuracy of estimated substructure costs.

Unit Total Structure Cost

Unit total structure cost is simply the sum of unit superstructure cost and unit substructure cost. In the previous section, the effect of substructure type on unit substructure costs was discussed. Whether this effect still remains in unit total structure costs was tested because the effect of substructure type might be reduced when added to unit superstructure costs. The same model used for the unit substructure cost analysis was used by replacing unit substructure costs with unit total structure costs.

Table 7 gives the ANOVA results. The homogeneity test was accepted at $\alpha = 0.001$. Anderson and McLean suggested that if the test is accepted between $\alpha = 0.01$ and 0.001, transformation is not needed unless there is a practical reason to transform (4). A histogram of raw data was plotted and it was found that total unit structure cost data were normally distributed. Raw data were transformed by common logarithm to see whether the scattering of data points was normally distributed. Two histograms showed basically the same shape and it was concluded that transformation of raw data was not required.

TABLE 5   TWO-WAY ANOVA DESIGN FOR UNIT SUBSTRUCTURE COST ANALYSIS

| Substructure Type | Superstructure Type | | | |
	Box Beam and RC Slab	Concrete I-Beam	Steel Beam	Steel Girder
Solid-stem piers				
N	27	30	13	13
Mean	13.60	14.19	14.29	12.88
SE	0.98	0.93	1.41	1.41
LL	11.68	12.37	11.53	10.12
UL	15.52	16.01	17.05	15.64
Pile-type piers				
N	91	7	7	
Mean	8.30	11.34	19.07	No sample available
SE	0.53	1.92	1.92	
LL	7.26	7.58	15.31	
UL	9.34	15.10	22.83	

NOTE: N = number of samples; mean = mean unit substructure cost ($/ft^2 of deck area); SE = standard error of the mean; LL = lower limit of 95 percent confidence interval; UL = upper limit of 95 percent confidence interval.

TABLE 6   ANOVA FOR SUPERSTRUCTURE TYPE BY SUBSTRUCTURE TYPE ON UNIT SUBSTRUCTURE COSTS

Source of Variation	Sum of Squares	Degrees of Freedom	Mean Square	F-Value	Significance of F
Within cells (error term)	4,669.91	181	25.80		
Constant	23,770.58	1	23,770.58	921.32	0
SUPTP	1,050.88	3	350.29	13.58	0[a]
SUBTP	354.38	1	354.38	13.74	0.0003[a]
SUPTP by SUBTP	381.55	2	190.77	7.39	0.001[a]

NOTE: Cochran C-statistic = 0.225; probability = 0.124 (approximately); SUPTP = superstructure type (main effect); SUBTP = substructure type (main effect); SUPTP by SUBTP = interaction effects of superstructure type by substructure type.

[a]Significant at the 0.05 level.

TABLE 7   ANOVA FOR SUPERSTRUCTURE TYPE BY SUBSTRUCTURE TYPE ON UNIT TOTAL STRUCTURE COSTS

Source of Variation	Sum of Squares	Degrees of Freedom	Mean Square	F-Value	Significance of F
Within cells (error term)	8,888.17	181	49.11		
Constant	272,007.30	1	272,007.30	5,539.20	0
SUPTP	4,577.20	3	1,525.73	31.07	0[a]
SUBTP	312.00	1	312.00	6.35	0.013[a]
SUPTP by SUBTP	218.08	2	109.04	2.22	0.112[b]

NOTE: Cochran C-statistic = 0.296; probability = 0.001 (approximately); SUPTP = superstructure type (main effect); SUBTP = substructure type (main effect); SUPTP by SUBTP = interaction effects of superstructure type by substructure type.

[a]Significant at the 0.05 level.
[b]Not significant at the 0.05 level.

The interaction was dramatically reduced and it became not significant at a 5 percent level (α = 0.112 with raw data). However, two main effects were still significant at a 5 percent level. From this analysis it can be said that the substructure type does affect unit total structure costs as well as does the superstructure type. Therefore, it will be better to compute total superstructure costs separately for the two substructure groups to better estimate replacement costs.

Approach Construction Cost

Approach construction costs for new bridges are difficult to estimate because of many factors affecting the construction of approach roads. Because of this diversity of site-specific factors, approach costs are often estimated as a lump-sum value relative to structure costs. However, at the state level of bridge management, prediction of approach costs is an important element because it would account for a substantial portion of the total construction cost once approach roads are needed. Approach length and amount of earthwork were selected as two classification factors. Approach length was defined as the length of the project after the bridge structure length has been subtracted. The earthwork was the sum of common excavation, borrow, and excavation for subgrade treatment.

Histograms of approach length and earthwork were plotted and samples were classified into three groups, each consisting of approximately one-third of the entire data set. Approach length was divided into three groups—short, medium, and long—whereas earthwork was divided into three levels—short, medium, and large. Ranges for these groups are as follows: (a) Approach length (L): short, 0 ft < L ≤ 500 ft; medium, 500 ft < L ≤ 1,000 ft; long, 1,000 ft < L ≤ 5,280 ft. (b) Approach earthwork (E): short, 0 yd^3 < E ≤ 2,000 yd^3 < E ≤

2,000 yd^3; medium, 2,000 yd^3 < E ≤ 8,000 yd^3; large, 8,000 yd^3 < E ≤ 50,000 yd^3.

Table 8 shows the ANOVA model used for this analysis. Although each cell did not have an equal sample size, each row and column had approximately one-third of the entire sample.

The homogeneity test was rejected at α = 0.001 for raw data and the transformation was made by using common logarithm (log 10). With the transformed data, the Cochran C-statistic was 0.208 and the homogeneity of variance was

TABLE 8   TWO-WAY ANOVA DESIGN FOR APPROACH COST ANALYSIS

Approach Length	Amount of Earthwork		
	Small	Medium	Large
Short			
N	47	15	3
Mean	80.1	121.1	179.8
LL	70.1	95.5	105.5
UL	91.6	153.7	306.2
Medium			
N	13	40	21
Mean	121.0	158.4	268.9
LL	93.7	136.9	219.9
UL	156.2	183.3	328.9
Long			
N	_[a]	7	46
Mean	—	257.8	330.7
LL	—	181.9	288.7
UL	—	365.4	378.8

NOTE: N = number of samples; mean = mean approach construction cost (in $1,000); LL = lower limit of 95 percent confidence interval; UL = upper limit of 95 percent confidence interval.

[a]No sample available.

TABLE 9 ANOVA FOR APPROACH LENGTH AND AMOUNT OF EARTHWORK ON APPROACH CONSTRUCTION COSTS

Source of Variation	Sum of Squares	Degrees of Freedom	Mean Square	F-Value	Significance of F
Within cells (error term)	7.698	184	0.0418		
Constant	946.677	1	946.677	22,626.59	0
LENGTH	8.705	2	4.353	104.03	0[a]
EARTH	1.773	2	0.887	21.19	0[a]
LENGTH by EARTH	0.0076	3	0.025	0.60	0.614[b]

NOTE: Cochran C-statistic = 0.208; probability = 0.110 (approximately); LENGTH = approach length (main effect); EARTH = amount of earthwork (main effect); LENGTH by EARTH = interaction effects of approach length by the amount of earthwork.

[a]Significant at the 0.05 level.
[b]Not significant at the 0.05 level.

accepted at $\alpha = 0.05$. The ANOVA model performed on approach construction costs was

$$\log_{10} A_{ijk} = \mu + L_i + E_j + LE_{ij} + \varepsilon_{(ij)k}$$

where

A_{ijk}	=	actual approach construction cost,
μ	=	the grand mean,
L_i	=	approach length,
E_j	=	amount of earthwork,
LE_{ij}	=	interaction of approach length by amount of earthwork, and
$\varepsilon_{(ij)k}$	=	the error term.

Two main factors were treated as fixed effects. Table 9 shows the ANOVA table for this model. It was found that the interaction of two factors was not significant (P-value = 0.614). Two main effects were, however, significant at a 5 percent level. This implied that two factors, approach length and approach earthwork, can be used as grouping factors for estimating approach construction costs.

Table 8 also shows 95 percent confidence intervals of the cell means. The measurement unit of cost is $1,000 in this table. It is shown that the cells in the diagonal position provide the best estimates. Cells with a small sample size had wider confidence intervals. Although this linguistic grouping approach was somewhat coarse, results appeared to be promising for making initial estimates of approach construction costs.

SUMMARY AND CONCLUSION

Results of statistical analyses on costs of bridge superstructure, substructure, and approach construction, which can be used to make initial cost estimates, have been discussed in this paper. Unit structure costs are often used to estimate total structure costs. FHWA requires the state to submit unit structure costs by highway system type and by superstructure type. The replacement cost analysis tested whether this classification could be adequate to account for variations in unit costs caused by the site-specific nature of bridge construction.

As for superstructure construction costs, the analysis was conducted only for primary and secondary highway systems. The difference in the mean unit costs for these two types of highway systems was not statistically significant. Adequate samples were not available for other highway systems, that is, Interstate, urban highway, and off-system roads.

Currently, substructure type is not used to categorize unit structure costs. However, it was found that substructure type significantly affects unit substructure and unit total structure costs. In this analysis, costs were considered in terms of two substructure types: with solid-stem piers and pile-type piers. This simple two-type grouping considerably improves the accuracy of estimates of substructure construction costs.

The analysis conducted on approach construction costs showed that the prediction of approach costs could be improved by grouping such costs in terms of approach length and amount of earthwork. For instance, the mean approach cost of a short approach with a small amount of earthwork was $80,000 and its confidence interval was $20,000. As the approach road becomes longer and the amount of earthwork becomes large, the confidence interval increases, indicating that there was more variation in such large construction.

In this paper the emphasis is on the use of statistical principles to assess the accuracy of unit bridge costs to be used for estimating future bridge construction costs. Often, average values are used as representative costs of that group, but unless the deviation of costs is known, one is not sure about their precision. Standard errors of the mean and 95 percent confidence intervals of the mean unit costs should help engineers and inspectors understand how much variability might be expected when average values are used.

REFERENCES

1. *Value of New Construction Put in Place.* Construction Report C30-86-3. Bureau of the Census, U.S. Department of Commerce, June–Oct. 1986.
2. *Recording and Coding Guide for the Structure Inventory and Appraisal of the Nation's Bridges.* FHWA, U.S. Department of Transportation, Jan. 1979.
3. C. H. Hull and N. H. Nie, eds. *SPSS Update 7-9: New Procedures and Facilities for Release 7-9.* McGraw-Hill, New York, 1981.
4. V. L. Anderson and R. A. McLean. *Design of Experiments: A Realistic Approach.* Marcel Dekker, Inc., New York, 1974.

Bridge Performance Prediction Model Using the Markov Chain

Yi Jiang, Mitsuru Saito, and Kumares C. Sinha

As part of a study to develop a comprehensive bridge management system for the Indiana Department of Highways (IDOH), a bridge performance prediction model using the Markov chain was developed. The model can be used to predict the percentages of bridges with different condition ratings as well as to develop performance curves of bridges. The Markov chain, a probability-based method, was used in the model to reflect the stochastic nature of bridge conditions. The study exhibited the power of the Markov chain approach in prediction or estimation of future bridge conditions. The procedure, although simple, was found to provide a high level of accuracy in predicting bridge conditions.

A major objective of a bridge management system is to assist bridge managers in making consistent and cost-effective decisions related to maintenance and rehabilitation of bridges. The decision making, either at the network level or at the project level, is based on current and future bridge conditions. Therefore, it is essential for a bridge management system to be capable of accurately predicting future bridge conditions.

A bridge performance model was developed for a bridge management system for the Indiana Department of Highways (IDOH). The model was developed using the Markov chain for predicting future bridge conditions. Predictions can be made for the condition rating of bridges and for the percentage of bridges at different condition ratings, both of which are important for a bridge management system.

Knowing the percentage of bridges at different condition ratings at present, a bridge manager may wish to know the percentage distribution in the future. Also, knowing the present condition rating of a bridge, he may want to predict the condition rating of the bridge in a given year. This model provides a tool for these predictions. To use the model, one simply has to input the present percentage distribution of bridge conditions or the present condition rating of a bridge.

This paper presents a brief introduction to the concept and use of the Markov chain approach. The development of transition matrices is also discussed. Their applications to the development of a bridge performance model are explained through examples.

DATA BASE

The complete data base included about 5,700 state-owned bridges in Indiana. A sample data set was selected from

Y. Jiang and K. C. Sinha, School of Civil Engineering, Purdue University, West Lafayette, Ind. 47907. M. Saito, Institute for Transportation, City College of New York, Convent Avenue at 138th Street, New York, N.Y. 10031.

bridges on State Roads 1, 2, 3, 4, 14, 16, 46, and 57. To evaluate the effects of bridge type and climate on bridge performance, structures were divided into steel and concrete bridges, and bridges in northern and southern regions were studied separately. The sample data set consisted of 170 concrete bridges and 106 steel bridges.

MARKOV CHAIN APPROACH

The Markov chain as applied to bridge performance prediction is based on the concept of defining states in terms of bridge condition ratings and obtaining the probabilities of bridge condition transition from one state to another. These probabilities are represented in a matrix form that is called the transition probability matrix, or simply transition matrix, of the Markov chain. If the present or the initial state of the bridges is known, the future condition can be predicted through multiplication of the initial-state vector and the transition probability matrix.

Using the FHWA bridge-rating system, bridge inspectors employ a range from 0 to 9, with 9 being the maximum rating number for near-perfect condition [1]. Ten bridge condition ratings are defined as 10 states, with each condition rating corresponding to one of these 10 states. For example, condition rating 9 is defined as State 1, rating 8 as State 2, and so on. Without repair or rehabilitation, the bridge condition rating decreases as the bridge age increases. Therefore, there is a probability that the condition will make a transition from one state, say i, to another state, j, during a given period of time, which is denoted $P_{i,j}$. Table 1 shows the correspondence of condition ratings, states, and transition probabilities.

Let the transition probability matrix of the Markov chain be P, given by

$$
P = \begin{vmatrix}
P_{1,1} & P_{1,2} & \cdots & P_{1,10} \\
P_{2,1} & P_{2,2} & \cdots & P_{2,10} \\
\cdot & \cdot & \cdots & \cdot \\
\cdot & \cdot & \cdots & \cdot \\
\cdot & \cdot & \cdots & \cdot \\
P_{10,1} & P_{10,2} & \cdots & P_{10,10}
\end{vmatrix}
\qquad (1)
$$

Then the state vector for any time T, $P^{(T)}$, can be obtained

TABLE 1 CORRESPONDENCE OF CONDITION RATINGS, STATES, AND TRANSITION PROBABILITIES

		R=9	R=8	R=7	R=6	R=5	R=4	R=3	R=2	R=1	R=0
		S=1	S=2	S=3	S=4	S=5	S=6	S=7	S=8	S=9	S=10
R=9	S=1	$P_{1,1}$	$P_{1,2}$	$P_{1,3}$	$P_{1,4}$	$P_{1,5}$	$P_{1,6}$	$P_{1,7}$	$P_{1,8}$	$P_{1,9}$	$P_{1,10}$
R=8	S=2	$P_{2,1}$	$P_{2,2}$	$P_{2,3}$	$P_{2,4}$	$P_{2,5}$	$P_{2,6}$	$P_{2,7}$	$P_{2,8}$	$P_{2,9}$	$P_{2,10}$
R=7	S=3	$P_{3,1}$	$P_{3,2}$	$P_{3,3}$	$P_{3,4}$	$P_{3,5}$	$P_{3,6}$	$P_{3,7}$	$P_{3,8}$	$P_{3,9}$	$P_{3,10}$
R=6	S=4	$P_{4,1}$	$P_{4,2}$	$P_{4,3}$	$P_{4,4}$	$P_{4,5}$	$P_{4,6}$	$P_{4,7}$	$P_{4,8}$	$P_{4,9}$	$P_{4,10}$
R=5	S=5	$P_{5,1}$	$P_{5,2}$	$P_{5,3}$	$P_{5,4}$	$P_{5,5}$	$P_{5,6}$	$P_{5,7}$	$P_{5,8}$	$P_{5,9}$	$P_{5,10}$
R=4	S=6	$P_{6,1}$	$P_{6,2}$	$P_{6,3}$	$P_{6,4}$	$P_{6,5}$	$P_{6,6}$	$P_{6,7}$	$P_{6,8}$	$P_{6,9}$	$P_{6,10}$
R=3	S=7	$P_{7,1}$	$P_{7,2}$	$P_{7,3}$	$P_{7,4}$	$P_{7,5}$	$P_{7,6}$	$P_{7,7}$	$P_{7,8}$	$P_{7,9}$	$P_{7,10}$
R=2	S=8	$P_{8,1}$	$P_{8,2}$	$P_{8,3}$	$P_{8,4}$	$P_{8,5}$	$P_{8,6}$	$P_{8,7}$	$P_{8,8}$	$P_{8,9}$	$P_{8,10}$
R=1	S=9	$P_{9,1}$	$P_{9,2}$	$P_{9,3}$	$P_{9,4}$	$P_{9,5}$	$P_{9,6}$	$P_{9,7}$	$P_{9,8}$	$P_{9,9}$	$P_{9,10}$
R=0	S=10	$P_{10,1}$	$P_{10,2}$	$P_{10,3}$	$P_{10,4}$	$P_{10,5}$	$P_{10,6}$	$P_{10,7}$	$P_{10,8}$	$P_{10,9}$	$P_{10,10}$

Note: R = Condition Rating

S = State

$P_{i,j}$ = Transition Probability from State i to State j

by the multiplication of the initial-state vector $P^{(0)}$ and the transition probability matrix P:

$$P^{(T)} = P^{(0)} * P * P \dots * P = P^{(0)} * P^T \qquad (2)$$

Thus, a Markov chain is completely specified when its transition matrix P and the initial-state vector $P^{(0)}$ are known. Because the initial-state vector $P^{(0)}$ is usually known for a bridge management system, the main problem of the Markov chain approach in this study is to determine the transition probability matrix.

TRANSITION PROBABILITY MATRIX

Since 1978 all federally supported bridges have been inspected every 2 years. The inspection includes ratings of individual components such as deck, superstructure, and substructure as well as of the overall bridge condition. Unless rehabilitation or repair is applied, bridge structures deteriorate gradually so that the bridge condition ratings either are unchanged or change to a lower number in the 2-year rating period. That is, a bridge condition rating should monotonically decrease as the bridge age increases. Therefore, the probability $P_{i,j}$ is null for $i > j$, where i and j represent the states in the Markov chain.

For the purpose of management, two kinds of predictions need to be performed: (a) the percentage of bridges with a particular condition rating at any given time and (b) the bridge conditions at different bridge ages.

Percentage of Bridges with a Particular Condition Rating

From the data base, the number of bridge-condition transitions from one state to another state was obtained. Let $n_{i,j}$ denote the number of transitions from State i to State j within the time period; then the number of bridges in State i before the transition can be defined as

$$n_i = \sum_j n_{i,j} \qquad (3)$$

It can be proved (2) that the estimated transition probability is

$$\hat{P}_{i,j} = \frac{n_{i,j}}{n_i} \qquad (4)$$

Consequently, the transition matrix is determined and the prediction can be performed by using Equation 2.

As an example, the transition matrix for deck conditions of concrete bridges in northern Indiana was obtained by this method. Because bridges are inspected every 2 years, a 2-year transition period was used; that is, $p_{i,j}$ was the probability of transition from State i to State j in a 2-year period. The numerical results of n_i, $n_{i,j}$, and the corresponding transition matrix are given in Tables 2 and 3.

Bridge Conditions at Different Bridge Ages

To develop a bridge performance curve, it is necessary to predict bridge conditions at different ages. The transition

TABLE 2 NUMBER OF STATE TRANSITIONS OF DECK CONDITION FOR CONCRETE BRIDGES

state	$n_{i,1}$	$n_{i,2}$	$n_{i,3}$	$n_{i,4}$	$n_{i,5}$	$n_{i,6}$	$n_{i,7}$	$n_{i,8}$	$n_{i,9}$	$n_{i,10}$	Σ
i=1	1	6	5	2	0	0	0	0	0	0	$n_1=14$
i=2	0	20	51	12	2	6	0	0	0	0	$n_2=91$
i=3	0	0	114	36	9	4	0	0	0	0	$n_3=163$
i=4	0	0	0	45	12	0	3	0	0	0	$n_4=60$
i=5	0	0	0	0	18	7	1	0	0	0	$n_5=26$
i=6	0	0	0	0	0	18	2	1	0	0	$n_6=21$
i=7	0	0	0	0	0	0	5	0	0	0	$n_7=5$
i=8	0	0	0	0	0	0	0	1	0	0	$n_8=1$
i=9	0	0	0	0	0	0	0	0	0	0	$n_9=0$
i=10	0	0	0	0	0	0	0	0	0	0	$n_{10}=0$

Note: The sample data were randomly chosen from the concrete bridge condition data from nothern Indiana.

TABLE 3 TRANSITION PROBABILITY MATRIX OF CONCRETE DECK CONDITION IN NORTHERN INDIANA

state	$P_{i,1}$	$P_{i,2}$	$P_{i,3}$	$P_{i,4}$	$P_{i,5}$	$P_{i,6}$	$P_{i,7}$	$P_{i,8}$	$P_{i,9}$	$P_{i,10}$
i=1	0.071	0.429	0.357	0.143	0.000	0.000	0.000	0.000	0.000	0.000
i=2	0.000	0.220	0.560	0.132	0.022	0.066	0.000	0.000	0.000	0.000
i=3	0.000	0.000	0.699	0.211	0.055	0.025	0.000	0.000	0.000	0.000
i=4	0.000	0.000	0.000	0.750	0.200	0.000	0.050	0.000	0.000	0.000
i=5	0.000	0.000	0.000	0.000	0.692	0.269	0.038	0.000	0.000	0.000
i=6	0.000	0.000	0.000	0.000	0.000	0.857	0.095	0.048	0.000	0.000
i=7	0.000	0.000	0.000	0.000	0.000	0.000	1.000	0.000	0.000	0.000
i=8	0.000	0.000	0.000	0.000	0.000	0.000	0.000	1.000	0.000	0.000
i=9	0.000	0.000	0.000	0.000	0.000	0.000	0.000	0.000	0.000	0.000
i=10	0.000	0.000	0.000	0.000	0.000	0.000	0.000	0.000	0.000	0.000

matrix used in this case is different from that in percentage prediction, which gives the proportion of bridges with a particular condition rating in a given year. Bridges with different ages may have the same condition ratings. However, a performance curve provides a direct relationship between bridge condition and bridge age.

The transition matrix presented in Table 3 cannot be used to develop bridge performance curves, because this matrix is independent of bridge age; in other words, it is not homogeneous with respect to bridge age. However, a Markov chain requires the homogeneity of a transition matrix (2). Therefore, to avoid overestimating or underestimating the bridge condition, a different approach, called a zoning technique, was used to obtain the transition matrix. This approach had been used by

Butt et al. for the development of pavement performance curves in a previous study (3).

Unlike in percentage prediction, a 1-year transition period was used in developing the performance curve. That is, $p_{i,j}$ was the transition probability from State i to State j in a 1-year period. Bridge age was divided into groups, and within each age group the Markov chain was assumed to be homogeneous. Groups consisting of 6 years were used, and each group had its own transition matrix, which was different from those of the remaining groups.

To make the initial computations simple, an assumption was made that the bridge condition rating would not drop by more than one state in a single year. Thus, the bridge condition would either stay in its current state or make the transition to

the next lower state in 1 year. The transition matrix therefore has the following form:

$$P = \begin{vmatrix} P(1) & q(1) & 0 & 0 & 0 & 0 & 0 \\ 0 & p(2) & q(2) & 0 & 0 & 0 & 0 \\ 0 & 0 & p(3) & q(3) & 0 & 0 & 0 \\ 0 & 0 & 0 & p(4) & q(4) & 0 & 0 \\ 0 & 0 & 0 & 0 & p(5) & q(5) & 0 \\ 0 & 0 & 0 & 0 & 0 & p(6) & q(6) \\ 0 & 0 & 0 & 0 & 0 & 0 & 1 \end{vmatrix} \quad (5)$$

where $q(i) = 1 - p(i)$.

It should be noted that the lowest recorded rating number in the data base was 3, indicating that bridges are usually repaired or replaced at a rating not less than 3. Consequently, the corresponding State 7 has the transition probability $p(7) = 1$.

To estimate the transition matrix probabilities, for each age group the following nonlinear programming objective function was formulated:

$$\min \sum_{t=1}^{N} |S(t) - E(t,P)| \quad (6)$$

subject to $0 \le p(i) \le 1, \quad i = 1, 2, \ldots, 6$

where

N = 6, the number of years in one age group;
P = $[p(1), p(2), \ldots, p(6)]$, a vector of length 6;
$S(t)$ = average of condition ratings at time t; and
$E(t,P)$ = estimated value of condition rating by Markov chain at time t.

The objective function was to minimize the absolute distance between the actual bridge condition rating at a certain age and the predicted bridge condition for the corresponding age generated by the Markov chain with the probabilities obtained by the nonlinear programming. The solution to this function was obtained by the gradient projection method (4).

To find the trend of a performance curve, a polynomial regression procedure (5) was performed first. The results of the regression were taken as the average condition ratings to solve the nonlinear programming. This method is explained in the following section through an example.

The maximum rating of bridge condition is 9, and it represents a near-perfect condition of a bridge component. It is almost always true that a new bridge has condition rating 9 for its deck, superstructure, and substructure. In other words, a bridge at age 0 has condition rating 9 for its components with unit probability. Thus, the initial-state vector $p^{(0)}$ for the deck, superstructure, or substructure of a new bridge is always (1, 0, 0, ..., 0), where the numbers are the probabilities of having condition ratings 9, 8, 7, ..., and 0, respectively, at age 0. That is, the initial vector of the first group for developing the bridge performance curve is known. Group 2 takes the last-state vector of Group 1 as its starting-state vector. In general, Group n takes the last-state vector of Group $n - 1$ as its starting-state vector. The rest of the work to obtain the overall bridge

performance curve or performance curve for bridge components is nothing but to conduct the following matrix multiplications:

$$p^{(1)} = p^{(0)} * P$$

$$p^{(2)} = p^{(0)} * P2$$

.

.

.

$$p^{(i)} = p^{(0)} * p^i \quad (7)$$

where $p^{(i)}$ represents the condition-state vector at age i.

APPLICATIONS

Once the transition matrix has been obtained, the prediction of the future condition by the Markov chain becomes a matter of simple multiplication of matrices. As stated earlier, this study used the Markov chain technique for two kinds of predictions: the percentage of bridges with a particular condition rating at any given time and the performance curve of bridges. The two applications are discussed in the following paragraphs.

Example of Percentage Prediction

The percentage of bridges with particular condition ratings in the base period can be readily obtained from the record of bridge condition ratings. For example, the fraction of concrete bridges with different deck condition ratings in northern Indiana in 1978 can be used as the initial-state vector:

$$P^{(0)} = (0.096, 0.559, 0.272, 0.059, 0.015, 0.000, 0.000,$$

$$0.000, 0.000, 0.000)$$

That is, in 1978 there were 9.6, 55.9, ..., and 0.0 percent of concrete bridges with deck condition ratings of 9, 8, ..., and 0, respectively.

Suppose that the expected percentages in 1984 are required, that is, the percentages after three rating periods, because bridge conditions are evaluated every 2 years. Using the transition probability matrix given in Table 3, the problem is only to get the three-step probability vector $P^{(3)}$ with the initial-state vector $P^{(0)}$ and the transition probability matrix P. From Equation 2,

$$P^{(3)} = p^{(0)} * P3 = (0.000, 0.009, 0.350, 0.323, 0.157,$$

$$0.110, 0.045, 0.006, 0.000, 0.000)$$

Figures 1 and 2 show the comparison of the actual and the predicted values for deck condition of concrete bridges in northern Indiana and steel bridges in southern Indiana, respectively, recorded in 1984.

The chi-squared goodness-of-fit test (6) was used to measure the closeness of the predicted and the recorded values. The computed chi-square is given by
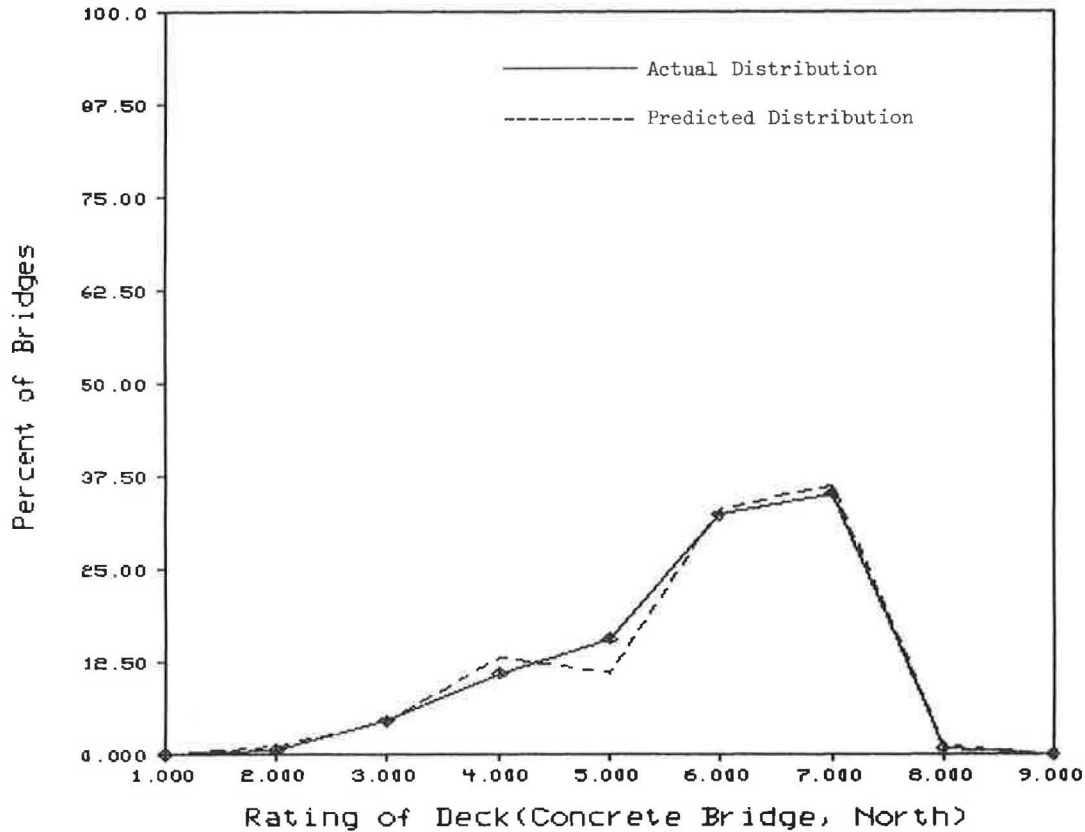
FIGURE 1 Actual versus predicted percentage of concrete bridges in northern Indiana in 1984 by deck condition rating.

TABLE 4 CHI-SQUARED GOODNESS-OF-FIT TEST OF PERCENTAGE PREDICTION OF DECK CONDITION RATING: CONCRETE BRIDGES, NORTHERN INDIANA

Rating	R_i	E_i	$(R_i-E_i)^2$	$\dfrac{(R_i-E_i)^2}{E_i}$
9	0.0%	0.0%	0.0	--
8	1.1%	0.9%	4.0×10^{-6}	4.4×10^{-4}
7	36.3%	35.1%	1.4×10^{-4}	4.1×10^{-4}
6	33.0%	32.3%	4.9×10^{-5}	1.5×10^{-5}
5	11.0%	15.6%	2.2×10^{-3}	1.4×10^{-2}
4	13.1%	11.0%	4.8×10^{-4}	4.4×10^{-3}
3	4.4%	4.5%	1.0×10^{-6}	2.2×10^{-5}
2	1.1%	0.6%	2.5×10^{-5}	4.2×10^{-3}
1	0.0%	0.0%	0.0	--
Σ	100.0%	100.0%		$x^2 = 0.024$

$$CHI_6^2 [x^2 \geqslant 0.024] > 0.995$$

$$\chi^2 = \sum_{i=1}^{k} \frac{(R_i - E_i)^2}{E_i} \tag{8}$$

where

k = number of observations,

R_i = recorded value of the ith observation,

E_i = expected value of the ith observations, and

χ^2 has a chi-squared distribution with $k - 1$ degrees of freedom.

The results are shown in Tables 4 and 5. As can be seen from Figures 1 and 2 and the statistical test results, the predicted values are very close to the recorded values.

Example of Performance Curve for Bridge Component

The deck performance curve of a concrete bridge in northern Indiana is used as another example. As mentioned in the last section, the initial-state vector of the first group for the deck, superstructure, or substructure of a new bridge is always (1, 0, 0, ..., 0). Therefore, the major problem is to obtain the transition matrix for bridge decks.

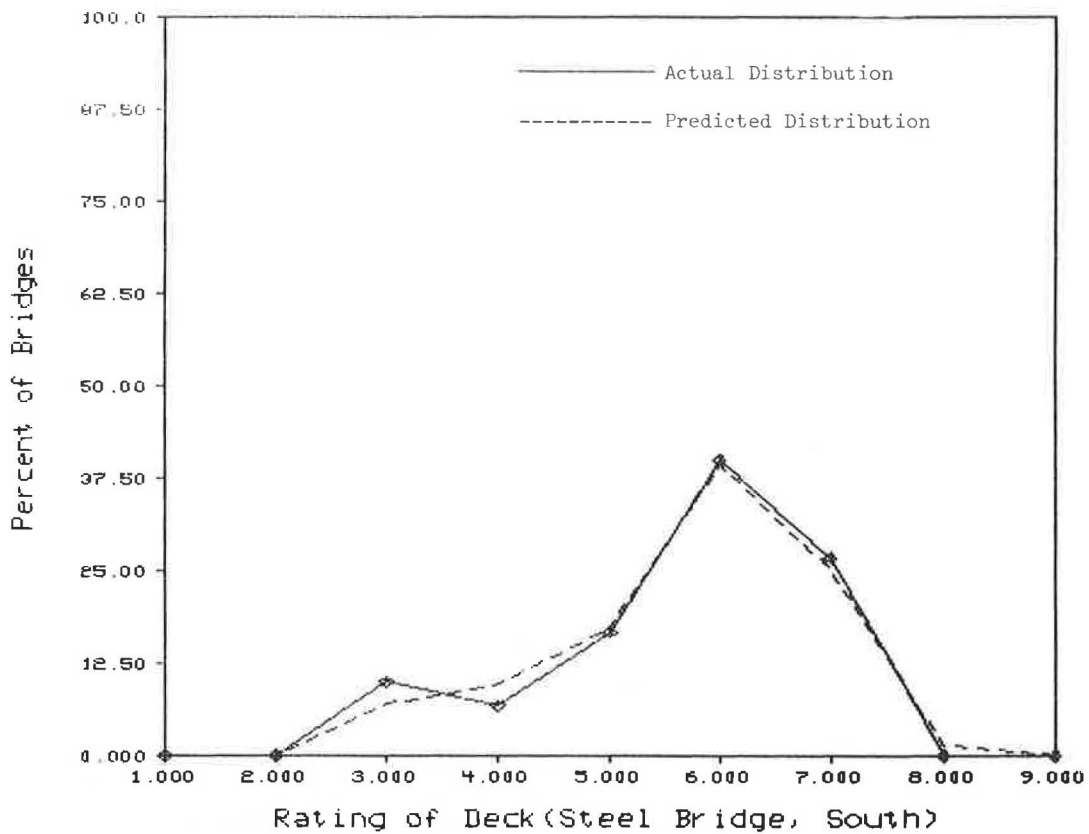A polynomial nonlinear regression model was assumed as follows:

FIGURE 2 Actual versus predicted percentage of steel bridges in southern Indiana in 1984 by deck condition rating.

TABLE 5 CHI-SQUARED GOODNESS-OF-FIT TEST OF PERCENTAGE PREDICTION OF DECK CONDITION RATING: STEEL BRIDGES, SOUTHERN INDIANA

Rating	R_i	E_i	$(R_i - E_i)^2$	$\dfrac{(R_i - E_i)^2}{E_i}$
9	0.0%	0.1%	1.0×10^{-6}	1.0×10^{-3}
8	0.0%	1.4%	2.0×10^{-4}	1.4×10^{-2}
7	26.7%	25.2%	2.2×10^{-4}	8.9×10^{-4}
6	40.0%	39.3%	4.9×10^{-5}	1.2×10^{-4}
5	16.6%	17.3%	3.6×10^{-5}	2.1×10^{-4}
4	6.7%	9.7%	9.0×10^{-4}	9.3×10^{-3}
3	10.0%	7.0%	9.0×10^{-4}	1.2×10^{-2}
2	0.0%	0.0%	0.0	--
1	0.0%	0.0%	0.0	--
Σ	100.0%	100.0%		$x^2 = 0.038$

$$CHI_6^2 [x^2 > 0.038] > 0.995$$

$$S(t) = A + Bt + Ct^2 + Dt^3 \qquad (9)$$

where

t = bridge age or number of years since last major reconstruction,
$S(t)$ = bridge deck condition rating, and
$A–D$ = coefficients to be determined.

Using the SAS (7) statistical package, the coefficients were obtained on the basis of the sample data, as shown below:

$$S(t) = 9.0 - 0.30266t + 0.00895t^2 - 0.00009t^3 \qquad (10)$$

The values of $S(t)$ obtained from Equation 10 were used to solve the nonlinear programming function in Equation 6. This solution provided transition probabilities corresponding to Equation 5 for different bridge age groups. Table 6 shows the transition probabilities for the nine age groups. For example, $p(1) = 0.69$ in Group 1, which means that 69 percent of the bridges in Group 1 (aged 6 years or less) that are in State 1 (condition rating 9) at present would remain in State 1 and that the remaining 31 percent of the bridges would deteriorate to State 2 (condition rating 8) in a 1-year period.

An example set of computations is given in the following. Using Equation 5 and information from Table 6, the transition matrix for Group 1 was obtained:

$$P = \begin{vmatrix} 0.69 & 0.31 & 0 & 0 & 0 & 0 & 0 \\ 0 & 0.77 & 0.23 & 0 & 0 & 0 & 0 \\ 0 & 0 & 0.92 & 0.08 & 0 & 0 & 0 \\ 0 & 0 & 0 & 0.91 & 0.09 & 0 & 0 \\ 0 & 0 & 0 & 0 & 0.90 & 0.10 & 0 \\ 0 & 0 & 0 & 0 & 0 & 0.79 & 0.21 \\ 0 & 0 & 0 & 0 & 0 & 0 & 1 \end{vmatrix} \quad (11)$$

The initial-state vector of Group 1 was $p^{(0)} = (1, 0, 0, ..., 0)$. Therefore, the state vector of Group 1 for year t can be obtained by Equation 7. For example, the state vectors for year 0 through year 6 are given below:

$p^{(0)} = (1, 0, 0, 0, 0, 0, 0, 0, 0, 0)$

$p^{(1)} = p^{(0)} * P$

$= (0.69, 0.31, 0.00, 0.00, 0.00, 0.00, 0.00, 0.00, 0.00, 0.00)$

$p^{(2)} = p^{(0)} * P2$

$= (0.48, 0.45, 0.07, 0.00, 0.00, 0.00, 0.00, 0.00, 0.00, 0.00)$

$p^{(3)} = p^{(0)} * P3$

$= (0.33, 0.49, 0.17, 0.01, 0.00, 0.00, 0.00, 0.00, 0.00, 0.00)$

$p^{(4)} = p^{(0)} * P4$

$= (0.23, 0.48, 0.27, 0.02, 0.00, 0.00, 0.00, 0.00, 0.00, 0.00)$

$p^{(5)} = p^{(0)} * P5$

$= (0.16, 0.44, 0.36, 0.04, 0.00, 0.00, 0.00, 0.00, 0.00, 0.00)$

$p^{(6)} = p^{(0)} * P6$

$= (0.11, 0.39, 0.43, 0.06, 0.01, 0.00, 0.00, 0.00, 0.00, 0.00)$

TABLE 6   TRANSITION PROBABILITIES FOR DIFFERENT BRIDGE AGE GROUPS

	p(1)	p(2)	p(3)	p(4)	p(5)	p(6)
Group 1	0.69	0.77	0.92	0.91	0.90	0.79
Group 2	0.42	0.86	0.86	0.69	0.72	0.56
Group 3	0.65	0.91	0.91	0.92	0.97	0.76
Group 4	0.10	0.07	0.96	0.95	0.98	0.93
Group 5	0.10	0.10	0.94	0.98	0.99	0.11
Group 6	0.10	0.10	0.99	0.98	0.95	0.99
Group 7	0.10	0.10	0.83	0.99	0.97	0.99
Group 8	0.10	0.10	0.57	0.92	0.95	0.99
Group 9	0.10	0.10	0.10	0.55	0.97	0.48

Then $p^{(6)}$ obtained above for Group 1 was taken as the initial-state vector of Group 2, and the corresponding transition matrix of Group 2 was used to continue the procedure.

By this procedure, the bridge condition at any time t can be predicted in terms of initial-state vector $p^{(0)}$ and transition matrix P. Figure 3 shows the deck performance curve of concrete bridges in northern Indiana obtained by this method. Performance curves can be developed similarly for other bridge components.

The trend of the predicted performance curve matched the actual bridge condition data well. The results indicated that bridge deck ratings dropped quickly at the beginning of a bridge's life, then became more stable as the bridge age increased, and dropped quickly again after the deck condition rating reached 5 or less. It should be noted that bridge condition ratings are subjective judgments of bridge inspectors and thus the trend may reflect inherent human bias. For example, bridge inspectors are generally reluctant to rate a condition "perfect" after the initial year and they also tend to consider the condition as rapidly deteriorating after the rating has reached 5.

A chi-squared goodness-of-fit test(6) was performed, and the results indicated that the difference between the predicted performance and the least-squares polynomial performance was not significant at $\alpha = 0.05$, as shown below:

$$\chi^2 = \sum_{i=0}^{60} \frac{(R_i - E_i)^2}{E_i} = 0.072$$

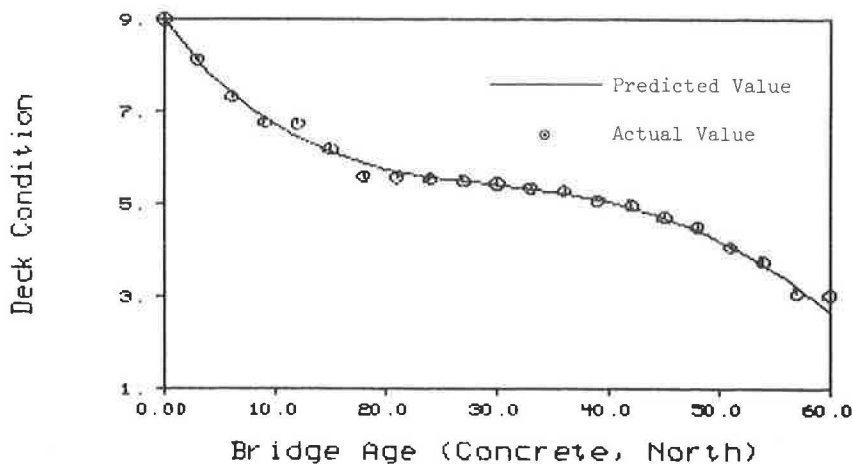$\text{Chi}^2_{60} \ (\chi^2 \geq 0.072) > 0.995 > \alpha = 0.05$

FIGURE 3 Performance curve of concrete-bridge deck condition in northern Indiana.

CONCLUSIONS

An accurate estimate of the future condition of bridges is essential for an effective bridge management system. The Markov chain is a powerful and convenient tool for estimating future bridge performance. The results obtained by a Markov chain model are particularly useful if dynamic programming is used for optimization in a bridge management system, because the transition probabilities are the basic parameters to determine before one can solve a dynamic program (*8*). Furthermore, performance curves give bridge managers a quantitative view of bridge conditions that is useful in selecting rehabilitation strategies.

A Markov chain is completely specified when its transition matrix P and the initial-state vector $p^{(0)}$ are known. Usually, the initial condition is known in a bridge management system. So the main task in using the Markov chain is to develop the transition probability matrix. In the present study, the effects of bridge age on bridge condition were emphasized. The effects of other factors on bridge performance, such as truck traffic and climate, are currently under study. The more factors a model considers, the closer it is to the reality of the problem.

ACKNOWLEDGMENT

REFERENCES

1. *Recording and Coding Guide for the Structure Inventory and Appraisal of the Nation's Bridges*. FHWA, U.S. Department of Transportation, Jan. 1979.
2. U. N. Bhat. *Elements of Applied Stochastic Processes*. John Wiley and Sons, Inc., New York, 1972.
3. A. A. Butt, K. J. Feighan, and M. Y. Shahin. Pavement Performance Prediction Model Using the Markov Process. In *Transportation Research Record 1123*, TRB, National Research Council, Washington, D.C. 1987, pp. 12–19.
4. D. G. Luenberger. *Linear and Nonlinear Programming*. Addison-Wesley Publishing Company, New York, 1985.
5. J. Neter and W. Wasserman. *Applied Linear Statistical Models: Regression, Analysis of Variance, and Experimental Designs*. Richard D. Irwin, Inc., Homewood, Ill., 1974.
6. E. D. Rothman and W. A. Ericson. *Statistics: Methods and Applications*. Kendall/Hunt Publishing Company, Dubuque, Iowa, 1983.
7. *SAS User's Guide: Statistics, Version 5 Edition*. SAS Institute Inc., Cary, N.C., 1985.
8. S. M. Ross. *Applied Probability Methods with Optimization Applications*. Holden-Day, Inc., Oakland, Calif., 1970.

Tie Girder Fracture in Siouxland Veterans Memorial Bridge

JOHN M. HANSON, MICHAEL J. KOOB, AND GILBERT T. BLAKE

The Siouxland Veterans Memorial Bridge, from Sioux City, Nebraska, to Sioux City, Iowa, was opened to traffic in January 1981. In May 1982 Iowa Department of Transportation personnel discovered a fracture across the full width of the top flange on the downstream tie girder. The investigation into the cause of the fracture included chemical and physical testing and fractographic and metallographic examinations. Results of the latter examinations showed that the fracture originated at a gas-flame-cut edge of the 2³/₄-in.-thick A588 flange plate. It arrested at least once at a depth of 0.37 in. and possibly earlier at a depth of about 0.05 in. before propagating in a brittle mode across the flange. The fracture surface was heavily corroded, indicating that the fracture had occurred long before its discovery. The physical tests indicated that the plate in which the fracture occurred did not meet the specified toughness requirements. Additional tests on samples of material extracted from other parts of the girders revealed highly variable toughness properties, some of which did not meet the requirements of the specifications either.

The Siouxland Bridge from Sioux City, Nebraska, to Sioux City, Iowa, a tied arch structure having a span length of 425 ft, was opened to traffic in January 1981. In May 1982 Iowa Department of Transportation (IDOT) personnel discovered a fracture across the full width of the top flange of the downstream tie girder. An investigation to determine the cause of the fracture was undertaken. The investigation included chemical and physical testing and fractographic and metallographic examinations. A summary of the testing and examinations and the authors' opinion of the cause of the fracture are reported in this paper.

BRIDGE DESCRIPTION

The Siouxland Bridge is a steel tied arch structure with continuous-welded plate-girder approach spans. A view of the 425-ft tied arch span, looking south, is shown in Figure 1. As shown in the elevation in Figure 2, the interior panels are 35 ft 0 in. long, and the end panels are 37 ft 6 in. long. The tie girders act in tension to counteract the compressive thrust of the arch, as well as in flexure to resist the live-load bending moment. Panel points are numbered from 0 to 6 to 0'.

A partial cross section of the bridge is shown in Figure 3. The reinforced-concrete deck slab, which carries four lanes of traffic, is supported on nine longitudinal stringers, which bear

Wiss, Janney, Elstner Associates, Inc., 330 Pfingsten Road, Northbrook, Ill. 60062.

on the top flanges of transverse floor beams located at each panel point. The floor beams frame into the tie girders at each panel point. The tie girders are supported by 1³/₄-in.-diameter strand hangers suspended from the arch rib.

The bridge was designed for an HS20-44 loading plus an allowance of 20 psf for a future wearing surface. The design was based on the 1973 specifications for highway bridges of the American Association of State Highway and Transportation Officials (AASHTO), plus their interim specifications, along with the draft version of Guide Specifications for Fracture Critical Non-Redundant Steel Bridge Members and *IDOT SP-229: Special Provisions for Missouri River Bridge.*

The tie girders, shown in Figure 4, are box members that are 2 ft 7¹/₂ in. wide by 6 ft 4 in. to 6 ft 5¹/₂ in. deep, fabricated from ASTM Grade A588 and A572 steel. The A588 flange plates vary in thickness between 2 and 2³/₄ in. The A572 web plates are 6 ft deep by ³/₄ in. thick and are inset ³/₄ in. from the edge of the flanges. The flange and web plate lengths vary from 8 ft 9 in. to 70 ft, depending on field splice locations. It is believed that the plates were flame cut without preheat. Welded construction was used throughout the tie girders, except for the high-strength bolted field splices. All welded details utilized in the bridge were Category C or better.

Steel for the bridge was provided by two suppliers, one who furnished most of the flange plates, and the other who furnished the remainder of the flange plates and all of the web plates.

EXAMINATION OF FRACTURE SURFACE AND TESTS OF ADJACENT MATERIAL

The fracture was located 6 ft 10 in. north of panel point 3 in the downstream tie girder, and extended in a nearly perpendicular direction across the top flange plate. The view shown

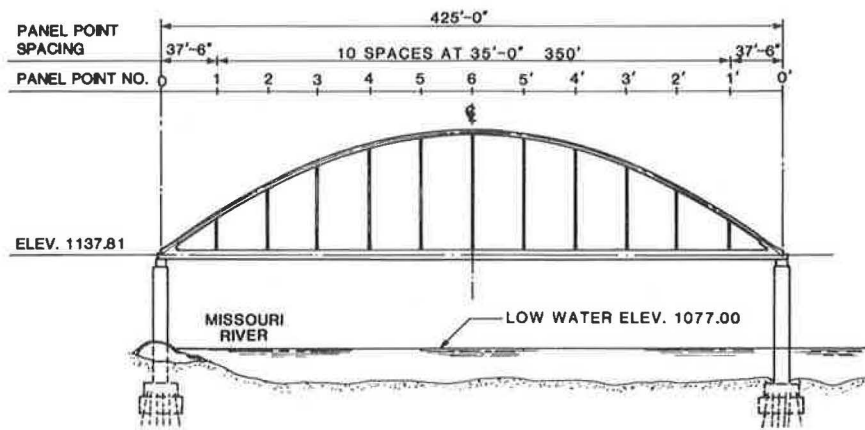FIGURE 1 Siouxland Bridge at Sioux City, Iowa.
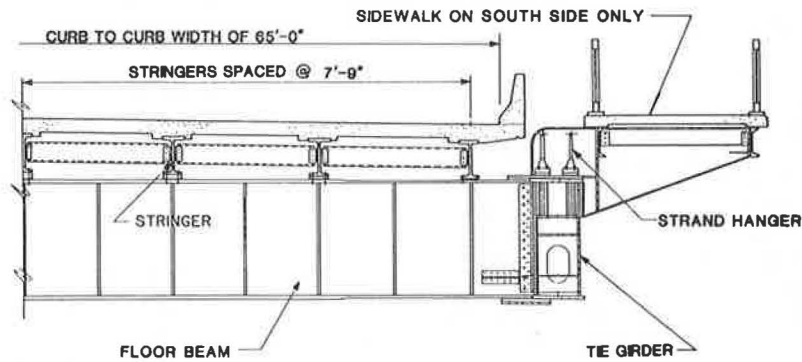
FIGURE 2 Elevation looking west.

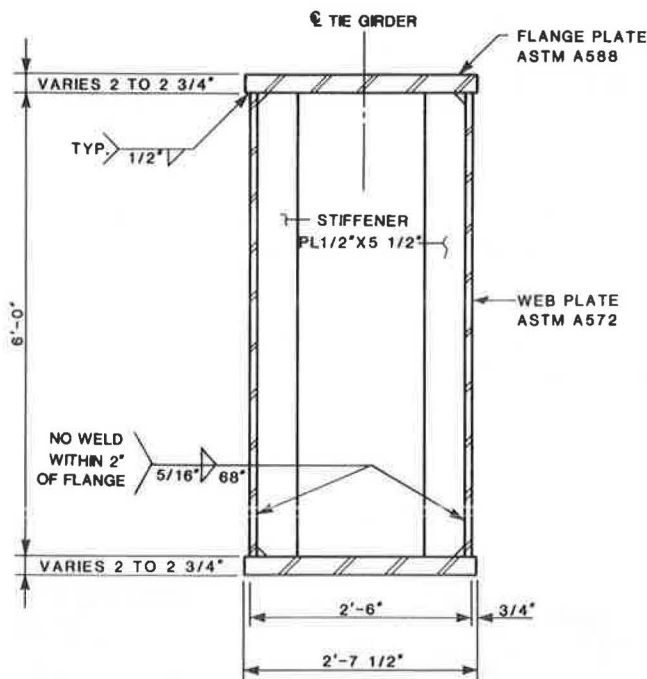**FIGURE 3 Partial cross section.**

FIGURE 4 Cross section of tie girder at typical intermediate stiffeners.

in Figure 5 was taken as a section of the flange containing the fracture was being cut and removed from the tie girder for laboratory testing. As a precaution against further propagation, IDOT personnel drilled a $^{15}/_{16}$-in.-diameter hole through the weld and web plate on each side of the tie girder to remove the crack tip, as shown in Figure 6. The measured widths of the crack varied from 0.05 to 0.08 in., as shown in Figure 7. There were no stiffeners or any other welded attachments in the vicinity of the crack.

The section taken from the flange is shown in Figure 8. One piece was about 5 in. long (in the direction of the tie girder), and the other was about 9 in. long. The fracture occurred in a region where the flanges and web plates had a fabricated length of 70 ft 0 in.

To preserve the fracture surface, a $^1/_2$-in.-thick slice adjacent to the fracture was made across the full width of the 9-in.-long piece of flange plate. The remainder was used to conduct chemical, tensile, Charpy V-notch impact, and compact tension toughness tests.

The 5-in.-long piece was given to the supplier of that material, who also removed and preserved a slice containing the fracture surface. Specimens were cut from the remainder for chemical, tensile, Charpy V-notch impact, and hardness tests. The supplier was also given four cores extracted from the top flange near the fracture for testing.
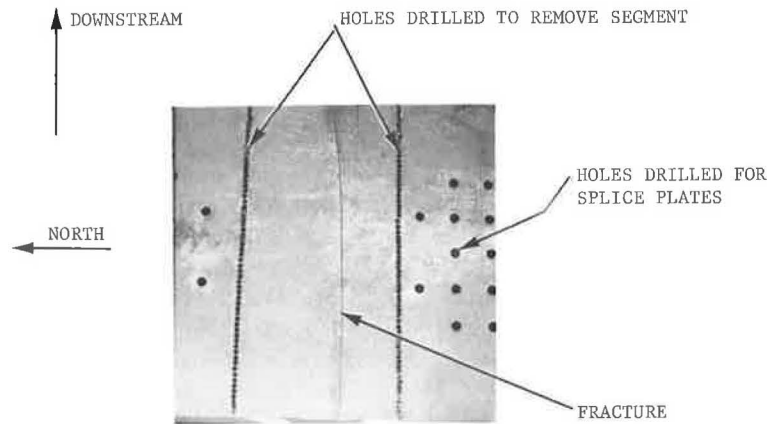
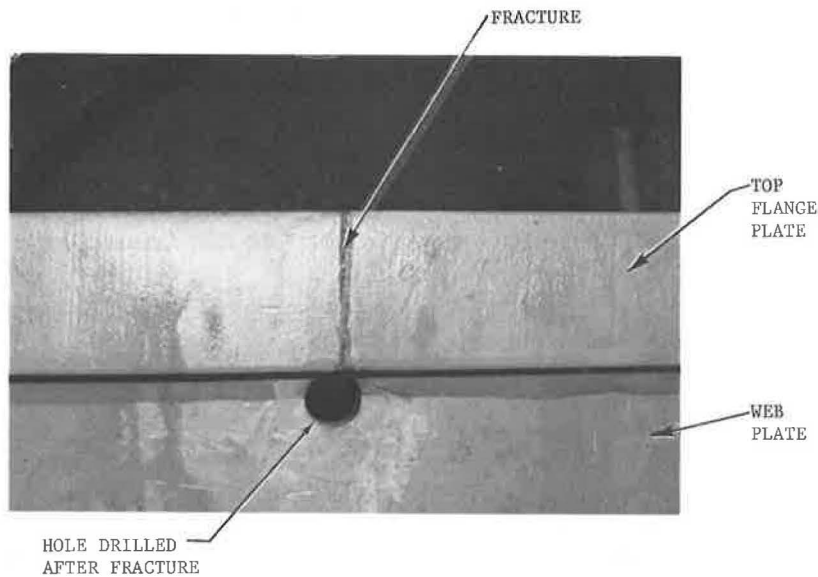FIGURE 5 Plan view of top flange, showing fracture.
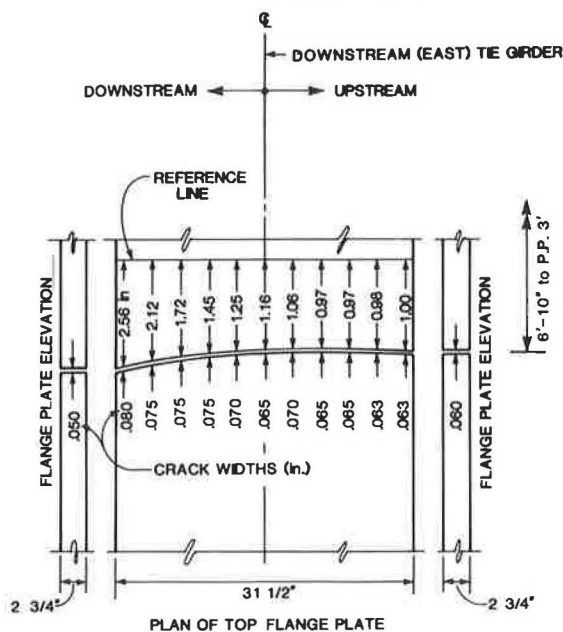

FIGURE 6 Elevation view of fracture.

FIGURE 7 Geometry of fracture and measurements of crack width.

Results of tests conducted by Materials Research Laboratory, Inc., on behalf of IDOT and by the supplier were in good agreement. The examinations and findings by the supplier were confirmed by Ed Ripling of Materials Research Laboratory, Inc. All of these test results are summarized in the following sections.

Chemical Properties

The chemical tests indicated that the steel conformed to the requirements of ASTM A588-77a, as specified. Carbon content was at or close to the maximum allowable value of 0.19 percent and the manganese content ranged from 1.10 to 1.15 percent.

Tensile Properties

ASTM A588 requires a minimum tensile strength of 70 ksi, a minimum yield strength of 50 ksi, and a minimum elongation of 19 percent for plates with thicknesses up to 4 in. Tensile tests on longitudinal (rolling direction) and transverse specimens indicated tensile strengths ranging from 90.3 to 103.1
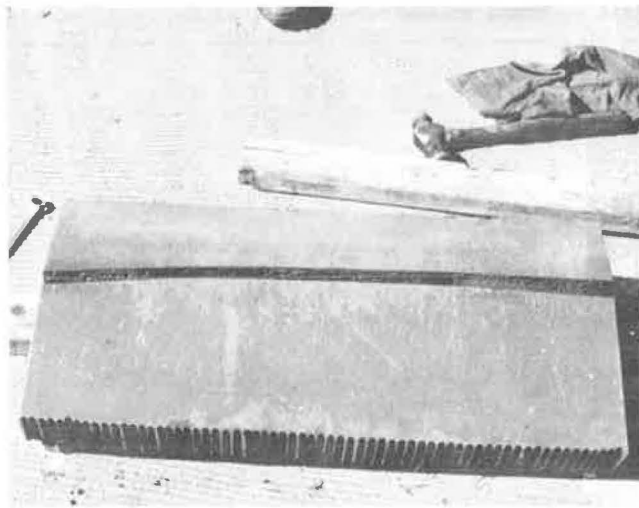
FIGURE 8 Pieces of A588 flange plate with fracture.

ksi, yield strengths from 58.5 to 68.1 ksi, and elongations from 21.5 to 27.5 percent. These results met the requirements for A588 steel.

Charpy V-Notch Impact Tests

Charpy V-notch (CVN) impact tests were conducted on specimens taken at the top, upper-quarter thickness, center, and bottom of the two pieces of flange plate. Specimens from the four cores were taken at the upper- and lower-quarter thicknesses. The tests were conducted in accordance with ASTM A370 at discrete temperature levels from −20°F to 100°F. Results of the tests are plotted in Figure 9. They exhibit significant variability, even for specimens taken from the same location. Of the 27 specimens tested at 40°F, only 5 met the

30 ft-lb minimum requirement of IDOT's special provisions (SP-229).

Plane-Strain Fracture Toughness Tests

Fracture toughness tests were conducted in accordance with ASTM E399, except that a loading rate of about 1 sec to failure (to represent an intermediate strain rate) was used. Three full-thickness compact specimens were cut from the flange plate. The average critical stress intensity factor K_{Ic} at −20°F was 40 ksi $\sqrt{in}$. The test results were valid according to criteria in E399, except that the fatigue precrack stress intensity of about 27 ksi $\sqrt{in}$. was somewhat higher than the allowable value of 23.9 ksi $\sqrt{in}$.

Additional tests were performed at 40°F on two smaller half-thickness compact tension specimens machined from the previously tested full-thickness specimens. The K_{Ic} values for these two specimens were about 45 ksi $\sqrt{in}$., indicating very little toughness increase for a 60°F increase in temperature.

Hardness Tests

Rockwell B hardness tests conducted on a through-thickness section of the flange gave values ranging from 87.5 to 94.5.

Fractographic and Metallographic Analyses

Fractographic and metallographic examinations were conducted to determine the origin and size of the initiating crack and the extension and characteristics of propagation.

A report by the supplier stated that the fracture began in the heat-affected zone of the gas-cut edge of the flange plate on the upstream side of the girder and propagated as a cleavage crack that appeared to have arrested 0.37 in. from the plate edge, and then subsequently from the crack arrest region
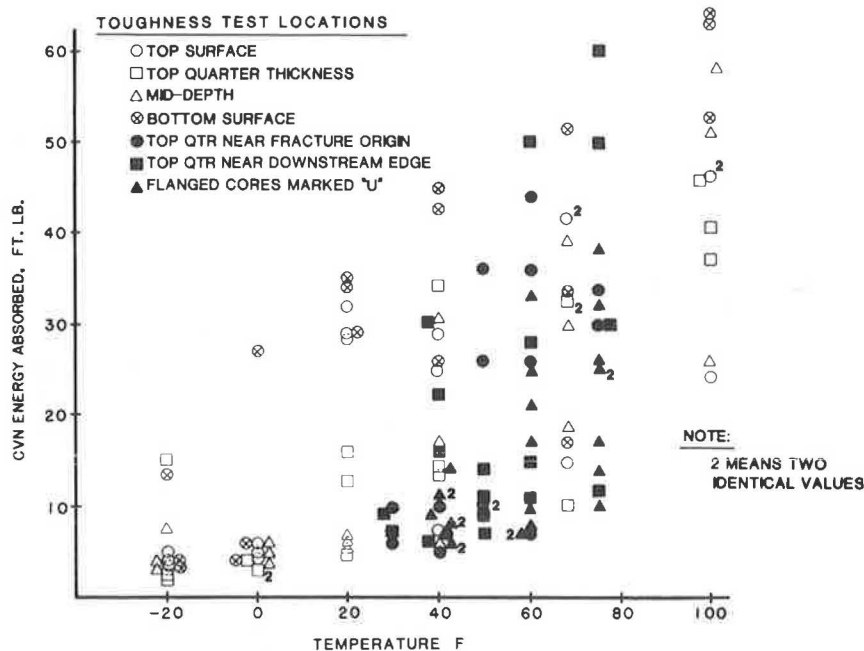

FIGURE 9 CVN test values from flange plate next to fracture.

across the flange width in a cleavage-fracture mode. Figure 10, provided by the supplier, shows the fracture surface.

The report by the supplier also indicated that a magnetic particle examination revealed an additional crack on the downstream edge of the piece of fractured plate. The crack was subsequently shown by metallographic examination to be 0.046 in. deep. It was located within the heat-affected zone of the gas-cut edge on the bottom corner of the plate. The crack surface, shown in Figure 11, exhibited intergranular cleavage and ductile tearing fracture characteristics.

ADDITIONAL TESTS OF FLANGE AND WEB MATERIAL

Because the CVN values for the steel adjacent to the fracture were low, additional samples were extracted from material representing each heat of steel used in the fabrication of the tie girder flanges and webs. All of these tests were conducted by Materials Research Laboratory, Inc., on behalf of IDOT. Initially, 4-in.-diameter cores, identified by the prefix M, were extracted from 16 selected locations. Chemical, tensile, and CVN impact tests were conducted on specimens machined from these cores.

Some of the results of the CVN tests exhibited scatter and thus did not meet the acceptance criteria of Section 22.2.1 of ASTM 370. Consequently two additional M-type cores were extracted for testing. Subsequently, additional cores, identified by the prefix S, were extracted for further material testing. Locations of all cores, including the four cores near the
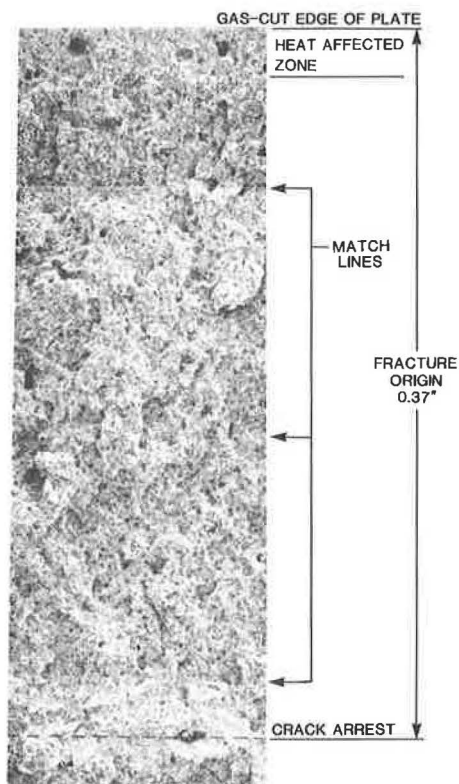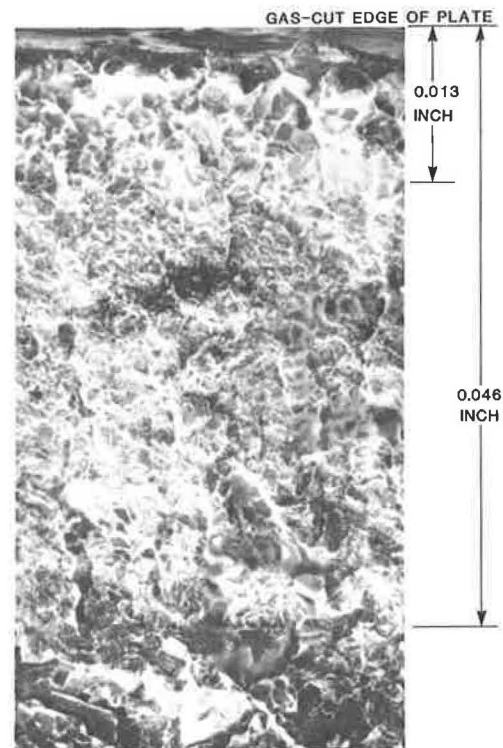

FIGURE 11 Fractograph of crack at downstream edge.

fracture marked U that were initially given to the supplier, are shown in Figure 12.

Tensile Tests

The results of tensile tests on specimens machined from the core samples indicated that tensile requirements of ASTM A-588-77a were met.

Chemical Tests

Results of all tests met the requirements of ASTM A-588-77a. Carbon and manganese contents of samples from material furnished by the supplier of the fractured plate ranged from 0.16 to 0.18 percent and from 1.02 to 1.17 percent, respectively. Corresponding carbon and manganese contents of samples from material by the other supplier were from 0.12 to 0.15 percent and from 0.85 to 0.97 percent, respectively. Other chemical contents of samples from material furnished by the supplier of the fractured plates that differed from the samples of material by the other supplier were as follows: silicon, 0.34 to 0.43 percent compared with 0.23 to 0.27 percent; nickel, 0.22 to 0.25 percent compared with 0.32 to 0.34 percent; and copper, 0.27 to 0.36 percent compared with 0.22 to 0.27 percent, respectively.

Charpy V-Notch Impact Tests

Specimens were machined from each core, and tests were conducted in accordance with ASTM A370 at temperatures ranging from $-20°$ to 70°F. A plot of the results of the Charpy

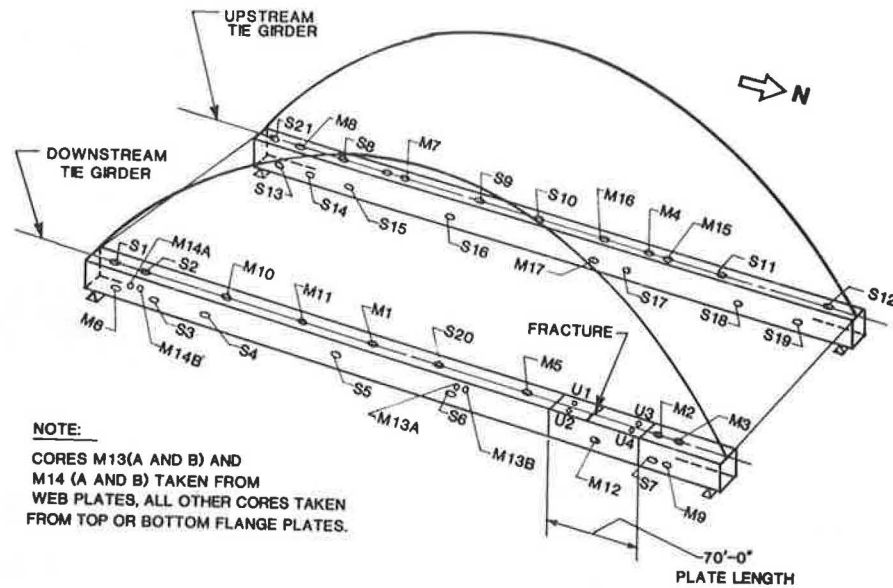FIGURE 10 Fracture at upstream edge of plate.
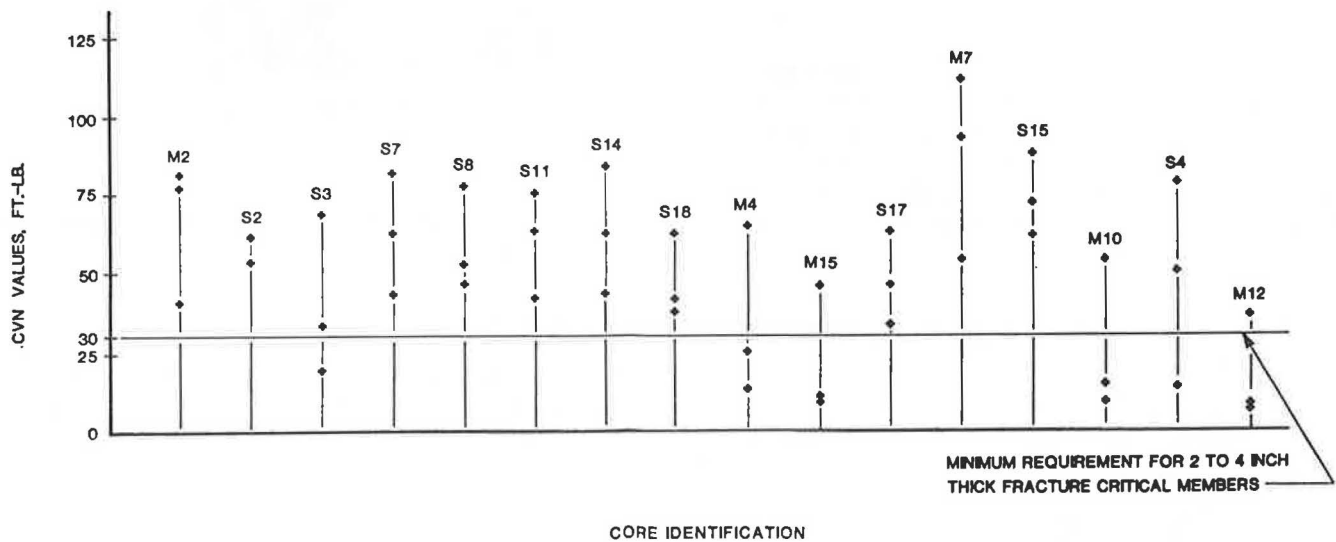
FIGURE 12 Core locations on girders.

FIGURE 13 CVN values at 40°F for all 2³/₄-in. flange material.

tests for three specimens from each of the 2³/₄-in.-thick cores that were tested at 40°F is shown in Figure 13. CVN values were found to be below the IDOT's SP-229 requirement of 30 ft-lb at 40°F in specimens from six core locations in the 2³/₄-in. plate and five locations in the 2¹/₂-in. plate.

DISCUSSION

The closing of the Siouxland Bridge following the discovery of the fracture imposed a severe hardship on the neighboring communities of Sioux City, Iowa, and Sioux City, Nebraska. The ensuing investigation was carried out expeditiously.

It was immediately evident from the results of the CVN tests on samples from the 2³/₄-in.-thick fractured plate (shown in Figure 9) that there was highly unusual scatter in the toughness properties of this material and that the material did not meet the specified minimum requirement of 30 ft-lb at

40°F. Some of the scatter was related to the position of the test specimen within the plate. According to the mill report for this plate, the CVN values at 40°F were 39, 39, and 43 ft-lb. These observations led to the conclusion that it was necessary to test representative samples of all the steel in the bridge.

As shown in the plot of CVN values at 40°F for all of the 2³/₄-in.-thick flange material in Figure 13, a number of locations were found where the toughness did not meet the specified requirement. Locations where 2¹/₂-in.-thick plates did not meet the requirement were also found. At this point in the investigation, an offer was made to IDOT by the supplier of the fractured plate to replace all flange plates that had been furnished by the supplier. This offer was accepted. Work to replace these flange plates was completed in spring 1983.

The metallurgical examinations were not completed until after work to replace the flange plates was under way. As described earlier, the examinations indicated that a small

crack, about 0.37 in. deep, was present in the edge of the flange plate before the fracture occurred. Some time after this plate had been painted, the crack propagated in a brittle mode across the full plate width. Another crack was found, about 0.05 in. deep, in the opposite flame-cut edge of the 5-in.-long piece of removed flange plate. It is believed that a crack of about the same depth had existed initially in the edge of the plate where the fracture occurred.

Alan Pense of Lehigh University provided an explanation for the initiation of a crack due to flame cutting and its extension and subsequent arrest. Stress at the tip of a crack would decrease as the crack propagated out of the zone of high residual stress that is associated with the martensitic material produced along the plate edge by the gas-flame-cutting operation. These residual stresses can be higher than the yield strength of the base material. Therefore, the crack that caused the fracture may have propagated in two stages, first during gas-flame-cutting to a depth of about 0.05 in., and then subsequently (possibly during handling) to the depth of 0.37 in.

When there is an edge crack with a depth of 0.37 in., a stress of about 33 ksi at the crack tip during very cold weather would induce a fracture under traffic conditions (K_{Ic} of 40 ksi $\sqrt{\text{in}}$. for a loading rate of about 1 sec to failure). Pense pointed out that a dynamic stress at the crack tip of about the same level (not necessarily during cold weather) could also produce a fracture. Considering the heavy corrosion associated with the fracture surface, it is likely that the fracture occurred very early during the life of the bridge. Cracking under these circumstances may have occurred during construction if the bridge had been subjected to an unusual construction loading or during the first or second winter of usage under conditions of an unusually heavy traffic loading.

The fracture may not have occurred in a plate with higher toughness. For example, an increase in K_{Ic} from 40 to 60 ksi $\sqrt{\text{in}}$. would mean that the stress required at the tip of a 0.37-in.-deep crack to initiate fracture in cold weather would increase from 33 to 50 ksi, an improbable condition.

REPLACEMENT OF THE FLANGE PLATES

To replace the tie girder flanges, it was necessary to relieve the bridge dead load. This was accomplished by temporarily supporting the superstructure on falsework erected in the river. Pilings were driven into the river bottom at four locations to form bents. Two bents were located beneath the expansion joints at panel points 4 and 4'. The other bents were located about 99 ft from the first two, toward each bridge abutment. Longitudinal and lateral beams were erected on top of the bents to provide support for the superstructure.

The dead load was relieved by lifting the superstructure onto temporary support pedestals located under each floor beam. Lifting was accomplished with hydraulic jacks in a computer-generated sequence of lift stages. Stresses in the tie girders were monitored with strain gauge instrumentation. After being lifted, the bridge was tested under a simulated traffic loading and then opened to limited traffic.

The top flange of each tie girder was removed with propane-fueled cutting torches mounted on girder-connected rails running the length of the bridge. This arrangement facilitated accurate cutting of the flange-to-web connection. The cut edges of the webs were ground smooth. The replacement plates were wider than the original plates and were prefabricated with welded side plates located adjacent to the outside faces of the webs. Holes were drilled in the webs through the predrilled holes in the side plates. After the drilling, the flanges were bolted into place. Care was taken to ensure that the internal hanger diaphragms were in contact with the flange plates across their full width.

After installation of the top flange plates had been completed, the bottom flanges were replaced in a similar manner. A reverse jacking sequence was used to remove the support pedestals and retransfer the dead load to the tie girders. The bridge was reopened to normal traffic in May 1983.

SUMMARY

Following the discovery of the fracture in the top flange of the downstream tie girder in May 1982, examinations of the fracture surface and tests of the adjacent steel were made by several parties. The examinations and tests showed that the fracture originated at the gas-flame-cut edge on the upstream side of the tie girder. It arrested at least once at a depth of 0.37 in., and possibly earlier at a depth of about 0.05 in., before propagating in a brittle mode across the flange. The fracture surface was heavily corroded, indicating that the fracture had occurred long before its discovery.

The $2^{3}/_{4}$-in.-thick A588 steel plate in which the fracture occurred did not meet the toughness requirements of IDOT specifications, and test values exhibited an extreme amount of scatter. Tests on samples of material extracted from other parts of the girders revealed highly variable toughness values, some of which did not meet the requirements of the specifications.

ACKNOWLEDGMENTS

Experimental Study of Washington State Precast Girders Without End Blocks

UMESH VASISHTH AND RAFIK Y. ITANI

This paper describes the research procedure followed to eliminate the end blocks from simply supported Washington Series 14 and 10 girders. Girders in the former series have 5-in. webs, are over 6 ft deep, and can be up to 140 ft long. The procedure consisted of an analytical study followed by full-scale testing, the monitoring of a girder in a bridge, and implementation of the end block removal. A finite-element analysis was first made of girders with and without end blocks. This was followed by a full-scale test of a 48-ft long, Series 14 girder manufactured without end blocks. A Series 10 girder was manufactured without end blocks and monitored in a bridge under actual service. The findings of this research were implemented by revising the girder standards. This resulted in about a 7 percent saving in the cost of simple span girders. A study is under way to see whether the end blocks can be removed from continuous girders.

An end block is a short section with a thickened web at the end of a prestressed concrete girder. In a posttensioned girder, the end block provides room for the bulky anchorage and the distribution of the prestressing force. All girders are pretensioned these days; posttensioned girders are no longer used. End blocks were eliminated from girders made with the specifications of the American Association of State Highway and Transportation Officials (AASHTO) with 6- and 8-in. webs. Washington series girders have 5-in. webs. The reinforcing steel becomes congested at the ends of these girders if there are no end blocks. There was also some concern about the proper fabrication, transportation, stability, and shear compression capacity of these girders. Series 14 girders can be up to 140 ft long and have a 6-ft 1½-in. depth and 5-in. webs. Series 10 girders have a 4-ft 10-in. depth and are sometimes 120 ft long.

Researchers estimated that about 7 percent of the cost of prestressed girders could be reduced if the end blocks were eliminated. Washington State Department of Transportation (WSDOT) decided to research whether the end blocks were necessary for these girders. Research findings show that end blocks are not necessary for simple span girders.

Phase 1 of the research project, dealing with simple span girders, has just been completed. It consisted of a literature survey, a finite-element study, two full-scale tests, monitoring of the field performance of a girder without end blocks, and implementation of the research findings. A second phase to study the removal of end blocks from continuous girders is now under way.

BACKGROUND

There have been many studies dealing with prestressed concrete girders. Marshall and Mattock (1) were among the first investigators whose primary goal was to measure stresses in the end-block region and to study horizontal cracks usually observed in the end regions. From the results of their field survey and experiments, they concluded that end blocks are not necessary and that their presence in pretensioned, prestressed girders does not ensure absence of horizontal cracks. They pointed out that vertical reinforcement close to the end face of such girders will ensure satisfactory performance of the end zones. Furthermore, they suggested that fine, short horizontal cracks will not affect the service performance of the girders.

Gergely et al. (2) developed a direct method of designing transverse reinforcement by assuming the initiation of a crack in the end zones. They determined that for an eccentric load, the spalling stresses were larger for a rectangular end block than for an I-shaped one. They also proposed design specifications that could be applied to the anchorage zone of pretensioned members.

In 1965, Arthur and Ganguli (3) conducted experimental studies and applied to pretensioned beams theories of posttensioned beams used in the design of end zones. They examined the theories of Magnel et al. (an adaptation of Bleich-Sievers's theory) and Guyon in their prediction of the vertical tensile stresses in the end zone at transfer. Arthur and Ganguli proposed a modification of Magnel's theory so that it could be applied to pretensioned beams, and in 1966, Marshall (4) proposed a modification to Sievers's approach (5) for determining maximum tensile stress in the web of a posttensioned beam so that the approach could be applied to pretensioned cases.

Hawkins (6) in 1966 suggested that rectangular end blocks should not be used for I-beams. Gergely and Sozen (7) in 1967 provided a method for designing vertical reinforcement to restrain longitudinal cracks in the end zones of girders. Their method was supported by a series of experimental results that agreed closely with their theoretical values.

Krishnamurthy (8) in 1970 developed expressions for obtaining maximum tensile stress on the end face of the beam and the stress distribution in the region. In order to reduce vertical tensile stresses in the end zone and to reduce the transmission length of prestressing wires, gradual transfer

U. Vasishth, Washington State Department of Transportation, Olympia, Wash. 98504. R. Y. Itani, Department of Civil and Environmental Engineering, Washington State University, Pullman, Wash. 99164.

should be used in the production of pretensioned beams. Krishnamurthy's equation predicted maximum stresses that compared well with the experimental results by Marshall and Mattock and those by Arthur and Ganguli.

Sarles and Itani (*9*) studied anchorage-zone stresses using linear elastic finite-element models. Their investigations were related, in particular, to the end blocks of WSDOT Series 10 and 14 girders. The study conclusions were that end blocks can safely be removed from such girders and that their use only serves to reduce the congestion of transverse vertical reinforcement.

The Sarles and Itani study was followed by laboratory and in-service testing of full-scale girders. The laboratory test included an evaluation of the performance of a Series 14 girder, whereas the in-service testing concentrated on measuring stresses in a Series 10 girder used in a bridge that was recently opened for traffic. The Series 10 girder was designed on the basis of the results of the laboratory test of the Series 14 girder. As mentioned earlier, the results obtained from both tests are described and presented in this paper.

LABORATORY TEST OF SERIES 14 GIRDER

The first part of the study was intended to establish the ultimate shear capacity of Series 14 girders without end blocks. Therefore, an attempt was made in the laboratory to cause shear failure in a 48-ft girder without end blocks. Details of the girder cross section are shown in Figure 1.

Each end of the girder was provided with a different type of vertical reinforcement (Figure 2) so that two separate tests could be conducted. The lightly reinforced end was called the unmarked end and the other end was referred to as the marked end. The reinforcement in the unmarked end was chosen to ensure shear failure whereas the marked end was designed
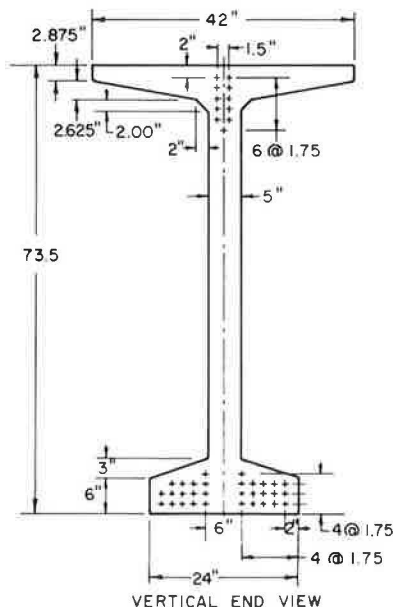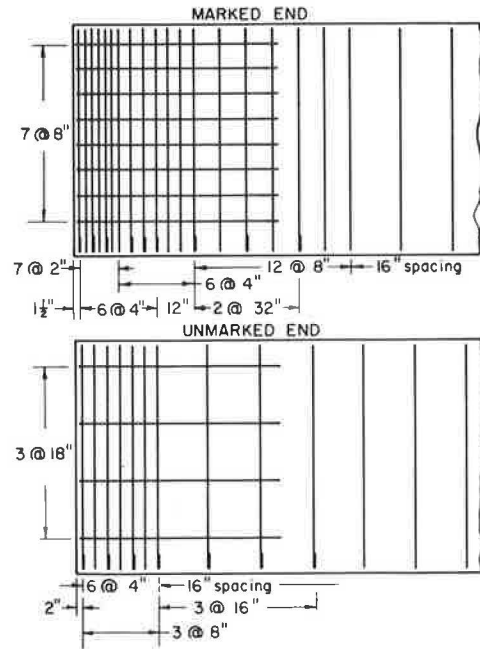
FIGURE 2   Steel reinforcement at the ends of Series 14 test girder.

according to AASHTO specifications and for an ultimate shear capacity of 400 kips. The WSDOT Series 14 girder is recommended for spans between 100 and 140 ft. The number of strands and the arrangement and profile of strands selected for this girder are identical to those used for a 110-ft long girder. Each of the 38 half-inch strands used (28 straight and 10 harped) was jacked to 28.9 kips.

Instrumentation of the girder consisted of both strain rosettes located on the concrete surface and strain gauges on stirrups and ties within the concrete. The gauges were placed so that the stress distribution from both prestress transfer and loading could be determined.

Seventeen SR-4 10-mm gauges were placed on seven stirrups at each end of the the test girder (Figure 3a and b). The gauges were located at points where maximum stresses in the steel stirrups were expected. For the first three stirrups from the ends, the gauges were placed 8, 22, and 36 in. from the bottom of the girder. The remainder of the instrumented stirrups contained only two gauges each, 8 in. and 36 in. from the bottom. For the marked end, the instrumented stirrups were placed $1\frac{1}{4}$, 6, 12, 22, 38, 70, and 102 in. from the end, whereas for the unmarked end, the instrumented stirrups were placed at 2, 6, 10, 22, 42, 74, and 106 in. Six 10-mm gauges were also mounted on ties confining the straight prestressing strands. Three instrumented ties in the marked end were located 2, 10, and 18 in. from the end, and in the unmarked end they were placed 2, 18, and 42 in. from the end. Reinforcing steel consisted of No. 4, Grade 60 bars.

Because of cost limitations, only the unmarked end of the girder was instrumented with concrete strain rosettes (Figure 3c). Twelve rectangular rosettes were placed in three rows of four, at distances of 2, 11, and 20 in. from the end of the girder. The rosettes were all located on the web region of the girder 10.5, 28.5, 46.5, and 64.5 in. from the bottom, forming a gridlike pattern.

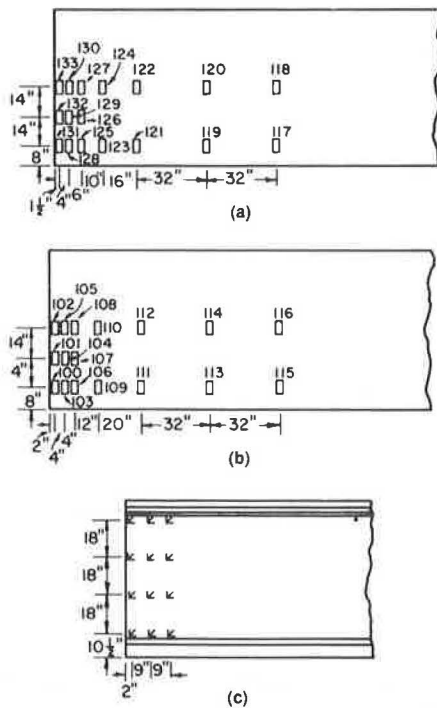FIGURE 1   Cross section of WSDOT Series 14 girder.

FIGURE 3 Locations of strain gauges and rosettes. (a) Location and number of stirrup strain gauges on marked end. (b) Location and number of stirrup strain gauges on unmarked end. (c) Location of rosettes on unmarked end.

The strains were recorded as the detensioning of the strands began. The only visible results from the prestress transfer test were two horizontal cracks in the unmarked end of the girder near the centroid and midway between the centroid and the bottom flange. These cracks were caused by tensile stresses resulting from the distribution of the concentrated compressive stresses at the end of the girder. The cracks were 0.1 and 0.06 mm wide and around 10 and 15 in. long. Because these cracks were not very long or wide, they were not expected to affect the performance of the girder under loading conditions and, in fact, did close. More than 15 girders with end blocks were inspected at detensioning. All of the girders exhibited cracks that were longer and wider than those observed in the test girder.

For the shear tests, the girder was placed on reinforced-concrete blocks topped with pin supports. On top of the support at the unmarked end was a $6 \times 1/4 \times 20$-in. Fabreeka pad, whereas on the other support was a frictionless Teflon pad, which caused it to behave like a roller. Therefore, the beam was simply supported.

The loading was induced by five hydraulic jacks that could be controlled manually to achieve specified end shears. These jacks were located closer to the end being tested to keep the other end from falling, and were also aligned symmetrically to prevent transverse bending or torsional stresses.

A shear test on the unmarked end was performed first. The 6-in. support was flush with the end of the girder, and the first 100-ton ram was located 10 ft from the end. The rest of the rams were spaced at 3-ft intervals, alternating between 30 and 100 tons. An initial load of 0.1 kip was applied to each jack, which combined with the dead weight of the girder to cause an initial end shear of 18.1 kips. The load was increased in stages, with strain readings taken between loadings (Table 1). At end shears of 44.7, 72.7, 101.0, and 128.5 kips, no changes were visible except that the cracks caused by the prestress transfer began to close. The girder sustained an approximate service load of 156.1 kips without any problems.

TABLE 1 TESTING OF UNMARKED END

Load Stage	Unmarked-End Shear (kips)	Comments
0	18.1	Splitting crack widths 0.004 and 0.0024 in.
1	44.7	No visible change
2	72.7	Splitting crack widths 0.002 and 0.002 in.
3	101.0	No visible change
4	128.5	Splitting crack widths less than 0.002 in.
5	156.1	Approximate service load; no visible change
6	183.9	Splitting cracks closed; diagonal crack appeared in bottom flange
7	212.0	Diagonal crack spread through web to approximately H/2
8	239.3	Diagonal crack grew in length and width; new crack formed parallel to first one
9	263.1	Girder failed in bearing/compression

NOTE: 1 in. = 25.4 mm.

The first sign of cracking occurred at an end shear of 183.9 kips when a diagonal crack appeared at the intersection of the web and bottom flange near the support. At this point, the shear stress was high because of the abrupt reduction in width of the cross section, and the longitudinal compression was reduced by the effect of the applied loads. Therefore maximum principal tensile stresses were produced, causing an inclined crack to form. As the load was increased to 212.0 kips, the diagonal crack extended through the web to a distance of about $h/2$. At 239.3 kips, the first crack continued to grow and a second crack formed parallel to the first one. As the load was increased to an end shear of 263.1 kips, the girder collapsed onto the floor. Although the girder was designed with a nominal shear of 300 kips, a maximum shear of only 260 kips was reached, which exceeded the ultimate design volume for many of the girders used. However, the failure was not caused by shear but rather by crushing of the concrete between the web and the bottom flange where the bearing area was not sufficient to carry the high compressive force. After the two cracks had opened, the load distribution at the edge-loaded short bearing did not represent actual design conditions. Subsequent to this failure, the beam was lifted and supported for the marked-end test.

For the marked-end test, the method of support was changed to simulate actual conditions and prevent failure due to bearing compression. The support width was doubled to 12 in. by using two 6-in. supports. A piece of plywood was used between the beam and the support to provide rotation. The support was also moved in from the end of the girder so that the centerline was 12 in. from the end. The girder was loaded in the same manner as in the unmarked-end test, except that the end shears were slightly less because of the shorter span

length. Again, strain readings were taken after each stage of the loading.

The load was increased from an initial end shear of 17.1 kips to 264.4 kips (Table 2) without any cracks or other problems. However, at an end shear of 291.7 kips, the reaction floor of the testing facility began to fail, so the loading was discontinued. No cracks were noticed.

TABLE 2   TESTING OF MARKED END

Load Stage	Marked-End Shear (kips)	Comments
0	17.1	Begin Test 3.1
1	43.5	No new cracks
2	71.3	No new cracks
3	99.5	No new cracks
4	126.7	No new cracks
5	154.3	No new cracks
6	181.9	No new cracks
7	209.3	No new cracks
8	237.0	No new cracks
9	264.8	No new cracks
10	291.7	Loading discontinued due to hold-down failure
0	17.2	Begin Test 3.2
11	153.5	No new cracks
12	181.0	No new cracks
13	208.0	No new cracks
14	235.6	Loading discontinued
0	17.3	Begin Test 3.3
15	152.3	No new cracks
16	179.5	Hairline diagonal crack
17	206.4	No new cracks
18	233.6	No new cracks
19	245.3	No new cracks
0	17.3	Cracks due to detensioning closed up

Stresses were computed from the strain readings. Several assumptions were made for analyzing the stresses. The researchers assumed that both the steel and the concrete were stressed within their elastic ranges and that the concrete remained uncracked. This latter assumption was unrealistic, and one should view the results of high principal stresses with caution. Another assumption was that the concrete behaved as an isotropic and homogeneous material. Because the strains were measured on an unstressed surface of the girder, a condition of plane stress existed. The combination of this condition with the assumption that deformations would be small made the condition of plane strain also valid. These assumptions provided the basis for analyzing the concrete stresses using the mechanics equations associated with linear elastic behavior, plane stress and strain, and Hooke's law. The stresses in the reinforcing steel were calculated by multiplying the strains by the modules of elasticity of the steel (29×10^6 psi).

FIELD TEST OF SERIES 10 GIRDER

The second phase of the study was to design and monitor the performance of a girder without end blocks during prestress transfer and under actual loading conditions. A bridge using Series 10 girders was selected for this purpose. An interior girder in one of the end spans was selected. The simply

supported end of the girder was designed without an end block. This end was monitored throughout the construction of the bridge.

Figures 4 and 5 show details of the girder. The particular end without an end block was provided with stirrup reinforcement similar to that used for the marked end of the girder used in the laboratory test.

The girder was instrumented with strain gauges on the reinforcing stirrups and strain rosettes on the surface of the concrete. Eight stirrups were instrumented, with the gauges located at points where cracks were most likely to develop (Figure 6). The first two stirrups, $1\frac{1}{2}$ and $5\frac{1}{2}$ in. from the end, each carried four strain gauges. The third, at $9\frac{1}{2}$ in., had three gauges, whereas the remainder, located at $15\frac{1}{2}$, $43\frac{1}{2}$, $63\frac{1}{2}$, and $91\frac{1}{2}$ in., each had two gauges. The gauges near the end were for determining the stresses induced by prestress transfer, whereas the gauges starting $43\frac{1}{2}$ in. from the end were provided mainly for monitoring the tensile stresses induced by shear.
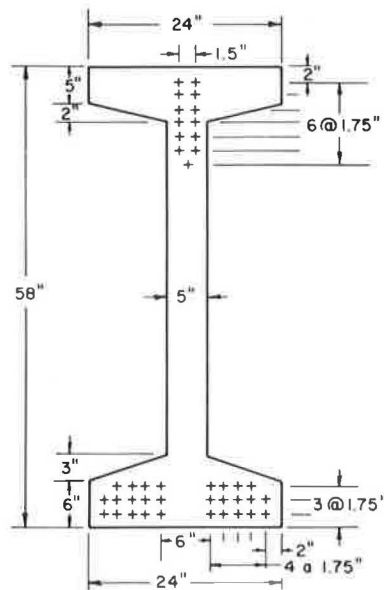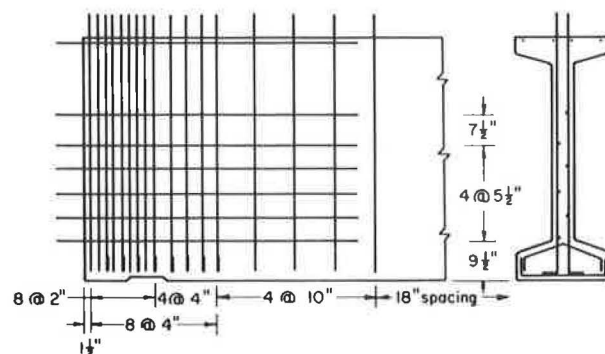

FIGURE 4   Cross section of WSDOT Series 10 girder.

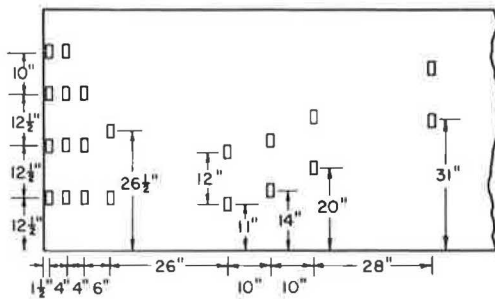**FIGURE 5   Details of steel reinforcement for Series 10 girder.**

FIGURE 6 Locations of gauges on stirrups.

Strain rosettes were installed on the surface of the concrete (Figure 7) before the prestressed strands were detensioned. Readings were taken during detensioning and after completion of the prestress transfer.

Approximately 28 days later the girder was transported to its proper location. Strain gauge readings were recorded after the 7¹/₂-in. concrete slab was placed. The resulting stresses were the most critical when the slab concrete was still wet.
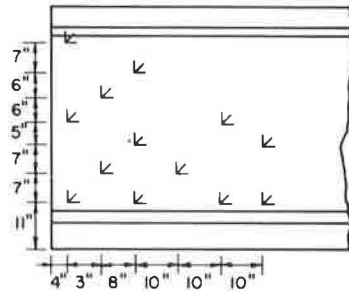

FIGURE 7 Locations of rosettes on concrete.

After the slab was cast, the final test was to place a known live load on the bridge and record the strains. The vehicle used for this purpose consisted of a cab and trailer on five axles. One axle was located under the cab and two sets of axles were under each end of the trailer. The spacing between the axles was 14.6, 4.3, 22, and 4.3 ft. The truck was weighed, and the gross vehicle weight was determined to be 78.6 kips. Each of the back axles weighed 17.1 kips, with the axle under the cab weighing 10.2 kips. The first strain reading was taken with the rear axle of the truck located directly over the end of the girder without an end block. This reading was followed by ones in which the axle was 5, 10, 25, 50, and 75 ft from that end. Strain readings were also taken with the rear axle of the truck located 10 and 5 ft from the opposite end of the girder, as well as 5, 10, and 25 ft from the end of the adjacent continuous span.

DATA REDUCTION

The collection of data from the strain gauges began during detensioning. The only noticeable effect during the prestress transfer was that the girder cambered upward, with a maximum deflection of 1 in. at the midspan. Also, a slight crack formed near the centroid of the girder end. With a length of

only 13 cm and a width of 0.1 mm, the crack would not have been detrimental to the service load capacity of the girder.

The stresses in the steel and the concrete were computed from strain data recorded by methods similar to those used in the laboratory tests. The modules of elasticity for concrete were obtained by using the following equation:

$$E_{ct} = 33w^{15} (f_c')t$$

where w was the weight of the concrete, assumed to be 155 pcf, and $(f_c')t$ was the compressive strength at the the time of interest. Poisson's ratio was assumed to be 0.2.

The strain readings recorded after the roadway slab was placed were increased by 6 percent because the zero reading was taken when the steel was already in place.

These stress values were obtained only for the slab load and were later combined with the stresses obtained after the prestress transfer. When these two stresses were superimposed, the latter was reduced by 25 percent to account for a loss in prestress due to creep and shrinkage of the concrete and relaxation of the prestressing steel. The strains recorded for the truck load test were very small.

RESULTS

The stresses computed for the laboratory test and the field test were compared with the appropriate AASHTO specifications for limited stresses in concrete and steel.

The variation of maximum tensile stress in the stirrups versus their distance from the end of the girder in the laboratory test is shown in Figure 8 for the marked end of the girder. The plot for the unmarked end showed a maximum stress of around 22,000 psi at the end, which decreased to zero at the approximate transfer length. The plot of the marked end indicates that the tensile stress was much less at that end of the girder, around 15,000 psi. However, it did not follow the same pattern as that of the unmarked end, perhaps because of the heavy vertical reinforcement.
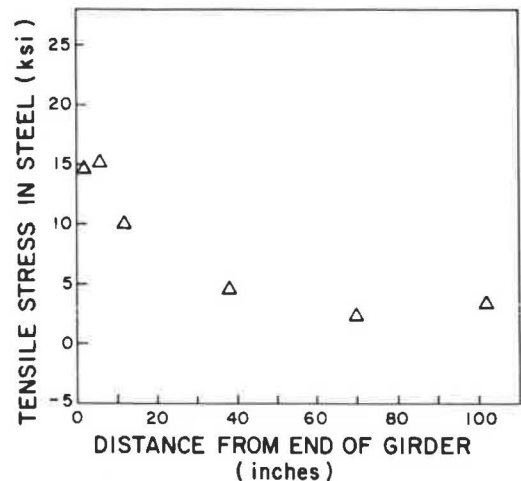

FIGURE 8 Stirrup stresses in marked end caused by prestress transfer.

During the shear test of the unmarked end, high tensile stresses were recorded for gauges 106, 109, 111, and 114 at an end shear of 239.3 kips, the final reading before failure. These agreed well with the locations of the cracks that formed (Figure 3 and Table 3). A compressive stress of around 35 ksi was indicated by the gauges located closest to the lower corner of the girder. This high stress confirmed that failure of the unmarked end was caused by the concrete at the support.

The shear test of the marked end did not produce any critical stresses in the end region of the girder (Figure 3 and Table 4). Only Gauge 121 measured tensile stress, which was well within the allowable tensile stress for the service load design of 24,000 psi for Grade 60 reinforcement. The rest of the gauges measured compressive stresses that were well above the support, but not of critical magnitude.

During the prestress transfer, the highest tensile and compressive principal stresses in the concrete were located near the bottom flange and slightly in from the end of the girder (Figure 9). (Unreliable stress values are indicated in Figures 9–12 by an asterisk.) These stresses were probably the combined result of bursting stresses produced by the straight prestressing strands and compressive stresses produced by the vertical reaction from the dead load of the girder. The magnitude of the compressive stress was well within the allowable limit (3,249 psi); however, the tensile stress exceeded the allowable limit (552 psi) by almost 800 percent. With that much stress, a microcrack forms, and the bonded steel reinforcement takes up the tensile stresses. Computations of stresses in the concrete became meaningless.

Figure 10 shows the principal stresses induced by the final stage of loading before the unmarked end of the girder failed. Tensile and compressive stresses exceeding their allowable values (557 and 3,249 psi) were indicated by the two gauges located near the bottom flange of the girder. The high principal compressive stress above the support again confirmed that failure of the unmarked end was caused by the crushing of the concrete in this area.

Finally, stresses caused by prestress transfer and the stresses at a simulated maximum service load shear of 156.1 kips were
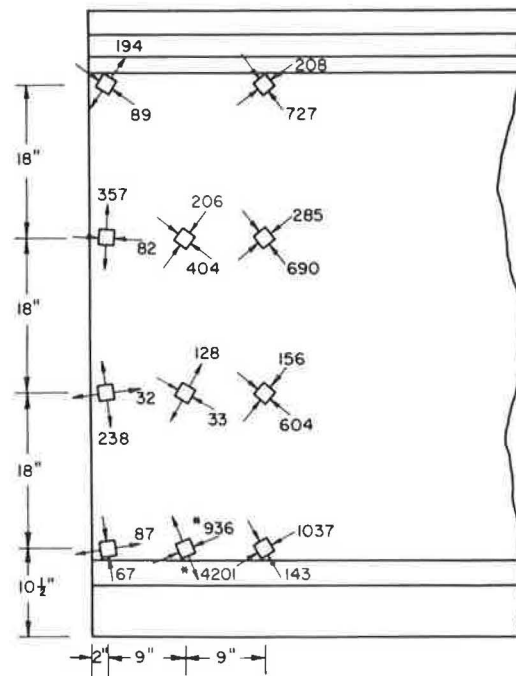

FIGURE 9 Principal stresses in concrete caused by prestress transfer (asterisk indicates unreliable value).

superimposed to give the principal stresses. The only principal stress that exceeded the allowable value was the tensile stress of 2,687 psi. However, this did not take into account losses due to creep and shrinkage of the concrete, or relaxation of the prestressing strands. Because the total losses were assumed to be 25 percent of the initial stresses, the horizontal, vertical, and shearing stresses (x, y, and xy) during the prestress transfer were reduced accordingly. These were again combined with the service load stresses to produce the principal stresses shown in Figure 11. This caused the highest principal tensile stress to decrease to 1,687 psi. Although it still exceeded the allowable value, this stress was greatly reduced from its initial

TABLE 3   STRESSES IN STIRRUPS DURING UNMARKED-END TEST

Gauge	Stress (psi) by End Shear (kips)								
	18.1	44.7	72.7	101.0	128.5	156.1	183.9	212.0	239.3
100	0	−3,538	−7,308	−11,165	−15,254	−19,720	−30,305	−40,339	−54,549
101	29	−3,161	−7,540	−10,556	−13,311	−15,660	−19,720	−22,707	−25,781
102[a]	−	−	−	−	−	−	−	−	−
103	87	−3,552	−5,278	−7,946	−10,614	−12,644	−16,530	−20,445	−25,230
104	0	−3,538	−7,482	−10,005	−12,122	−13,978	−17,225	−19,633	−22,069
105	58	−2,813	−6,612	−9,715	−12,093	−14,065	−17,110	−18,966	−20,735
106	29	−1,624	−2,929	−3,886	−4,524	−3,248	−5,394	10,266	10,382
107	29	−2,233	−4,872	−6,554	−8,149	−9,454	−11,745	−13,137	−14,442
108	29	−1,798	−4,524	−6,873	−8,584	−9,860	−11,890	−13,311	−14,442
109	0	−2,610	1,305	−4,350	−1,305	435	11,774	27,492	55,419
110	87	−841	−1,914	−2,956	−3,451	−3,799	−4,031	−3,712	−3,393
111	0	−203	−145	−145	−116	203	58	203	25,143
112	29	−203	−261	−522	−551	−174	−696	−464	696
113	29	−261	−145	−377	−464	−406	−406	−406	−377
114	29	−116	0	−87	−29	145	145	10,034	35,409
115	928	783	6,815	4,582	4,350	8,249	2,291	1,537	5,974
116	58	−203	−116	−145	−203	−145	−464	−406	2,958

[a]Not functioning.

TABLE 4   STRESSES IN STIRRUPS DURING MARKED-END TEST

Gauge	Stress (psi) by End Shear (kips)										
	17.1	43.4	71.3	99.5	126.7	154.3	181.9	109.3	237.0	264.8	291.7
117	−58	−522	−638	−551	−725	−667	−812	−696	−580	−1,160	−667
118	29	0	0	0	−174	−145	−116	−145	−116	−261	−551
119	0	0	−145	−203	−435	−522	−522	−638	−609	−5,220	−580
120	0	0	0	0	0	0	0	0	0	0	29
121	0	174	0	0	−174	−116	0	145	290	377	725
122	−58	0	−232	−435	−696	−783	−783	−986	−1,044	−1,131	−1,131
123	0	−580	−1,769	−3,074	−4,727	−6,003	−8,207	−7,859	−8,671	−9,570	−1,044
124[a]	−	−	−	−	−	−	−	−	−	−	−
125[a]	−	−	−	−	−	−	−	−	−	−	−
126	0	−1,479	−3,509	−5,075	−6,641	−7,540	−8,460	−8,512	−10,353	−11,368	−12,470
127	−29	−406	−1,044	−1,769	−2,668	−3,219	−3,886	−4,437	−4,959	−5,597	−6,380
128	−29	−1,769	−4,321	−6,090	−7,917	−9,077	−10,498	−11,774	−1,305	−14,297	−16,240
129	0	−1,421	−3,741	−5,684	−7,511	−8,044	−9,396	−10,556	−11,571	−12,702	−14,036
130[a]	0	0	0	0	0	0	0	0	0	0	0
131	−58	−1,856	−4,437	−6,119	−7,424	−8,625	−9,280	−10,237	−11,049	−12,064	−13,311
132	−29	−1,450	−3,828	−5,771	−7,453	−8,613	−9,918	−11,136	−11,716	−13,166	−14,500
133	−116	−1,102	−2,552	−3,915	−5,452	−6,264	−7,395	−8,352	−8,961	−9,918	−10,904

[a]Not functioning.
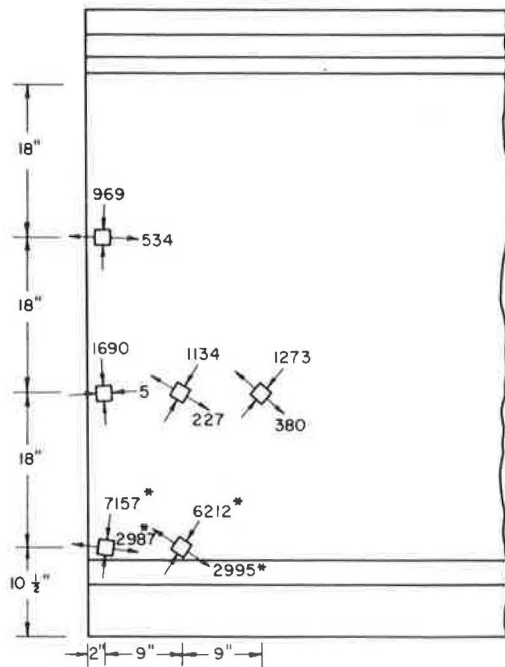
FIGURE 10   Principal stresses in concrete
caused by a shear of 260 kips (asterisk indicates
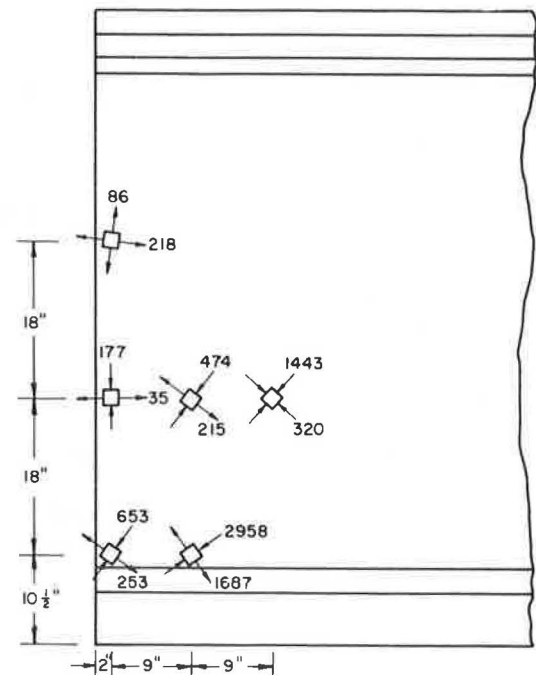unreliable value).

FIGURE 11   Principal stresses in concrete caused
by superposition of prestress transfer and service
load with reduction for losses.

value after detensioning of 4,201 psi. A tensile stress of this magnitude indicates that a crack has probably formed and that the bonded steel reinforcement is being stressed.

The highest stress in the steel stirrups was 13.5 kips for the field test girder. The highest stress was located in the stirrup closest to the end face of the girder and decreased to a minimum at a distance approximately equal to the transfer length from the end of the girder. A maximum stress of around 15,000 psi was recorded when the girder was picked up; however, this was well within allowable limits, and it also decreased when the girder was placed on supports.

The principal stresses due to prestress transfer and their orientations were recorded at the end of the girder. Many of

the principal tensile stresses exceeded the allowable value. This was the result of microcracks forming in the concrete because of tensile stresses. However, visual inspection of the end of the girder indicated no visible cracks in these areas. The principal compressive stresses were well within the allowable limit, indicating that the end of the girder was capable of handling the transfer of prestress effectively, without the need for an end block. The principal stresses induced by the addition of the slab were rather small, except at three of the gauges. The high compressive stresses are probably caused by the reaction of the bearing, which was 13 in. wide, with the centerline located 15 in. from the end of the girder. However,

these stresses did not represent the actual condition. To get an idea of the actual stress condition, it was necessary to combine these stresses and the stresses at prestress transfer.

Figure 12 shows the principal stresses due to a combination of prestress transfer stresses and stresses from the addition of the roadway slab. The principal stresses in Figure 12 are adjusted for a 25 percent loss in prestressing. A comparison of these with the AASHTO allowable stresses of 3,112 psi compression and 529 psi tension revealed that a few of the stresses exceeded the limits. According to Lin (10), the compressive stresses on which the girder design is based are horizontal stresses, although the principal compressive stresses at that point are somewhat greater in magnitude. Whenever the principal tensile stress indicated by the rosette gauge was greater than 1,058 psi $[= 12 \, (f_c')^{1/2}]$, a surface tension crack probably existed under the strain gauge. In such a case both the principal stresses, tension and compression, obtained from that rosette gauge were unreliable. The tensile stresses that exceeded the allowable value are not critical because when the concrete cracks, the tensile force is transferred to the stirrups.
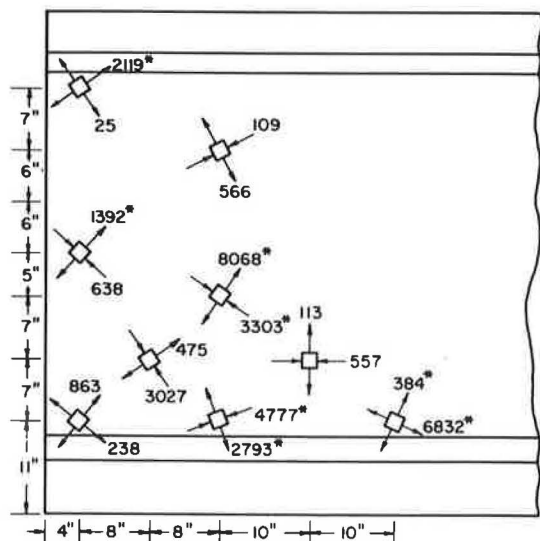
FIGURE 12 Principal stresses caused by superposition of prestress transfer and slab stresses with reduction for losses for Series 10 girder (asterisk indicates unreliable value).

The strains recorded for the truck loading on the girder were rather small. Strain gauges mounted on the stirrups indicated strains in the steel ranging from +10 microstrains to 0.35 microstrain, with 70 percent indicating compression (−). This converts to a range in stress from 290 psi tension to 1,015 psi compression for the stirrups.

Similarly, the strains indicated by the rosettes on the concrete ranged from a maximum tensile strain of +20 microstrains to a maximum compressive strain of 0.12 microstrain. Conversion of the strains into principal stresses produced values ranging from 183.9 psi in tension to 98.1 psi in compression; both extremes occurred when the rear of the truck was located at or near the end of the girder.

CONCLUSION

The results of the ultimate load test indicated that the modified ends perform effectively under both prestress transfer and service load conditions. The vertical stirrup reinforcement designed according to AASHTO shear and anchorage-zone requirements is an effective replacement for end blocks. The ties and longitudinal reinforcement are not affected by the change, and are therefore provided according to standard practice.

Production of the Series 10 and 14 girders for this project proved that steel placement and compaction of concrete in the end regions were possible with a 5-in. web.

Of interest to this project is the investigation of horizontal cracking in the end regions of WSDOT series girders. The perception that end blocks reduce horizontal cracking caused by detensioning of the prestressing strands is incorrect. However, examination of a random sample of approximately 15 Series 10 and 14 girders with end blocks showed that the end regions of all the girders contained as many as two to five cracks, with widths ranging from 0.2 to 0.3 mm (0.008 to 0.012 in.). The Series 10 and 14 girders without end blocks each had only one or two cracks 0.1 mm wide (0.004 in.) or less. Therefore, the modified design is effective in reducing the creation of cracks during prestressed transfer.

Finally, the removal of end blocks from WSDOT's simple span, pretensioned concrete girder series is not only possible and desirable but also economical, and would result in thousands of dollars in savings each year.

IMPLEMENTATION

As a result of this research project, end blocks have been eliminated in simple span, prestressed concrete girders and at the free end of continuous girders. Details of the reinforcing steel in the current, standard WSDOT Series 14 girder are similar to those used for the test girders.

FUTURE RESEARCH

A research project to determine whether the end blocks from continuous girders can be eliminated is currently under way. A full-scale specimen has been tested to a force of 500 kips. The results are not yet available.

ACKNOWLEDGMENTS

REFERENCES

1. W. T. Marshall and A. H. Mattock. Control of Horizontal Cracking in the Ends of Pretensioned Prestressed Concrete Girders. *PCI Journal*, Vol. 7, No. 5, Oct. 1962, pp. 56–74.
2. P. Gergely, M. A. Sozen, and C. P. Seiss. *The Effect of Reinforcement on Anchorage Zone Cracks in Prestressed Concrete Members*. Structural Research Series 271. University of Illinois, Urbana, July 1963.
3. P. D. Arthur and S. Ganguli. Tests on Endzone Stresses in Pretensioned Concrete I-Beams. *Magazine of Concrete Research*, Vol. 17, No. 51, June 1965, pp. 85–96.
4. W. T. Marshall. A Theory for End Zone Stresses in Pretensioned Concrete Beams. *PCI Journal*, Vol. 11, April 1966, pp. 45–51.
5. H. Sievers. Stress Conditions in the Vicinity of Anchorage Plates in Prestressed Tendons of Prestressed Concrete Structural Units. *Der Bauingenieur*, Vol. 31, No. 4, 1965, pp. 134–135.
6. N. M. Hawkins. Behavior and Design of End Blocks for Prestressed Concrete Beams. *Civil Engineering Transactions* (Institution of Engineers, Australia), Vol. CE8, No. 2, Oct. 1966, pp. 193–202.
7. P. Gergely and M. A. Sozen. Design of Anchorage Zone Reinforcement in Prestressed Concrete Beams. *PCI Journal*, Vol. 12, No. 2, April 1967, pp. 63–75.
8. D. Krishnamurthy. A Method for Determining the Tensile Stresses in the End Zones of Pretensioned Beams. *Indian Concrete Journal*, Vol. 45, No. 7, July 1971, pp. 286–297 and 315.
9. D. Sarles and R. Y. Itani. Anchorage Zone Stresses in Prestressed Concrete Girders. *PCI Journal*, Vol. 29, No. 6, Nov./Dec. 1984, pp. 100–114.
10. T. Y. Lin. *Design of Prestressed Concrete Structures*, 2nd ed. John Wiley & Sons, Inc., New York, 1963, p. 213.

Seismic Design of High-Strength-Concrete Bridge Piers and Columns

ROBERT L. CHEN AND JOHN A. VAN LUND

The structural design applications and mechanical properties of high-strength concrete (HSC) are briefly reviewed. Analytical design studies of reinforced HSC bridge piers and columns subjected to static and seismic loadings are presented. Flexible and rigid foundation systems are incorporated into the analysis. The results of this study show that the use of HSC will reduce column size and stiffness. As the columns become more flexible, seismic shears and moments are reduced. Cost estimates show that the use of HSC with minimum reinforcing steel provides the most economical solution for bridge piers and columns. Economy is also achieved because smaller foundations can be used.

The production and placement of high-strength concrete (HSC) in either precast or cast-in-place (CIP) construction using conventional materials and methods with close cooperation among the engineer, contractor, concrete producer, and testing agency are technically and economically feasible (1-16).

HSC with a 28-day uniaxial compressive strength, $f'c$, of 6,000 to 14,000 psi (41.4 to 96.6 MPa) is rapidly gaining acceptance in building design in the United States. When used in buildings, the number of columns and their sizes can be reduced, resulting in two economic advantages to the building owner: (a) more space to lease and (b) lower construction costs (1-3). If HSC can be produced and placed by the building construction industry, the bridge construction industry should be able to do the same.

With some exceptions, bridge designers in the United States have been slow to accept HSC and are still specifying strengths of 3,000 and 4,000 psi (20.7 and 27.6 MPa) for concrete. Normal-strength concrete (NSC) has a 28-day compressive strength ranging from 3,000 to 6,000 psi.

Nearly 20 years ago, HSC with a strength of 6,000 psi was used in the on-site fabrication of the precast posttensioned concrete T-beams used for the Willows Bridge in Toronto, Ontario, Canada (4).

In today's precast prestressed concrete industry, bridge girders can be produced utilizing HSC under manufacturing plant conditions. In the Pacific Northwest, precast prestressed concrete bridge girders with strengths as high as 7,000 and 9,000 psi (48.3 and 62.1 MPa) have been used (5, 6). The majority of precast prestressed girder bridges designed by the Washington State Department of Transportation (WSDOT) have concrete with a 28-day strength of 6,000 psi, with 5,000 psi (34.5 MPa) permitted at the strand release. On the Pasco-

Washington State Department of Transportation, Transportation Building, Olympia, Wash. 98504.

Kennewick cable-stayed bridge over the Columbia River in eastern Washington, the precast prestressed girder segments had an average 28-day strength of 7,500 psi (51.7 MPa) based on a specified 6,000-psi design mix (7).

The current upper limit for CIP concrete in U.S. bridge construction appears to be 6,000 psi. Concrete with this strength has been used successfully on several major bridge projects to reduce the size and weight of structural elements. On the Houston Ship Channel bridge, the subcontractor substituted 5,500-psi (37.9-MPa) concrete for the pier construction and 6,000-psi concrete for the CIP posttensioned box girders. Originally, concrete with a strength of 3,600 psi (24.8 MPa) had been specified for the substructure and concrete with a strength of 5,000 psi for the superstructure (8). On the East Huntington cable-stayed bridge over the Ohio River, concrete with a 28-day strength of 8,000 psi (55.2 MPa) was specified for the precast hybrid concrete-and-steel deck segments and 6,000 psi for the CIP "wishbone" tower (9, 10).

In 1979, FHWA, through the U.S. Department of Transportation, authorized a study, Applications of High Strength Concrete for Highway Bridges (11, 12). This study explored the potential for using HSC in precast prestressed girder beams, bulb-tees, posttensioned box girders, segmentally posttensioned box girders, compression members, and thin-walled precast plate elements. In addition, a square hollow pier was tested. The study concluded that HSC permitted the use of longer spans, reduced dead loads, and provided higher load capacities.

Society expects aesthetically pleasing and durable structures that combine strength with simplicity for the least cost. Furthermore, these structures should be relatively maintenance free. HSC will satisfy these needs. Would the use of HSC in bridge construction result in more economical bridge structures? This paper examines one aspect of that question, the design of bridge piers and columns subject to static and seismic loadings.

MECHANICAL PROPERTIES OF HSC

Some of the mechanical properties of HSC are different from those of NSC. A brief summary follows.

Stress-Strain Behavior

As shown in Figure 1, the slope of the ascending part of the stress-strain curve is more linear and steeper up to a higher stress/strength ratio, the strain at maximum stress level is
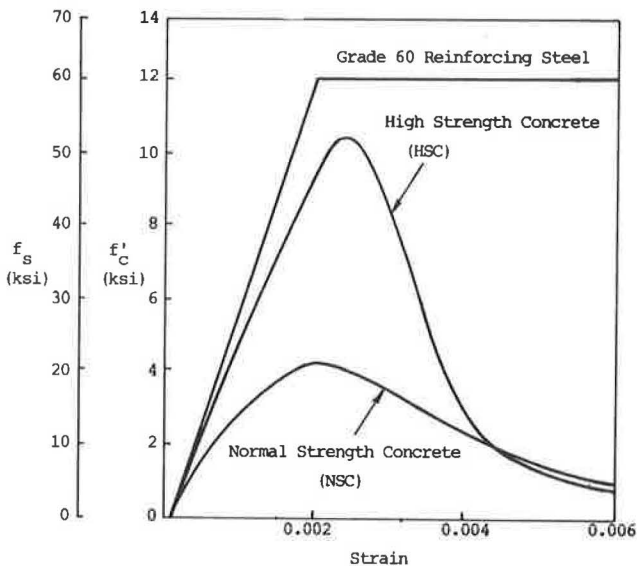
FIGURE 1 **Stress-strain curves for steel reinforcement and concrete.**

higher, and the slope of the descending portion of the curve is steeper when compared with the curve for NSC (*13, 16–18*).

Poisson's Ratio

The value of Poisson's ratio is in the range of 0.20 to 0.28 for normal-weight HSC; it is independent of compressive strength, coarse aggregate size, and age of specimen (*13, 16, 19*).

Static Modulus of Elasticity

For concrete with a dry unit weight of 145 lb/ft^3 (2320 kg/m^3), the 1983 ACI Building Code (ACI 318-83) recommends the following equation for predicting the static modulus of elasticity of concrete (*20*):

$$Ec = 33\,w^{1.5}(f'c)^{0.5} \quad \text{or} \quad 57{,}000\,(f'c)^{0.5} \quad \text{(psi)} \tag{1}$$

For other dry unit weights, Equation 1 can be used in the following form:

$$Ec = 57{,}000\,(f'c)^{0.5}\,(w/145)^{1.5} \tag{2}$$

For concrete with compressive strengths over 6,000 psi, this equation overestimates the value of Ec by as much as 15 percent.

For concrete with a dry unit weight of 145 lb/ft^3 and a compressive strength over 3,000 psi and less than 12,000 psi (82.8 MPa), a better correlation can be obtained from the following expression (*13*):

$$Ec = [40{,}000\,(f'c)^{0.5} + 1.0 \times 10^6]\,(w/145)^{1.5} \tag{3}$$

Equation 3 is valid for lightweight concrete, 90 to 145 lb/ft^3 (1440 to 2320 kg/m^3), when the compressive strength is between 3,000 and 9,000 psi.

Other empirical equations for predicting the modulus of elasticity are (*21*)

$$Ec = w^{2.5}(f'c)^{0.325} \quad \text{(psi)} \tag{4}$$

$$Ec = 27.55\,w^{1.5}(f'c)^{0.5} \quad \text{(psi)} \tag{5}$$

Tensile Strength

For concrete with a compressive strength between 3,000 and 12,000 psi, ACI Committee 363 recommends the following empirical equations to predict the average modulus of rupture ($f'r$) and tensile splitting strength ($f'sp$) (*17*):

$$f'r = 11.7\,(f'c)^{0.5} \quad \text{(psi)} \tag{6}$$

$$f'sp = 7.4\,(f'c)^{0.5} \quad \text{(psi)} \tag{7}$$

Other empirical expressions that give lower tensile strengths than those proposed by ACI Committee 363 are (*18, 21*)

$$f'r = 2.30\,(f'c)^{2/3} \quad \text{(psi)} \tag{8}$$

$$f'sp = 4.34\,(f'c)^{0.55} \quad \text{(psi)} \tag{9}$$

Effects of Confinement Reinforcement

Transverse reinforcing steel places lateral confining pressure on the concrete core, which is in a state of triaxial stress. This increases the axial strength and strain capacity of the concrete, causing the column to exhibit a ductile, post-peak-strength behavior. Therefore, HSC columns, together with adequate reinforcing steel, can withstand seismic forces.

For normal-weight HSC, the axial strength of a confined column can be determined from the following expression (*17*):

$$f''c = f'c + 8.0 Asp \times fsp\,(1 - S/D)/SD \tag{10}$$

where

$f''c$	=	compressive strength of confined column,
$f'c$	=	compressive strength of unconfined column,
Asp	=	area of confinement reinforcement,
fsp	=	actual stress in confinement reinforcement at maximum load,
S	=	spacing of confinement reinforcement, and
D	=	core diameter of column.

ANALYTICAL DESIGN STUDY

Slenderness Effects

A state-of-the-art survey conducted by Poston et al. (*22*) indicated that multiple-pier bents accounted for 83 percent of the bridge piers used and single-pier bents accounted for 17 percent. The use of solid cross sections was much more prevalent than hollow cross sections. However, the study found that the use of hollow cross sections increased dramatically with height (*22*). The use of HSC in lieu of NSC will reduce the column cross section and stiffness. The magnification of moment due to this increase in slenderness for compression members not braced against sidesway must be considered in the design. When the slenderness ratio, l/r, exceeds 100, both the AASHTO Specifications (*23*) and the ACI Building Code 318-83 (*20, 24*) recommend a second-order frame analysis that considers sidesway, nonlinear effects due to cross-section cracking, creep, and stress-strain behavior of the concrete.

Note that the significantly lower creep coefficient and increased modulus of elasticity of HSC will affect the value of the effective flexural rigidity, *EI*.

HSC Column Design

Static Analysis

As shown in Table 1, the axial load capacity for a column with a constant cross section can be increased twofold or more when the concrete compressive strength is increased from 4,000 to 12,000 psi, depending on the slenderness ratio.

For the column subjected to axial load and biaxial bending, increases in the bending moments are possible with HSC. As the interaction diagram in Figure 2 shows for an axial load of 1,620 kips (7,205 kN) on a 5- by 7-ft (1.5- by 2.1-m) cross section, the nominal transverse moment capacity increases 20 percent and the nominal longitudinal moment capacity increases 10 percent. These increases occur when the concrete compressive strength is increased from 4,000 to 12,000 psi.

When slenderness effects are considered, the use of HSC is beneficial. Figure 3 shows the interaction diagram for a 6- by 6-ft (1.8- by 1.8-m) column using NSC with $f'c = 4,000$ psi and HSC with $f'c = 12,000$ psi for various slenderness ratios. This illustrates that compression members are an excellent application for HSC. Smaller cross sections can be used for a given member, or fewer members can be used. In addition to weight, material costs are reduced.

Seismic Analysis

The bridge shown in Figure 4 was subjected to seismic motion to study the effects of using HSC in the columns. Concrete compressive strengths ranged from 4,000 to 12,000 psi, with data obtained at every 2,000-psi (18.3-MPa) interval. The column cross sections corresponding to the appropriate value of concrete compressive strength are shown in the lower part of Figure 4 and in Figure 5.

A three-dimensional response spectrum analysis using the computer program SEISAB (Seismic Analysis of Bridges) was performed for each column cross section and compressive strength to obtain the overall response of the structure. SEISAB contains both single-mode and multimodal response spectrum techniques and includes a linear transient analysis capability (25). To understand the influence that the foundation type has on the overall response of the structure, flexible (vertical-pile) and rigid (battered-pile or drilled-shaft) foundation systems were modeled by introducing low and high foundation spring constants into the analysis. The unreduced ground response spectrum used in the analysis is shown in Figure 6.

Vibration Characteristics

A comparison of the vibration characteristics of the bridge structure for the different column concrete strengths is shown

TABLE 1   AXIAL LOAD CAPACITY FOR 5 × 7-FT RECTANGULAR PIER

Slenderness Ratio, l/r	Concrete Strength (ksi)	e=0 P/P4	e=0.1D* P/P4	e=0.2D* P/P4
0	4	1.00	1.00	1.00
	8	1.88	1.85	1.80
	12	2.76	2.65	2.60
50	4	1.00	1.00	1.00
	8	1.85	1.81	1.72
	12	2.68	2.65	2.50
100	4	1.00	1.00	1.00
	8	1.75	1.60	1.40
	12	2.43	2.25	2.05

Note: P4 — Axial load capacity of pier with 4,000 psi concrete compressive strength and 32-#11 reinforcing bars

ϕ factor — 0.90-0.2 P_u/0.1Agf'c
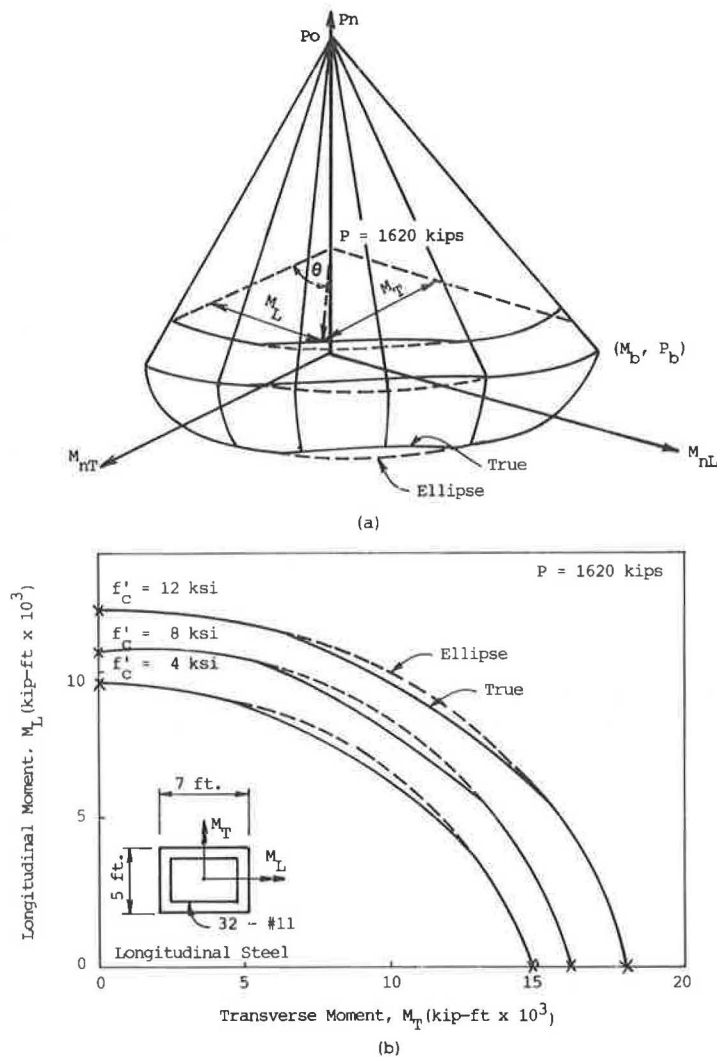
* — eccentricity in the weak direction

FIGURE 2 Biaxial bending on pier: (a) interaction diagram; (b) moment contour at axial load of 1,620 kips.

in Figure 7. As the column strength increases, the natural period of the structure increases and the Elastic Seismic Response Coefficient (ESRC) decreases. ESRC is commonly thought of as the ratio of transverse inertia force to static dead load and is used as a comparison with other bridges with similar characteristics that have been previously analyzed.

The ESRC is lower for the bridge with a flexible foundation than for the one supported by a rigid foundation. The flexible foundation system effectively lengthens the columns of bridges supported by such a foundation system.

Displacement

A comparison of the Complete Quadratic Combination (CQC) displacements at the top of Pier 4 for the different concrete strengths is shown in Figure 8. The data presented show that higher displacements result when the concrete strength of the columns is increased. As expected, the displacement at the top of the column supported by the flexible foundation exceeds the displacement when a rigid foundation is used. The higher values of the displacement for slender columns with a flexible

foundation imply that the moment magnifier for these columns will be increased.

Forces and Moments for Columns and Foundations

Figure 9 shows how the shears and moments at the top of Pier 4 vary as the concrete strength is increased. The reduction is much higher for the rigid foundation system than for the flexible foundation system. When a comparison is made between the flexible and the rigid foundation systems, the shears and moments of the flexible foundation system are much less than those of the rigid foundation system. This is because the flexible foundation provides less stiffness to the columns and overall system than the rigid foundation; consequently, less inertial force is attracted to these flexible columns. However, as the concrete strength approaches 12,000 psi, it appears that the foundation stiffness makes less difference in the top of column shears and moments.

Bending deformations in rigid foundation systems will generate high reaction force. Figure 10 shows that the reduction in
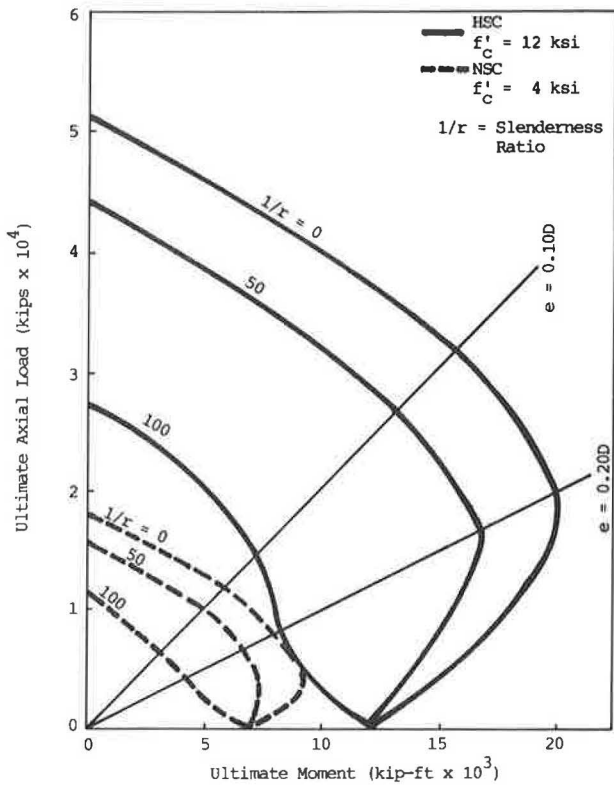
FIGURE 3 Interaction diagram for 6- by 6-ft (1.8- by 1.8-m) column.

the seismically induced axial force at the top of the pile is much greater for the rigid foundation system when compared with that for the more flexible foundation system. This is due to the transmission of lower foundation forces and bending moments from the flexible columns. On the other hand, the

large relative lateral displacements of the flexible foundation system induce high bending moments at the top of the piles.

Economic Considerations

The current economic situation places increasing pressure on designers to use stronger materials. In most concrete structures, the cost of materials amounts to a small percentage of the total cost. To examine the savings of using HSC over NSC, cost estimates for the columns of the bridge shown in Figure 4 were computed and are shown in Figure 11. The column dimensions and concrete strengths used are those shown in the lower part of Figure 4. Longitudinal steel varied from 1 to 4 percent. Typical material costs for comparison purposes are as follows (1):

Description	Unit Price
Reinforcing steel ($/lb)	0.40 (or $800/ton)
Concrete ($/yd^3)	
4,000 psi	45
6,000 psi	59
8,000 psi (1)	82
10,000 psi	102
12,000 psi	124
14,000 psi (1)	145
Formwork ($/ft^2)	3

For the rigid foundation system and using Figure 11, the cost per foot for the 5-ft by 7-ft 4,000-psi cross section with 48 No. 11 reinforcing bars (1.5 percent) is $285/ft and for the 3-by 4-ft (0.9- by 1.2-m) column cross section using 12,000-psi concrete with 28 No. 11 reinforcing bars (2.5 percent) is $190/ft. The difference is $95/ft, for a 33 percent savings in material cost. As shown, the use of HSC is more cost-effective in piers and columns with the smallest cross-sectional area and minimum reinforcing steel.
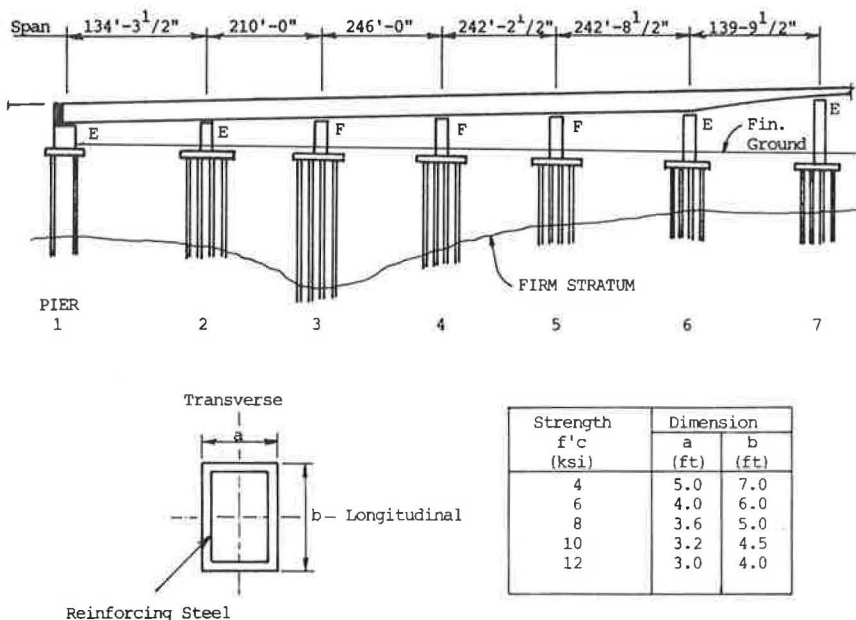

Strength f'c (ksi)	Dimension	
	a (ft)	b (ft)
4	5.0	7.0
6	4.0	6.0
8	3.6	5.0
10	3.2	4.5
12	3.0	4.0

FIGURE 4 *Top:* Elevation of bridge used in seismic analysis. *Bottom:* Pier cross-section dimensions and concrete compressive strength used in seismic analysis.
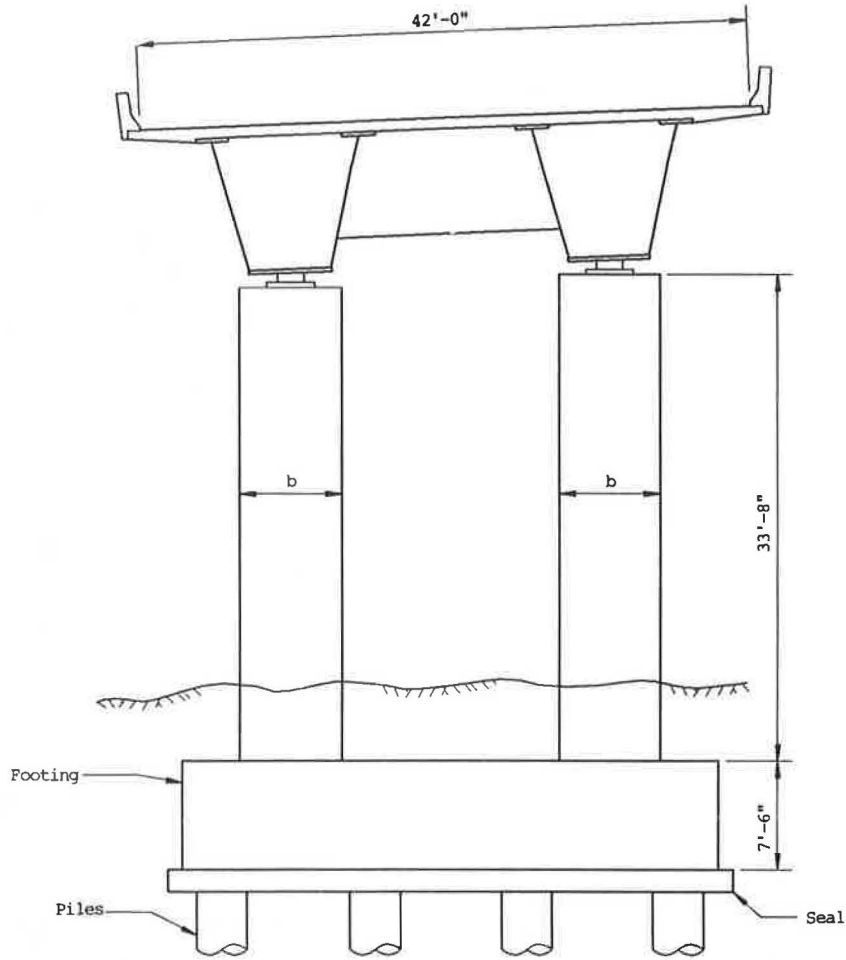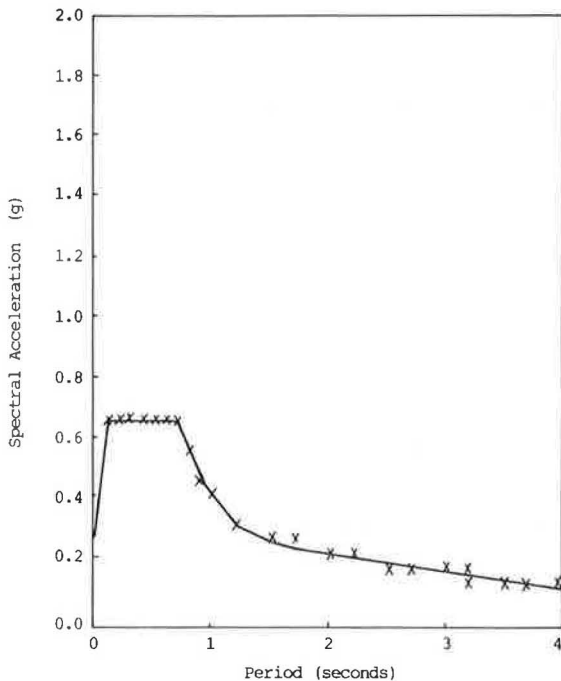
FIGURE 5 Section at Pier 4.

FIGURE 6 Response spectrum.

CONCLUSIONS AND RECOMMENDATIONS

The use of HSC in bridge piers and columns supported by rigid foundation systems can potentially reduce column shears and moments due to seismic loading. Savings of up to 33 percent in the material cost of the piers may be possible when HSC is used in lieu of NSC. Additional economy is achieved because smaller bearings and foundations can be used.

For piers and columns that are supported by flexible foundation systems, HSC will not reduce column shears and moments due to seismic loading as much as rigid foundation systems. However, cost savings will still be possible because less material is required in the columns.

Because foundations represent a significant portion of the cost of a bridge, greater savings can be realized by using HSC in the piers and columns of bridges supported by rigid foundations instead of in those supported by flexible foundations.

Additional research and small-scale testing should be conducted to further study the behavior of HSC used in slender columns on rigid and flexible foundation systems when subjected to seismic motion and subsequent cost savings.
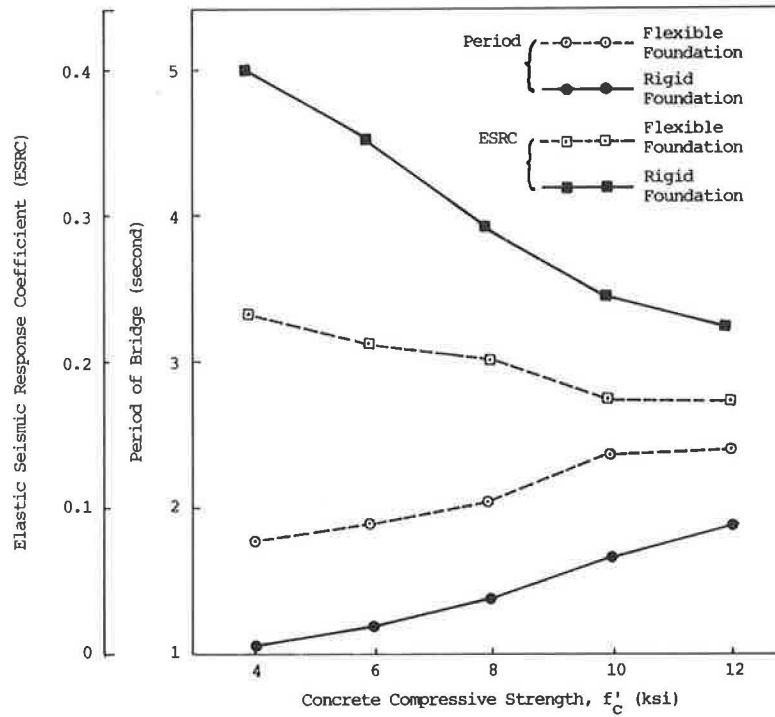
FIGURE 7 Comparison of vibration characteristics of bridge structure for different pier concrete strengths.
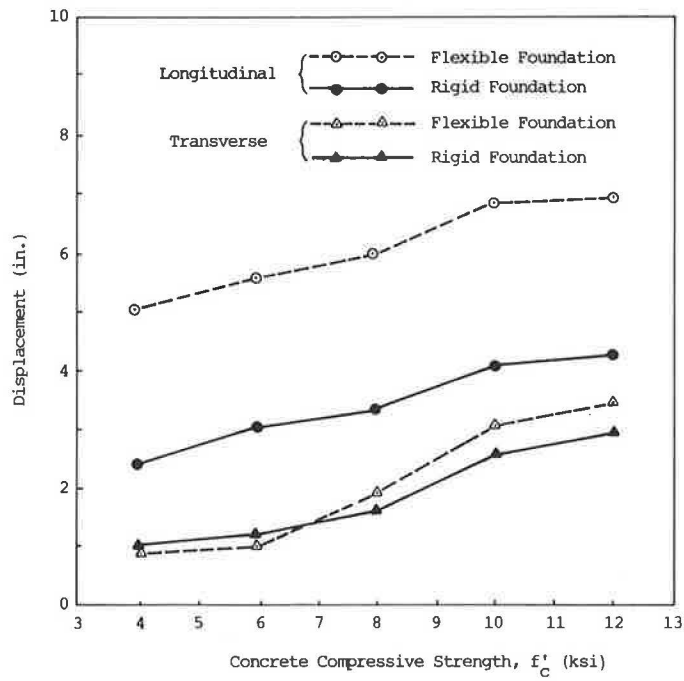

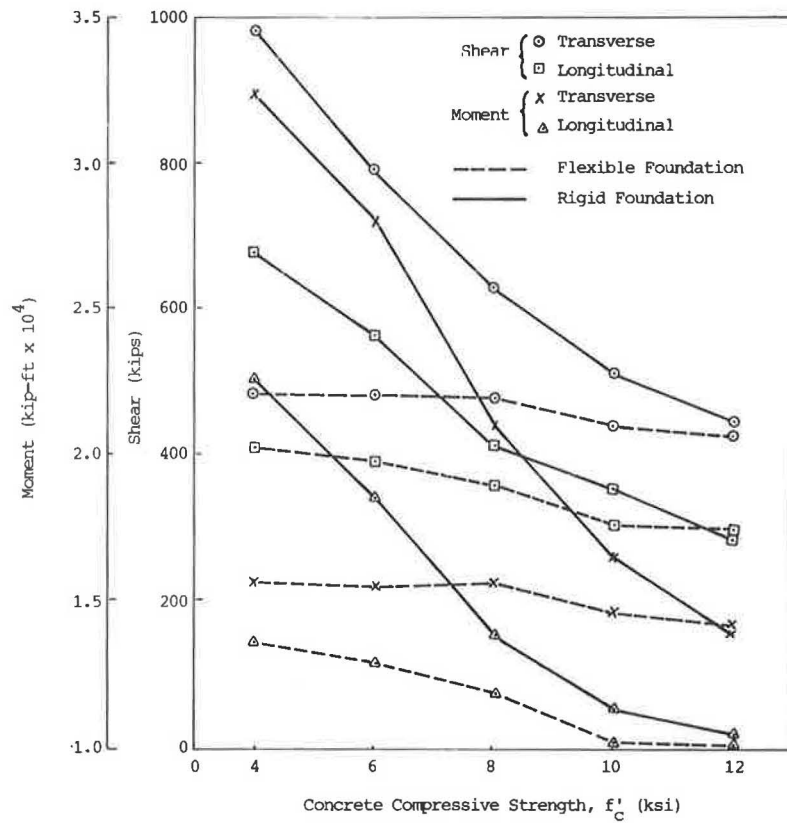**FIGURE 8** Comparison of CQC horizontal displacements at top of Pier 4 for different concrete strengths.

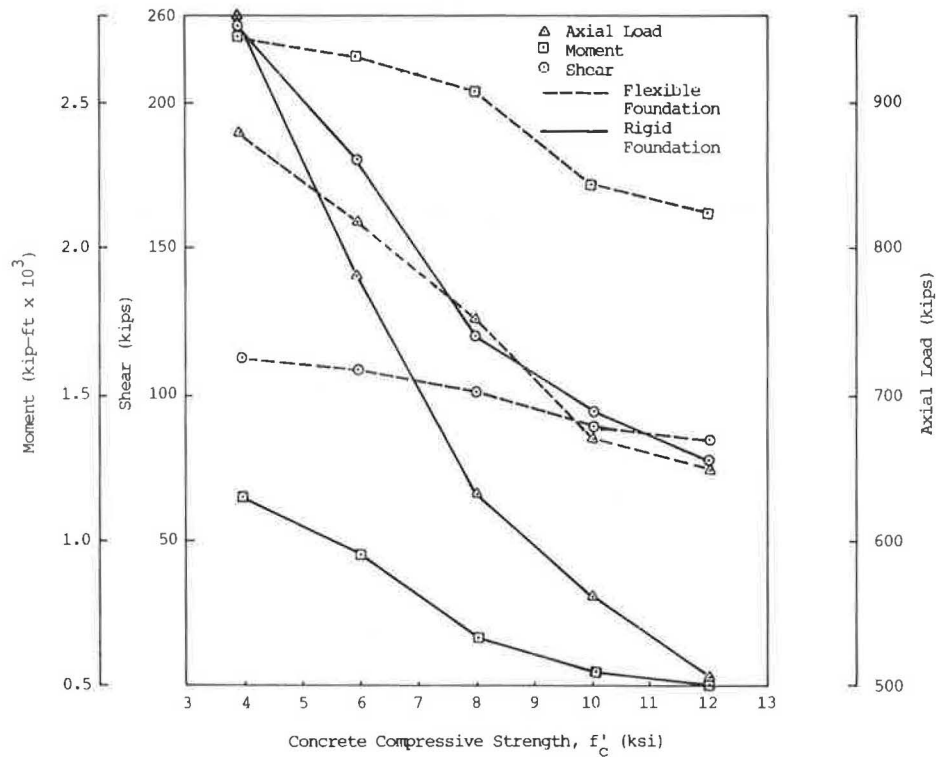**FIGURE 9   Comparison of CQC forces at top of Pier 4 for different concrete strengths.**

FIGURE 10   Comparison of CQC forces to top of piles at Pier 4 for different concrete strengths.
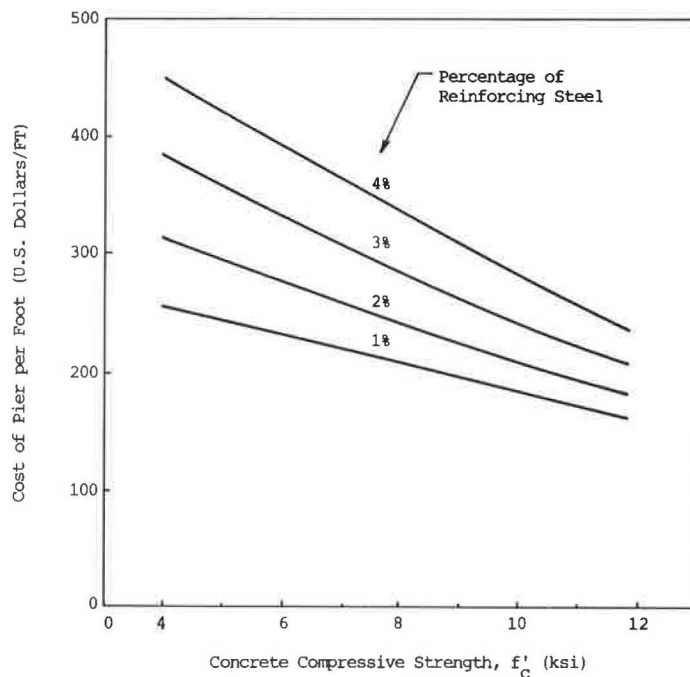
FIGURE 11   Material cost of piers for different concrete strengths and reinforcing steel ratios.

ACKNOWLEDGMENT

REFERENCES

1. Strong New Concrete Muscles into Market. *Engineering News Record*, March 19, 1987, p. 21.
2. *High Strength Concrete in Chicago High-Rise Buildings*. Task Force Report 5. Chicago Committee on High-Rise Buildings, Chicago, Ill., 1977, pp. 1–7.
3. H. G. Russell. *High Strength Concrete*. Special Publication SP-87. American Concrete Institute, Detroit, Mich. 1985, 278 pp.
4. A. J. Burgess, J. Ryill, and J. Bunting. High Strength Concrete for the Willows Bridge. *Journal of the American Concrete Institute*, Vol. 67, No. 8, Aug. 1970, pp. 611–619.
5. Mountain View Road Bridge. *Journal of the Prestressed Concrete Institute*, Vol. 29, No. 2, March-April 1984, pp. 148–151.
6. Tower Road Bridge. *Journal of the Prestressed Concrete Institute*, Vol. 29, No. 2, March-April 1984, pp. 144–147.
7. A. P. Grant. Pasco-Kennewick Bridge—The Longest Cable-Stayed Bridge in North America. *Civil Engineering—ASCE*, Vol. 47, No. 8, Aug. 1977, pp. 62–66.
8. S. B. Quinn. Record Concrete Box Girder Spans Houston Ship Channel. *Civil Engineering—ASCE*, Vol. 53, No. 11, Nov. 1983, pp. 46–50.
9. A. P. Grant. Design and Construction of the East Huntington Bridge. *Journal of the Prestressed Concrete Institute*, Vol. 32, No. 1, Jan.-Feb. 1987, pp. 20–29.
10. Hybrid Girder in Cable Stayed Debut. *Engineering News Record*, Nov. 15, 1984, pp. 32–36.
11. J. E. Carpenter. Applications of High Strength Concrete for Highway Bridges. *Public Roads*, Vol. 44, No. 2, Sept. 1980, pp. 76–83.
12. H. J. Jobse and S. E. Moustafa. Applications of High Strength Concrete for Highway Bridges. *Journal of the Prestressed Concrete Institute*, Vol. 29, No. 3, May-June 1984, pp. 44–73.
13. R. L. Carrasquillo, A. H. Nilson, and F. O. Slate. *The Production of High-Strength Concrete*. Report 78-1. Structural Engineering Department, Cornell University, Ithaca, N.Y., May 1978, 90 pp.
14. L. J. Parrott. *The Selection of Constituents and Proportions for Producing Workable Concrete with a Compressive Cube Strength of 80 to 110 MPa*. Technical Report 416. Cement and Concrete Association, Wexham Springs, Slough, England, May 1969, 12 pp.
15. S. Freedman. *High Strength Concrete*. Publication 15176. Portland Cement Association, Skokie, Ill., 1971, 19 pp.
16. R. L. Chen. Behavior of High-Strength Concrete under Biaxial Compression. Ph.D. dissertation. University of Texas at Austin, Nov. 1984, 299 pp.
17. ACI Committee 363. State-of-the-Art Report on High Strength Concrete. *Journal of the American Concrete Institute*, Vol. 81, No. 4, July-Aug. 1984, pp. 364–411.
18. S. P. Shah, U. Gokoz, and F. Ansari. An Experimental Technique for Obtaining Complete Stress-Strain Curves for High-Strength Concrete. *Cement, Concrete and Aggregates*, Vol. 3, No. 5, May 1981, pp. 21–27.
19. W. F. Perechio and P. Klieger. Some Physical Properties of High Strength Concrete. Research and Development Bulletin RD056.OIT. Portland Cement Association, Skokie, Ill., 1978, 7 pp.
20. ACI Committee 318. *Building Code Requirements for Reinforced Concrete*. ACI 318-83. American Concrete Institute, Detroit, Mich., 1983, pp. 29, 39.
21. S. P. Shah and S. H. Ahmad. Structural Properties of High Strength Concrete and Its Implications for Precast Prestressed Concrete. *Journal of the Prestressed Concrete Institute*, Vol. 30, No. 6, Nov.-Dec. 1985, pp. 92–119.

22. R. W. Poston, M. Diaz, and J. E. Breen. Design Trends for Concrete Bridge Piers. *Journal of the American Concrete Institute*, Vol. 83, No. 1, Jan.-Feb. 1986, pp. 14–20.
23. *Standard Specifications for Highway Bridges*, 13th ed. AASHTO, Washington, D.C., 1983.
24. ACI Committee 318. *Commentary on Building Code Requirements for Reinforced Concrete*. ACI 318-83. American Concrete Institute, Detroit, Mich., 1983, p. 45.

25. R. A. Imbsen et al. *SEISAB-I, Seismic Analysis of Bridges: User's Manual*. Manual Version 1.3.3. Engineering Computer Corporation, Sacramento, Calif., Aug. 1985.

Beam Models for Nonlinear and Time-Dependent Analysis of Curved Prestressed Box Girder Bridges

ANTONIO R. MARÍ, SERGIO CARRASCÓN, AND ANGEL LOPEZ

Two analytical models developed to study the structural response of curved prestressed concrete box girder bridges are presented. The first one consists of a filament beam model, with arbitrary longitudinal and sectional geometry. Concrete and steel are assumed to be subjected to a uniaxial stress state. Material nonlinearities such as cracking of concrete, yielding of steel, and so forth are taken into account. Flexural and torsional behaviors are considered uncoupled. Time-dependent effects due to load history, creep, shrinkage, and aging of concrete and relaxation of prestressing steel are also included. In the second approach, a box-beam straight element of nondeformable cross section composed of concrete panels with steel layers is used to model the bridge. Concrete is assumed to be subjected to a biaxial stress state. Material nonlinearities are also considered. Longitudinal and transverse prestressing can be included. Coupling between flexural, torsional, and shear response of the cross section is considered. A curved prestressed box girder bridge constructed in Spain is analyzed by the two models presented under different loading conditions. Short-term analyses with increasing overload to failure demonstrate the applicability of the uncoupled model when either bending or torsion is dominant, whereas for other cases coupling is necessary to accurately predict the structural response. A time-dependent analysis under permanent loads is made, followed by a long-term overload analysis showing the effects of time in the structural response. The influence of transverse prestressing on the structural behavior is also studied.

In recent years reinforced and prestressed concrete curved box girder bridges have been widely used for overcrossings and viaducts. Characteristic features that have made box girders an attractive alternative for bridge designers include their structural efficiency (high flexural and torsional stiffness combined with light weight) and their pleasing aesthetic qualities (the clean lines of the closed section and the ability to use single, slender piers as supports).

Present and past designs of box girder bridges have usually been based on linear elastic analysis using simplified models of uncracked, homogeneous systems. These models are able to predict adequately the behavior of prestressed concrete bridges at service load levels. However, if such a structure is loaded beyond the working stress range, excessive cracking of the concrete and eventual yielding of the reinforcement no longer justify the use of linear elastic models.

In addition, bending and torsional moments in curved bridges are coupled, which means that the bending moment

Universitat Politècnica de Catalunya, Barcelona, Spain.

and torque cannot be obtained separately. When a section subjected to combined actions cracks, its stiffness decreases significantly. Generally the loss of torsional stiffness is proportionally greater than the loss of flexural stiffness, so the structural response under increasing load will be nonlinear after cracking.

In curved prestressed concrete bridges over simple intermediate supports, very high torsional moments are originated, particularly under certain loading cases (if only the exterior lanes are loaded). The longitudinal prestressing designed to prevent flexural cracking at service load levels may not be sufficient to avoid cracking caused by torsion, so the girder flanges are usually prestressed transversely. Such prestressing will influence the torsional response and therefore the overall structural behavior.

Time-dependent effects such as creep and shrinkage of concrete and relaxation of prestressing steel may change the prestressing force of the tendons as well as the stresses and strains of concrete and steel. Consequently the structural response under increasing load up to failure will depend, to a certain extent, on the load history.

It is evident that a complete understanding of such complex structural behavior requires an important effort from the experimental and theoretical viewpoints. In this paper, two mathematical models developed by the authors (1, 2) for the nonlinear analysis of reinforced and prestressed concrete curved box girder bridges are briefly described. The paper will focus particularly on the structural response of a curved prestressed box girder bridge, drawing conclusions regarding the behavior of such structures and the applicability of the proposed analytical models.

DESCRIPTION OF ANALYTICAL MODELS

General Remarks: Common Assumptions

The behavior of single box girder bridges can be reasonably simulated by means of beam theory when the ratio of span to cell width is greater than approximately 5. In such a range of span–cell-width ratio, the influence of transverse distortion and warping of the cross section on the longitudinal stresses may be, for the usual prestressed concrete box girders, very small (3), which means that assumptions can be made about the nondeformability of sections in their plane, as well as about the deformation of Navier's plane sections.

The analytical models developed can be described by attending essentially to four aspects: structural idealization, material models used, sectional analysis, and structural analysis. In the following, a brief description of the characteristics of each model is given.

Model 1: Filament Beam with Uncoupled Torsional-Flexural Behavior

Structural Idealization

The structures that can be analyzed with this model are general three-dimensional reinforced and prestressed concrete frames composed of prismatic or nonprismatic members, with arbitrary cross section, and straight or curved in space. The members are interconnected by structural nodes. Such nodes are strictly necessary only at the actual structural joints, not inside the element. However, for integration purposes, a number of sections along the member are considered, in which a local coordinate system is defined (Figure 1).
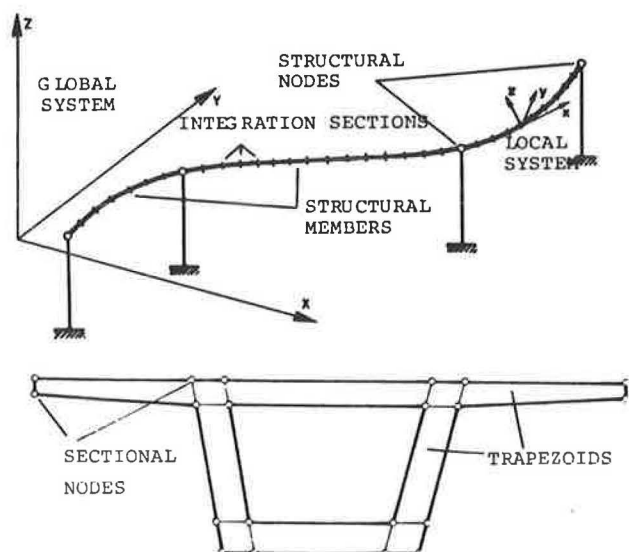
FIGURE 1 Structural idealization (Model 1).

Six degrees of freedom are considered at the end of each member: three translations and three rotations. Such longitudinal idealization allows the modeling of large structures with a small number of long elements, reducing the global matrix stiffness size at the expense of greater computer time because of the integration process along the bars.

Loads or moments can be applied either over the nodes or along the member length with any position and orientation in space. Imposed displacements and constraints at supported nodes can also be applied in any direction.

The cross section is discretized by means of trapezoids (Figure 1), each one defined by a four-sectional vertex. The trapezoids are made into squares by means of a parametric transformation. Then, a 5×5-point mesh over each square together with a two-dimensional Simpson rule are used for integration over the cross section. Mechanical properties as well as sectional forces can be obtained very accurately with this system.

Reinforcing steel bars are considered embedded elements parallel to the longitudinal member reference line. The area and position of each bar in local coordinates of the section are given as input data.

Pretensioned and posttensioned longitudinal tendons can be considered in this model. Each tendon can be extended to any length of the structure. A prestressing tendon may be composed of several segments, each of them of different profile (straight or parabolic, with or without end slope constraints). Jacking can be done from either of the two ends; friction losses and anchorage slip are taken into account.

Material Constitutive Equations

Concrete and steel are assumed to be subjected to a uniaxial longitudinal stress state. Total concrete strain at a given time and point in the structure is taken as the direct sum of mechanical strain (stress-produced strain) and nonmechanical strain, consisting of creep strain, shrinkage strain, and thermal strain.

The nonlinear constitutive relationship for concrete is shown in Figure 2a. This model is based on the one suggested by Sargin (4), including load reversal branches parallel to the initial slope. Eleven possible material states are considered.

For the reinforcing steel, a bilinear stress-strain relationship is assumed with load reversals, making four different material states, as shown in Figure 2b. A multilinear stress-strain curve is used for prestressing steel (Figure 2d). In addition, the usual empirical formulas are used for stress relaxation and friction properties of the prestressing steel.

Creep strain ε_c of concrete is evaluated by an age-dependent integral formulation based on the principle of superposition. Thus

$$\varepsilon_c (t) = \int_0^t c(t, t - \tau) \ \frac{\partial \sigma(\tau)}{\partial \tau} \ d\tau \qquad (1)$$

where $c(t, t - \tau)$ is the specific creep function, dependent on the age of loading. It can be seen from Equation 1 that for the determination of creep strain at any instant t, it is necessary to know all the stress history at each point. This problem can be avoided by using a Dirichlet series for the specific creep function, such as

$$c(t, t - \tau) = \sum_{i=1}^{n} a_i (\tau) \ \{ 1 - \exp [- \lambda_i (t - \tau)] \} \qquad (2)$$

where $a_i(\tau)$ and λ_i are parameters to be determined from experimental or empirical creep curves. Using such a creep function incorporates the historic effects by successively updating only one stress increment, instead of the entire stress history (5).

Sectional Analysis

The sectional deformation is characterized in this model by six components: axial strain of the reference sectional center, two flexural curvatures, an average twist, and two shear deformations.

In additional to Navier's plane-section hypothesis, uncoupling between normal and tangential responses and a perfect bond between steel and concrete are assumed.

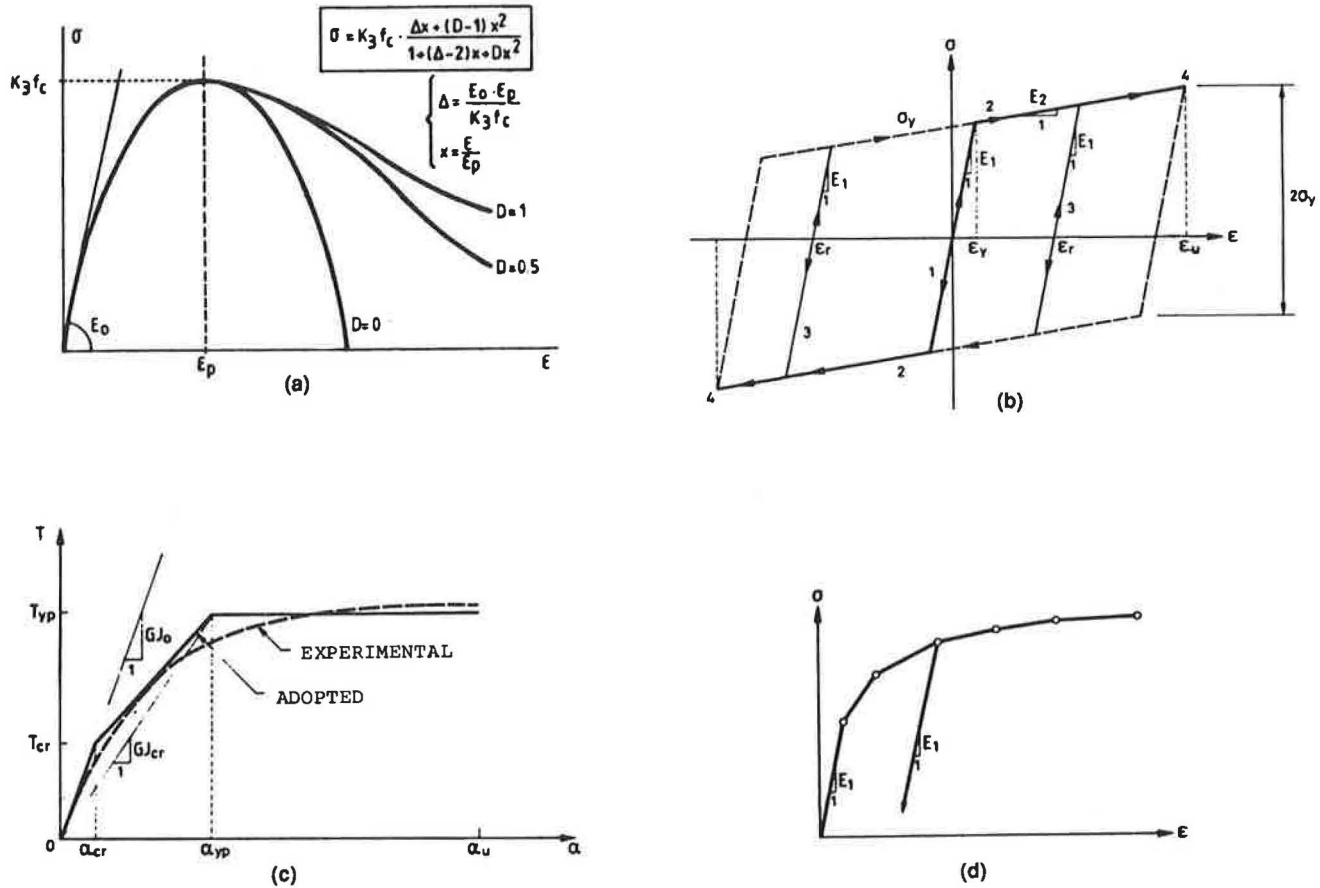**FIGURE 2** Material properties and torsional behavior (Model 1).

The sectional behavior can be expressed by a general constitutive equation derived by combining equilibrium equations between stresses and forces, compatibility of strains over the section, and material constitutive relations at each point. Such an equation, incrementally expressed, takes the following form:

$$\Delta \vec{\sigma}_s = \mathbf{k}_s \cdot \Delta \vec{\epsilon}_s + \Delta \vec{\sigma}_s^0 \qquad (3)$$

where $\Delta \vec{\sigma}_s$ is the vector of sectional forces, composed of axial force, two bending moments, torque, and two shear forces; $\Delta \vec{\epsilon}_s$ is a vector of sectional deformations; $\Delta \vec{\sigma}_s^0$ is vector of initial stresses; and $\mathbf{k}_s$ is the tangent sectional stiffness matrix, which takes into account the material state at each point (cracked, yielded, crushed, etc.), including the contributions of reinforcing and prestressing steel. Therefore, material nonlinearities are included in the sectional stiffness matrix.

The uncoupling hypothesis leads to a sectional stiffness matrix such as the following:

$$\begin{Bmatrix} \Delta N \\ \Delta M_y \\ \Delta M_z \\ \Delta T \\ \Delta V_y \\ \Delta V_z \end{Bmatrix} = \begin{bmatrix} k_{11} & k_{12} & k_{13} & & & \\ & k_{22} & k_{23} & & \mathbf{0} & \\ & & k_{33} & & & \\ & & & k_{44} & k_{45} & k_{46} \\ & & & & k_{55} & k_{56} \\ & & & & & k_{66} \end{bmatrix} \begin{Bmatrix} \Delta \epsilon_0 \\ \Delta \phi_y \\ \Delta \phi_z \\ \Delta \alpha \\ \Delta \gamma_y \\ \Delta \gamma_z \end{Bmatrix} + \begin{Bmatrix} \Delta N^0 \\ \Delta M_y^0 \\ \Delta M_z^0 \\ \Delta T^0 \\ \Delta V_y^0 \\ \Delta V_z^0 \end{Bmatrix} \quad (4)$$

in which the flexural forces are related only to longitudinal deformations.

The term k_{44} represents the torsional stiffness, which depends on the load level. In this model a trilinear torque-twist relationship is assumed in which k_{44} is the slope of such a diagram. The representative parameters of the torsional model are the initial stiffness GJ_0, the torque at first cracking T_{cr}, the cracked torsional stiffness k_{11}, the torque at full yielding T_{yp}, and the ultimate twist (6). Inelastic unloading parallel to the initial stiffness GJ_0 is assumed, as shown in Figure 2c.

Structural Analysis Procedure

The method of nonlinear structural analysis is developed on the basis of the classic matrix structural analysis of curved bars in space, extended to take into account material nonlinearities and time-dependent effects on reinforced and prestressed concrete three-dimensional frames.

The member stiffness matrix is derived by setting the three basic equations at the element level, expressed in global coordinates:

1. Incremental equilibrium equations:

$$\Delta \vec{\sigma}_{sxy}(s) = N(s) \cdot \Delta \vec{P}_B + \Delta \vec{\sigma}_{sxy}^*(s) \qquad (5)$$

where

$\Delta\vec{\sigma}_{sxy}(s)$ = vector of internal forces at any section of the member;

$N(s)$ = equilibrium matrix, depending on the beam geometry;

$\Delta\vec{P}_B$ = vector of applied loads at one of the member ends; and

$\Delta\vec{\sigma}^*_{sxy}(s)$ = vector of forces acting at any section, caused by applied loads over the member, in a statically determinate configuration.

Such an equation comes from integration of the differential equilibrium equation of the beam, with the appropriate boundary conditions.

2. Incremental kinematic equations:

$$\Delta\vec{d} = \int_A^B N^T(s) \cdot \Delta\vec{\varepsilon}_{sxy}(s) \, ds \qquad (6)$$

where $\Delta\vec{d}$ is the vector of relative displacements between both member ends, and the other terms are as defined previously.

3. Constitutive sectional Equation 3, transformed to global coordinates: If the above equations are combined and completed for the rest of the member degrees of freedom, the general member force-displacement relationship is obtained:

$$\Delta\vec{F} = K \cdot \Delta\vec{\delta} + \Delta\vec{F}^* + \Delta\vec{F}^0 \qquad (7)$$

where

$\Delta\vec{F}$ = vector of applied loads at both member ends,

K = member tangent stiffness matrix,

$\Delta\vec{\delta}$ = vector of member end displacements,

$\Delta\vec{F}^*$ = vector of fixed end forces due to applied loads over the member length, and

$\Delta\vec{F}^0$ = vector of fixed end forces due to initial stresses.

By assembling the elementary equations for the complete structure, a similar global expression is obtained.

For the nonlinear time-dependent analysis, the time domain is divided into a number of time intervals, separated by time steps. At time step t_{n-1} all nodal displacements, total strains, nonmechanical strains, and stresses in every part of the structure are known. The increments of nonmechanical strain due to creep and shrinkage of concrete and temperature changes occurring during time steps t_{n-1} and t_n are evaluated as explained in the section headed 'Material Constitutive Equations.

At each section, incremental forces due to nonmechanical strains are obtained by sectional integration. Such forces, added to the sectional prestressing primary forces existing if any prestressing operation is carried out at the beginning of the current time interval, are integrated over the member length so that the incremental initial stress load vector $\Delta\vec{F}^0$ is obtained. A similar procedure is followed for the sectional forces due to loads applied over the member length, obtaining the term $\Delta\vec{F}^*$.

Finally, the unbalanced-load vector $\Delta\vec{F}^u$ from the last time step is added, so that the load increment $\Delta\vec{F}_n$ at time step t_n to be applied to the structure is obtained by

$$\Delta\vec{F}_n = \Delta\vec{F}_n^{ext} + \Delta\vec{F}_n^u + \Delta\vec{F}^* + \Delta\vec{F}_n^0 \qquad (8)$$

The total load increment may be divided into several smaller load increments for incremental load analysis. Unbalanced load iterations can be performed following standard iterative procedures, with or without changing the structural stiffness matrix.

Model 2: Panel Beam with Coupled Torsional-Flexural Behavior

Structural Idealization

The structure is divided longitudinally into a number of short, straight elements connected by nodes. Inside each element, a short number of integration sections is considered. Loads or moments must be applied only at the structural nodes.

With such a longitudinal scheme, a large number of joints is necessary to idealize medium-sized structures; nevertheless, the longitudinal integration along the elements is extremely simple, making the global process of structural analysis probably faster than with Model 1.

The cross section is considered to be composed of panels (Figure 3), which can resist only normal and shear stresses in their middle plane. The position and thickness of the panel, as well as of the concrete cover, which is allowed to spall, are known. Also, several reinforcing steel layers with any orientation and a layer of transverse prestressing can be defined at each panel.

Longitudinal prestressing tendons are individually defined, giving their steel area, position, and slopes at the integration sections with respect to the longitudinal axis. The active effect of prestressing is introduced in this model by means of an initial strain in the prestressing steel, which is calculated taking into account the friction losses.

Material Properties

Concrete is assumed to be subjected to a biaxial stress state. Before cracking, a biaxial isotropic elastic constitutive model is used, with a variable modulus of elasticity. Given the panel strains ε_x, ε_y, and γ, the principal strains ε_1 and ε_2 and their orientation β at the middle plane are obtained by means of bidimensional elasticity equations.

Once the principal strains on the middle plane are known, as well as the curvature in their direction induced by bending and torsion (7), the principal strains throughout the panel thickness can be obtained (Figure 3). Then the stress ratio α is

$$\alpha = \frac{\sigma_1}{\sigma_2} = \frac{\varepsilon_1 + \nu\varepsilon_2}{\varepsilon_2 + \nu\varepsilon_1} \qquad (9)$$

where ν is Poisson's ratio, assumed constant.

With such a value, the ultimate stress and strain for the maximum compressive direction are determined, according to the Kupfer and Gerstle failure envelope (8) (Figure 4). By
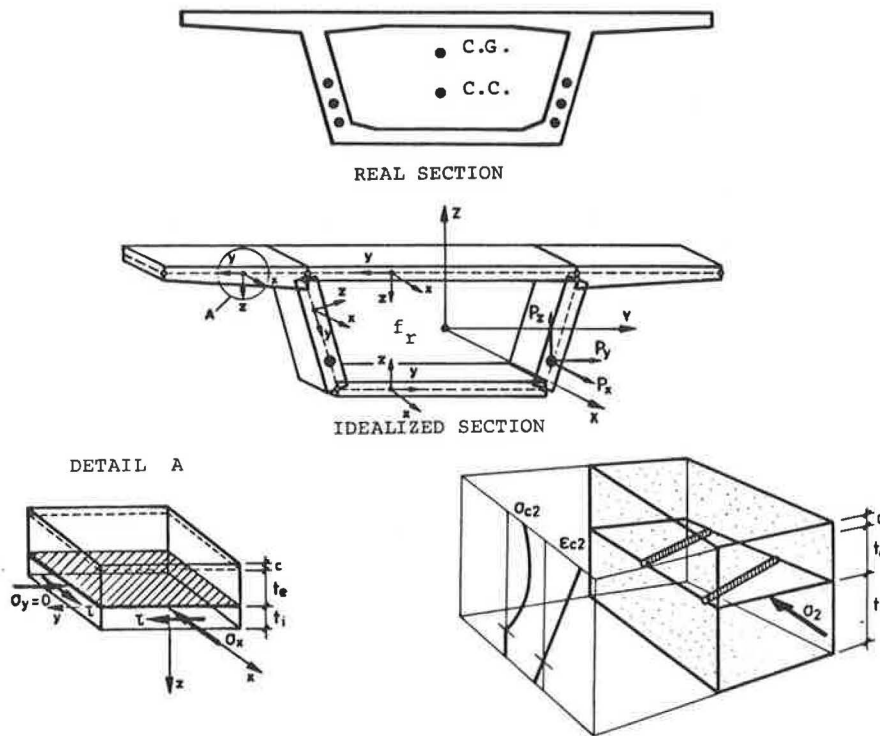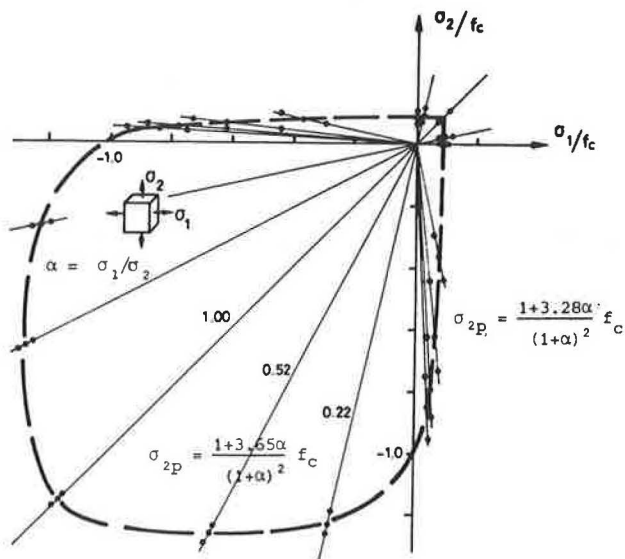
FIGURE 3 Structural idealization (Model 2).

FIGURE 4 Failure envelope for concrete under biaxial stresses.

using Saenz's equation (9) to represent the concrete behavior, an apparent elasticity modulus for concrete is obtained:

$$E_a = \frac{\sigma_2}{\varepsilon_2} = \frac{E_{c0}}{1 + \left(\frac{E_{c0}\,\varepsilon_{2p}}{\sigma_{2p}} - 2\right)\left(\frac{\varepsilon_2}{\varepsilon_{2p}}\right) + \left(\frac{\varepsilon_2}{\varepsilon_{2p}}\right)^2} \qquad (10)$$

The principal stresses are then

$$\sigma_1 = \frac{E_a}{1 - \nu^2}\,(\varepsilon_1 + \nu\varepsilon_2)$$

$$\sigma_2 = \frac{E_a}{1 - \nu^2}\,(\varepsilon_2 + \nu\varepsilon_1) \qquad (11)$$

For cracked concrete, the evolutive truss analogy with stress reduction, according to Vecchio and Collins (10), is adopted to represent the panel behavior. In such a case, the ultimate stress and strain for the maximum compressive direction are determined by the following equations:

$$\sigma_{2p} = \frac{f_c}{\lambda} \qquad \varepsilon_{2p} = \frac{\varepsilon_{c0}}{\lambda}$$

$$\lambda = \left(\frac{\gamma m}{\varepsilon_2} - 0.3\right)^{1/2} \qquad \gamma m = \varepsilon_1 - \varepsilon_2 \qquad (12)$$

The stress in the direction orthogonal to the cracks is assumed to be zero.

For the reinforcing steel the same constitutive relations as those in Model 1 are assumed for the direction in which the layer is oriented. Prestressing steel is assumed to be subjected to uniaxial stress with a stress-strain relationship similar to that in Model 1.

Sectional Analysis

The sectional behavior is governed by three sets of fundamental relationships: (a) compatibility between panel strains and sectional deformations, (b) constitutive relationships of the materials, and (c) equilibrium between sectional forces and stresses over the panels.

It is not possible to arrive, in this model, at an explicit constitutive equation at the sectional level, such as the one expressed for Model 1 by Equation 3. Then, to solve the sectional analysis, the process is the following:

1. The strains at each point of the section are obtained, by means of geometrical relationships, from the six general sectional deformations assuming Navier's plane-section hypothesis and nondeformability of sections in their plane;

2. Once the strains are known, stresses are obtained by means of the constitutive relationships of the materials (see previous section); and

3. Sectional forces are obtained by integration of stresses over the panels.

It is remarkable to note that this model does not separate torsional, flexural, axial, and shear behavior, making it possible to accurately predict the sectional response under combined actions. It is possible to capture failures due to crushing of concrete compression trusses, yielding of transverse steel, or yielding of longitudinal steel, depending on the load combinations.

Structural Analysis

The structural analysis method used in this model is essentially the same as that for Model 1, taking into account the particularities of the structural idealization (straight elements, loads applied only at structural joints, etc.). Unbalanced forces and prestressing effects are introduced as the initial stress loading vector. No time-dependent effects are considered in this model.

STRUCTURAL RESPONSE OF CURVED PRESTRESSED BOX GIRDER BRIDGE

The objectives of the present study are to show the capabilities of both analytical models, to compare their results when applied to the analysis of the same structure, and to study the response of a prestressed concrete box girder bridge under different loading conditions.

Description of Bridge Analyzed

The structure chosen for the present study is a curved prestressed concrete bridge actually constructed in Pamplona, Spain, in 1975 (11). The bridge superstructure consists of a three-span continuous beam whose total length is 88 m (28 m + 32 m + 28 m), with both ends torsionally fixed, supported without intermediate diaphragms over two single piers without torsional restraint. The geometry in plan consists of a circular curve of 120-m radius, followed by a spiral of parameter $A = 80$ (see Figure 5).

The cross section is a single box with side cantilevers 3.10 m long, making a total platform width of 12.85 m. The bottom slab is 5.75 m wide and the webs, 0.70 m thick, are included with a 2/1 slope. The bridge has a constant depth of 1.30 m, a top-deck constant thickness of 0.24 m, and a bottom-deck thickness of 0.20 m that increases to 0.35 m over the supports (see Figure 6).

The longitudinal prestressing is composed of 26 tendons 12T13 of 346 cm² total area, anchored in both ends of the superstructure by means of stressing anchorages. Because of the platform width and the large torsional span, which causes high stresses near the abutments, the top and bottom slabs are transversely prestressed along the final 7 m by means of tendons of 12 ϕ7 separated 0.67 m and 0.51 m, respectively.

The structure was constructed by means of a framework, directly soil supported, extended along the whole bridge length.

Idealization of Bridge and Analyses Performed

The centerline of the bridge was idealized as a circular curve of 120-m radius. The transverse and longitudinal discretizations are shown in Figure 7. Two equivalent tendons are
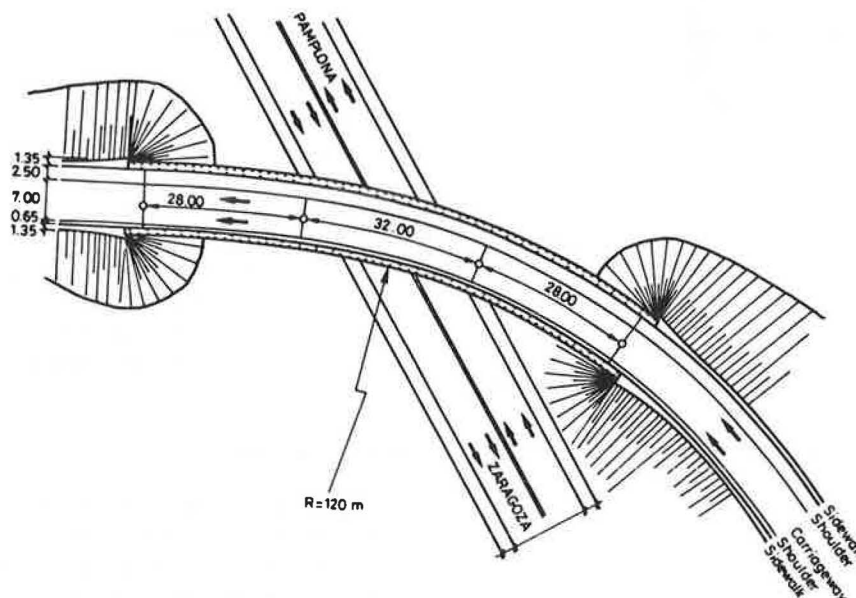

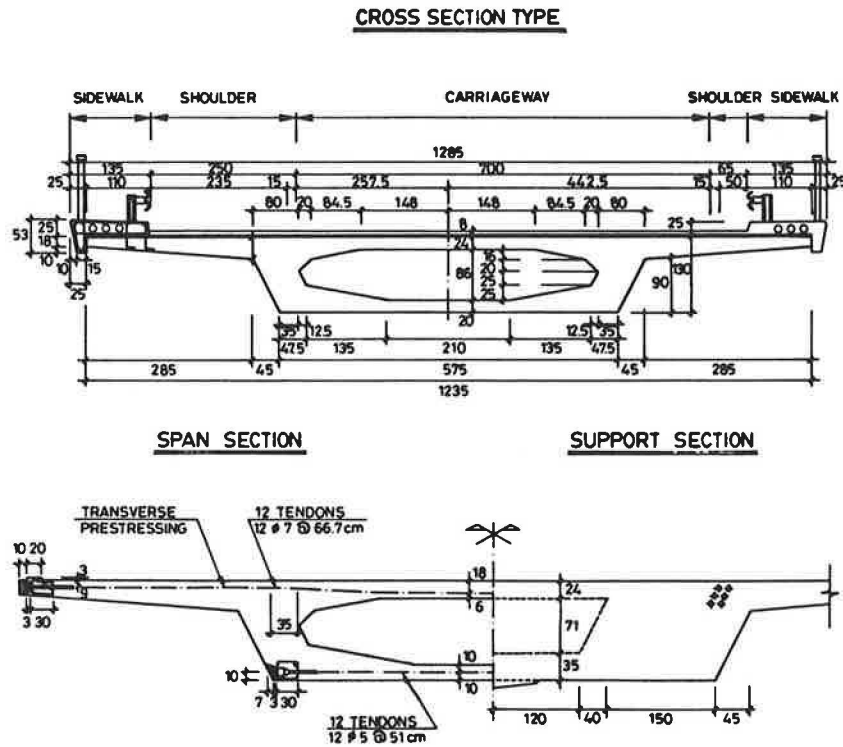FIGURE 5 General plan of the bridge.

CROSS SECTION TYPE

FIGURE 6 Cross section of the bridge.

used to represent the longitudinal prestressing with a total anchorage force of 19 000 kN each. The tendon layout is shown in Figure 8. For analysis purposes, the reinforcing steel arrangement has been divided into four zones, described in Figure 8.

Concrete properties assumed for the analysis are initial modulus E_c = 36 000 MPa; compressive strength f_c' = 35 MPa; tensile strength f_t = 3.5 MPa; peak strain ε_0 = −0.002; and ultimate strain ε_u = 0.0035. The reinforcing steel properties assumed are initial modulus E_s = 210 000 MPa; no strain hardening; strength f_s = 410 MPa; and ultimate strain ε_{su} = 0.01. The prestressing steel has been assumed to have an initial modulus E_p = 200 000 MPa; a yielding stress f_{py} = 1500 MPa; and a strength f_{pmax} = 1700 MPa.

Time-dependent properties of concrete have been considered according to the Model Code of the Comité Euro-International du Béton and International Federation of Prestressed Concrete (CEB-FIP) (*12*), assuming a medium ambient humidity (50 percent), no shrinkage strain, and a constant temperature of 20°C. The concrete strength is assumed to increase with time, from 35 MPa at t = 30 days to 50 MPa at t = 10,000 days. Also the deformational modulus varies, from E_c = 36 000 MPa to E_c = 42 400 MPa, so that aging of concrete is taken into account. The final relaxation of the prestressing steel is assumed to be 5 percent of the initial stress. Transverse prestressing tendons are assumed to be initially stressed at 70 percent of their yielding stress.

No anchorage slip has been considered. Friction coefficients adopted are μ = 0.20 and k = 0.0012. Jacking is assumed to be done from both ends simultaneously.

The loads considered in the analysis are the self weight of the bridge (*SW*), a dead load (*DL*) of 2.0 kN/m², and a live load (*LL*) of 4.0 kN/m² that can be extended to any surface and length of the bridge. No truck loads have been considered in the analysis. The following loading cases have been considered:

Load Case 1: *SW* + *DL* + *LL* extended over the whole bridge length and width.
Load Case 2: *SW* + *DL* + *LL* extended over the whole bridge length and the exterior half-width only.
Load Case 3: *SW* + *DL* + *LL* extended over the whole bridge length and the interior half-width only.

The analyses performed are the following:

Analysis 1: short-term (t = 30 days after casting); Models 1 and 2; Load Case 1 with increment of *LL* to failure.
Analysis 2: short-term (t = 30 days after casting); Models 1 and 2; Load Case 2 with increment of *LL* to failure.
Analysis 3: short-term (t = 30 days after casting); Models 1 and 2; Load Case 3 with increment of *LL* to failure.
Analysis 4: time-dependent; only Model 1; Load Case 1; *SW* at 30 days, *DL* at 60 days, *LL* at 10,000 days increasing to failure.
Analysis 5: short-term (t = 30 days after casting); Models 1 and 2; Load Cases 1, 2, and 3, including transverse prestressing.

Results of Analyses

Analysis 1: Centered Live Load

Figure 9 shows the load-deflection and load-force curves, respectively, for that case. Cracking appears in the support
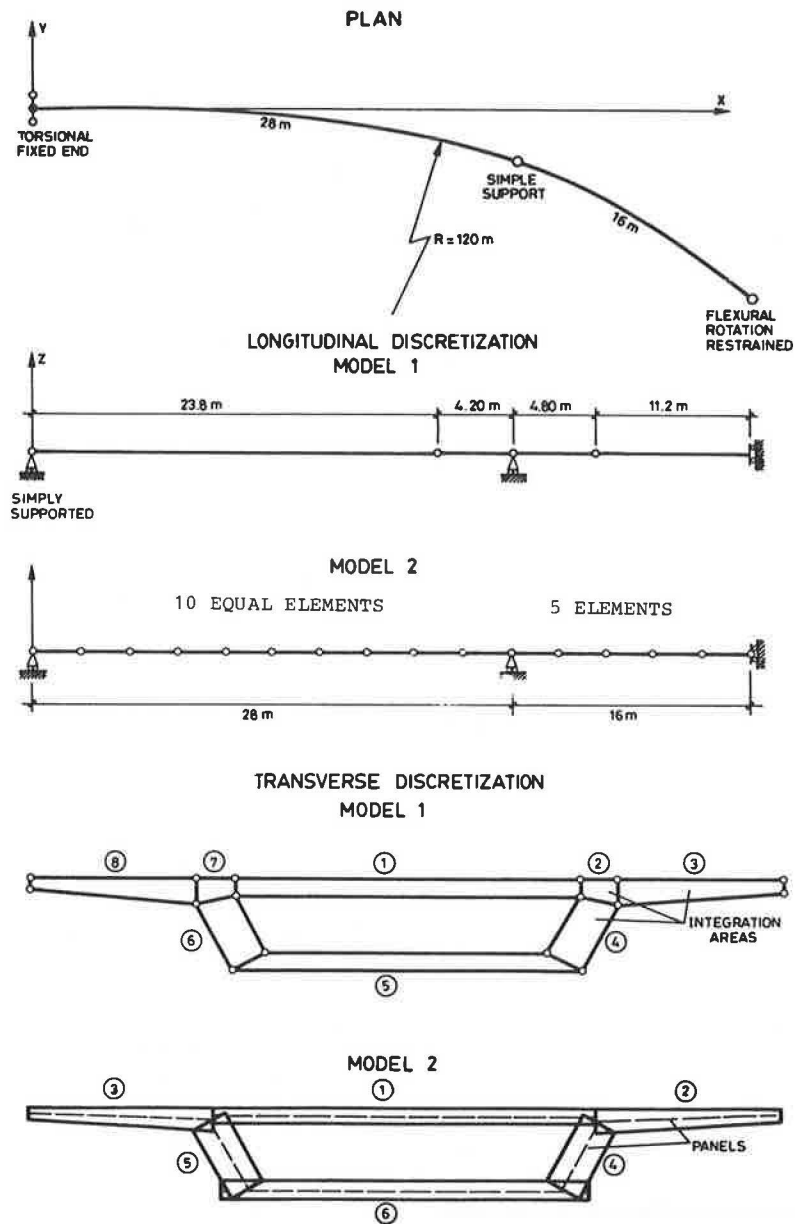
PLAN

FIGURE 7 Longitudinal and transverse idealization of the bridge.

section at about 8.0 times the live load, whereas flexural rupture due to prestressing steel yielding in the same section is produced at approximately 11.5 times the *LL*.

A very small redistribution of forces takes place for this loading case. The bending moment at the middle of the central span decreases, whereas in the support section a 4 percent increase takes place in the ultimate state.

In general, good agreement is obtained between the results of both models, which indicates that for dominant flexural behavior, the uncoupled model can be used with reasonable accuracy in these kinds of structures.

Analysis 2: Eccentric External Live Load

In this case, the opposite situation is found: the torsional behavior is dominant, and bending moments are very small.

Figure 10 shows the load-deflection and load-force curves. Cracking appears at the abutments because of the important torsional moment acting, at 4 times the live load, according to Model 1. Model 2 predicts cracking at a higher value of the overload factor. Such a difference is due to the effect of shear stresses coming from external loads and to the prestressing slope at the end of the beam, both of which are taken into account in Model 2. After cracking, a reduction of the moment at the middle of the central span and an increase of the support moment are produced with increasing load. Such a redistribution of bending moments that are due to the variation of the EI/GJ ratio along the bridge reaches 66 and 37 percent at the center and support sections, respectively, when failure occurs. Model 2 also predicts a sudden increase of the central deflection after cracking. Failure occurs at about 8.8 times the live
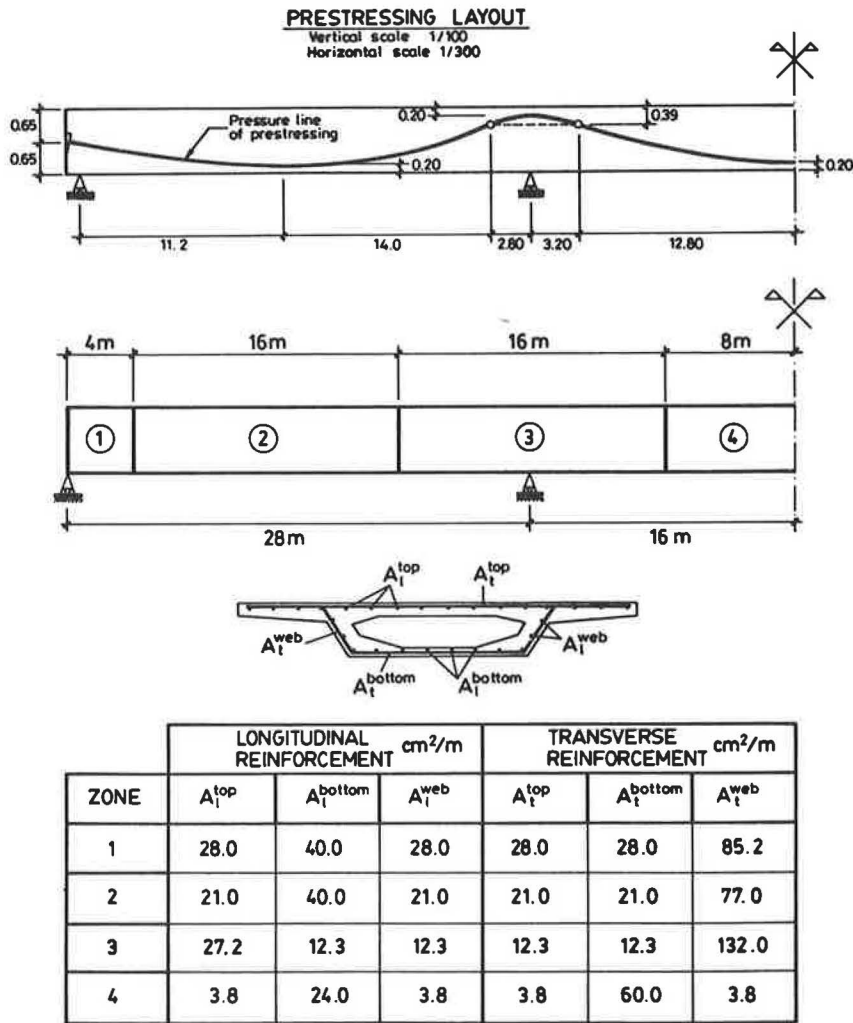
FIGURE 8 Prestressing and reinforcing steel arrangement adopted for the analysis.

load, when the ultimate torque is reached at the abutments, because of yielding of the transverse reinforcement.

In general there is excellent agreement between the results of both models, which indicates that even when torsional behavior is dominant, the uncoupled model provides good results.

Analysis 3: Eccentric Interior Live Load

Figure 11 shows the load-deflection and load force curves for this analysis. Good agreement is obtained also, although differences are a little larger than those under other loading conditions.

Failure at the abutments due to torsion is reached at practically the same time as flexural rupture in the central span section, at approximately 11.8 times the live load. Cracking is detected in both models at about 7.0 times the live load. Then a redistribution of bending moments opposite the one produced in Analysis 2 occurs for the same reason. The bending moment in the support section is about 30 percent smaller than the elastic value in the ultimate state.

In this bridge the sections subjected to maximum torque and maximum bending moment are different and very separated. Practically no cross section is being subjected simultaneously to torsion and bending of similar importance. Therefore, the uncoupled model can be used for any load combination with reasonable accuracy, because there is no deformational interaction between torsion and bending at any section.

Analysis 4: Time-Dependent Analysis

The objective of such an analysis is, on one hand, to determine the influence of time-dependent effects on the ultimate load capacity of the bridge, assuming no evolutive construction. On the other hand, a comparison of the computer results and the ones made by hand for design purposes is established.

Figure 12 shows the time-deflection diagram for the middle of the central span. From that curve it can be seen that the central deflection, after the dead load has been applied, remains practically constant with time, with a slight tendency to decrease, which means that prestressing and permanent loads are equilibrated.
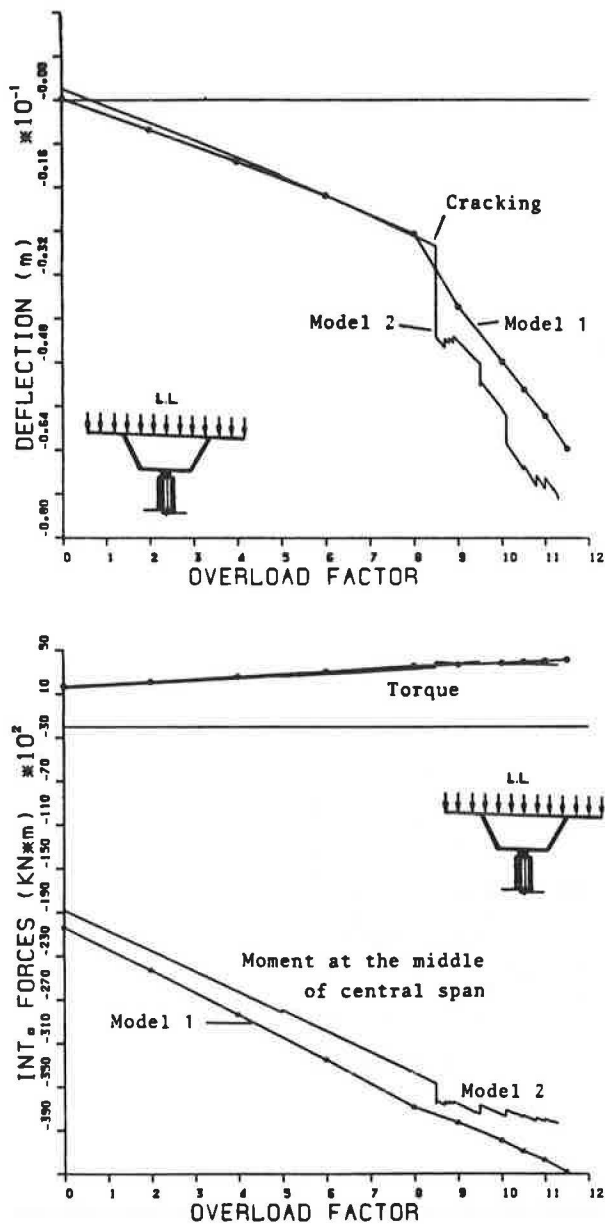
time and that cracking is advanced because of the loss of prestressing force.

Analysis 5: Transverse Prestressing

The objective of this analysis is to use Model 2 to study the influence of transverse prestressing of the top and bottom slabs near abutments on the structural response of the bridge under the three loading cases. Transverse prestressing is designed to avoid a great decrease in the torsional rigidity under high torsional moments, which may produce important variations in the longitudinal bending moments.

Figure 16 shows redistribution of the bending moments at the support section for the three loading cases, with and
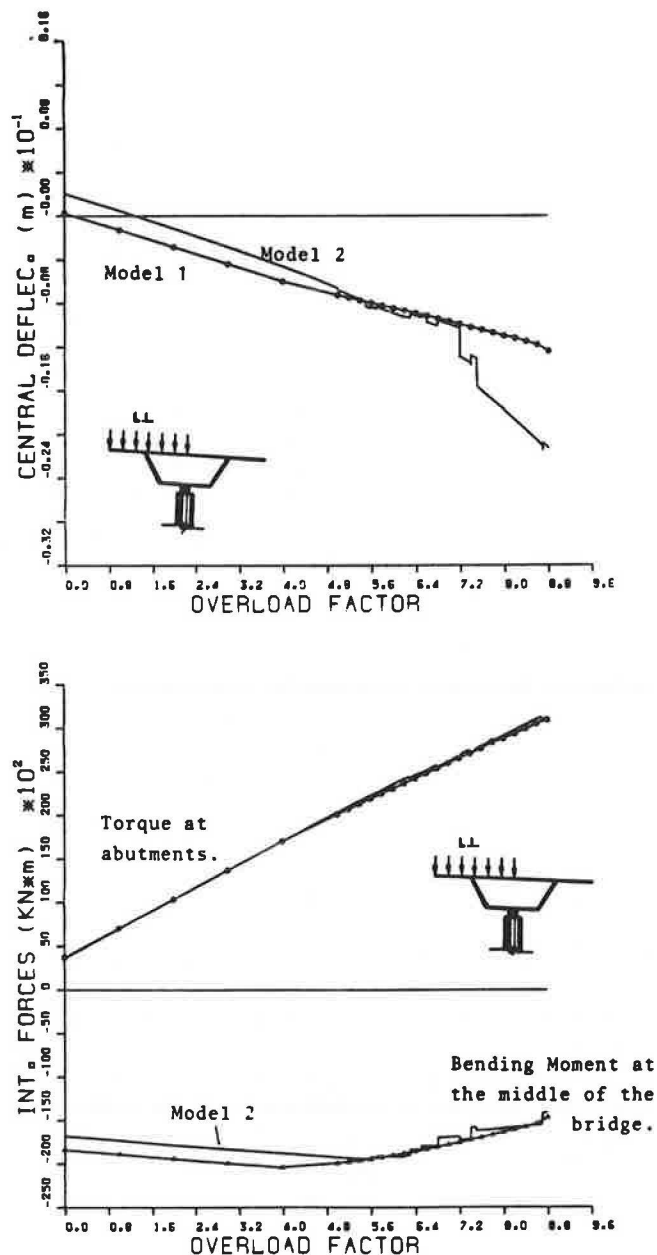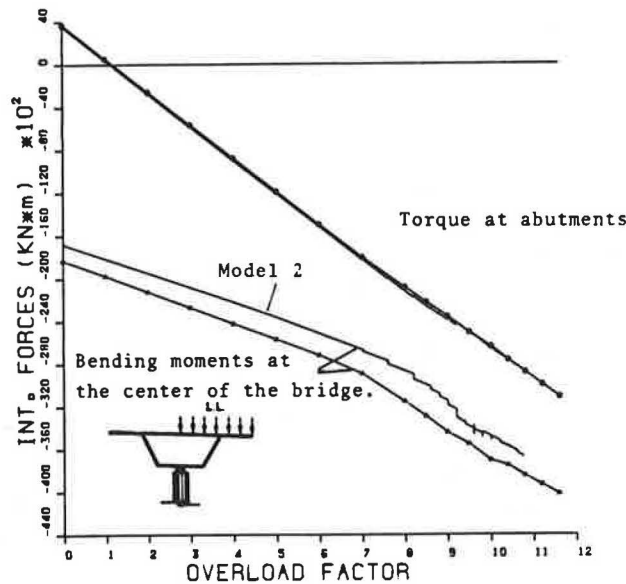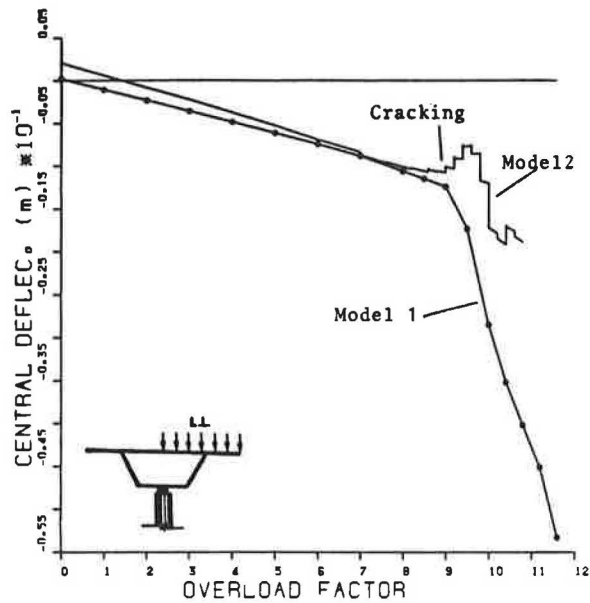
FIGURE 9   Results of Analysis 1.

The small redistribution of bending moments that occurs with time is due to the existence of prestressing and reinforcing steel on the compression side, which restrains the time deformation of concrete by increasing its compressive stress about three times (Figure 13).

The force along the three tendons is shown in Figure 14 for different times. It can be observed that, in addition to a general decrease of the tendon force because of creep and relaxation losses, there is a tendency to lose uniformity of the force along the tendons. A total loss of 3700 kN at the middle of the central span (about 12.5 percent) is obtained, which is a little lower than the results obtained by hand calculation (no shrinkage is taken into account in this analysis).

Figure 15 shows load-deflection curves at 30 and 10,000 days for a centered live load increasing to failure. From these curves it can be seen that ultimate capacity is constant with

FIGURE 10   Results of Analysis 2.
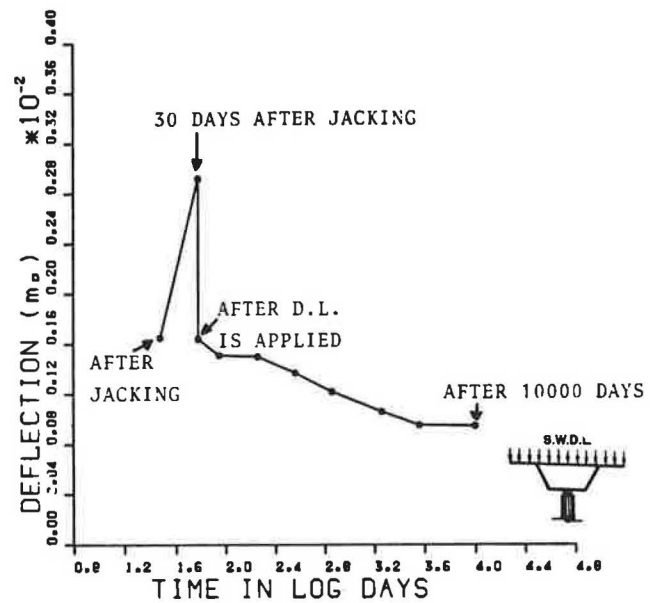
FIGURE 11   Results of Analysis 3.

FIGURE 12   Deflection at the middle of the central span.
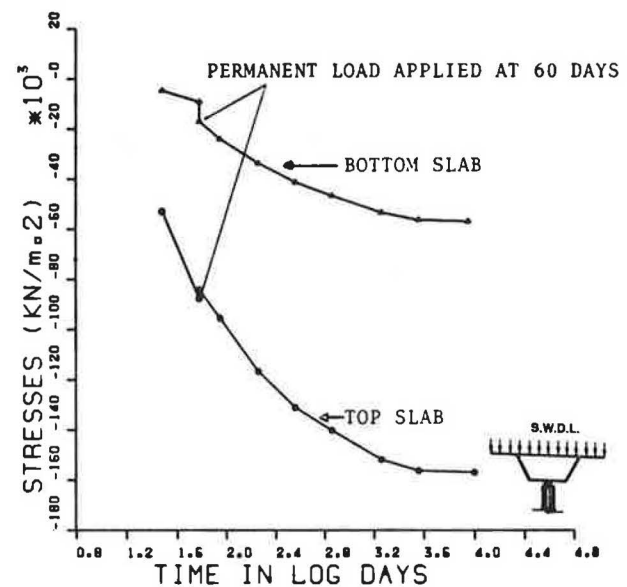
FIGURE 13   Stresses in the longitudinal reinforcing steel over the support versus time.

without transverse prestressing. It can be seen that the cracking load is slightly increased by transverse prestressing and the ultimate load capacity remains the same.

CONCLUSIONS

1. The structural response of curved prestressed box girder bridges supported over intermediate piers without torsional restraints is highly nonlinear after cracking under increasing loads.

2. The kind and degree of redistribution of internal forces depend, essentially, on the loading cases considered. For an external live load, a 37 percent increase in the bending moment over the support occurs at failure. For a centered live load such an increase is only 4 percent, whereas for an internal eccentric live load a decrease of about 30 percent takes place for the bridge studied.

3. The kind of failure depends on the load case considered. For a centered overload, flexural rupture takes place; for an external live load the failure is due essentially to torsion at the bridge ends; and for an internal overload, failure occurs simultaneously by flexural rupture at the support section and by torsion at the abutments.

4. When there is no evolutive construction, the ultimate load capacity of the bridge remains constant with the passage of time. However, the cracking load may be reduced because of prestressing losses. Redistribution of moments takes place with time because of the restraint that the reinforcing and prestressing steel introduces in the deformation of the section.

5. Transverse prestressing of top and bottom slabs introduces variations in the cracking load. However, it has no
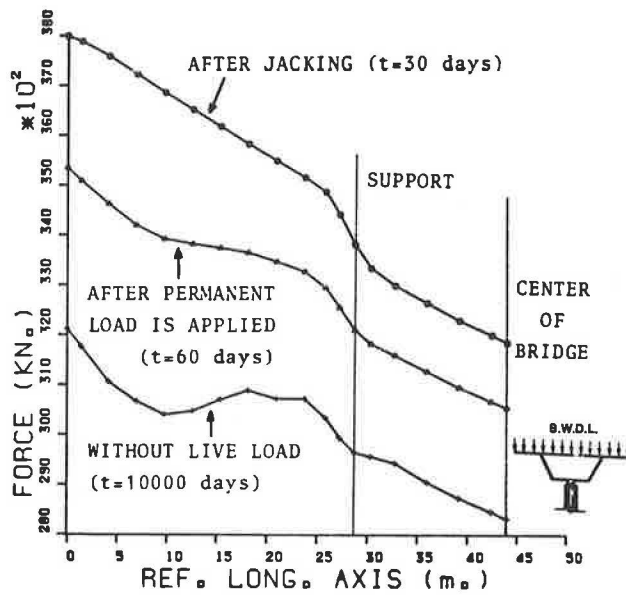
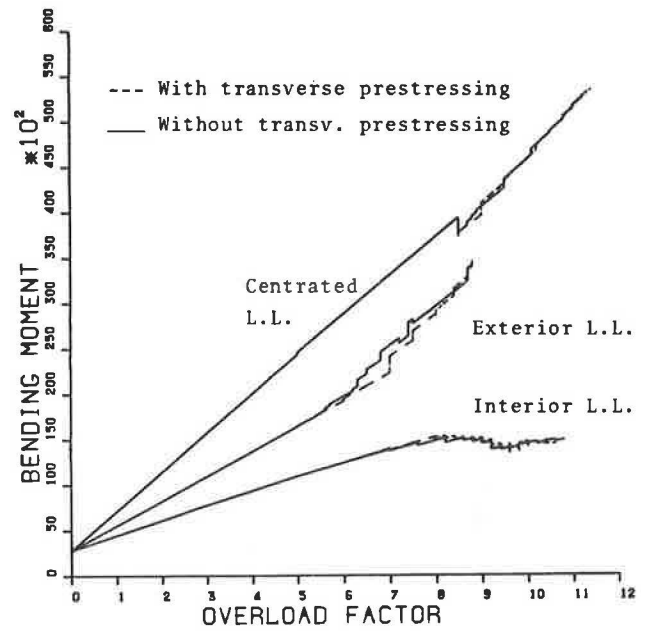FIGURE 14   Tendon force along the bridge length at different times.

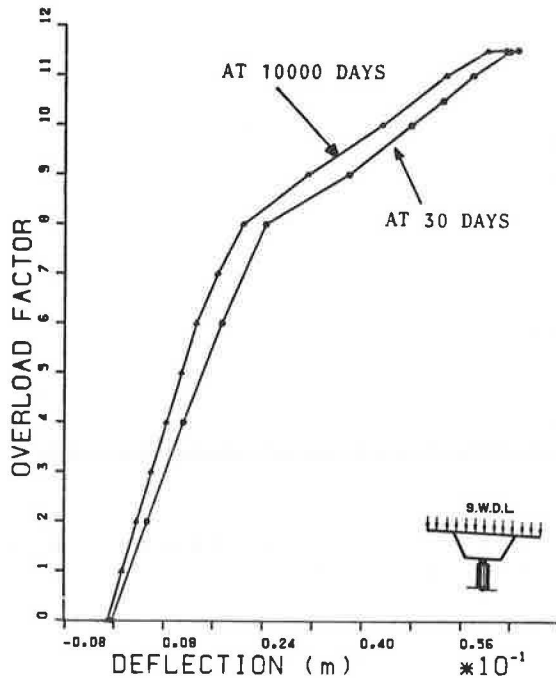FIGURE 16   Bending moments at the support section (Analysis 5).

FIGURE 15   Live load deflection at the middle of the central span.

7. However, in other kind of structures, such as straight skew bridges or longer curved bridges with or without intermediate torsional restrained supports, bending and torsion interact on the same sections. Then coupled models must be used to simulate the structural behavior.

ACKNOWLEDGMENTS

noticeable influence over the ultimate load capacity if the total mechanical ratio of transverse steel remains constant.

6. When either torsion or bending is dominant, uncoupled models can be used to predict the nonlinear response of reinforced and prestressed concrete structures. This circumstance occurs for the curved bridge studied, where, in addition, the sections subjected to maximum bending moment and maximum torque are different.

REFERENCES

1. S. Carrascón, A. R. Marí, and I. Carol. *Nonlinear Time Dependent Analysis of Curved Reinforced and Prestressed Bridges* (in Spanish). Report ES-015. Department of Civil Engineering, Universitat Politècnica de Catalunya, Barcelona, Spain, March 1987.
2. A. Lopez. A Study of the Behavior Under Increasing Loads, up to Failure, of Curved or Skew Continuous Prestressed Concrete Bridge Decks (in Spanish). Ph.D. thesis. Department of Civil Engineering, Universitat Politècnica de Catalunya, Barcelona, Spain, March 1987.
3. J. Manterola. *Opened and Closed Sections Under Eccentric Loading* (in Spanish). Monografía 15. Agrupación de Fabricantes de Cemento de España, 1976.
4. M. Sargin. *Stress-Strain Relationship for Concrete and the Analysis of Structural Concrete Sections.* Study No. 4. Solid

Mechanics Division, University of Waterloo, Waterloo, Ontario, Canada, 1970.

5. Y. J. Kang and A. C. Scordelis. Nonlinear Analysis of Prestressed Concrete Frames. *Journal of the Structural Division,* ASCE, Vol. 106, No. ST2, Feb. 1980.

6. P. Lampert. Postcracking Stiffness of Reinforced Concrete Beams in Torsion and Bending. In *Special Publication 35.* American Concrete Institute, Detroit, Mich., 1973.

7. M. Pre. Etude de la torsion dans le béton precontraint par la méthode du treillis spatial evolutif. *Annales de l'Institut Technique du Bâtiment et des Travaux Publics,* No. 385, July-Aug. 1980.

8. H. B. Kupfer and K. H. Gerstle. Behavior of Concrete under Biaxial Stresses. *Journal of the Engineering Mechanics Division,* ASCE, Vol. 99, No. EM4, Aug. 1973.

9. L. P. Saenz. Discussion of Equation for the Stress-Strain Curve of Concrete by Desay and Krishnan. *Journal of the American Concrete Institute,* Vol. 61, Sept. 1964.

10. F. Vecchio and M. P. Collins. Stress-Strain Characteristics of Reinforced Concrete in Pure Shear. Presented at International Association for Bridge and Structural Engineering Colloquium on Advanced Mechanics of Reinforced Concrete, Delft, Netherlands, 1981.

11. J. J. Arenas and A. C. Aparicio. Paso superior en la carretera de Zaragoza. Autovía Ronda Oeste de Pamplona. *Realizaciones Españolas,* ATEP, pp. 30–33, 1975.

12. Comité Euro-International du Béton and International Federation of Prestressed Concrete. *CEB-FIP Model Code for Concrete Structures.* American Concrete Institute, Detroit, Mich., 1978.

Structural Analysis and Response of Curved Prestressed Concrete Box Girder Bridges

Deepak Choudhury and Alex C. Scordelis

A numerical procedure for linear-elastic analysis and non-linear material analysis of curved prestressed concrete box girder bridges is demonstrated through two examples. A curved nonprismatic thin-walled box beam element is used to model the bridges. The cross section of the element is a rectangular single-cell box with side cantilevers. Eight displacement degrees of freedom, including transverse distortion and longitudinal warping of the cross section, are considered at each of the three element nodes. Prestressing, consisting of posttensioned bonded tendons in the longitudinal direction, is considered. For nonlinear material analysis, the uniaxial stress-strain curves of concrete, reinforcing steel, and prestressing steel are modeled. The shear and the transverse flexural responses of the box beam cross section are modeled using trilinear constitutive relationships based on cracking, yielding, and ultimate stages. The first example demonstrates the versatility of the numerical method in determining the linear-elastic distribution of forces in a three-span prestressed box girder bridge of curved plan geometry and variable cross section. Dead load, live load, and prestressing load cases are analyzed. In the second example, overload behavior and ultimate strength of a three-span curved prestressed concrete box girder bridge under increasing vehicular load are investigated. The different response characteristics of the bridge induced by different transverse locations of the overload vehicle are presented.

Prestressed concrete box girder bridges have gained importance as economic and esthetic solutions for the overpasses, underpasses, separation structures, and viaducts found in today's highway system. These bridges are often continuous-span structures (Figure 1a). Transverse diaphragms are placed at the end and interior support sections, and additional diaphragms are sometimes used between the supports. The typical cross section of such a box girder bridge consists of a top slab and a bottom slab connected monolithically by vertical webs to form a cellular or boxlike structure (Figure 1b). Design and esthetic considerations often call for longitudinal variations in the cross-sectional dimensions. In plan, the bridge can have a straight or curved geometry. Sometimes part of the bridge may be straight and part of it may be curved (Figure 1c). The complex spatial nature of a curved box girder bridge with a variable cross section (nonprismatic) makes it difficult to predict the structural response to a general loading

D. Choudhury, T. Y. Lin International, 315 Bay Street, San Francisco, Calif. 94133. A. C. Scordelis, Department of Civil Engineering, University of California, Berkeley, Calif. 94720.
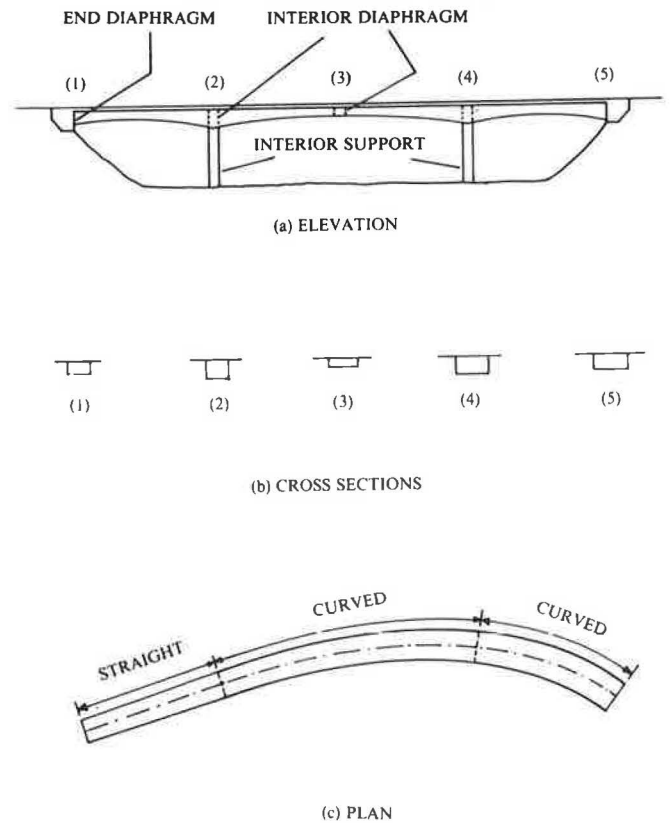
FIGURE 1 Curved nonprismatic box girder bridge.

case accurately. The presence of prestressing further complicates the analysis. Even with the assumption of homogeneous linear-elastic material, the accurate analysis of such a structure remains a formidable challenge to the engineer. Highway bridges are being subjected to increasing vehicular loads and traffic densities. A better understanding of the overload behavior of these bridges beyond the service load range is necessary. Also, in order to assess the degree of safety against failure, an accurate estimate of the ultimate load has to be made. A nonlinear analysis procedure incorporating the effects of nonhomogeneity of the material, concrete cracking, and nonlinearities in the stress-strain relationships of concrete reinforcing steel and prestressing steel is thus required. The objective of this paper is to demonstrate the capabilities of a numerical procedure for linear-elastic analysis and nonlinear material

analysis of curved nonprismatic prestressed concrete box girder bridges. The overall response of the structure, rather than the local behavior, is studied.

METHOD OF ANALYSIS

The method of analysis employed in the present study uses a finite-element formulation based on thin-walled beam theory (*1, 2*). The theoretical details, summarized briefly in this paper, have been presented elsewhere (*3*).

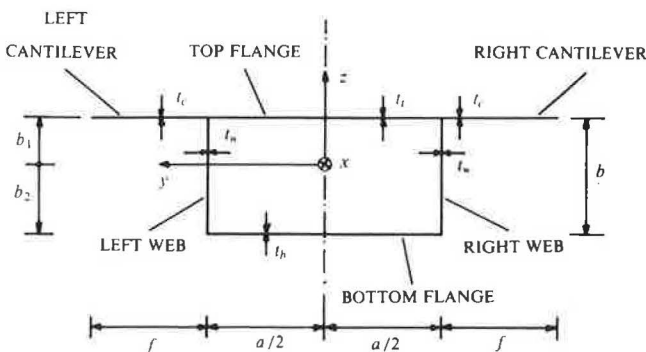### Curved Nonprismatic Box Beam Element

Thin-walled box beam elements have been used by several investigators (*4–6*) for linear-elastic analysis of box girder bridges. These elements are capable of capturing the dominant structural actions, but at considerably reduced computational effort. The simplicity and reduced computational effort inherent in a beam-type element make it particularly suitable for nonlinear analysis, which requires much greater central processing unit time and storage space in the computer than linear-elastic analysis. Thus in the present study, certain aspects of the formulations used by Bazant and El Nimeiri (*4*) and by Zhang and Lyons (*5*) are combined to develop a curved nonprismatic thin-walled box beam element that can be easily extended to nonlinear analysis.

The three-node element is shown in Figure 2. Its axis lies in the global *X-Y* plane and may be curved. The cross section of the element perpendicular to its axis is a rectangular, single-cell, thin-walled box with side cantilevers. The dimensions of the box cross section, indicated in Figure 2b, can all vary along the length of the element. The geometry of the element is defined using an isoparametric mapping between the three nodes. The shape functions associated with the three nodes are second-order Lagrangian polynomials.

At each element node, eight generalized displacement degrees of freedom are considered. These are the usual six degrees of freedom associated with the rigid body translations and rotations of the cross section and, in addition, a longitudinal warping mode and a transverse distortional mode of the cross section (Figure 3). A generalized strain and its associated generalized stress are used to represent the strain energy contribution from transverse bending of the walls of the box cross section caused by the transverse distortional mode (Figure 3b). Also, the longitudinal normal strains and stresses and the shear strains and stresses acting in the plane of the cross section along the walls of the box are monitored.
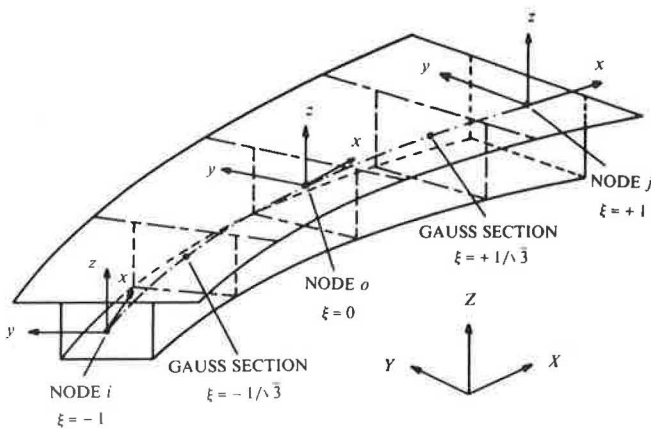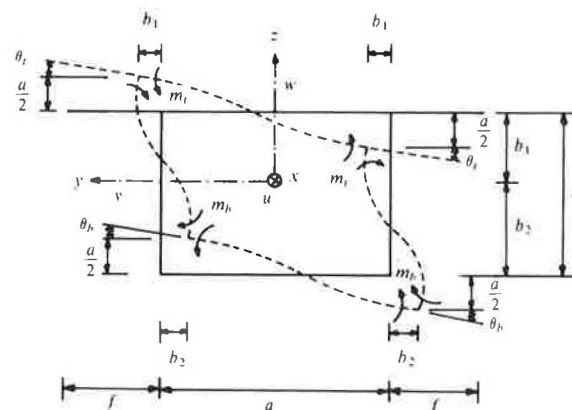

(a) ISOMETRIC VIEW

(b) CROSS SECTION

FIGURE 2 Curved nonprismatic thin-walled box beam element.
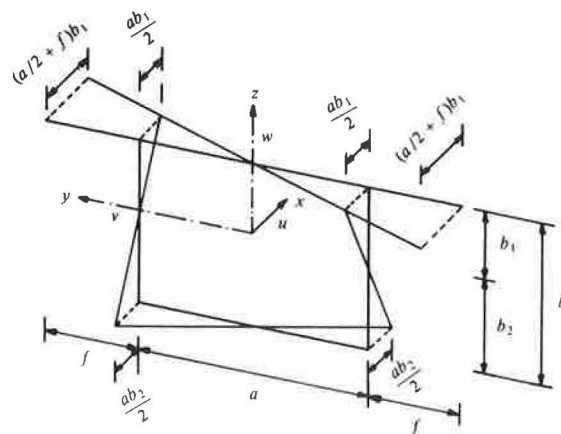
(a) UNIT LONGITUDINAL WARPING

(b) UNIT TRANSVERSE DISTORTION

FIGURE 3 Longitudinal warping and transverse distortional modes.

The element property matrices are obtained numerically using two-point Gaussian quadrature along the element axis. This is found to eliminate the spurious shear stiffness usually associated with beam and shell formulations, including shear deformations. Spurious shear effects relative to the torsional, distortional, and warping degrees of freedom are also eliminated by this reduced order of integration.

Prestressing

Prestressing, by means of posttensioned tendons in the longitudinal direction, is considered. The tendons are idealized as straight prestressing steel segments between the nodes of the box beam elements. Friction and anchorage slip losses are considered. For linear-elastic analysis of the structure under prestressing, the effect of prestress is represented by a set of equivalent loads applied at the nodes of the box beam elements. For the analysis at transfer of prestress in a nonlinear analysis, the prestressing is similarly represented by a set of

FIGURE 4   Box cross section discretized into concrete and longitudinal reinforcing steel filaments.

equivalent nodal loads, and the structure is analyzed as if it were of ordinary reinforced concrete. The contribution of the prestressing steel to the overall structural stiffness is neglected because at this stage the steel is unbonded. For the subsequent application of external loads, the prestressing steel is assumed to be bonded to the concrete (i.e., grouted), and the prestressing steel stiffnesses are included in the overall structural stiffness.

Nonlinear Analysis Procedure

For nonlinear material analysis, the box beam elements are considered to be concrete elements reinforced with steel in the longitudinal and transverse directions. In order to model the response of the reinforced concrete box beam element under longitudinal normal strains and stresses, the element cross section is idealized as concrete and longitudinal steel filaments that are assumed to be in a state of uniaxial stress (Figure 4). The uniaxial stress-strain curve adopted for the concrete filaments is based on the widely used relationship in compression suggested by Hognestad (7), together with cracking in tension at the tensile strength. With additional assumptions for load reversal, a total of 11 possible material states are obtained (Figure 5a). For the longitudinal steel filaments, a bilinear stress-strain relationship with load reversal is used (Figure 5b). Four different material states are possible. In addition, the tension-stiffening effect between the concrete and the steel filaments is modeled with a "steel-referred" method.

The trilinear constitutive relationship shown in Figure 5c is used to represent the shear response of the walls of the box section. The model incorporates the cracking, yielding, and ultimate stages. The postcracking behavior is based on the 45-degree truss analogy. The possibility of load reversal is considered, which gives a total of five different material states.
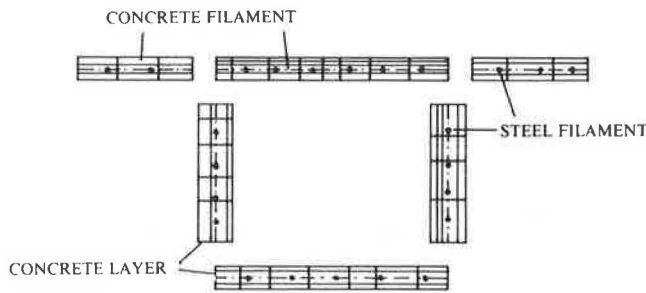

(a) CONCRETE

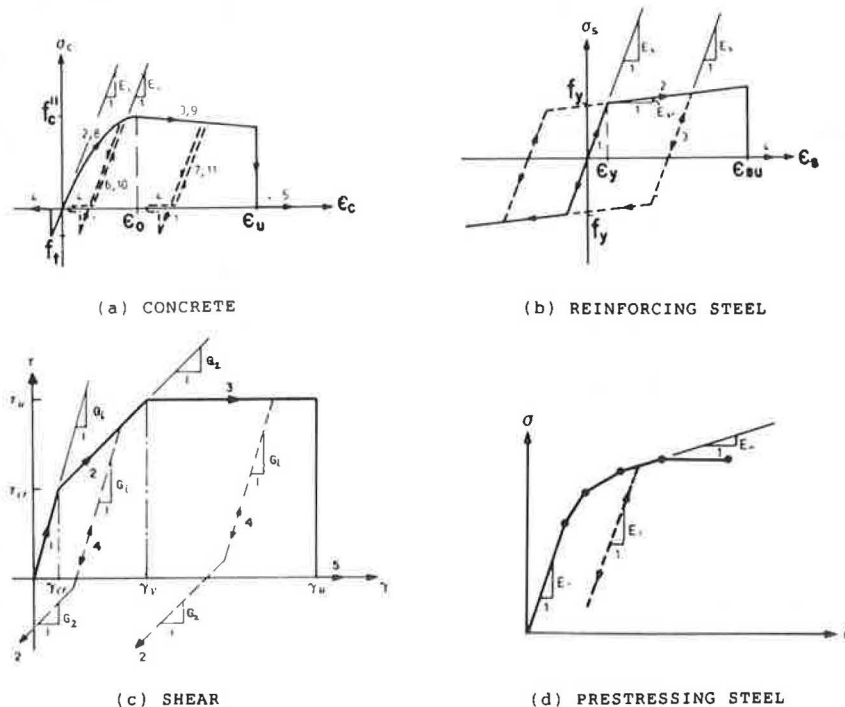(b) REINFORCING STEEL

(c) SHEAR

(d) PRESTRESSING STEEL

FIGURE 5   Nonlinear constitutive models.

The constitutive relationship for transverse flexure is obtained from a flexural analysis of the box beam cross section as a transverse reinforced concrete frame of unit width in the longitudinal direction. The resulting response is modeled with a trilinear relationship similar to the one used for shear (Figure 5c).

The uniaxial stress-strain relationship of the prestressing steel segments is modeled by using a multilinear idealization with load reversal (Figure 5d).

Because of the nonlinearities in the constitutive relationships, the equilibrium equations of the structure are nonlinear. These nonlinear equilibrium equations are solved in increments. Increments of either prescribed loads or displacements are applied, and for each increment unbalanced load iterations are performed until certain predefined convergence criteria are satisfied. With this nonlinear analysis procedure, the structural response can be traced throughout the elastic, inelastic, and ultimate load ranges.

COMPUTER PROGRAMS

The method of analysis has been incorporated into two computer programs: LAPBOX for linear-elastic analysis, and NAPBOX for nonlinear material analysis. The basic input for both programs consists of structure geometry and boundary conditions, material properties, prestressing data, structure loading, and locations for stress output. In addition, NAPBOX requires data on concrete and longitudinal steel filaments, transverse steel, and convergence tolerances. The various generation schemes implemented in the programs allow accurate modeling of complex bridge geometries, loadings, and prestressing tendon profiles on the basis of a few simple input parameters.

The computer programs LAPBOX and NAPBOX have been verified (*3*). Linear-elastic solutions from LAPBOX were compared with the folded-plate elasticity method (*8*), the finite-strip method (*9*), and the experimental results from a tapered box girder (*10*). NAPBOX results were compared with the computer program PCFRAME (*11*) for the special case of planar loading. PCFRAME, which is capable of performing nonlinear analysis of planar prestressed concrete frames, has been extensively tested (*11, 12*).

Detailed information on the theoretical basis, input and output, and a computer tape containing the source listings for LAPBOX and NAPBOX is available by writing to the second author.

EXAMPLE 1: LINEAR-ELASTIC ANALYSIS

Example 1 demonstrates the applicability of the proposed method and the capabilities of the computer program LAPBOX in determining the linear-elastic distribution of forces in a complex prestressed concrete box girder bridge of curved plan geometry and variable cross section.

Structure Details and Analytical Modeling

A hypothetical three-span continuous prestressed concrete box girder bridge (Figure 6) is analyzed. In plan (Figure 6a), the bridge has a straight span of 140 ft between supports S1 and S2, and two circularly curved spans of 240 ft between supports S2 and S3 and 180 ft between supports S3 and S4. The radius
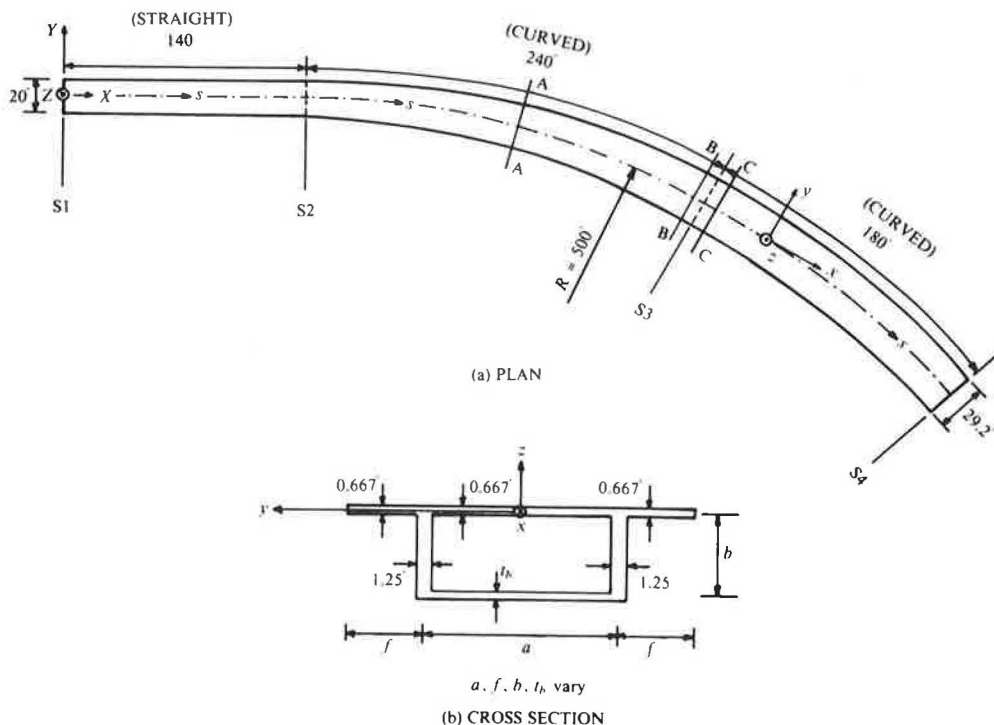

FIGURE 6 Example 1: three-span curved nonprismatic prestressed concrete bridge. (a) Plan view, (b) cross section.

of the circularly curved spans is $R = 500$ ft to the centerline. For convenience, a coordinate s is defined along the centerline with its origin at S1 and directed toward S4. At each of the four supports of the bridge, vertical movement, twist, and transverse distortion of the cross section are prevented.

The cross section of the bridge is shown in Figure 6b. The following equations define the variation of the cross-sectional dimensions a, f, b, and t_b (all in feet) in terms of the s-coordinate. A modulus of elasticity of 608,256 kips/ft^2 and a Poisson's ratio of 0.18 are assumed for the concrete.

$$
\begin{array}{lll}
a & = 12 + s/100 & \text{for } 0 < s < 560 \text{ ft} \\
f & = 4 + 9s/2800 & \text{for } 0 < s < 560 \text{ ft} \\
b & = 6 + s/70 & \text{for } 0 < s < 140 \text{ ft} \\
  & = 52/3 - s/15, & \text{for } 140 \text{ ft} < s < 200 \text{ ft} \\
  & = 4 & \text{for } 200 \text{ ft} < s < 320 \text{ ft} \\
  & = -52/3 + s/15, & \text{for } 320 \text{ ft} < s < 380 \text{ ft} \\
  & = 110/9 - s/90 & \text{for } 380 \text{ ft} < s < 560 \text{ ft} \\
t_b & = 3/5 + s/200 & \text{for } 0 < s < 140 \text{ ft} \\
  & = 67/30 - s/150 & \text{for } 140 \text{ ft} < s < 260 \text{ ft} \\
  & = -37/30 + s/150 & \text{for } 260 \text{ ft} < s < 380 \text{ ft} \\
  & = 25/9 - 7s/1800 & \text{for } 380 \text{ ft} < s < 560 \text{ ft}
\end{array}
$$

The bridge is prestressed with 14 different tendons, 7 in each web (Figure 7). The jacking forces and the geometry data of each tendon are given in Table 1. Each tendon numbered 1 through 6 has a vertical profile along its span consisting of one parabolic segment. Each of the other 8 tendons has two parabolic segments connected by a linear segment in the middle. All the tendons are stressed simultaneously from both ends. A wobble friction coefficient of 0.0002/ft, a curvature friction coefficient of 0.2/radian, and no anchorage slip are assumed.

Three different load cases are considered. They may be summarized as follows:

Case 1: Dead load due to a unit weight density of 160 pcf.
Case 2: Prestressing.
Case 3: Uniform live load of 0.15 kip/ft^2 over the full width of the the top deck and between $s = 180$ ft and 340 ft.

TABLE 1   EXAMPLE 1: PRESTRESSING TENDON DATA

TENDON NO.	JACKING FORCE	LOCATION OF END A		LOCATION OF END B		LOCATION(S) OF ZERO TENDON SLOPE	
	(kip)	s (ft)	z (ft)	s (ft)	z (ft)	s (ft)	z (ft)
1, 2	300	0	-2.470	120	-4.044	60	-6.357
3, 4	700	420	-3.646	560	-2.410	490	-6.278
5, 6	600	180	-2.473	340	-2.463	260	-3.500
7, 8	2500	80	-3.343	200	-1.710	120; 160	-0.500
9, 10	3000	320	-1.840	440	-3.283	360; 400	-0.500
11, 12	1000	40	-2.911	240	-1.710	80; 200	-0.500
13, 14	1250	280	-1.710	480	-4.089	320; 440	-0.500

The bridge is analyzed by using 56 curved nonprismatic box beam elements, each 10 ft long. All load cases are represented by equivalent nodal loads generated automatically within the program LAPBOX.

An additional analysis is performed for load case 3 with the computer program SAP IV (*13*) using 56 one-dimensional (straight) beam elements, each spanning 10 ft (measured along the actual axis of the bridge). Each element is prismatic, so the nonprismatic bridge can only be modeled approximately by using different cross-sectional properties for each element.

Results

Table 2 gives a summary of the support reactions obtained from LAPBOX for all load cases. In the last two columns, the total of all the vertical reactions is compared with the total applied load calculated by hand from the actual geometry and loading of the structure. The agreement is perfect, which is indicative of the high accuracy with which the box beam elements can be used to model the geometry and loading of a curved nonprismatic bridge. The support reactions obtained from the SAP IV analysis for load case 3 are also shown in Table 2. The agreement between the LAPBOX and the SAP IV results is good, particularly for the vertical reactions.
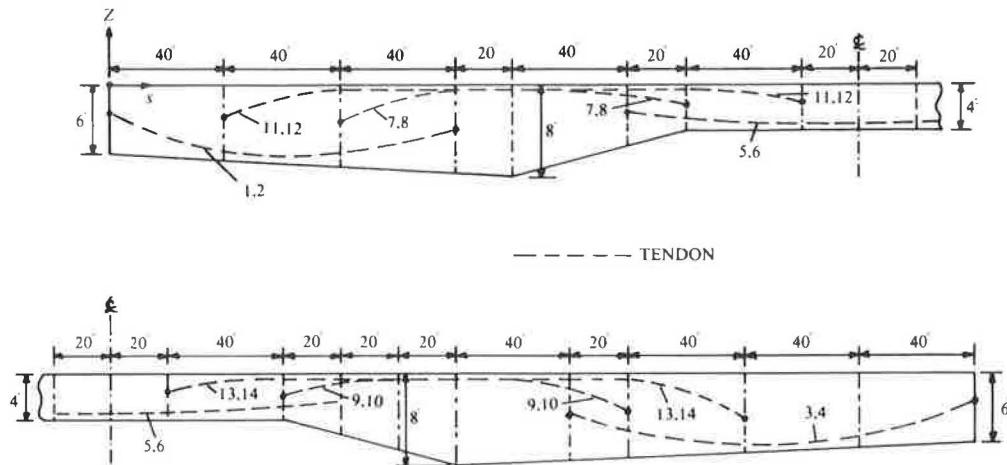

FIGURE 7   Example 1: three-span curved nonprismatic prestressed concrete bridge—longitudinal section along centerline.

TABLE 2   EXAMPLE 1: SUMMARY OF SUPPORT REACTIONS

LOAD CASE	FORCE QUANTITY	SUPPORT S1	SUPPORT S2	SUPPORT S3	SUPPORT S4	TOTAL VERTICAL REACTION (kip)	TOTAL APPLIED LOAD (kip)
DEAD LOAD	Distortional Moment M_d (kip·ft)	-0.2	782.4	2233.6	-125.1	—	—
	Vertical Force V_z (kip)	237.8	1491.9	1853.2	493.8	4076.7	4076.7
	Torque M_s (kip·ft)	-2.8	-867.9	-2026.8	1545.0	—	—
PRE-STRESS	Distortional Moment M_d (kip·ft)	-0.1	260.1	572.3	14.6	—	—
	Vertical Force V_z (kip)	-30.8	26.4	34.2	-29.8	0.0	0.0
	Torque M_s (kip·ft)	-1.6	-1103.6	-1954.8	-267.3	—	—
LIVE LOAD (LAPBOX)	Distortional Moment M_d (kip·ft)	-0.1	430.3	1035.3	8.0	—	—
	Vertical Force V_z (kip)	-116.2	404.0	385.2	-90.5	582.5	582.5
	Torque M_s (kip·ft)	-1.6	-322.9	-2359.2	-860.3	—	—
LIVE LOAD (SAP IV)	Vertical Force M_z (kip)	-115.7	403.4	385.2	-90.4	582.5	582.5
	Torque M_x (kip·ft)	0	-344.2	-2384.0	-848.0	—	—

The longitudinal variations of the vertical centerline displacements are shown in Figure 8. The plotted values for the live load case represent both the LAPBOX and the SAP IV analyses, which predicted practically the same vertical displacements. The transverse distributions of the vertical displacements at the middle of the interior span ($s = 260$ ft) are shown in Figure 9. The vertical displacements are larger at the outer web than at the inner web, with almost a linear variation across the bridge width, which indicates a twist of the cross section with little transverse distortion.

Longitudinal variations of bending moments for dead load, prestressing, and live load are shown in Figures 10 through 12,
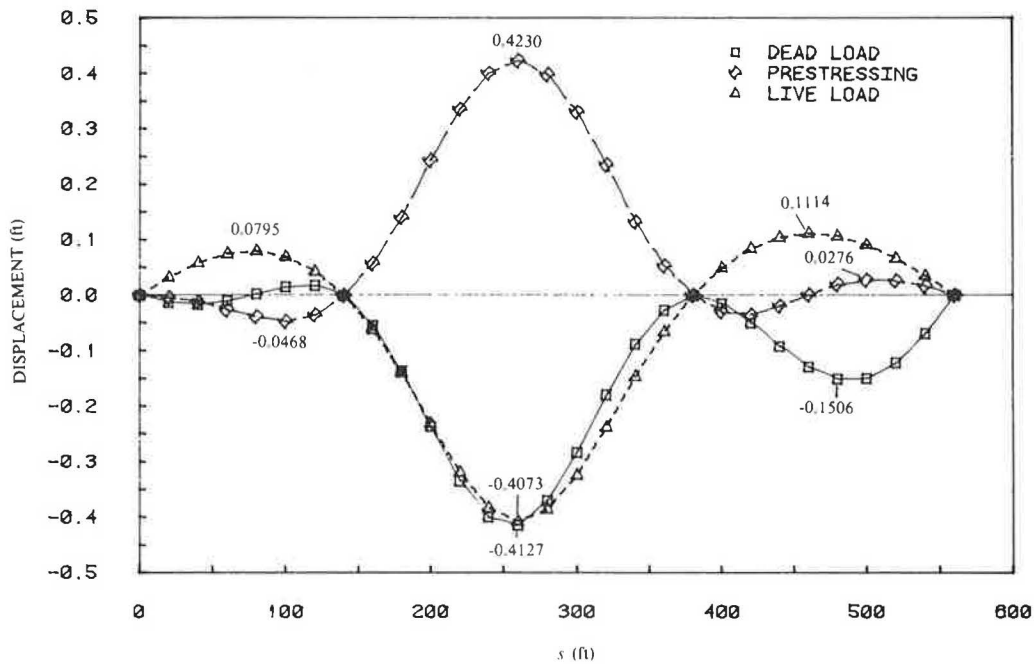

FIGURE 8   Example 1: longitudinal distributions of vertical centerline displacements.

respectively. It should be noted that the moments are with respect to the local y-axes of the cross sections (Figure 6b). When axial loads are present, which is the case with prestressing, the plotted moments will differ from the moments about the neutral axes of the cross sections. The locations of
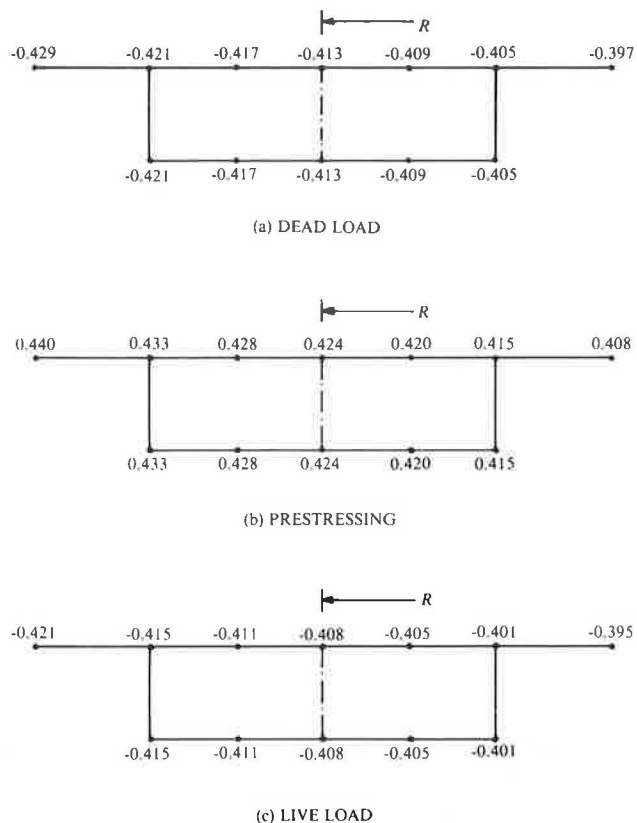

(a) DEAD LOAD

(b) PRESTRESSING

(c) LIVE LOAD

FIGURE 9 Example 1: transverse distributions of vertical displacements ($s = 260$ ft).

the discontinuities in the prestressing moment diagram (Figure 11) correspond to the tendon ends. The live load moments (Figure 12) obtained from the LAPBOX and the SAP IV analyses are found to agree closely.

The close agreement between the LAPBOX and the SAP IV results for the live load case indicates that the longitudinal flexural behavior of the bridge was not affected significantly by transverse distortion and longitudinal warping of the cross sections. However, ordinary beam theory (SAP IV) cannot predict the transverse distribution of stresses and the transverse flexural moments (not reported), which can be obtained from thin-walled beam theory (LAPBOX).

EXAMPLE 2: NONLINEAR ANALYSIS

Example 2 demonstrates how the proposed nonlinear analysis procedure can be used to trace the response of a curved prestressed concrete box girder bridge throughout the elastic, inelastic, and ultimate load ranges. Overload behavior and ultimate strength of the bridge under increasing vehicular load are investigated. The different response characteristics of the bridge, induced by different transverse locations of the overload vehicle, are presented.

Structure Details and Analytical Modeling

The three-span, curved, continuous, prestressed concrete box girder bridge considered in this example is shown in Figure 13. Its span arrangement is symmetric, with spans of 160, 200, and 160 ft. The axis of the bridge is circularly curved in plan with a radius of $R = 496.5$ ft to the centerline. Full restraint against vertical translation, twist, and transverse distortion of the cross section at the four supports is assumed.

For the sake of simplicity, the cross section (Figure 13b) is assumed to be constant from one end of the structure to the
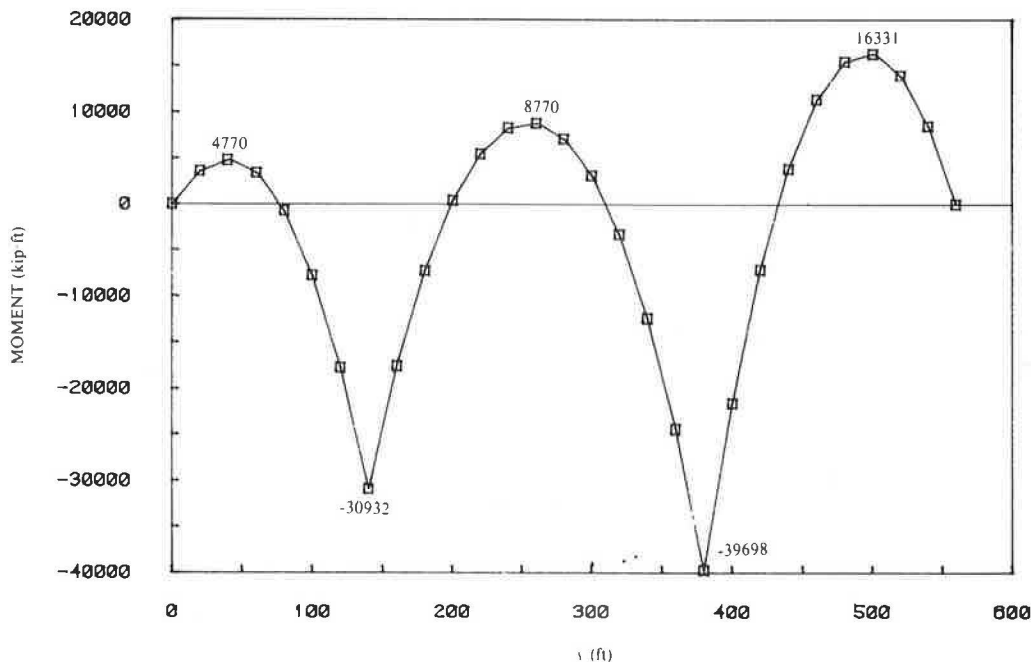

FIGURE 10 Example 1: longitudinal distribution of bending moment M_y due to dead load.
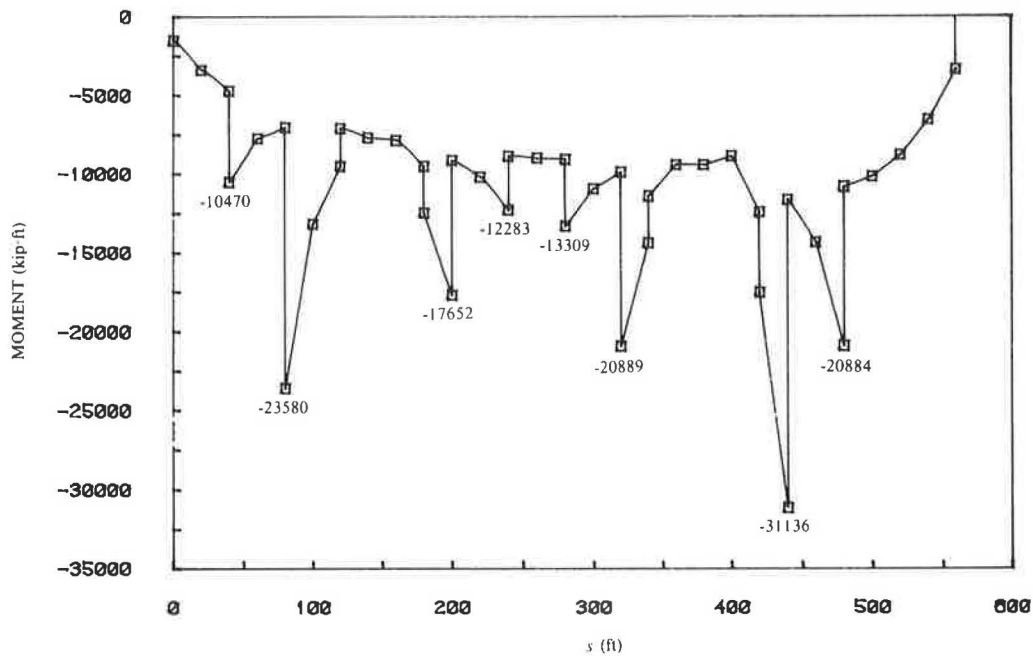
FIGURE 11 Example 1: longitudinal distribution of bending moment M_y due to prestressing.
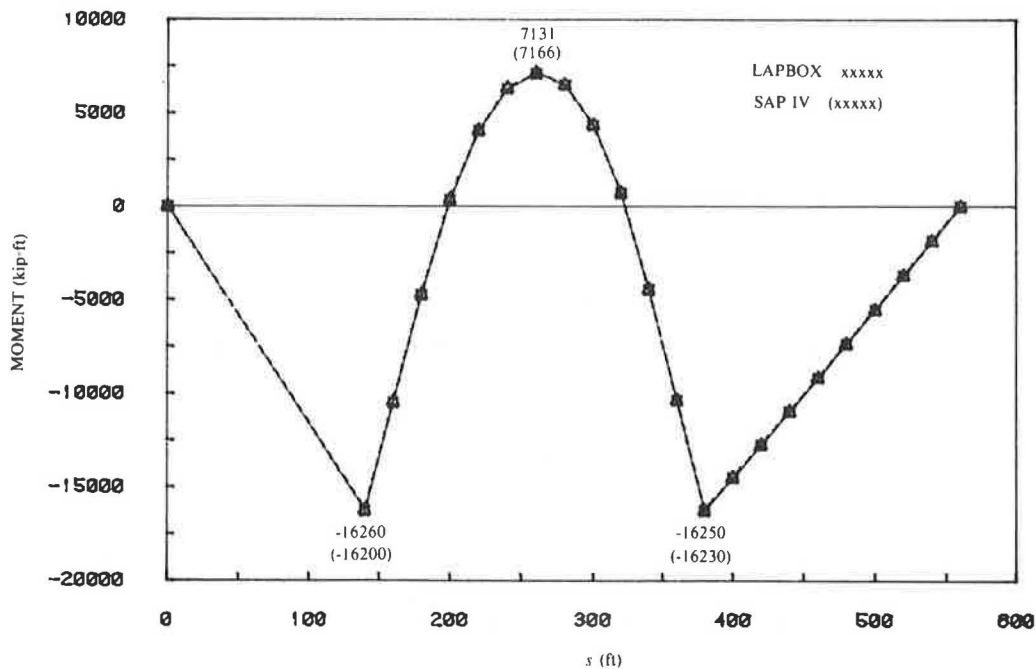

FIGURE 12 Example 1: longitudinal distribution of bending moment M_y due to live load.

owner, although design considerations often call for thickening of the bottom flange or the webs, or both, in regions near the supports. The total top deck width of 34 ft is typical of a two-lane highway bridge.

The prestressing in the bridge consists of two tendons in the longitudinal direction, one in each web. The prestress is achieved by posttensioning from both ends simultaneously, after which the prestressing steel is grouted and hence bonded to the concrete. The tendon profile along the curved webs is the same in each web, and is shown in Figure 13c.

The following conditions are assumed: concrete compressive strength of 4,000 psi, mild steel yield strength of 60 ksi, prestressing steel ultimate strength of 270 ksi, wobble friction coefficient of 0.0002/ft, curvature friction coefficient of 0.25/radian, anchorage slip at each jacking end of 0.25 in., and unit weight of composite structure of 155 pcf.

(a) PLAN

(b) CROSS SECTION
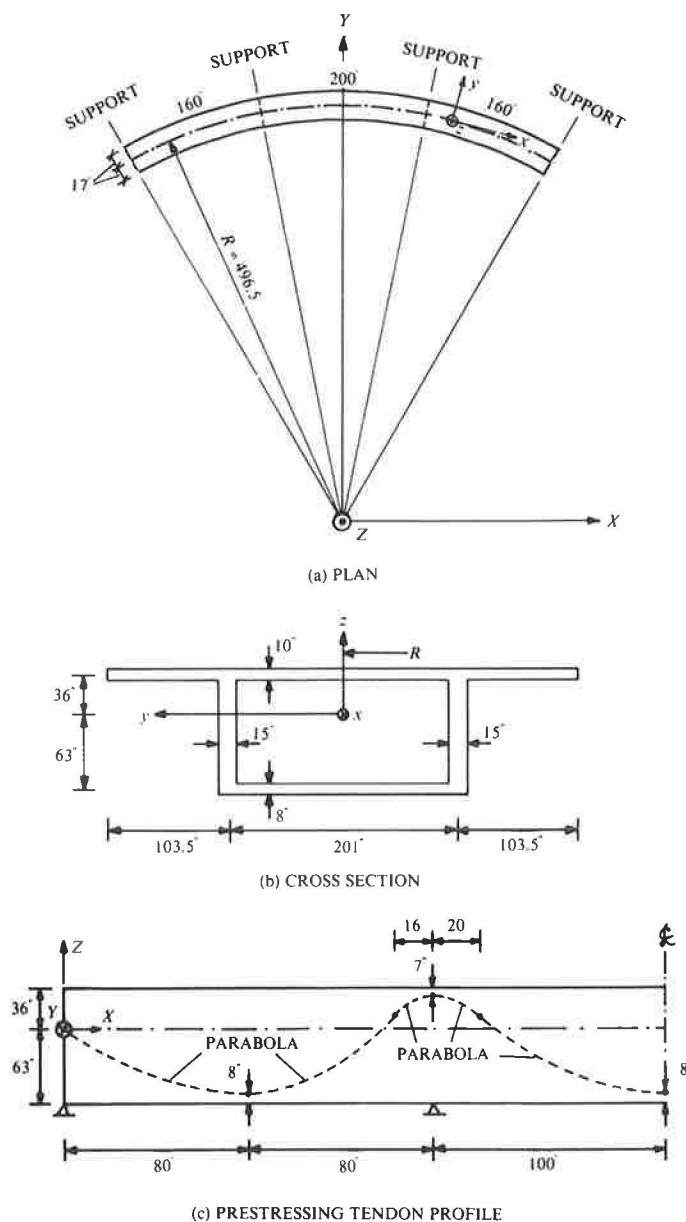
(c) PRESTRESSING TENDON PROFILE

FIGURE 13   Example 2: three-span curved prestressed
concrete bridge.

Structural design of the box girder is based on State of
California standard criteria (*14*). The prestressing steel re-
quirements are calculated by considering HS20 lane loading in
each of the two lanes, impact factors on the basis of span
lengths, and an allowable tensile stress of 6 $(f_c')^{1/2}$ psi in
concrete after all prestressing losses have occurred. A total of
172 seven-wire strands with 0.5-in. diameter (86 strands per
web), which gives a total prestressing steel area of 26.32 in.^{2},
is provided. The required jacking force is 2,660 kips per web.
Ultimate strength under factored loads is checked. In the load
factor design, an additional overload vehicle, designated a P13
truck (Figure 14), is considered.

Longitudinal mild steel reinforcement corresponding to 0.3
percent of the concrete area is provided in each wall of the box
cross section. This steel is not required because of strength
considerations, but is provided for construction purposes. The

transverse reinforcement consists of two legs of No. 5 stirrups
at 4-in. longitudinal spacing in each web and two legs of No. 5
stirrups at 10-in. longitudinal spacing in each slab.

The response of the bridge structure is studied under in-
creasing levels of vehicular overload. The overload vehicle,
the P13 truck (Figure 14), is typical of the heaviest vehicles
found on California's highways. In order to take advantage
of the symmetry of the structure, the P13 truck loading in
Figure 14b is approximated with the symmetric loading in
Figure 14d. This symmetric truck loading is positioned in the
middle of the center span of the bridge (Figure 15a), and the
structural load vector due to its weight is increased in incre-
ments until ultimate failure occurs. For convenience in presen-
tation of results, P is used to denote the factor of truck load
applied. Thus $P = 1$ represents the overload due to one truck
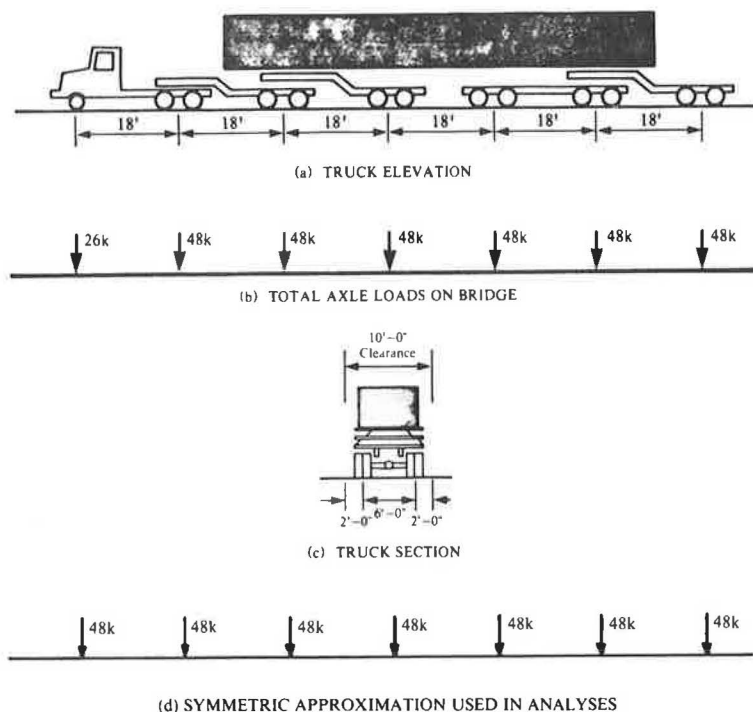(Figure 15a).

(a) TRUCK ELEVATION

(b) TOTAL AXLE LOADS ON BRIDGE

(c) TRUCK SECTION

(d) SYMMETRIC APPROXIMATION USED IN ANALYSES

FIGURE 14   Example 2: P13 truck loading.

(a) LONGITUDINAL POSITION OF TRUCK LOAD
FOR LOAD CASES 1, 2 AND 3

(b) TRANSVERSE POSITION OF TRUCK LOAD
FOR LOAD CASE 1

(c) TRANSVERSE POSITION OF TRUCK LOAD
FOR LOAD CASE 2

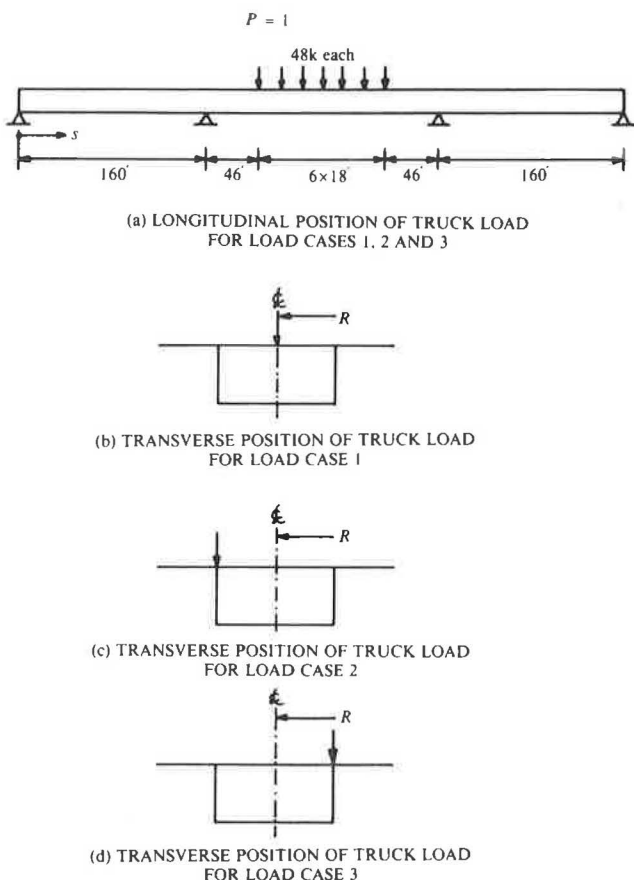(d) TRANSVERSE POSITION OF TRUCK LOAD
FOR LOAD CASE 3

FIGURE 15   Example 2: position of truck load for different load cases.

Three different load cases are considered:

Case 1: Truck load positioned over bridge centerline (Figure 15b).

Case 2: Truck load positioned over outer web (Figure 15c).

Case 3: Truck load positioned over inner web (Figure 15d).

Because of the symmetry of the structure and the loadings, only half the length of the bridge is analyzed. Forty curved box beam elements of varying lengths are used. The cross section is discretized into 52 concrete and 26 longitudinal steel filaments.

Results

Figures 16 through 18 show the vertical web displacements at the middle of the center span under increasing truck loads for load cases 1, 2, and 3, respectively. It is evident from the load-displacement curves that the structure responds quite differently depending on the transverse position of the truck load.

Load case 1 (Figure 16), with the truck load over the centerline, yielded the highest ultimate load of $P = 5.6$. Failure occurred because of the yielding of concrete filaments in compression at the bottom flange over the interior supports. The small differences between the vertical displacements at the two webs indicate that the overall response of the bridge was governed by its longitudinal flexural behavior.

In Figure 17, the differences between the vertical displacements at the two webs are seen to be quite significant for load case 2, in which the truck load is positioned over the outer
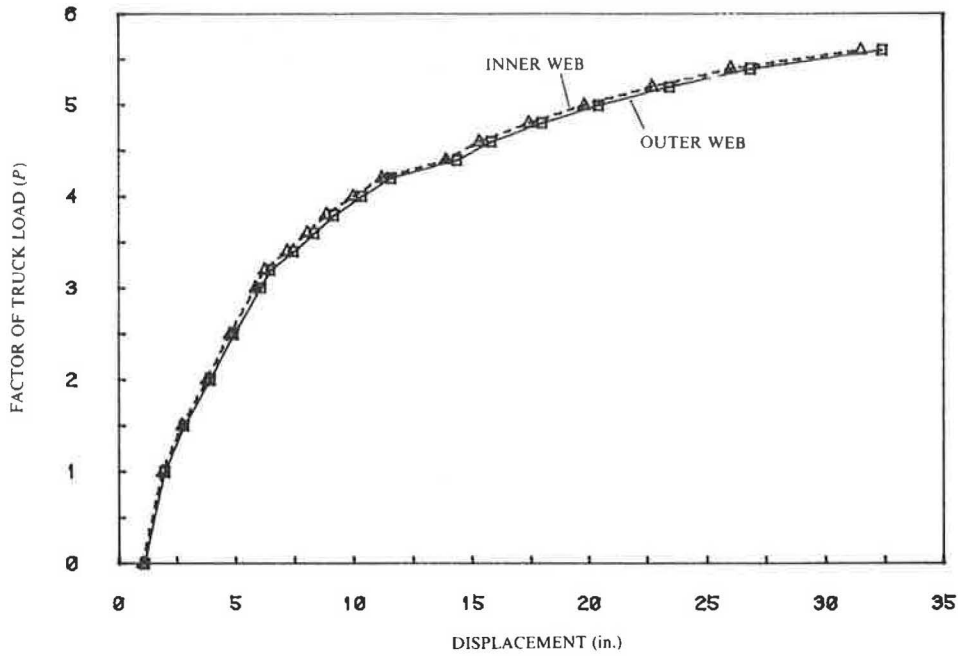
FIGURE 16   Example 2: load versus vertical web displacements at middle of center span (load case 1).
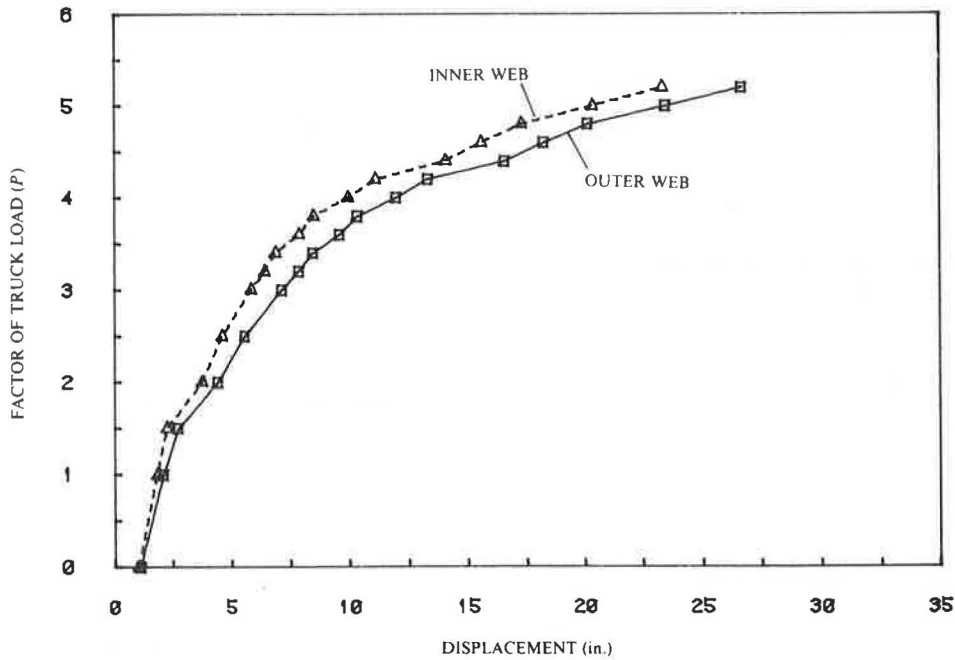

FIGURE 17   Example 2: load versus vertical web displacements at middle of center span (load case 2).

web. The differential web displacements, which increase with increasing load levels, are primarily due to the twist of the cross section and were caused by rapid deterioration in the torsional stiffness of the bridge. The ultimate load of the bridge was reduced to $P = 5.2$. Failure occurred when the shear stress reached its ultimate value at the outer web of the sections just to the inside of the interior supports.

An ultimate load of only $P = 4.0$ was obtained for load case 3 (Figure 18), with the truck load positioned over the inner web. This loading produced rapid deterioration in the
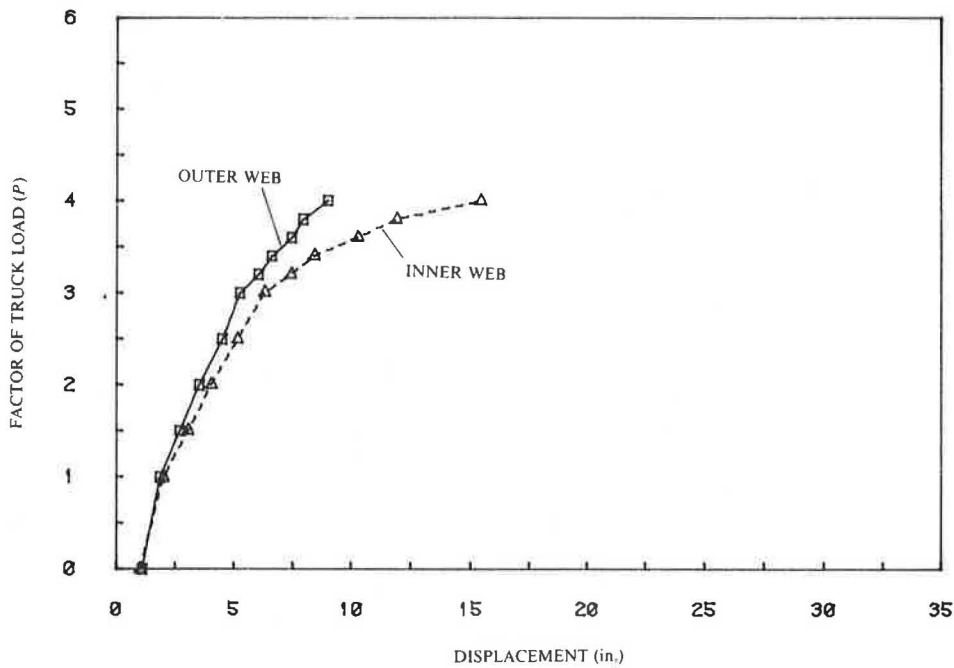
FIGURE 18 Example 2: load versus vertical web displacements at middle of center span (load case 3).

transverse flexural rigidity of the bridge. The transverse distortion of the cross section at the middle of the center span increased rapidly, and this is reflected in the increasingly large differences between the vertical displacements at the two webs. Failure was due to the ultimate transverse distortion of the cross section at the middle of the center span, which is governed by the plastic hinge rotation capacities at the four corners of the box section.

The cross-section twists at the middle of the center span are shown in Figure 19 for all three load cases. The rapid deterioration in the torsional stiffness of the bridge for load case 2 is evident. Of the three load cases considered, load case 2 represents the most severe torsional loading. The outer web loading tends to twist the cross section in the same direction as the dead load and prestressing, and hence produces the largest cross-section twists. Load case 1 produces a less severe
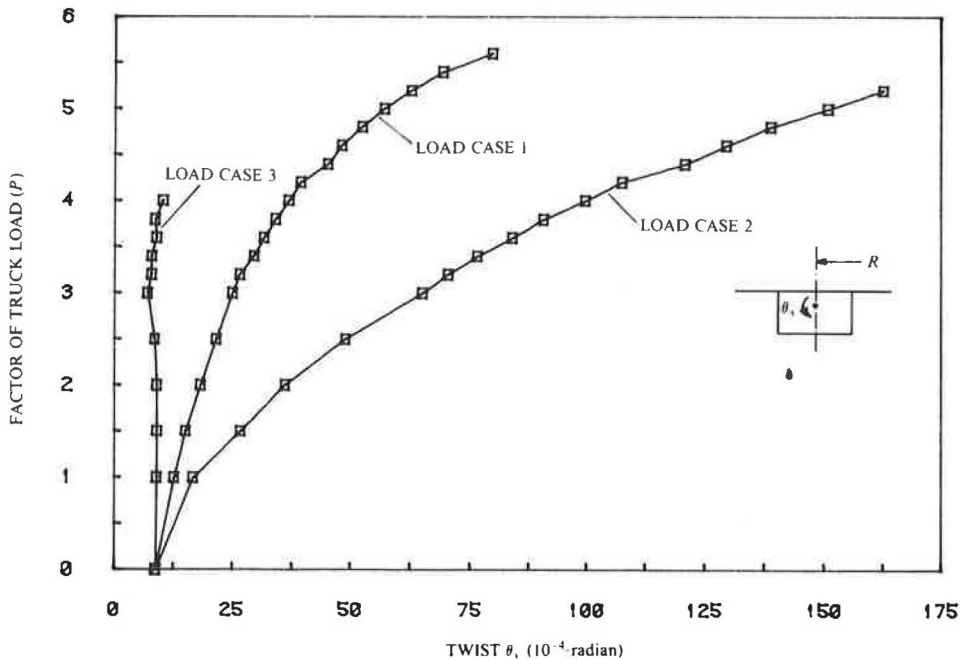

FIGURE 19 Example 2: load versus cross-section twist at middle of center span (load cases 1–3).

torsional response of the bridge. Because of the curvature of the bridge axis, the centerline loading does tend to twist the cross section, but its effect is not as pronounced as that of load case 2. Load case 3 represents the least severe torsional loading. The inner web loading tends to decrease the cross-section twist due to dead load and prestressing. The net result is that the cross-section twist remains almost constant with increasing truck load levels.

The transverse distortions of the cross section at the middle of the center span are shown in Figure 20 for the three load cases. Load case 3 is now found to produce the most severe response. The inner web loading tends to distort the cross section in the same direction as the dead load and prestressing. The combined effect is to cause rapid deterioration in the transverse flexural rigidity of the cross section. Initial cracking due to transverse flexure was observed at the middle of the center span at the very first load step of $P = 1.0$. This was followed by transverse flexural yielding at the same location at $P = 2.5$. Beyond $P = 2.5$, the transverse distortions increased rapidly as the transverse flexural yielding spread longitudinally. At the ultimate load of $P = 4.0$, the yielding spread to about 82.5 ft from the middle of the center span. The transverse distortions for load cases 1 and 2 are seen in Figure 20 to be much smaller than those for load case 3. No serious deterioration in the transverse flexural rigidity was observed for either of these load cases.

The prestressing steel segment stresses at two critical locations, one near the middle of the center span and the other near the interior support, are shown in Figure 21 for load cases 1 and 2 and in Figure 22 for load case 3. For each location, the prestressing stresses in both webs are shown. The differences between the initial stresses in the two webs are very small because the higher wobble friction losses in the outer web

more or less balance out the higher curvature friction losses in the inner web.

The load levels at which initial cracking of concrete filaments was observed at the middle of the center span and at the interior support are summarized in Table 3. These cracking loads can be identified in Figures 21 and 22 as the points at which large increases in the tendon stresses occur.

The differences between the tendon stresses in the two webs, evident in Figures 21 and 22, provide further insight into the behavior of the bridge under the three different loading conditions. A higher tendon stress in one or the other web indicates that a greater proportion of the load is carried by that web. Figure 21a shows that for load case 1, a greater proportion of the load is carried by the inner web near the middle of the center span. Near the interior support, the outer web carries a greater proportion of the load. However, the small differences between the tendon stresses in the two webs at both locations also indicate that the centerline truck loading is distributed fairly uniformly across the width of the bridge. In Figure 21b, practically equal proportions of the outer web loading are found to be carried by the two webs near the middle of the center span. Near the interior support, the outer web carries a considerably greater proportion of the load. Figure 22 shows that for load case 3, increasingly greater proportions of the inner web loading are carried by the inner web with increasing load levels. At both critical locations, the differences between the tendon stresses in the two webs increase rapidly after the initiation of concrete filament cracking. Near the middle of the center span, the outer web tendon stresses in fact start to decrease near the ultimate, whereas the inner web tendon stresses continue to increase rapidly. The increasing deterioration in the ability of the box section to distribute the eccentrically applied inner web loading transversely is due

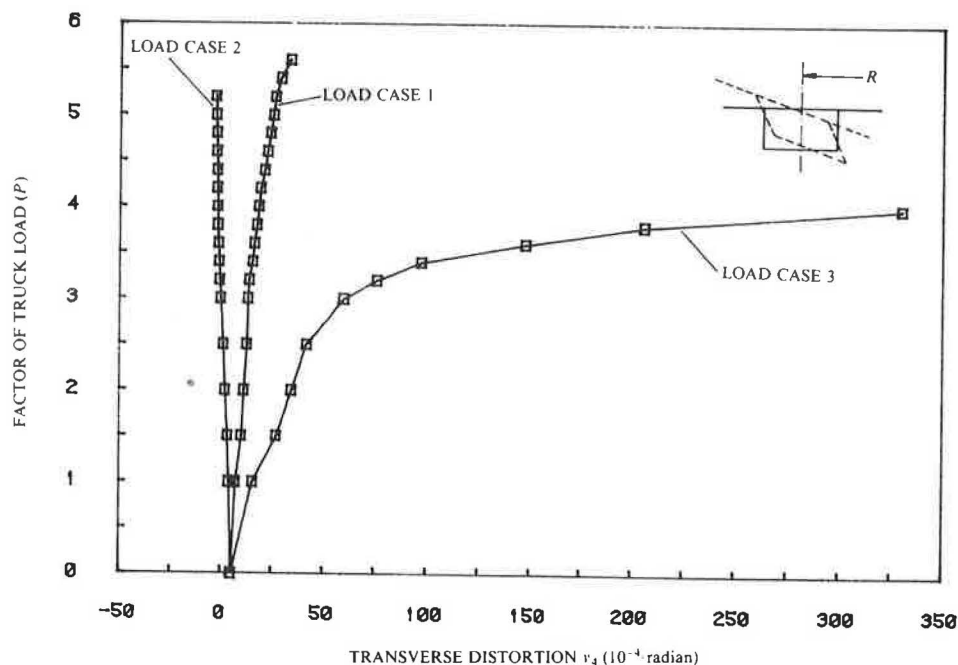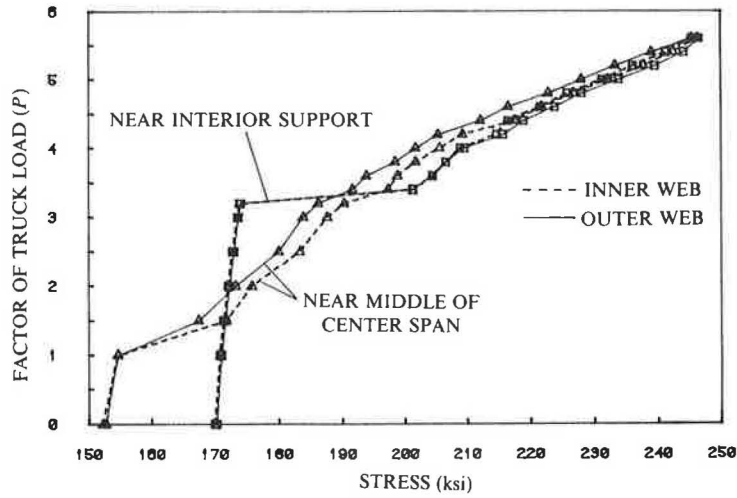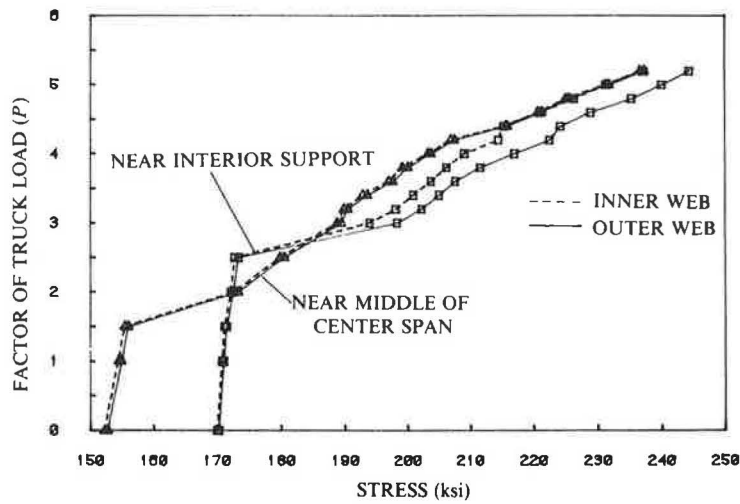**FIGURE 20 Example 2: load versus transverse distortion of cross section at middle of center span (load cases 1–3).**

(a) LOAD CASE 1

(b) LOAD CASE 2

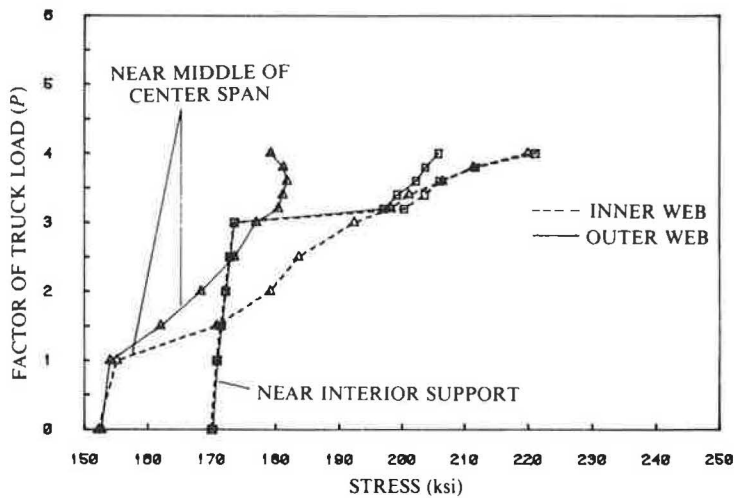**FIGURE 21 Example 2: load versus prestressing steel segment stresses at critical locations (load cases 1 and 2).**

FIGURE 22 Example 2: load versus prestressing steel segment stresses at critical locations (load case 3).

TABLE 3   SUMMARY OF CRACKING
LOADS

LOAD CASE	INITIAL CRACKING AT MIDDLE OF CENTER SPAN	INITIAL CRACKING AT INTERIOR SUPPORT
CENTERLINE LOAD	$P = 1.5$	$P = 3.4$
OUTER WEB LOAD	$P = 2.0$	$P = 3.0$
INNER WEB LOAD	$P = 1.5$	$P = 3.2$

to the rapid deterioration in the transverse flexural rigidity of the bridge.

CONCLUSIONS

The capabilities and usefulness of the proposed analytical method for curved prestressed concrete box girder bridges have been amply demonstrated. The nonlinear analysis procedure is shown to be capable of capturing the dominant structural behavior in the elastic, inelastic, and ultimate load ranges. Internal strains and stresses in concrete, reinforcing steel, and prestressing steel can be determined at all loading stages. Useful information on overload behavior and ultimate strength can be obtained from such a detailed analysis. Depending on the structure and the loading, warping, distortional, and torsional effects can influence structural behavior significantly. They not only affect the internal force distribution within the box structure, but also may govern the failure mode and the ultimate load.

ACKNOWLEDGMENT

REFERENCES

1. V. Z. Vlasov. *Thin-Walled Elastic Beams*. Israel Program for Scientific Translations, Jerusalem, Israel, 1961.
2. R. Dabrowski. *Curved Thin-Walled Girders: Theory and Analysis*. Springer-Verlag, New York, 1968.
3. D. Choudhury. *Analysis of Curved Nonprismatic Reinforced and Prestressed Concrete Box Girder Bridges*. Structural Engineering, Mechanics and Materials Report UCB/SEMM-86/13. University of California, Berkeley, Dec. 1986.
4. Z. P. Bazant and M. El Nimeiri. Stiffness Method for Curved Box Girders at Initial Stress. *Journal of the Structural Division*, ASCE, Vol. 100, No. ST10, Oct. 1974, pp. 2071–2090.
5. S. H. Zhang and L. P. R. Lyons. A Thin-Walled Box Beam Finite Element for Curved Bridge Analysis. *Computers and Structures*, Vol. 18, No. 6, 1984, pp. 1035–1046.
6. M. J. Mikkola and J. Paavola. Finite Element Analysis of Box Girders. *Journal of the Structural Division*, ASCE, Vol. 106, No. ST6, June 1980, pp. 1343–1357.
7. E. Hognestad. *A Study of Combined Bending and Axial Load in Reinforced Concrete Members*. Bulletin Series 399, Bulletin 1. University of Illinois Engineering Experiment Station, Urbana-Champaign, Nov. 1951.
8. A. DeFries-Skene and A.C. Scordelis. Direct Stiffness Solution for Folded Plates. *Journal of the Structural Division*, ASCE, Vol. 90, No. ST3, June 1964, pp. 15–47.
9. Y.K. Cheung. Finite Strip Method Analysis of Elastic Slabs. *Journal of the Engineering Mechanics Division*, ASCE, Vol. 94, No. EM6, Dec. 1968, pp. 1365–1378.
10. V. Kristek. Tapered Box Girders of Deformable Cross Section. *Journal of the Structural Division*, ASCE, Vol. 96, No. ST8, Aug. 1970, pp. 1761–1793.
11. Y. J. Kang and A. C. Scordelis. Nonlinear Analysis of Prestressed Concrete Frames. *Journal of the Structural Division*, ASCE, Vol. 106, No. ST2, Feb. 1980, pp. 445–472.
12. J. Hellesland, D. Choudhury, and A. C. Scordelis. *Nonlinear Analysis and Design of RC Bridge Columns Subjected to Imposed Deformations*. Structural Engineering and Structural Mechanics Report UCB/SESM-85/03. University of California, Berkeley, April 1985.
13. K. Bathe, E. L. Wilson, and F. E. Peterson. *SAP IV: A Structural Analysis Program for Static and Dynamic Response of Linear Systems*. Earthquake Engineering Research Center Report EERC 73-11. University of California, Berkeley, June 1973.
14. *Standard Specifications for Highway Bridges*. American Association of State Highway and Transportation Officials, Washington, D.C., 1983, 13th edition. Revised by California Department of Transportation.

Design and Construction of Transversely Posttensioned Concrete Bulb Tee Beam Bridge

JAMES J. HILL, LAURIE G. MCGINNIS, WILLIAM R. HUGHES, AND ARUNPRAKASH M. SHIROLÉ

A six-span prestressed concrete bulb tee beam bridge, designed to eliminate the need for a conventional cast-in-place concrete deck, was constructed in Minnesota in 1986. Two end spans of this 484.7-ft (147.8-m) long structure were 70 ft (21.3 m) clear, and four interior spans were 85 ft (25.9 m) clear. Bars 1 in. (2.54 cm) in diameter were used to transversely posttension 6-ft (1.8-m) wide top flanges of five 40-in. (100-cm) deep bulb tee beams. A slip-formed, cast-in-place, reinforced concrete railing limited required formwork to only the low-slump wearing course, expansion devices, and pier diaphragms. A 2-in. (5.1-cm) minimum concrete overlay provided a good riding surface. Construction of this structure was completed in just 5 months at a cost of $450/yd² ($538/m²), with a savings of about 25 percent over a conventional design.

This discussion covers the design and construction of a six-span prestressed concrete bulb tee bridge that was built at the Northern States Power Company plant in Red Wing, Minnesota, in 1986. The bridge consisted of two 70-ft (21.3-m) spans and four 85-ft (25.9-m) spans, with an overall length of 484.7 ft (147.8 m). Five bulb tee beams, each 6 ft (1.8 m) wide, placed side by side constituted the deck width. Final deck width of 30.3 ft (9.2 m) included a 3-in. (7.6-cm) accumulation of horizontal beam total curvatures resulting from fabrication (Figure 1).

GEOMETRIC CONSTRAINTS

Several vertical constraints required grades of 6.05 and 5.38 percent with a sharp vertical curve of 140 ft (42.7 m) over a set of railroad tracks. One constraint was a minimum vertical clearance of 23 ft (7.0 m) over the railroad tracks. The railroad also required a minimum horizontal clearance of 22 ft (6.7 m). Another constraint was the elevation difference of 40 ft (12.2 m) between the power plant yard and Trunk Highway 61 (Figure 2).

Spans at all five piers were fixed, and expansion was taken up completely at the abutments because of steep grades. Strip-seal-type expansion devices were used, which allow a total expansion of 6 in. (15.2 cm).

J. J. Hill, Minnesota Department of Transportation, Room 615, Transportation Building, John Ireland Boulevard, St. Paul, Minn. 55155. L. G. McGinnis and W. R. Hughes, Howard Needles Tammen & Bergendoff, 6700 France Avenue South, Minneapolis, Minn. 55435. A. M. Shirolé, City of Minneapolis, 203 City Hall, Minneapolis, Minn. 55415.

FOUNDATION CONSTRAINTS

The elevation differential of bedrock at the bridge site presented another design obstacle. At the south abutment and adjacent pier 1, footings were keyed directly into bedrock. At the other four piers and the north abutment, steel H-piles driven to bedrock were used.

A special hinge was placed in the column base of pier 1 to allow the pier to rotate longitudinally (Figure 3).

AESTHETICS OF PIERS

To minimize costs and achieve aesthetically pleasing piers, a common hammerhead cap on a 10- by 3.75-ft (3.0- by 1.1-m) shaft with rounded ends was chosen. Horizontal rustication was placed on the shaft at 4-ft (1.2-m) intervals to enhance the aesthetic appeal.

UNIQUE DESIGN FEATURES

In the conventional method for holding bulb tee beams together welded bar ties are spaced on 4-ft centers, which generally results in longitudinal joint cracks. The design of this bridge used transversely posttensioned bars instead. To accomplish this, bulb tee beams were fabricated with 3-in. (7.5-cm) diameter galvanized metal spiro ducts. The ducts were centered in the top flange 3.38 in. (8.6 cm) from the top of the beams.

The bulb tee beams were standard shapes, 40 in. (101.6 cm) deep with 6-in. (15.2-cm) wide webs (Figure 4). These beams were longitudinally pretensioned to the required loads with 0.5-in. (1.25-cm) diameter low relaxation strands.

Blockouts of 4.75 by 10.25 in. (12.0 by 26.0 cm) were placed in the outside edges of the facia beams for anchorage assemblies. Vertical 0.83-in. (2.1-cm) grout tubes were connected to spiro ducts in facia beams under the railing.

Actual spacing of the metal spiro ducts was 2.92 ft (88.9 cm). All the reinforcement, including tie wires in the bulb tee beams but not the low-relaxation strands, was epoxy coated.

Two lifting cranes were needed to handle and place beams that weighed 34.5 and 41.4 tons (34.0 and 40.7 metric tons). Because these beams were placed at a slight slope to follow the final roadway transverse slope, special bearing plates were used.
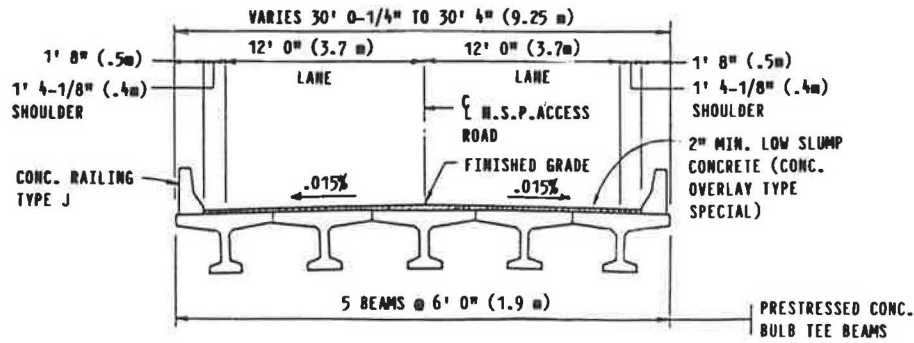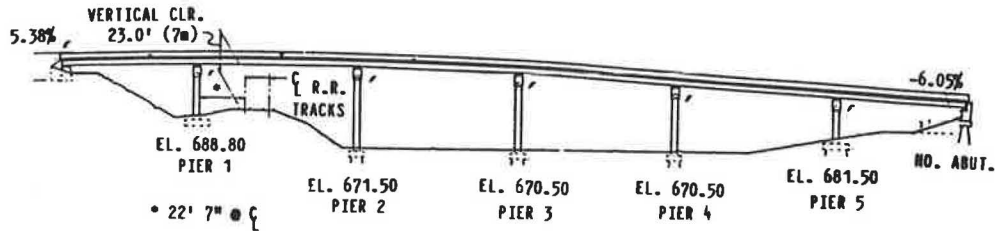
FIGURE 1 Cross section of bridge.

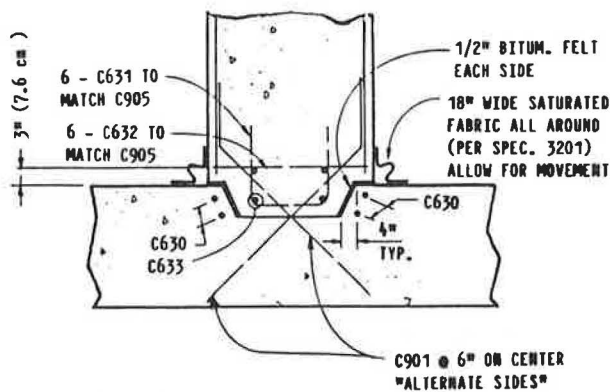**FIGURE 2 Elevation of bridge.**

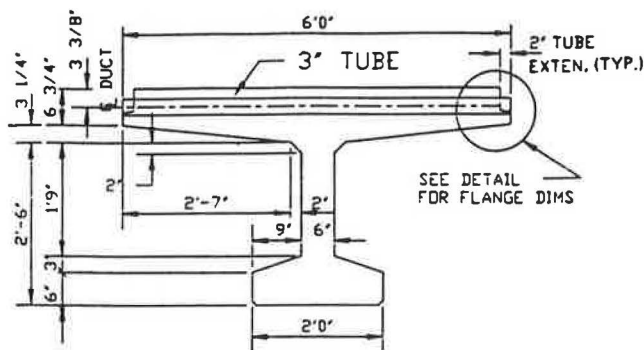**FIGURE 3 Hinge detail at base of pier 1.**

FIGURE 4 Typical beam section.

The bearing plates were tapered in two directions to take into account longitudinal grade and transverse crown slopes of the roadway. Use of longitudinally curved plates in the bearing assemblies ensured good bearing on the elastomeric bearing pads. There were some difficulties in placing and tilting beams correctly on the bearing assemblies. These could have been

greatly reduced by placing and using two additional lifting device points in adequately redesigned cantilever sections of the beam flange. Differential camber was not experienced as a problem. Joint openings between beams and vertical match-up of spiro ducts were negatively affected by the handling techniques of one pick point on each end of the beams. However, all transverse posttensioning bars were easily pushed through the spiro ducts.

In order to minimize rotational stresses at mid-span of the facia beams, steel intermediate transverse diaphragms were used at the middle of the spans. Concrete diaphragms were used at abutments and piers to restrain beams against lateral rotation at these locations. Design of each bulb tee beam for live load was based on Section 3.23 of the American Association of State Highway and Transportation Officials (AASHTO) specifications. Beams were longitudinally pretensioned using 22 low-relaxation 0.5-in. (1.27-cm) diameter strands for the short end spans and 34 low-relaxation 0.5-in. diameter strands in the longer interior spans. Six and 14 strands were draped in the end-span and center-span beams, respectively, to maintain compressive stresses in the concrete below an allowable stress value of 2,400 psi (16 540 kPa) based on $F'c$ of 6,000 psi (41 360 kPa).

JOINTS BETWEEN BEAMS

A 2-in. (1.5-cm) wide by 4-in. (10.2-cm) deep notch along the interior longitudinal edges of the top flange formed a joint key between the beams. This standard joint key accounted for the horizontal bowing of beams that results from fabrication and handling. During construction, a polystyrene rope was worked down into the joints between the beams to hold the grout above it. Because this opening between beams varied, it was recommended by construction personnel that a rubber tee or equivalent be used on future jobs (Figure 5). Couplings were used initially to reduce leakage and intrusions into the ducts
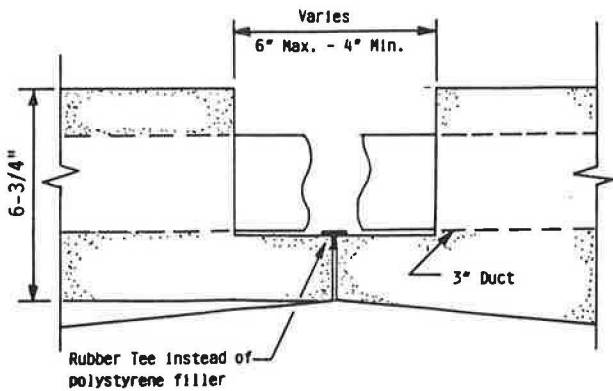
FIGURE 5 Beam joints.

during placement of mortar grout. On the final spans, the contractor simply secured the spiro-duct joints with tape. This procedure worked fairly well during pressure grouting; however, use of couplings would ensure tight joints.

The joint key between the beams was filled with concrete nonshrink grout with the appropriate admixtures. This grout was required to have 6,000-psi strength (based on a maximum water/cement ratio of 0.45) before transverse posttensioning.

TRANSVERSE POSTTENSIONING DESIGN AND DETAIL

The contractor used threadbars 29.67 ft (9.0 m) long with 1-in. diameter to posttension the beams transversely. These threadbars were epoxy coated, except for their heads. Steel anchor plates 4 by 8.25 by 1.5 in. (10.2 by 21.0 by 3.8 cm) thick were used to bear against the concrete and maintain the concrete stress of less than 3,000 psi (20 680 kPa). All contact surfaces and the hexagonal anchor nuts were uncoated to achieve uniform and consistent stresses in the threadbars. The threadbars, which were spaced at 2.92 ft (88.9 cm), were tensioned to 101,000 lbf (45 810 kgf) progressively across each span. This force was required to pull the beams together and prevent tensile stresses at the longitudinal joints. Threadbar elongation was calculated at 1.375 in. (3.5 cm), with an anchor set of 0.06 in. (1.52 mm). All exposed uncoated surfaces were epoxy coated after posttensioning. The actual elongations were measured at 1.375 in. (3.5 cm) when the jacking force of 101,000 lbf was achieved.

GROUTING OF SPIRO DUCTS

In the first attempts at grouting the spiro ducts with a cement-and-water mixture under 100 psi (698 kPa) pressure, the grout

was blown out of the joints. A commercial grout mix pumped into the ducts at 80 psi (552 kPa) proved to be effective. Grout was pumped into one end of the spiro duct through one grout tube and air was let out of the other end of the spiro duct through the opposite grout tube.

RAILING AND WEARING COURSE

To further reduce construction time, Type J railings were placed by slip forming, which is a common practice in Minnesota. To take up the unevenness in the beam surfaces, a 2-in. (5.1-cm) low-slump dense concrete wearing course was applied as a final riding surface.

CONSTRUCTION ADVANTAGES

Use of the foregoing special time-saving construction techniques and absence of deck forming resulted in a construction time for the bridge of only 5 months. This is about half of the conventional construction time for a bridge of this size. Another significant advantage was that the actual construction cost of the bridge was $450/yd^2 ($538/m^2) of deck surface. A conventional bridge of this type in Minnesota would have cost about $65/ft^2 ($70/m^2), which amounted to about a 25 percent savings in the cost of construction.

CONCLUSIONS

• During the first year of service, no cracks appeared in the concrete wearing surface over the longitudinal joints.

• This type and size of bridge construction requires only one construction season of 6 months.

• Cost savings of 20 to 25 percent may be achieved using transversely posttensioned deck bulb tee beams.

• Maintenance costs would be lower because of the smaller amount of exposed steel and lack of joint weldments, which easily fatigue and break.

• Rubber tees, if used in the joints between beam flanges, would provide a tolerance of up to 1 in. to properly cover differential openings between the beams.

• Additional handling devices should be used in properly designed beam flanges to facilitate tilting and placement of the beams on their bearing supports.

Transverse Load Distribution in a 536-ft Deck Arch Bridge

DAVID R. ANDERSON, RICHARD M. JOHNSON, AND ROBERTO LEON

An instrumentation and load-testing analysis of the 536-ft, two-span, open spandrel arch-rib Hennepin Avenue Bridge over the Mississippi River in Minneapolis, Minnesota, was conducted to measure the transverse load distribution among the six arches of the bridge and to determine whether the buckled webs of the arch ribs carry any load. When the structure was rated for Hennepin County in 1983, the load distribution and the ability of the buckled web plates to carry axial stress were questioned. Thus, an instrumentation analysis under static load was performed. The bridge was instrumented with 18 strain gauges and was loaded with three 27.5-ton tandem dump trucks positioned in nine different loading arrangements. Strain readings were averaged for each loading to determine the magnitude of load carried by each arch rib and then compared with a computer-modeled (linear) transverse distribution. It was found that the arch ribs carried not only axial stress, but also stress due to bending moments. It was concluded from the study that the floor beams and diaphragms do not transfer loads from one side of the bridge to the other. The results of the web testing demonstrated that a nominal axial load was being carried by the web, and that, although buckled, it was working effectively through a tension-field mechanism similar to that of a simple truss.

The Hennepin Avenue Bridge (S.B. 90589) over the Mississippi River in Minneapolis, Minnesota, is a historically significant, unique structure functioning as the second-longest solid arch-rib bridge span known to be in use today. Although this is the third bridge on this site, its earliest predecessor was the first recorded bridge across the Mississippi River. Constructed directly north of the Falls of St. Anthony and situated between the Burlington-Northern Railroad flats area and Nicollet Island, the steel arch bridge is now part of the St. Anthony Falls Historic District, birthplace of the City of Minneapolis. The bridge continues to function as a major transportation artery linking downtown Minneapolis with the northern and eastern metropolitan areas.

Of historic and technical significance, the steel bridge was constructed in longitudinal halves, with two 258-ft spans and supports, a 56-ft roadway, and two 12-ft sidewalks. The north half of the bridge was constructed in 1888 of 3 three-hinged arch ribs. In an attempt to reduce deflections and vibration, the design of the south half of the bridge was revised from a three-hinged to a two-hinged arch. The combination of three- and two-hinged solid arch ribs is the most unusual structural feature of the historic bridge.

An instrumentation and structural analysis of the Hennepin Avenue Bridge was undertaken in mid-1983 to determine its load-carrying capacity and the feasibility of rehabilitating the bridge. During the field inspection, many arch-rib web plates were found to be bowed or buckled out of their vertical plane. Therefore, the ability of the buckled web plates to carry compressive loads was questioned. During the structural analysis, it became apparent that the methods (and effectiveness) of transferring live loads in the transverse direction between the arch ribs were ambiguous. As a means of establishing the transverse load distribution and determining the ability of the buckled web plates to carry compressive loads, the bridge was monitored with strain gauges under known loading conditions.

What follows is an overview of the structural nomenclature of the Hennepin Avenue Bridge, a cursory summary of the instrumentation procedure, and a discussion of conclusions reached as a result of the study. The basis of this paper is a report prepared in June 1984 (1).

BRIDGE DESCRIPTION

Figures 1 and 2 show the structural components of the Hennepin Avenue Bridge in typical section views and the nomenclature used throughout this paper to describe the components. A brief description of the individual components follows:

1. Batten plates: These plates (splice plates) are composed of $3/8$-in. steel and serve to keep the individual arch-rib panels in place.
2. Diaphragms: The diaphragms are located at each panel throughout the bridge between the arch ribs.
3. Sway bracing: The sway bracing (diagonals) runs diagonally between the top and bottom of adjacent spandrel columns. These are circular rods with turnbuckles for length adjustment. Because of their slenderness, they transmit only tension forces.
4. Wind bracing: The wind bracing consists of round bars, again with turnbuckles. This bracing is located in the same plane as the top and bottom flanges of the arch ribs and forms an X within each panel. Similar to the sway bracing, these members transmit only tension forces.
5. Web plates: These plates are riveted between the flange angles to form the web of the arch rib.
6. Floorbeams: These members carry the stringer loads to the spandrel columns. The floorbeams are hinged at the center of the bridge as a direct consequence of the original staged construction, and thus provide no moment transfer at that point.

D. R. Anderson and R. M. Johnson, Howard Needles Tammen & Bergendoff, 6700 France Avenue South, Minneapolis, Minn. 55435. R. Leon, Department of Civil and Mineral Engineering, University of Minnesota, 500 Pillsbury Drive S.E., Minneapolis, Minn. 55155.
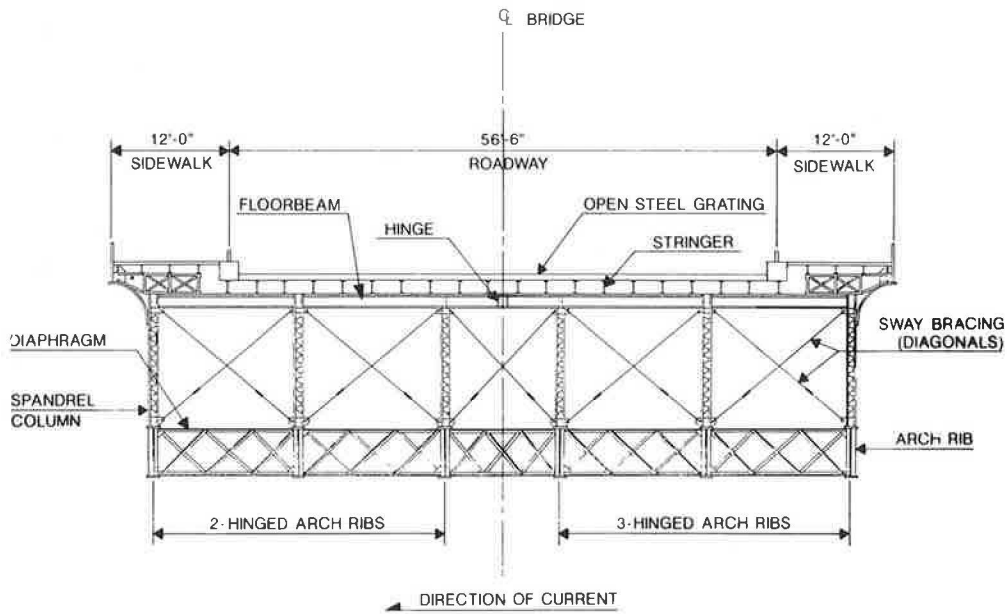
FIGURE 1   Typical section.
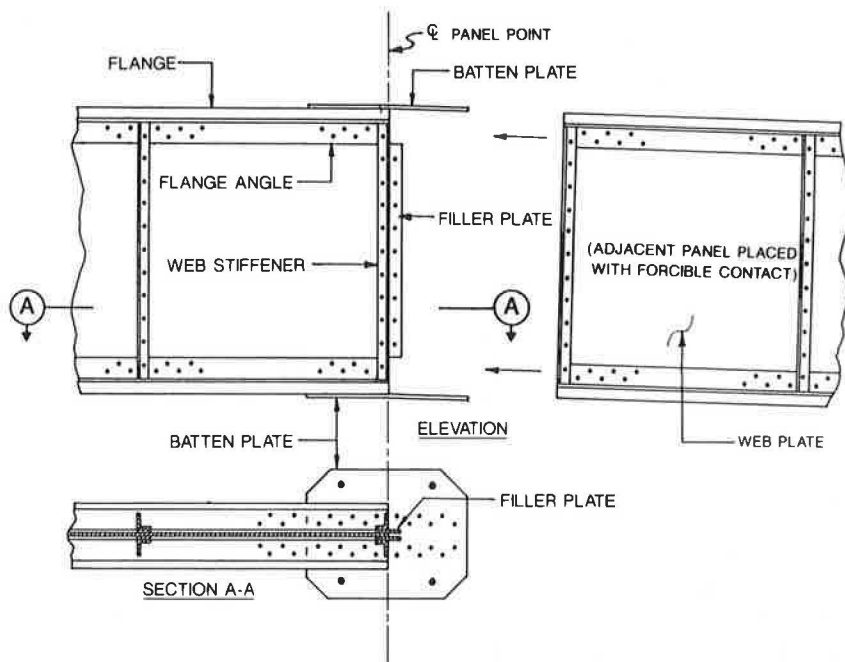
FIGURE 2   Typical arch section.

Figures 2 and 3 show a typical arch section and a plan and elevation view of the bridge, respectively. It should be noted that the arch ribs are not continuous members but a series of 42 panels constructed segmentally. This design feature limits the arch's ability to function as a beam (i.e., to carry bending stresses).

INSTRUMENTATION GOALS

The mechanism by which loads are transferred in the transverse direction and the effectiveness thereof were initially questioned after the following observations were made:

• Section properties of each arch are dissimilar by original design;

• Three of the arches are two-hinged, and three are three-hinged;

• Conventional analysis demonstrated that exterior arch ribs carried more load than design specifications would allow;

• A two-dimensional analysis could not accurately model all structural members, given the complicated three-dimensional aspects of the bridge; and

• Tension-only members, loose members, and the rigidity of connections are conditions that vary throughout the bridge.

FIGURE 3 Bridge plan and elevation.

As previously mentioned, it was thought that the web plates would carry little, if any, compressive loads because of their buckled condition. It was speculated that the flange plates would accept additional loads and would therefore be stressed at a higher level than would otherwise be expected.
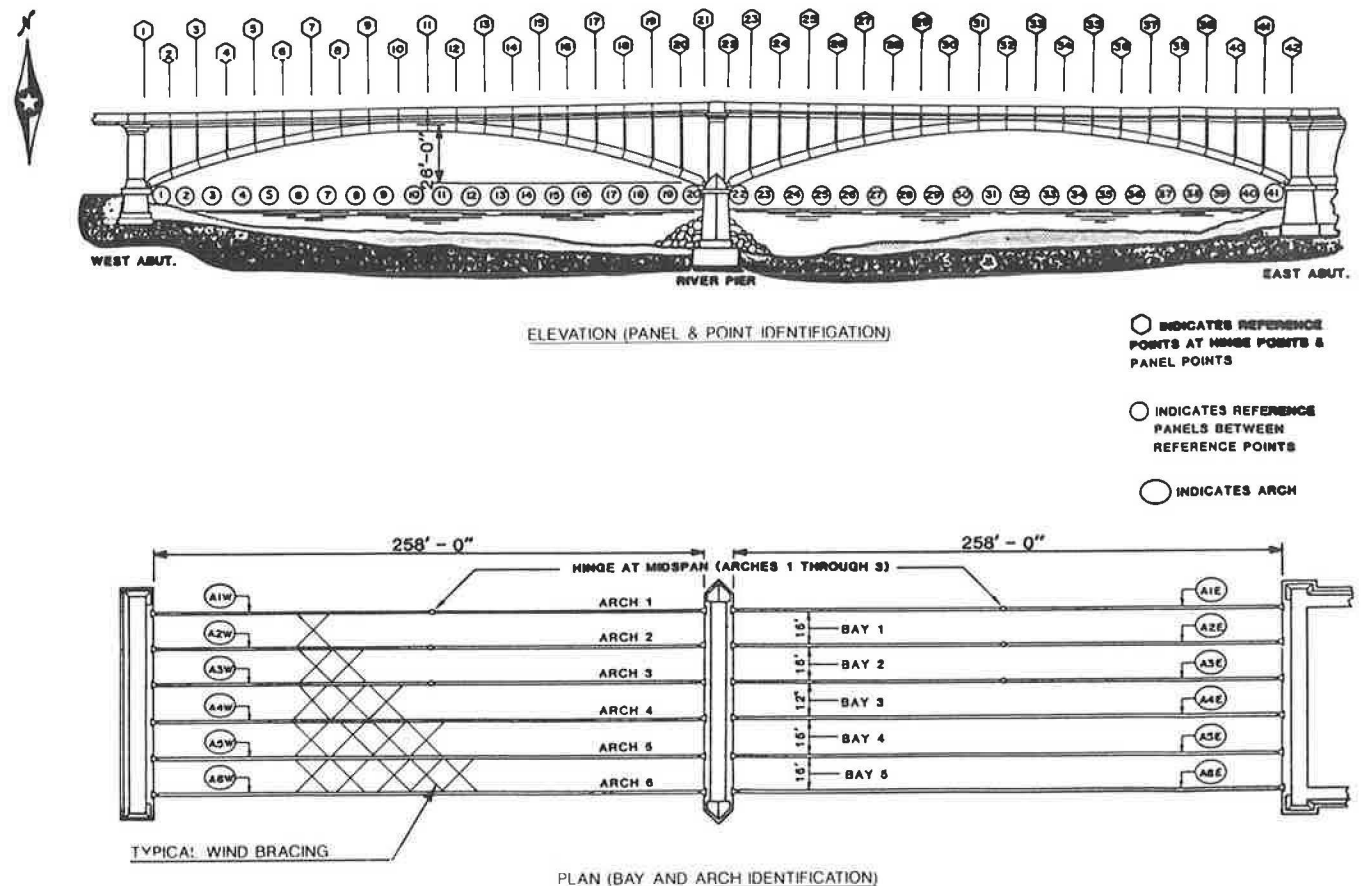
PURPOSE OF TESTING

The purpose of the testing was to monitor the bridge under a known loading condition. This would provide a correlation between the loads applied to the bridge and the corresponding strains (and hence stresses) in each of the arch ribs. This information would allow the prediction of the loads accepted by each of the arch ribs under a given loading condition and the documentation of the transverse distribution of loads. In addition, the web plates were monitored to determine whether they were contributing to the arch-rib section in a normal manner and accepting some of the compressive loads.

TESTING PROCEDURES

The Department of Civil and Mineral Engineering at the University of Minnesota was retained to provide the instrumentation for the load test. A total of 18 strain gauges were installed in a line near the east abutment, 18 in. from reference point 40 on panel 40 (see Figure 3). Twelve of the gauges were installed on the flanges of the main plate girders, with all the

bottom flanges instrumented on the inside face and the top flanges on the outside face. The top flange gauge in Arch 4 was placed on the inside face because of the unevenness of the outside face. Three gauges were installed on two web faces at angles of approximately −45, 0, and +45 degrees to the horizontal (strain gauge rosette) in areas where the web was buckled. An external dummy gauge was also used to compensate for the temperature variation throughout the duration of the loading.

Three dump trucks, each with a gross weight of 27.5 tons, were used to produce nine different test load patterns. Some of the load patterns were mirror images. This was to see whether the load distribution from one longitudinal half of the bridge to the other was symmetric about the middle. The strain gauges were read twice during each load position and were then rezeroed before the beginning of the next loading.

TEST FINDINGS

The data obtained during the testing were recorded and interpreted as follows:

1. The live load distribution between the arch ribs could be approximated from the data provided. Careful analyses of the magnitude of forces and moments were made to ensure that these quantities were reasonable. It should be noted that given the buckled condition of many of the webs, the usual assumption of a linear strain distribution is questionable. The readings

obtained from the midweb horizontal gauges suggested a distribution very different from that expected by a straight line distribution between the top and bottom flange gauges. It was therefore concluded that calculations using linear-elastic theory and the measured strains would not be expected to correlate well with the results of a linear-elastic analysis of the structure using the entire section properties.

2. The plates making up the arch ribs carried not only compressive stress, but also stress from bending moments. The trends through the test clearly showed that the compression produced by the dead loads on the bottom flange was relieved by the live loads. The results indicated that the arches were not acting as simple compression members.

3. The webs, although buckled, seemed to be working effectively through a tension-field mechanism. Thus, the webs were able to transfer forces by forming diagonal bands in tension, which resulted in a structural action similar to that of a truss. If this model is correct, the flanges are likely to be carrying higher stresses than the elastic theory would predict, whereas the webs are carrying lower stresses. This was supported by the experimental observations, which indicated that although very little or no force was present in the horizontal direction at the mid-depth of the web, the gauges at 45 degrees to this direction showed significant levels of stress.

4. The floor beams, diagonals, and diaphragms did not seem to transfer significant forces from one side of the bridge to the other; when the loads were placed on only one side of the bridge, very little load was transferred to the outside arch at the other side.

5. Investigation and analysis of the lack of rigidity of the panel point connections between the members making up the arches, although these connections do have a finite rotational stiffness, resulted in slightly lower moments and higher axial loads, but not by more than 10 to 15 percent. The main difference in these analyses came from the deflections, which began to increase rapidly as the rotational stiffness was diminished. As the stiffness was reduced to about 1,000,000 kips/radian, the centerline deflection of the arch with a truck (55-kip) load at joint 3 increased to about 5.5 in.

Inclement weather and technical problems were experienced during the instrumentation of the Hennepin Avenue Bridge. Ambient temperatures during the test dates in December 1983 averaged +20°F, which created problems with the attachment of strain gauges. Falling debris from the steel grating that served as the bridge deck made working conditions hazardous. The strain gauge placed on the bottom flange of Arch 2 failed just before the testing, preventing a complete independent measurement of the load distribution on one of the arch ribs. Financial considerations limited the level of instrumentation effort, and lack of equipment prevented dynamic load testing.

The recorded strain values were smaller than desirable to achieve precise analysis. The presence of utilities on the bridge also resulted in significant electrical noise. However, the values obtained were determined to be valid for the purposes of the test. Additional test load weight on the bridge would have provided larger strain values, but also presented the danger of permanent structural damage.

SUMMARY

The unique two-hinge and three-hinge arch design of this 100-year-old bridge made the determination of live load distribution an obvious issue. The limited bending capacity of the critical arch members because of their "segmental design," the badly deteriorated batten plates, the known decreases in structure dead load and increases in live load, and the buckled web plates all made the issue of load distribution a critical one. For a meaningful evaluation of the bridge, a determination of the load distribution was required.

The instrumentation of the bridge was successful in providing data for making better decisions about the key issues of transverse distribution and buckled web behavior.

The successful testing also played a major role in the rating of the bridge. It was determined that the entire section of the arch was not contributing to the section properties, thereby increasing stresses in the flanges of the arches. The interior two-hinged arch closest to the three-hinged arches was found to be carrying more than its share, making this arch critical over the more lightly designed exterior arches. The instrumentation revealed that the compression in the lower arch flange was being completely relieved and subjected to tension. This last finding revealed that the seriously deteriorated batten plates were controlling the rating. Immediate repairs to the batten plates were required to ensure safety of the bridge.

Finally, the test findings were very helpful in developing alternatives for possible rehabilitation of the bridge. They confirmed that any alternative would have to address improvements in relative load distribution to the arches. Alternatives studied included regrouping of the two- and three-hinged arches so that all the same designs would be placed in the same spans, introducing a center longitudinal joint separating the arch designs, and developing a stiffer deck to assist in load distribution.

ACKNOWLEDGMENTS

REFERENCE

1. *Hennepin Avenue Bridge Structural Analysis Inspection Report.* Howard Needles Tammen & Bergendoff, Minneapolis, Minn., June 1984.

Behavior of Open Steel Grid Decks Under Static and Fatigue Loads

Hota V. S. GangaRao, William Seifert, and Hagop Kevork

Open steel grid decks are factory assembled, lightweight, and easy to install. They are commonly used to rehabilitate older bridges by being welded to stringers, floor beams, or both. The American Association of State Highway and Transportation Officials (AASHTO) load distribution procedures for open steel grid decks are found to be in error; hence realistic load distribution procedures have been developed to prevent cracking of grid deck bars and plug welds. The research work presented here, however, deals only with the effects of main-bar spacing, direction of main bars with respect to traffic flow, load position, composite action, fatigue effects due to repetitive loads and residual stress build-up in grids during fabrication, braking and accelerating forces, galvanization, and composite action between the deck and stringer. Twenty-six grid deck specimens were tested under static and fatigue loads. Reduction in bending stresses due to composite action is found to be marginal. Allowable fatigue stresses for commercially available welded grid decks are found to be very close to those given for Category E in the AASHTO specifications. However, heavy-duty welded grid decks subjected to fatigue loads have developed no welded cracks after up to 1.5 million cycles. Under fatigue, riveted decks have performed better than the most common welded decks. Finally, welded decks that have been galvanized have a longer service life than decks without galvanization.

The rehabilitation or replacement cost of bridges in the United States is estimated to be about $50 billion in 1982 dollars (1). One of the most economical ways to increase the load-carrying capacity of a bridge and improve its safety is to rehabilitate the bridge deck with an open steel grid deck system. An open steel grid deck is factory assembled and consists of main and cross bars positioned so that they are perpendicular to each other and mechanically interlocked and plug welded, or riveted, at their intersections (Figures 1 and 2). Occasionally diagonal bars are added to produce a grid of higher stiffness in its plane.

The successful use of open grid decks can be attributed to their light weight (approximately 16 psf), ease of installation, decreased construction costs, ease of adaptability to the composite mode of construction, and use as temporary bridges or even as decking on movable bridges (2). Typically, open steel grid decks are welded to their stiffening system, usually wide-flange stringers, floor beams, or both. Because of increases in traffic intensity as well as in volume, open steel grid decks

develop cracking of plug welds, which eventually leads to the failure of cross or main bars. Such failures are primarily attributed to poor design, which is the result of lack of understanding of the behavior of grid decks under static and fatigue loads. The current specifications for bridges from the American Association of State Highway and Transportation Officials (AASHTO) (3) suggest design procedures to determine both the distribution of wheel loads within an open grid deck and the distribution between the deck and its stiffening system. As discussed in the literature (2, 4, 5), design procedures consider only the stringer spacing and the number of traffic lanes. They do not account for other parameters such as stringer stiffness and spacing, deck stiffness, span length, composite action, fatigue behavior, and load location. Also, the AASHTO load distribution procedures for open grid decks (3) are in error in that they lead to a decrease in load intensity on the main bar as the main-bar spacing increases (2, 6). Hence, more realistic load distribution formulas have been developed by the authors to adequately design open grid decks for static and fatigue loads and to improve their service life. These distribution formulas are of two types: within an open steel grid deck and between the grid deck and steel stringer.

The major objective of this research paper is to present details on the behavior of open steel grid decks under static and fatigue loads so that designers can have a more complete understanding of the overall performance of the grid deck, which would lead to reduced maintenance costs. More specifically, research work is presented that evaluates deck performance with reference to main-bar spacing, direction of main bars with respect to traffic, braking-force effects, load range, composite action of the deck, type of deck, galvanization, effects of residual stress, static performance after fatigue loading, and load influence on adjacent panels.

A comprehensive experimental testing program has been devised and the aforementioned problem parameters have been varied in a systematic manner to study their influence on the overall behavior of grid decks. The scope of this paper is limited to the behavior of open steel grid decks under static and fatigue loads. The design formulas derived from the information gained during this research are presented in a separate paper for the sake of clarity and brevity. More comprehensive details on both the behavior and design equations may be found in the final report, available from the West Virginia Department of Highways or Bridge Flooring Manufacturers Association of Pittsburgh, Pennsylvania (7).
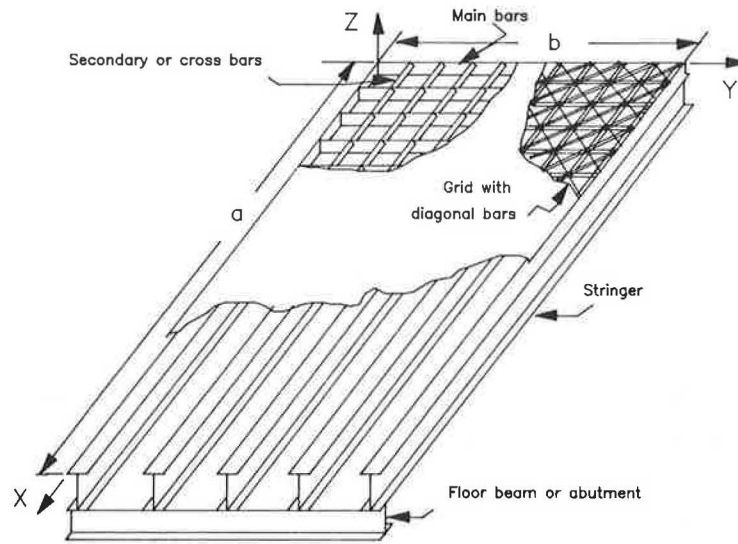
Civil Engineering Department, West Virginia University, Morgantown, W. Va. 26506-6101.

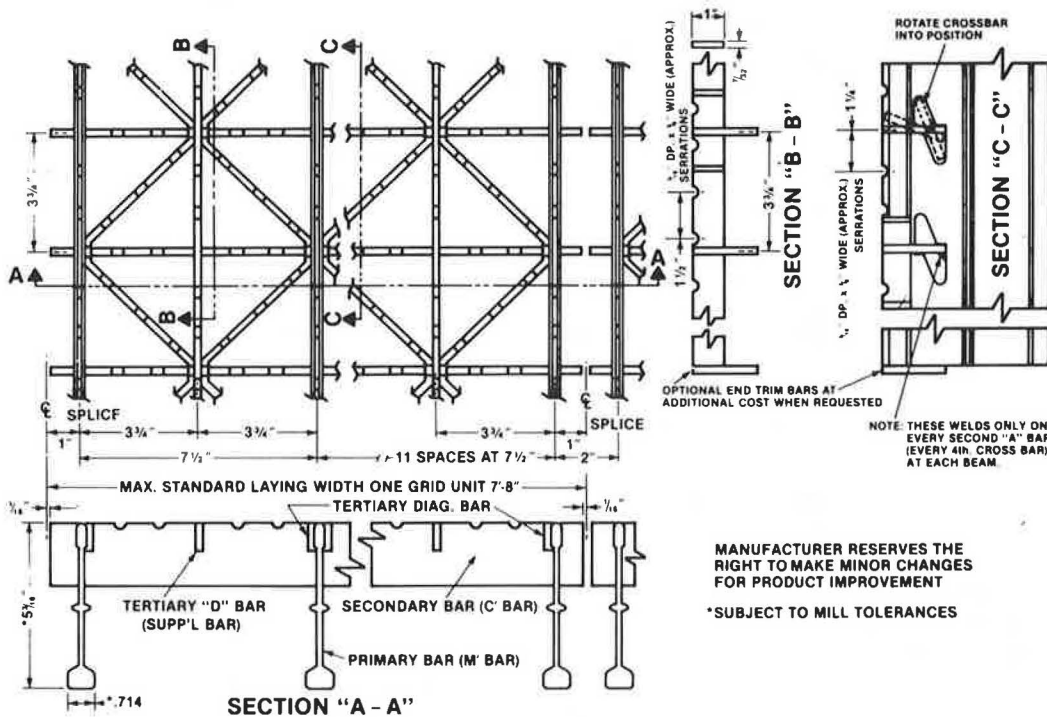**FIGURE 1   Open-deck–wide-flange stringer bridge system.**

FIGURE 2   Diagonal open grid deck details.

TEST SETUP AND SPECIMEN TESTING

A schematic diagram of a typical test setup is shown in Figure 3. A typical setup consists of an open grid deck placed over steel stringers and stiffened by steel floor beams. The floor beams are supported on concrete blocks, which are placed directly under each stringer. The load was applied through a hydraulic ram for static tests and through a closed-loop MTS actuator for fatigue tests. The loading was spread over a 10- by 20-in. area of the grid deck with steel plate and elastomeric pad for proper simulation of dual wheel loads. Some experiments were conducted by using a wedge effect on the actuator or ram to simulate the in-plane forces due to braking or

accelerating of trucks on grid decks. The grid decks are welded either fully or partially to the stiffening system to study their composite behavior. Additional details are given in the final report (7).

Three typical specimen sizes (6 by 10 ft, 16 by 7.58 ft, and 6 by 24 ft) are used in the tests for static and fatigue loads. To date, a total of 26 different static and fatigue tests have been conducted on various commercially available grid decks (diagonal and riveted decks with main-bar spacing of 4, 6, and 8 in., and a 5-in., four-way grid deck). These open grid deck specimens were randomly chosen from the general stockpile and were not specifically fabricated for the test purposes. The
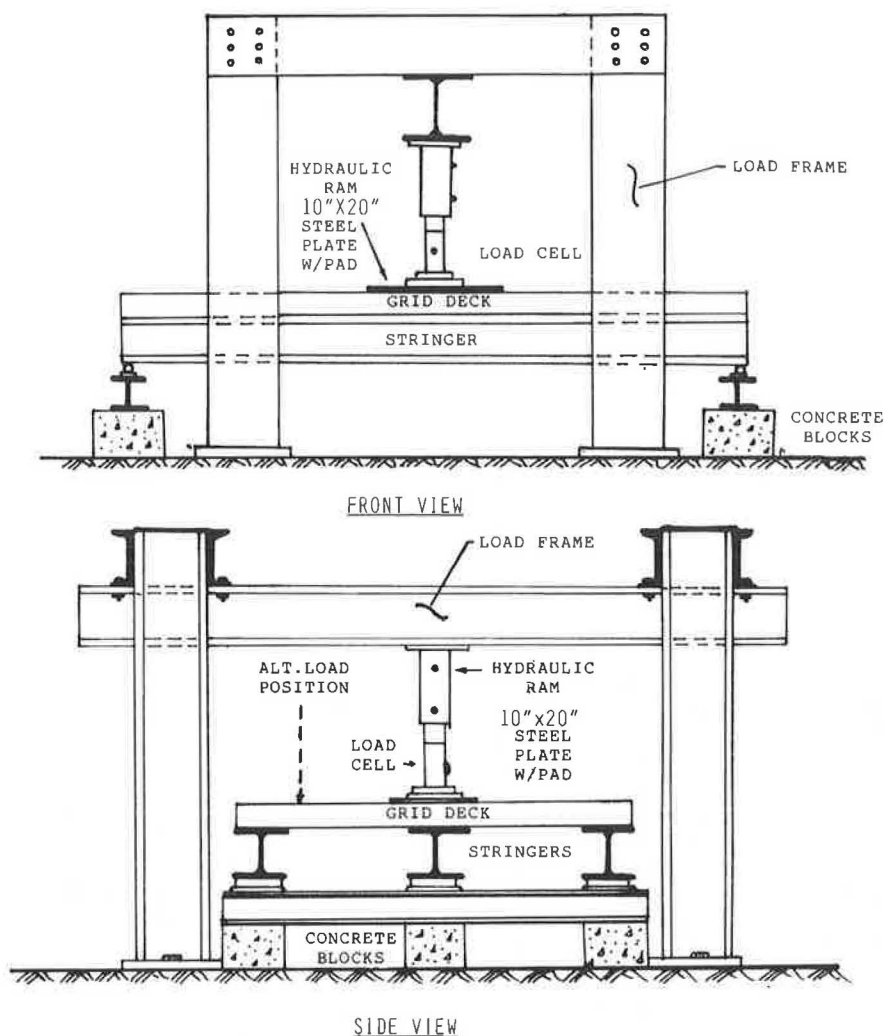
FIGURE 3   Typical test setup.

5-in., four-way grid deck was introduced on the basis that in-plane force resistance and rideability would be better with this grid than they are with the rectangular grids. However, it was not recognized that the concentrated force transfer from the diagonal bars to the center of the cross bars would be detrimental to the fatigue resistance.

Static tests on each panel were conducted by applying incremental loading from 0 to 30 kips, whereas fatigue tests were performed with the aid of a 50-kip capacity MTS system with stress ranges from 8 to 37.8 ksi and a maximum of 1.5 million cycles. It should be noted that static tests were performed on specimens subjected to repetitive loads at the end of every 50,000 cycles to measure the specimen degradation due to fatigue cracking.

Strain and dial gauges were mounted at several locations on grid decks and also on stringers and floor beams. In addition, residual stresses in the grid decks were measured through a strain relief test devised and perfected by the authors (7).

TEST RESULTS AND SYNTHESIS

Static and fatigue tests of open steel grid decks stiffened by steel stringers were performed in the Major Units Laboratory

of the Civil Engineering Department at West Virginia University. The effects of 10 different variables were systematically researched for steel grid decks under static and fatigue loads. These variables are main-bar spacing, traffic flow with main-bar direction, braking force effects, range of applied loads, composite action of grid deck and steel stringers, type of deck, galvanization, residual and induced stress effects, static versus fatigue behavior, and applied load influence on adjacent grid panels.

Main-Bar Spacing

Test results of grid decks with main-bar spacing of 4, 6, 7$\frac{1}{2}$, and 8 in. revealed that deck deflections and main-bar stresses increased with spacing. The variation in deflections and stresses is shown in Table 1. The data indicate that stiffness of open grid decks decreases with increases in main-bar spacing.

Traffic Flow with Main-Bar Direction

Varying the direction of traffic with respect to the main bars on a grid deck–stringer system revealed no significant variation in

TABLE 1 STRESSES AND DEFLECTIONS
CORRESPONDING TO 20-KIP LOAD

Main-Bar Spacing (in.)	Stresses on Main Bar (ksi)		Deflection of Main Bar (in.)
	Top	Bottom	
4	13.8	12.9	0.108
6	25.0	19.6	0.116
7.5[a]	20.8	21.3	0.128
8	27.2	19.4	0.157

NOTE: The open grid flooring consisted of commercially available panels fabricated from ASTM A 588 steel with allowable steel stress fs of 27 ksi. This value was suggested by the manufacturers (Greulich, Inc., Belleville, N.J.). Properties of main bars whose spacing is 4, 6, and 8 in.:
  Weight = 6.09 lb/ft; I = 5.108 in.4; depth = 5.196 in. (see Figure 2); cross-bar and supplementary-bar sizes are $2 \times 1/4$ in. and $1 \times 5/16$ in., respectively.
Properties of main bars whose spacing is 7.5 in. (5-in., four-way grid):
  Weight = 4.83 lb/ft; I = 4.137 in.4; depth = 5.188 in.; cross-bar, supplementary-bar, and diagonal-bar sizes are $2^1/16 \times {}^{13}/64$ in., $1 \times {}^7/32$ in., and $1 \times {}^7/32$ in.
Additional details of open steel grid deck panels are shown in Figure 2, and other design information can be obtained from the manufacturer's catalogs, which can be obtained from the Bridge Grid Flooring Manufacturers Association, 231 South Church Street, Mount Pleasant, Pa. 15666.

[a]Bending stresses and deflections increase with increases in bar spacing except when the main-bar spacing is 7.5 in. This grid deck has diagonal bars and supplementary bars that alter the load distribution within the deck. For additional explanations, see final report (7).

deflection. However, moment variations in the main bars of a 4-in. spaced deck were found to be about 11 percent for two identical grid decks, one set up with main bars parallel to and another with main bars perpendicular to traffic (see Table 2). Such a difference in moments is attributed to the presence of five main bars under the load in the parallel direction and only two in the perpendicular direction. Typically, strain and deflection measurements tend to be larger when the main bars are perpendicular to the traffic flow than when the main bars are parallel to the traffic flow.

Braking Force Effects

Braking or accelerating forces were simulated in the laboratory by using a wedge under the wheel load that transfers a portion of the applied vertical load in the plane of the grid. When in-plane forces act along the length of the main bar, they induce compressive stresses that are superimposed on compressive stresses induced from vertical wheel loads. However, if braking forces are perpendicular to the main bars, they dissipate a portion of the main-bar stress, and in this case, in-plane compressive forces are induced on a portion of the top of the cross bars. Similarly, tensile forces are induced on other portions of the cross bars. Therefore, the critical wheel load position is when the traffic is parallel to the cross bars, because these are found to be most vulnerable to failure under fatigue-induced loads. The design equations developed reflect this critical load position.

Range of Applied Loads

The fatigue life (number of cycles) in the case of constant amplitude load testing decreases with an increase in bending stress range. This can be found from the results given in Table 3. Commercially available grid decks subjected to fatigue loads showed no crack propagation at stress ranges below 10 ksi. The most significant factor controlling fatigue life of a welded grid deck is the spacing of the main bars; for example, the fatigue life of a deck with 4-in. main-bar spacing was 700,000 cycles versus 500,000 cycles for a deck with 6-in. main-bar spacing. All the fatigue cracks were formed at the tops of the cross bars. The cracks were perpendicular to the longitudinal direction of the cross bars and very close to the main- and cross-bar junctions. This implies that bending stress on cross bars is the predominant factor in the fatigue failure of grid decks. The cross bar does not have a uniform cross section because of notches; thus, these experiments revealed that the effective moment of inertia is based on only 70 percent of total height.

The standard bending stress range of cross bars versus the number of cycles (*S-N* curves on a log-log scale) for welded grid decks was developed on the basis of the experimental information derived from this study. From these test results, it is concluded that a welded grid deck system (excluding 5-in., four-way grids) stiffened by being welded to stringers, floor beams, or both can be classified under Category E of the AASHTO specifications (see Figure 4). The controlling factor is the bending stress range of the grid cross bars subjected to a typical truck load, in which the transverse load distribution factor has to be determined in accordance with the formula developed by the authors (7).

TABLE 2 EFFECT OF DIRECTION OF TRAFFIC WITH RESPECT TO MAIN BARS

Bridge Component	Main-Bar Spacing (in.)	Moment (kip·in.) by Direction of Traffic		Deflection (in.) by Direction of Traffic	
		Parallel to Main Bars	Perpendicular to Main Bars	Parallel to Main Bars	Perpendicular to Main Bars
Main bar	4	23.78	26.79	0.100	0.104
Cross bar	6	5.07	5.07	0.298	0.299
Stringer	6	398.05	398.05	0.174	0.178

NOTE: The 20-kip load is positioned at midspan and centered between the stringers. Moments are computed from the strain readings. The change in direction of traffic from parallel to perpendicular is simulated by rotating the 10×20-in. loading plate over a 90 degree angle. All cross bars ($2 \times 1/4$ in.) have a center-to-center distance of 4 in.

TABLE 3   STRESS RANGE VERSUS
FATIGUE LIFE

Main-Bar Spacing (in.)	Constant Amplitude Stress Range (ksi)	Fatigue Life (cycles to failure)
6	15.4	500,000
4	13.5	700,000
4	11.4	750,000
4	8.5	1.5×10^6

NOTE: All fatigue tests are performed on 6- × 10-ft open steel grid decks stiffened by three W10×22 stringers, two at the ends and one in the middle with 5-ft spacing. Frequency of fatigue load is 1.6 Hz. A dual tire loading is simulated over an area of 10 × 20 in. and is applied by means of a 0.5-in.-thick steel plate and elastomeric rubber pad.

A more realistic approach in designing a welded grid deck for fatigue resistance is to properly account for residual stress effects as well as induced stresses (see section headed Residual and Induced Stress Effects), which are due to differential elevation between stringers or curvature variations within a grid deck. The authors found that if the vertical axis of the S-N curve is represented by a log value of the maximum stress (maximum stress in a member from applied loads plus residual stress, which varies with bar spacing and pattern, plus induced stresses), the design S-N curve for welded decks has to be classified as Category A (see Figure 4). Once again, the test data were extensively synthesized before this conclusion was derived; additional information may be found in the final report (7). From the design viewpoint, it would be ideal to shim the gaps between the grid deck and the stringers over the full stringer flange width before welding. If the deck is not properly supported by stringers or is forced down for welding, the induced stress will be high and detrimental to service life.

Composite Action of Grid Deck and Steel Stringers

Before presentation of the details on composite action, it should be noted that the term "composite action" in this paper always refers to the effect of the grid deck on a supporting stringer that is transverse to the main bar of the grid deck.

Results in Table 4 indicate that, under static loads, a maximum increase of about 8 percent in the composite action of the grid deck–stringer system is observed when every fourth main bar is welded to the stringers as compared with the noncomposite deck–stringer system. However, other results in Table 4 indicate that there is no significant increase in composite action when every second bar is welded to the stringers instead of every fourth bar. Hence, it would be economical to weld only every fourth bar. Two identical decks were tested under identical fatigue loads; one deck has a noncomposite system and the other has every fourth main bar welded to the stringers. At the end of a million fatigue cycles, the noncomposite deck lost twice as much stiffness as the deck that was sparsely welded to the stringers, which leads to the conclusion that deck service life under fatigue improves when the deck is welded to the stringers.

Type of Deck

Load deformation tests were performed on welded as well as riveted decks. No fatigue failure was observed on riveted decks even after they were subjected to 1.5 million cycles. This may be attributed to frictional damping in riveted decks. Nevertheless, crack initiation takes place in most welded decks at about 400,000 to 500,000 cycles at high stress ranges because of high stress concentrations or stress raisers near reentrant angles, residual stress buildup during fabrication, and large openings in main bars. However, riveted decks are found to be more flexible than welded decks. This is attributed to excessive slack in a riveted deck system.

Galvanization

Two identical grid decks (with and without galvanization) were tested under identical fatigue load ranges. A fatigue life of 1 million cycles was observed for galvanized decks, whereas 700,000 cycles was noted for nongalvanized decks. A similar improved service life in galvanized decks was noted through field observations (personal communication, Ackrow Corporation, April 1987). Furthermore, a 10 percent variation in main-bar stresses was noted at the top of the deck with
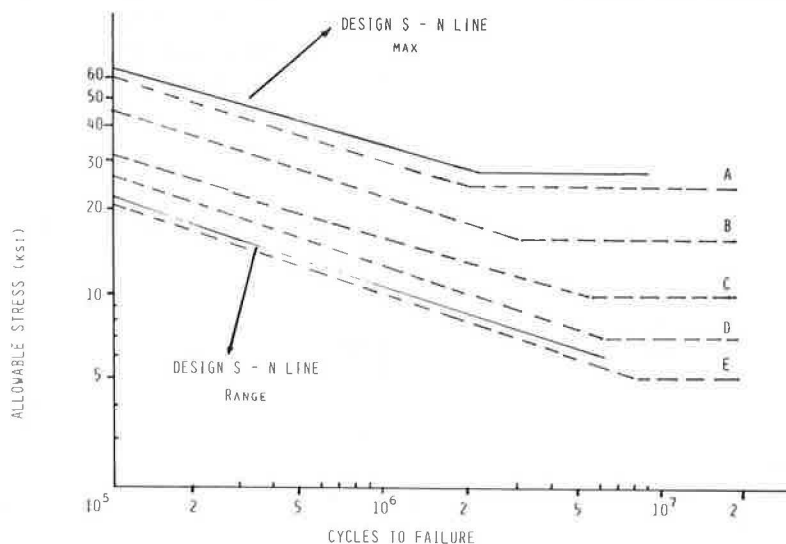

FIGURE 4   Design *S–N* lines for open steel grid decks.

TABLE 4   COMPOSITE ACTION

Type	Load (kips)	Deflection (in.)
Every fourth bar welded[a]	20	0.314
Every second bar welded[a]	20	0.306
Noncomposite[b]	20	0.133
Composite with every fourth bar welded[b]	20	0.122

[a]Dial gauge directly under load on main bar. Test specimen 16 by 7.58 ft. with 6-in. main-bar spacing.
[b]Dial gauge directly under load on main bar. Test specimen 6 by 10 ft with 4-in. main-bar spacing. Test grid loaded at middle of two consecutive stringers.

identical stress at the bottom. This may be due to residual stress relief at the top of the deck during the galvanization process, which consists of heating to 860°F and cooling to ambient temperatures.

Residual and Induced Stress Effects

Residual Stresses

Residual stresses in welded joints result primarily from shrinkage due to cooling. These joints are restrained by adjacent parts that have not been heated to high temperatures (1700° to 1800°F). The effects of welding-induced residual stress in open grids are substantial. Residual stresses in grid decks were measured in the laboratory by using electrical strain gauges to observe the decrease in strain (and consequently stress) after the removal of a welded joint connecting the main and cross bars. Because the residual stresses are localized at regions surrounding the weld joints, the removal of such a region should relieve the stresses in the remaining main and cross bars. The magnitude of residual stress in grid decks was measured to be as high as 27 ksi, even though some scatter was noted in the experimental data. The residual stresses were found to be higher for decks with closer main-bar spacing. However, for 5-in., four-way grid decks, residual stresses are lower because of the better in-plane stress distribution provided by diagonal bars. Similarly, galvanized decks have lower residual stresses than nongalvanized decks.

Induced Stresses

Grid decks are often not in full contact with top flanges of supporting stringers because of differential elevations of stringers or warping of grids during fabrication. According to the AASHTO specifications, the grid deck should be forced down and welded to the top flange of the stringer or floor beam. Laboratory testing of a commercially available grid deck with 6-in. main-bar spacing and a 3/4-in. differential elevation over a 6-ft stringer spacing revealed an induced main-bar stress of 17.3 ksi. This clearly proved that induced stress can be very high under typical field conditions and may create adverse effects on grid deck performance.

Static Versus Fatigue Behavior

Test results have shown conclusively that grid deck stiffness decreases with the increase in number of cycles. However, test results revealed that fatigue has no significant effect on welds between the deck and the stringers. This proves that fatigue is a local problem in open steel grid decks. The cross bars do not rest fully on the main bars, and plug welds are not structural welds. Hence, the deck does not act like a perfect plate (less than 100 percent torsional moment transfer). The deck is subjected to relative movement of bars at main- and cross-bar junctions and also is free to move at the bottom of the cross bars because of oversized notching in the main bars for fabrication purposes. This leads to additional slackness in the deck system.

Applied Load Influence on Adjacent Grid Panels

Strain measurements were taken on all panels of the grid deck that are continuous over the stringers, whereas the loading was applied on one panel only. Test results revealed that the strain and deflection effects of the load on an adjacent panel were no more than 8 percent of the strain or deflection on the loaded panel. Also, strain relief on the adjacent panel over the full fatigue life of a deck is insignificant. This is a very significant observation in the case of structures subjected to moving loads. It implies that the interaction of loads from adjacent panels is insignificant and that a deck can be designed on the basis of average daily truck traffic only, without incorporating the influence of trucks on contiguous deck panels in the deck design.

A significant amount of research work has been carried out to develop theoretical and design equations for load distribution, displacements, and moments in steel grid decks stiffened by a stringer-and-diaphragm system. That work and a large volume of experimental and theoretical data are not reported here because of space limitations. It should be noted, however, that the experimental and theoretical correlations are found to be excellent; they are reported elsewhere (7).

CONCLUSIONS AND RECOMMENDATIONS

The following conclusions are drawn on the basis of the experimental program on open steel grid decks:

1. Reduction in bending stresses due to composite action is found to be a maximum of 8 percent when the applied load is between stringers or at any general location.
2. Moments of a grid deck–stringer system are lower by about 11 percent when main bars are parallel to traffic rather than perpendicular to traffic.
3. Laboratory results indicate that the stresses and deflections of a grid deck–stringer system are lower when the main bars are parallel to the traffic. Furthermore, main-bar direction should be such that braking or accelerating forces are parallel to the main bars, to avoid additional compressive stresses on the cross bars.
4. Field-induced stresses can be very high (approximately 30 ksi), and the practice of forcing the deck to the stringer and welding it in place should be avoided.

5. Residual stresses obtained experimentally by material removal tests are found to be considerable (approximately 27 ksi), and they seem to have a direct effect in reducing the fatigue life of a deck.

6. Fatigue life (number of cycles before cracking of plug welds) decreased with the increase in main-bar spacing and the increase in stress ranges. An open welded grid deck system (except 5-in., four-way diagonal grids) can be classified under AASHTO Category E with no field-induced stresses if the stress range is considered to be the vertical-axis parameter. However, a more realistic approach, which covers all types of grid decks and all the construction details, is to classify a grid deck under AASHTO Category A by altering the vertical-axis parameter to maximum stress, that is, the sum of maximum stress from applied loads, residual stresses in a grid, and induced stresses in the field.

7. Galvanized welded grid decks have a longer service life than nongalvanized decks, which is attributed to the stress relief caused by the galvanization process.

8. Riveted decks have a longer fatigue life for many reasons, for example, fewer stress raisers, frictional damping, and higher flexibility at junctions of the main and cross bars.

REFERENCES

1. *Special Report 202: America's Highways: Accelerating the Search for Innovation.* TRB, National Research Council, Washington, D.C., 1984.
2. H. V. S. GangaRao. *Feasibility of Steel Grid Decks for Bridge Floors.* Final Report. West Virginia University, Morgantown, July 1980.
3. *Standard Specifications for Highway Bridges.* American Association of State Highway and Transportation Officials, Washington, D.C., 1983, and current interim specifications.
4. J. H. Daniels and R. G. Slutter. *Behavior of Modular Unfilled Composite Steel Grid Bridge Deck Panels.* Fritz Engineering Laboratory Report 200.84.795.1. Lehigh University, Bethlehem, Pa., Jan. 1985.
5. U.S. Steel Corporation. *Test Data Showing Full Composite Action Between Concrete Filled Steel Grid Deck and Supporting Stringers.* Bridge Grid Flooring Manufacturers Association, Pittsburgh, Pa., Aug. 19, 1960.
6. V. K. Hasija. *Concrete Filled Steel Grid Floors for Bridges.* Reliance Steel Products Company, July 1975.
7. H. V. S. GangaRao, W. Seifert, and H. Kevork. *Behavior and Design of Open Steel Grid Decks for Highway Bridges.* Final Draft Report. West Virginia University, Morgantown, Oct. 1987.